UNIVERSITÀ DI PARMA

UNIVERSITA' DEGLI STUDI DI PARMA

DOTTORATO DI RICERCA IN
"*Scienze del Farmaco*"

CICLO XXXV

Combining Phenotypic and Targeted Approaches for the Identification of New Broad-Spectrum Antiviral Agents (BSAAs)

Coordinatore:
Chiar.mo Prof. Marco Mor

Tutore:
Chiar.mo Prof. Marco Radi

Dottoranda: Maria Grazia Martina

Anni Accademici 2019/2020 – 2021/2022

Abstract

The ongoing COVID-19 pandemic caused by the emergence of SARS-CoV-2 in 2019, along with the growing concern about old re-emerging viruses (such as Dengue virus, Zika virus, Ebola virus, etc.) and new potentially pandemic viruses, strongly highlight the need of new antivirals to fight future outbreaks of unknown origin or known viruses for which no drugs are available yet.

The highly specific “one drug, one virus” strategy should be therefore substituted by a less selective "one drug, multiple viruses" approach, which exploits highly conserved viral targets or host cell proteins for the design of pan-viral drugs. These broad-spectrum antiviral agents (BSAAs) can inhibit the replication of multiple viruses and may therefore be used to treat a variety of viral illnesses.

The two main approaches can be employed for the development of new BSAAs: i) a *target-based approach*, which has the advantage of allowing an easy optimization of the drug candidates via structure-based refinement; and ii) a *phenotypic approach*, which has the advantage of quickly identifying new drugs with the desired functional effect in a complex system independently from their mechanism of action. The main goal of this Ph.D. thesis has been the exploitation of both approaches to speed up the identification of new antiviral agents able to inhibit the replication of multiple viruses.

In the **first part**, an evolution-inspired phenotypic approach based on the modification of the formamide prebiotic model was used to identify novel antiviral heterobases with potential broad-spectrum antiviral activity. This approach stems from the idea that, when life originated on our planet, ancestral viruses, already obligated parasites that rely exclusively on the host to survive and replicate themselves, co-evolved with primordial eukaryotic cells (the Last Universal Common Ancestor; LUCA) by sharing and exploiting the same chemical toolset. Thus, a modification of the prebiotic chemical conditions that originated common precursors to viruses and LUCA may lead to new molecules unable to sustain the replication of viruses but still tolerated by eukaryotic cells thanks to their defence mechanism. Next, a system-oriented optimization of 2,6-diaminopurine heterobases is presented, demonstrating how phenotypic studies may allow the identification of new promising BSAAs independently from the exact knowledge of their mechanism of action. Finally, the conversion of the most promising 2,6-diaminopurine antivirals into the corresponding base-modified nucleosides was conducted, in the attempt to create dual-acting drugs that could act against viruses both directly through the nucleoside itself and indirectly through the antiviral nucleobase that might be formed after metabolic cleavage of the glycosidic bond.

The **second part** of this thesis was focused on the target-based approach to new BSAAs. SARS-CoV-2 helicase nsp13, which has a highly conserved structure with common features among highly pathogenic human coronaviruses (HCoVs), was chosen as a promising target to identify pan-coronavirus inhibitors. The inhibition of the host helicase DDX3 by the same target compounds was also taken into account, since DDX3 is involved in the replication of multiple viruses and less prone to drug resistance selection. Finally, new inhibitors of the host kinase PI4KIIIß, which is exploited by several viruses for their replication, were also developed and evaluated against multiple viruses belonging to different families.

SUMMARY

ABBREVIATIONS

ABTS 2,2'-azino-bis (3-ethylbenzothiazoline-6-sulfonic acid)

ADME Absorption, Distribution, Metabolism, and Excretion

BSAA Broad-Spectrum Antiviral Agent

CC_{50} 50% cytotoxic concentration

CC_{90} 50% cytotoxic concentration

CCR5 C-C chemokine receptor type 5

CFTR Cystic Fibrosis Transmembrane Conductance Regulator

COVID-19 Coronavirus disease 2019

CPE Cytopathic effect

DAAs Direct acting antivirals

DCE Dichloroethane

DCM Dichloromethane

DDX3X DEAD-box helicase 3 X-linked

DENV Dengue virus

DIPEA N,N-diisopropylethylamine

DMAP Dimethylaminopyridine

DMF Dimethylformamide

DMSO Dimethyl sulfoxide

DNA Deoxyribonucleic acid

DYRA Direct Yield Reduction Assay

EC Electrochemistry

ESI Electrospray ionization

EVs Enteroviruses

FDA Food and Drug Administration

FLU Influenza

HA Hemagglutinin

HBV Hepatitis B Virus

HCMV Human cytomegalovirus

HCV Hepatitis C Virus

HDAs Host-directed antivirals

HIV Human Immunodeficiency Virus

HIV-1 Human Immunodeficiency virus type 1

HIV-2 Human Immunodeficiency virus type 2

hRVs human Rhinoviruses

HSV-1 Herpes Simplex Virus type 1

IC_{50} 50% inhibitory concentration

IMPDH Inosine 5′-monophosphate dehydrogenase

LUCA Last Universal Common Ancestor

MCR Multicomponent Reaction

MERS-Cov Middle East Respiratory Syndrome-Coronavirus

MMOA Molecular mechanism of action

MS Mass Spectrometry

NS3 Non-structural protein 3

NS5 Non-structural protein 5

Nsp13 Non-structural protein 13

PDD Phenotypic Drug Discovery

PI3KR1 Phosphoinositide-3-kinase regulatory subunit 1

PI4KIIIβ Phosphatidylinositol kinase type IIIβ

PIK Phosphatidylinositol kinases

PIP Phosphoinositides

PRA Plaque Reduction Assay

RdRp RNA-dependent RNA-polymerase

RNA Ribonucleic acid

ROs Replication Organelles

RSA Radical scavenging activity

SAR Structure Activity Relationship

SARS-CoV-2 Severe acute respiratory syndrome-Coronavirus-2

SI Selectivity Index

SYRA Secondary Yield Reduction Assay

TDD Target-based Drug Discovery

THF Tetrahydrofuran

WNV West Nile Virus

ZIKV Zika Virus

1. GENERAL INTRODUCTION

1.1 Broad-Spectrum Antiviral Agents (BSAAs)

Over the course of human history, viral pathogens have represented a serious threat that has significantly affected the health and evolution of entire populations. The increasing globalization and climatic changes have significantly contributed to relocate several viruses from their original habitat, thus allowing the infection of naive populations and spreading of new pandemics: the twenty-first century alone has recorded more than ten epidemic and pandemic viral emergence events, including the disastrous Coronavirus disease 2019. Recently, there has been a growing concern for old re-emerging (e.g. Dengue virus, Zika virus, Ebola virus, etc.) and new emerging viruses (e.g. SARS-CoV-2, MERS-Cov, and related viruses) for which there are no treatments available. Depending on the infectivity of these viruses, they cannot only cause major health problems but also negatively impact the economy, as demonstrated by the recent COVID-19 pandemic[1]. The latter disease, caused by worldwide spreading of SARS-CoV-2, has been causing more than 100 million reported cases and greater than 2 million deaths[2]. In 2023, the COVID-19 pandemic is still ongoing, and there is no doubt that its medium/long-term consequences will affect us for a long time. SARS-CoV-2 has certainly highlighted the need for prompt countermeasures, but emerging widespread viruses with a moderate mortality rate (e.g. Flaviviruses) may also pose a significant epidemic threat[3]. The epidemic potential of Flaviviruses may be also favored by their rapid diffusion through mosquito vectors. Overall, several viruses belonging to different families are still untreatable, and coinfections by viruses from the same or different families, are also a global concern for public health. As viral infections from emerging viruses are expected to increase in the future, new approaches to fight potential outbreaks are highly needed. To fight this menace, the standard antiviral strategy in which each virus is treated separately should be revised and implemented with new drugs endowed with a broad-spectrum antiviral activity by acting on highly conserved viral targets or host cell factors[4]. These broad-spectrum antiviral agents (BSAAs) can inhibit the replication of multiple viruses and could be used for the treatment of different viral infections, following the new paradigm “one drug, multiple viruses”[5]. This approach could help in the prompt intervention against new pandemics since these antivirals act on multiple viruses by targeting some commonality in their life cycle. For their wide range of coverage, BSAAs might be also useful in the case of viral co-infections that, nowadays, represent the most serious challenge in the treatment of patients with severe infections by multiple viruses[6].

The concept of BSAAs was introduced in 1972 when it was demonstrated that ribavirin is active against 16 DNA and RNA viruses[7]. Different mechanisms have been suggested to clarify the broad-

range antiviral properties of ribavirin, which include inhibition of RNA capping activity, and direct inhibition of viral polymerases[8], as well as the inhibition of inosine 5′-monophosphate dehydrogenase (IMPDH)[9]. The BSAAs field is still in its early development, and only two drugs (ribavirin and interferon-alpha) have been approved by FDA to treat infections from viruses belonging to different families. However, repurposing of existing antiviral agents against other virus infections should be a quick approach to find new BSAAs. In fact, hundreds of compounds have characteristics that allow to classify them as broad-spectrum antiviral agents[10] (Figure 1). For example, favipiravir, approved in Japan, is RNA dependent RNA polymerase inhibitor of Influenza, but exhibits broad spectrum RNA virus activity with efficacy also against the polymerase of Ebola and Lassa fever[11,12]; cidofovir, a nucleotide analog, has activity against DNA viruses including herpes, adeno, polyoma and pox viral families; brincidofovir, although didn't show human efficacy, it has been shown to have in vitro activity not only on DNA viruses, but also against the RNA-genome filovirus Ebola[13,14]; ganciclovir, approved against CMV, also inhibits two other DNA viruses in vitro: adenovirus and hepatitis B virus[15]; remdesivir, nucleoside analogues, has been shown to have effect against both coronaviruses and filoviruses[16]; tenofovir, in addition to its activity against HIV and HBV, is active against the DNA polymerase of HSV[17]; foscarnet, a pyrophosphate analog that blocks the pyrophosphate binding sites of viral polymerase is an antiviral used exclusively for resistant herpesvirus infections but has also demonstrated activity against the reverse transcriptase of HIV-1 and HIV-2; the HIV protease inhibitor lopinavir, in combination with ritonavir, has been repurposed for use in the treatment of coronaviruses SARS and MERS[18]; interestingly, an anti-parasitic and anti-bacterial drug, nitazoxanide, has been shown to have also antiviral activity against hepatitis B, hepatitis C, dengue virus, rotavirus, yellow fever, Japanese encephalitis, HIV, and influenza[19].

An extensive therapeutic window for the inhibition of virus replication can be created by the field of broad-spectrum antiviral agents (BSAA), as evidenced by the previously unheard-of broad spectrum antiviral activity of drugs originally developed to target a single agent.

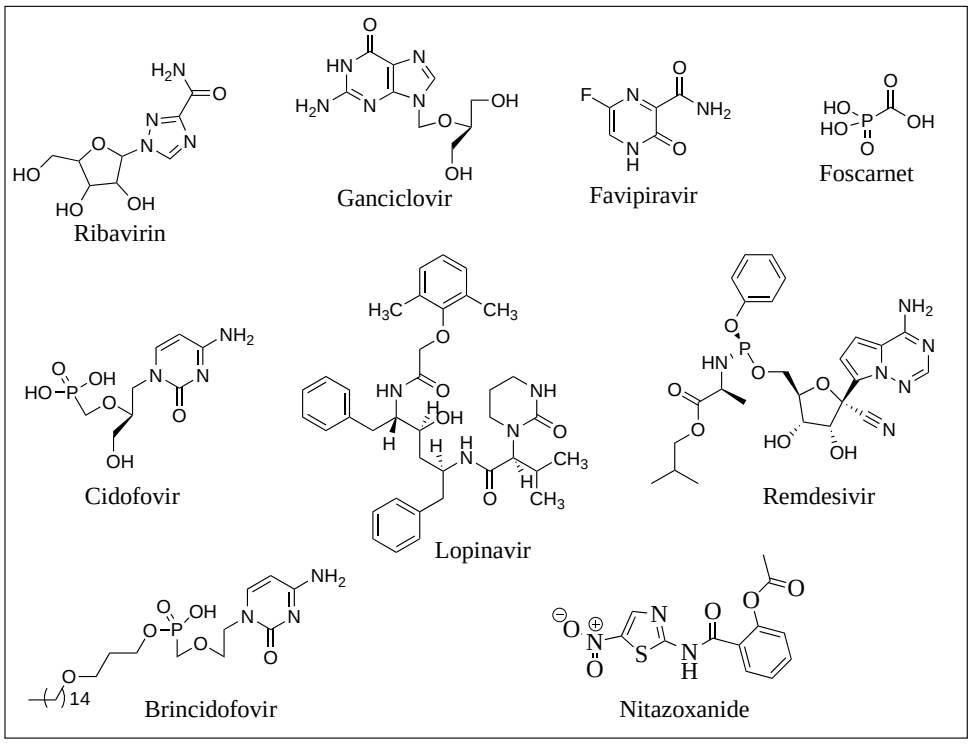

Figure 1. The chemical structure of broad-spectrum antiviral agents (BSAAs).

Drug discovery strategies can be mainly divided into *target-based approaches* and *phenotypic approaches*. The target-based approach is certainly advantageous because the successive chemical optimization of drugs identified with this approach can be achieved faster and easily, thanks to the possibility to apply molecular and chemical knowledge to investigate specific molecular hypotheses. Over the past 25 years, molecular target-based drug screening has become the main drug discovery paradigm exploited in both the pharmaceutical industry and academic research[20]. David C. Swinney & Jason Anthony proposed that poor identification of new drugs with a target-based approach is partly because it doesn't take in account the molecular complexities of the drugs' action, which is reflected in molecular mechanism of action (MMOA)[21]. This has stimulated a debate about the most effective way of discovering new drugs between target-based approaches (target-first, forward chemical biology) or phenotypic approaches (function-first, reverse chemical biology)[22,23,24,25].

Fortunately, there has been an interest in the use of phenotypic screening as an alternative to target-based screening, that facilitated the identification of first- in-class medicines and their respective MMOAs. Recent studies proved the phenotypic approaches to be the most successful strategy for small-molecule, first-in-class medicines [21,26,27].

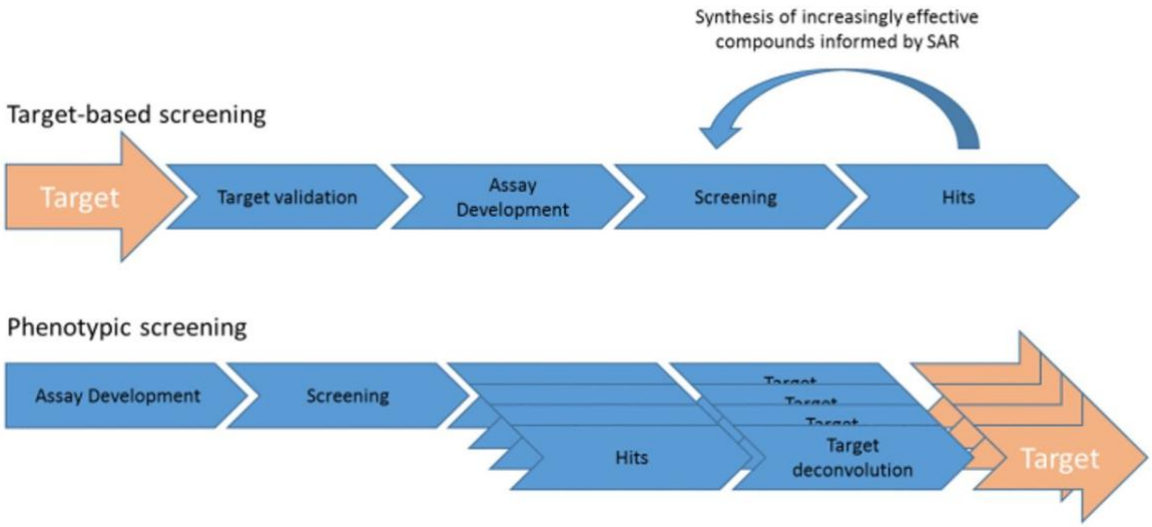

Figure 2. Target-Based vs. Phenotypic Drug Discovery for First-in-Class Medicines

The phenotypic approach does not require prior understanding of the molecular mechanism of action (MMOA), and this could lead to faster detection of new innovative medicines. This aspect obviously led to a disadvantage that is the challenge of optimizing the candidate drugs without the design parameters provided by prior knowledge of the MMOA.
Considering this scenario, the more interesting approach is to use an appropriate combination of a target-based approach and a phenotypic approach to enable good ideas to successfully move forward.

1.2 Phenotypic approach to new BSAAs

An antiviral drug-discovery campaign centered on phenotypic screening has the advantage of quickly identifying new drugs with the desired functional effect in a complex system (e.g. an infected cell) independently from their mechanism of action, thus avoiding the slow optimization process need to bring a drug candidate from target inhibition to efficacy in a higher disease model.

To achieve the challenging aim of identifying new small molecules endowed with broad-spectrum antiviral activity, we started from the consideration that all viruses are small microorganisms that cannot grow outside of living cells because they cannot replicate on their own. For this reason, they are obligate parasites that exploit host cell components to replicate their DNA or RNA. This relationship dates back to the origin of life on our planet, when ancestral viruses co-evolved with the Last Universal Common Ancestor (LUCA) by sharing and exploiting the same chemical toolset. However, while LUCA has later evolved in a complex machine equipped with complex defence mechanisms against harmful and unrecognized substances, viruses are still simple organisms that may not survive if unable to “speak” the same chemical “language” of their host, which is needed to use the host machinery and building blocks[28].

We thought that by modifying the prebiotic conditions that led to earliest life forms from simple inorganic precursors it would be possible to generate non-natural organic precursor (nucleobases and nucleosides) capable of reducing viral replication but still tolerated by eukaryotic cells thanks to their defence mechanisms (Figure 3).

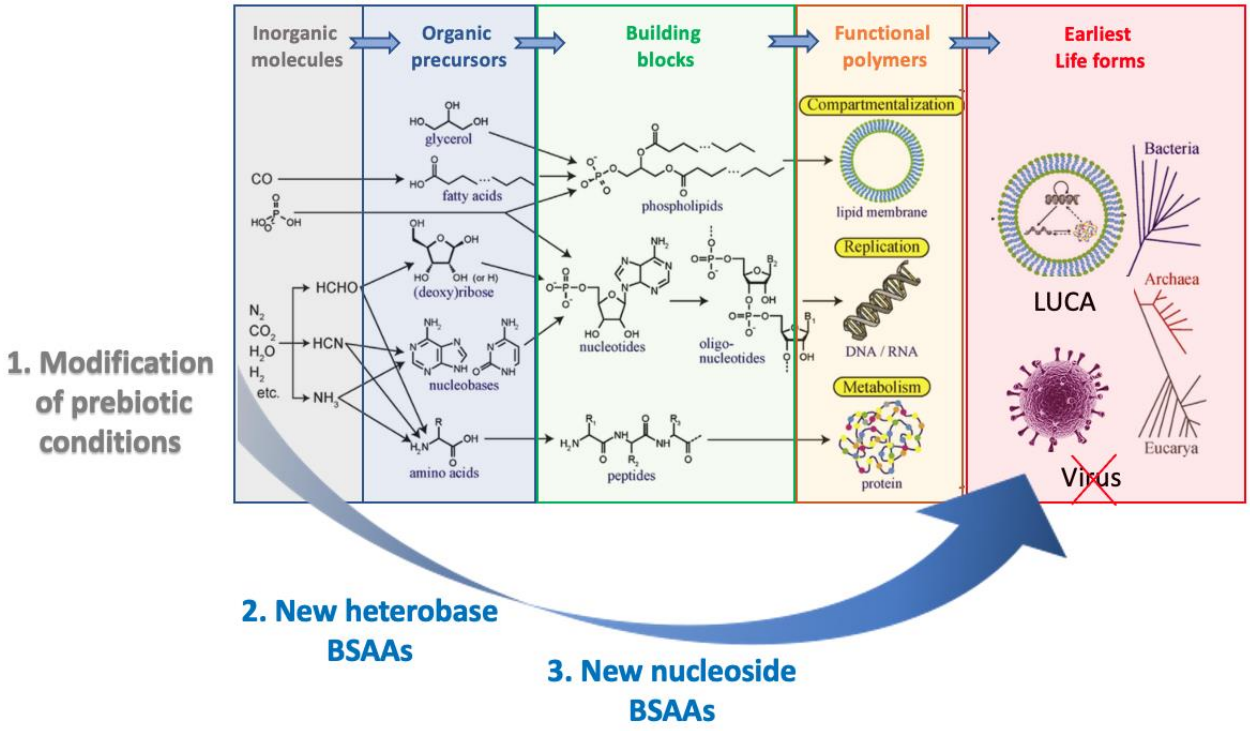

Figure 3. Evolution-inspired approach to new BSAAs (adapted from Ref. 29)

In **Chapter 2.1**, I will describe an evolution-inspired approach based on the modification of the formamide prebiotic model to identify new antiviral heterobases with potential broad-spectrum antiviral activity. The following **Chapter 2.2** will describe a system-oriented optimization of 2,6-diaminopurine heterobases as new antiviral agents active on multiple families of viruses, thus showing how phenotypic-based studies may allow to identify new promising BSAAs independently from the exact knowledge of their mechanism of action.

Finally, in **Chapter 2.3** I will describe the conversion of the more promising 2,6-diaminopurine antivirals from the previous chapter into the corresponding nucleoside derivatives, a preliminary effort to create dual-acting drugs that would be able to fight viruses both directly through the nucleoside itself and indirectly through the antiviral nucleobase that might be generated after metabolic cleavage of the glycosidic bond.

1.3 Target-based approach to new BSAAs

Most approaches for the development of antiviral agents focus on targeting viral components (virus-targeting antivirals) or modulating host cell factors (host-targeting antivirals).

The majority of FDA approved antiviral drugs target viral proteins, especially viral enzymes and their catalytic domains[30]. These antivirals are called direct-acting antivirals (DAAs)[31]. DAA strategy is based on the study of a virus and identify a specific viral protein as a drug target in order to limit potential toxicity and to increase drug efficacy. However, viruses are subjected to continuous evolution to survive and cope with available drugs, as well as with the immune response of the host cells. Viral infection diseases are characterized by a high rate of mutations with the emergence of drug-resistant virus variants[32,33]. Particularly those with an RNA genome have a high mutation rate, allowing resistance to develop rapidly[34,35,36]. For this reason, the available drugs directly targeting virus factors lose very quickly their efficacy. Moreover, considering the increasing diversity among viruses of the same family and in different family's viruses, infectious viral diseases seem a never-ending challenge that makes it impossible to have an arsenal to fight the magnitude of re-emerging and emerging viruses. The difficulty to identify a critical protein belonging to different viruses or critical cellular processes used by different viruses makes the design of BSAAs virus targeting problematic because of the structural diversity among several viruses and the high mutation rate of viral components or virally encoded proteins. Nevertheless, virus-specific antiviral research remains a successful and essential strategy to combat viral infections, and historically, broad-spectrum antivirals have first been discovered by serendipity through simple screening assays of these DAAs against different viruses[7,37]. Therefore, undeniably, we can say that they contributed to the development of BSAAs.

However, the emergence of resistance to virus-targeting antivirals leads to considering alternative antiviral strategies to combine with it.

Viruses are small parasites constituted of a segmented nucleic acid surrounded by a protein coat, that cannot grow outside of living cells because they cannot replicate on their own. They exploit some host proteins for their replication, which are dispensable for host cells, but essential for viral replication cycles[38,39]. Thus, various types of host cellular components can aid viruses in the viral infection process. Because cellular factors have less genetic variability than viral factors, they are less prone to mutate and lead to antiviral drug resistance[7,33]. Thus, instead of targeting the highly mutating viral proteins, also host cell proteins can be targeted to interfere with viral infections. This strategy is known as host-directed antiviral agents (HDAAs). Even if the main disadvantage of host-targeted antivirals is the higher risk for host toxicity, an advantage is represented by the fact that the host

proteins involved in virus replication are often common to many viruses and can be studied before a new virus emerges.

In summary, one efficient strategy to fight new viral outbreaks can be represented by the developing of drugs able to target highly conserved viral proteins and, at the same time, host proteins exploited by viruses for their replication.

Chapter 3 will be focused on the design and synthesis of new BSAAs targeting both host (PI4KIIIß and DDX3) and viral proteins (nsp13).

2. PHENOTYPIC DRUG DISCOVERY

2.1 Evolution-inspired synthesis of antivirals

2.1.1 Introduction

Viruses and cells have intertwined since the dawn of evolution because viruses, by their nature, are obligate parasites that cannot multiply or carry out living processes outside the cells. This relationship dates back to the origin of life on Earth. Biologists have long agreed to the idea that all known life forms on Earth arose from a common ancestor and the concept of a Last Universal Common Ancestor (LUCA) is central to the study of early evolution and life's origin[40]. Ancestral viruses have co-evolved with LUCA, which was initially constituted by a minimal set of essential genes to support cellular life[41]. Nevertheless, LUCA has later evolved into a complex machine equipped with a convoluted defense mechanism, while viruses are still simple organisms that are not able to survive if they don't rely on the host machinery[42,43]. The common "chemical language" is represented by building blocks (e.g. nucleic acids, proteins, carbohydrates, and lipids), which are tools used by all life forms on Earth to store and transmit genetic information. The origin of the common "chemical language" can be traced back to a few keys starting inorganic molecules in a prebiotic environment, which were transformed into primary and secondary heterocyclic metabolites (organic precursors) via Multi-Component Reactions (MCR)[44]. The following 'evolution' of these simple organic molecules into a higher level of organization and complexity has later generated the first life forms on our planet[29]. MCR at the origin of life on Earth generated awesome chemical diversity, setting the basis for the emergence of LUCA. MCR usually involves three or more substrates, which are combined either simultaneously or by a sequential addition, to rapidly build up the final product in a one-pot procedure. The first documented MCR reproduced in a lab environment was the Strecker synthesis of α-amino cyanides in 1850, which are versatile intermediate for the synthesis of α-amino acids[45,46]. Later, several chemists wondered how life originated from an inanimate mixture of inorganic and organic compounds on the primordial Earth. Although the issue remains one of the most important open questions in science, different prebiotic MCR were attempted in laboratories to simulate the origin and evolution of life on Earth.

Among the key chemical precursors that could have served as starting materials, hydrogen cyanide (HCN)[47] and formamide (NH_2CHO)[48,49] have received increasing attention as possible precursors of building blocks. One of the most accredited MCR models to explain the prebiotic origin of life on Earth is represented by the formamide-based prebiotic chemistry. According to this model, formamide derived from the hydrolysis of HCN could accumulate in sufficiently high amounts to serve as backbone and reaction medium for the synthesis of the first biogenic molecules, nucleic

bases, acyclonucleosides, nucleotides, biogenic carboxylic acids, sugars, amino sugars, amino acids, and condensing agents (Figure 4)[50].

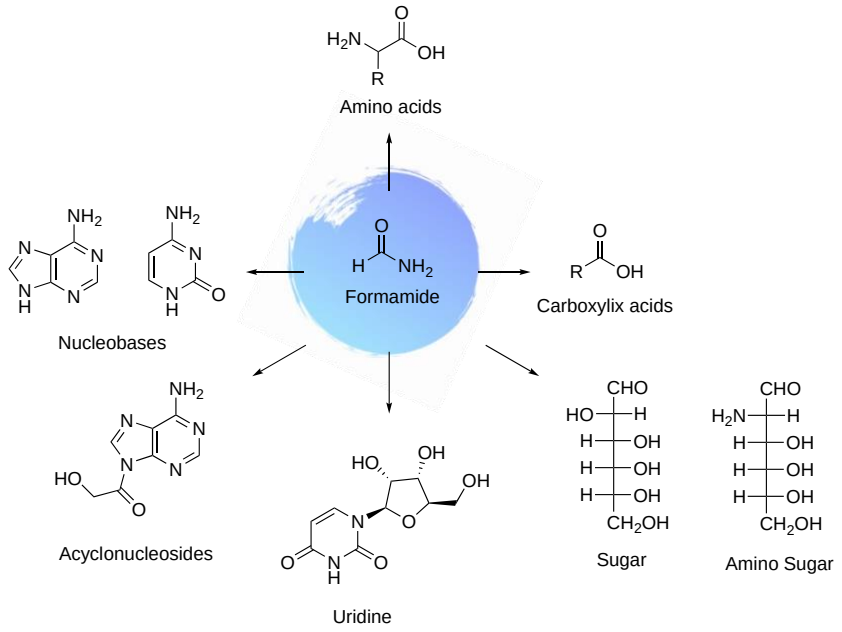

Figure 4. Formamide-based prebiotic chemistry model. Adapted from Rif. 50

Saladino and colleagues demonstrated in fact that heating formamide in the presence of terrestrial and non-terrestrial (meteoritic origin) catalysts, triggered a cascade of MCR that ultimately produces a complex mixture of nucleobases, amino acids, sugar, and other important organic precursors [51,52,53]. It is well-known that all biological reactions occur in boundary structures, of which phospholipids represent the main constituents, capable of encapsulating and harboring other biomolecules. In the late 1920s, Deamer et al noted the importance of membranes also in the origin of life[54]. Later on, it has been amply demonstrated that the prebiotic molecules must be assembled inside a compartmentalized system, semipermeable compartments that enveloped the essential components required for replication, translation, and transcription[55]. Obviously, the primordial membranes were much simpler than those of modern cells, but, also in the prebiotic soup, amphiphilic molecules found their proper space, which self-assembly spontaneously into complex supramolecular structures[56]. Therefore, amphiphilic micelles and vesicles could constitute a suitable microenvironment capable of harboring biomolecules and in which diverse chemical reactions could occur. Several works highlighted how phospholipids could be achieved abiotically from different types of amphiphilic molecules that have been proposed as possible prebiotic lipids[57,58,59,60,61]. Among these, fatty alcohols (long-chain alcohols with C4-C6) were considered constituents of prebiotic membranes[62]. The precursors of phospholipids, in order to assemble into vesicles, required an aqueous phase. There is no doubt that water had a crucial role in the origin of life[63] and it was recognized as the main solvent in the famous Miller-Urey experiment, as well as a catalyst in prebiotic chemistry[64].

A modification of the prebiotic MCR that originated common precursors to viruses and LUCA, may result in the generation of new molecules able to inhibit viral replication but well tolerated by eukaryotic cells thanks to their complex defense mechanisms. The modification and modernization of the formamide-based prebiotic chemistry model with innovative chemical techniques, such as microwave, electrochemistry, and catalysis with terrestrial and extra-terrestrial minerals, could offer the possibility to speed up the non-natural evolution of new heterocyclic compounds. An antiviral drug-discovery program centered on the phenotypic screening of evolution-inspired heterocyclic libraries may represent an innovative approach in the search for new non-natural organic precursors, possibly endowed with broad-spectrum antiviral properties.

2.1.2 Aim of the work

According to the formamide prebiotic chemistry model, life was originated in the primordial soup by random multicomponent reactions starting from formamide. We planned to modify this "natural" model by adding an early intermediate of our in house antivirals as a sort of doping agents,[65] in order to force the formamide-based MCR to generate a non-natural mixture enriched with heterocyclic analogues that may display antiviral activity. The planned workflow can be represented by an iterative series of steps consisting in: 1) a modified prebiotic reaction with different doping agents; 2) isolation of the mixture fraction soluble in MeOH:H_2O 90:10) cell-based antiviral assay on the isolated mixture; 4) analysis and deconvolution of active mixtures followed by modification of the prebiotic conditions until the identification and isolation of an antiviral compound. (Figure 5)

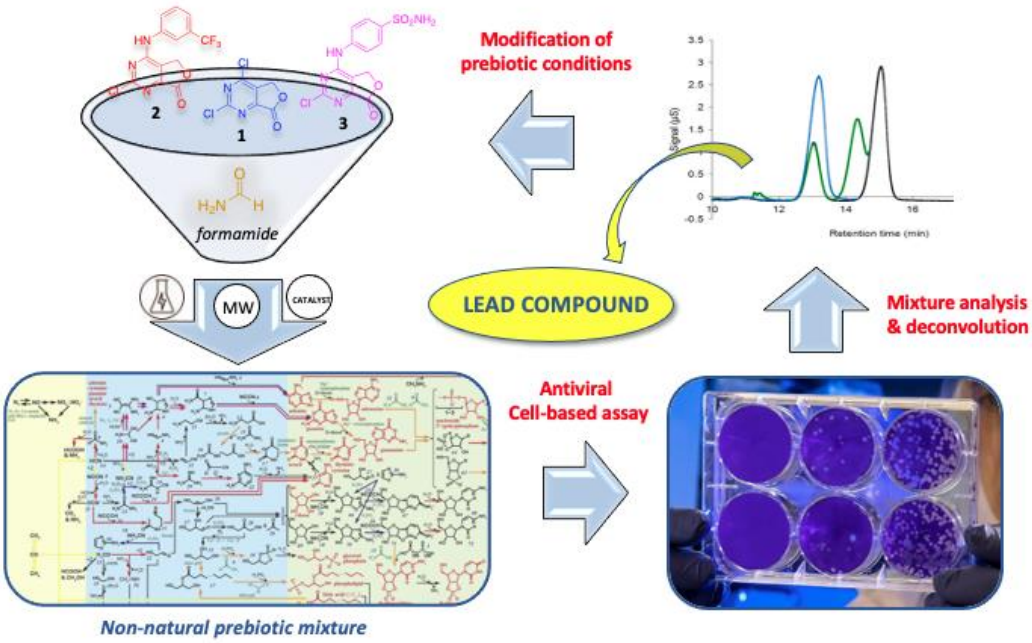

Figure 5. Workflow of the evolution-inspired antiviral drug-discovery approach

2.1.3 Results and discussion

A collection of various complex mixtures was obtained by microwave heating formamide in the presence of selected doping agents (**1-3**). Different sets of experiments were performed: dissolving the reaction mixture in pure pentanol or water, in pentanol/water (1:1), or using formamide as solvent, and heating at 140-180 °C for different times as shown in Scheme 1. Pentanol and water were selected solvents, considering their plausible presence in prebiotic Earth as already explained in the above paragraph 2.1.1.

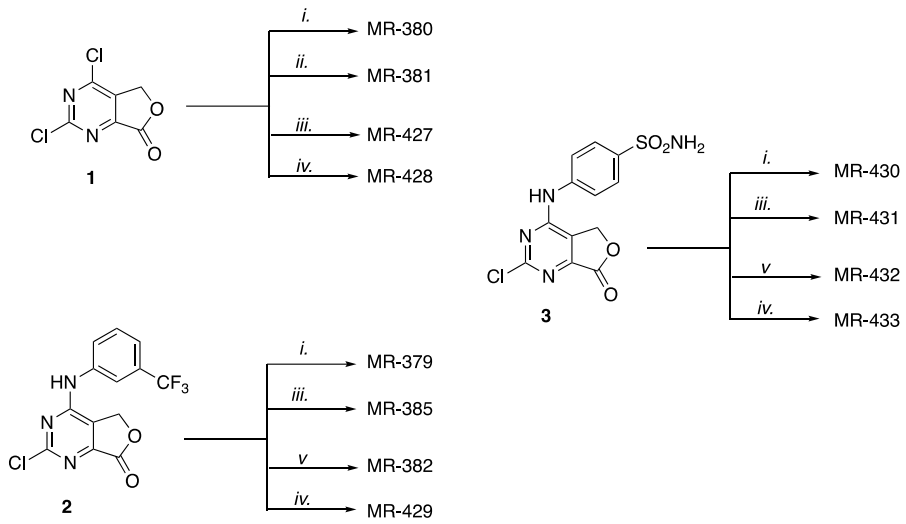

Scheme 1. *Reagents and conditions: i.* NH_2CHO (10 eq.), n-pentanol, 180 °C μW, 1h; *ii*. NH_2CHO (10 eq.), n-pentanol, 180 °C μW, 30'; *iii.* NH_2CHO (1 mL), 180 °C μW, 5'; *iv*. NH_2CHO (10 eq.), H_2O/n-pentanol (1:1), 140 °C μW, 15'; *v.* NH_2CHO (10 eq.), H_2O 180 °C μW, 5'.

In analogy with literature MCR for the one-pot synthesis of life's building blocks resulted in a very complex mixture of products, also the modification of the formamide-based prebiotic chemistry model furnished a large panel of products. The obtained complex mixtures of non-natural heterocyclic compounds may contain an innovative antiviral molecule non-selected by the natural MCR process.

2.1.4 Biological results and analytical analysis

Mixtures of heterocycles were tested against a large panel of viruses, including West Nile virus, Dengue virus, and Retrovirus HIV-1. As reported in Table 1, no mixtures resulted toxic in two different cell lines (Huh7 and H9) except for MR-429, with low CC_{50} values in both cell lines, and MR-428, which presented high toxicity in Huh7 cells. Among the different reaction mixture, MR-379 turned out to be the most interesting in terms of antiviral activity: it inhibited, at low micromolar concentrations, the replication of viruses belonging to the Flaviviridae family with no toxicity on the used cell lines.

Table 1: Cytotoxicity and antiviral activity of mixtures obtained through the modified prebiotic conditions.

	WNV		**DENV**		**HIV**	
Cmpd	CC_{50}[a] (*Huh7*)	IC_{50} [b] WNV	IC_{50} DENV		CC_{50} *(H9)*	IC_{50}
		DYRA[c]	DYRA	SYRA[d]		
MR-379	160	7.95	ND	18.2	65	NA
MR-382	100	NA[e]	NA	NA	100	NA
MR-385	50	NA	NA	NA	60	NA
MR-429	30	12.1	4.95	3.2	45	NA
MR-434	60	22.9	12	11	45	NA
MR-430	140	7.95	ND	NA	100	15,60
MR-431	>200	NA	ND	NA	>100	NA
MR-432	>200	NA	ND	NA	>100	NA
MR-433	>200	12.1	ND	NA	>100	NA
MR-380	>200	7.95	ND	28	100	NA
MR-381	>200	9.9	ND	NA	120	NA
MR-427	180	NA	ND	NA	100	NA
MR-428	23	ND[f]	ND	ND	>100	NA

[a]CC_{50}: half-maximal cytotoxic concentration (μM); [b]IC_{50}: half-maximal inhibitory concentration (μM); [c]DYRA: direct yield reduction assay; [d]SYRA: secondary yield reduction assay; [e]NA: Not active; [f]ND: Not determined.

In the attempt to further evaluate the spectrum of antiviral activity of this promising mixture, it was also evaluated against a negative-strand RNA virus, Influenza A (Table 2). MDCK and A549 cell lines were used to evaluate cytotoxicity and antiviral potency against Influenza. The selected mixture did not display cytotoxicity on both cell lines. In particular, the MR-379 showed a high SI (selective index) on MDCK and a lower CC_{50} value on A549. Finally, MR-379 was evaluated against SARS-CoV-2 (Table 2): albeit the mixture was endowed with a moderate toxicity in Caco-2 cells, a low micromolar activity (IC_{50} = 9.1 μM), against the new pandemic virus was shown, allowing us to consider this prebiotic mixture as promising source of BSAAs for further investigations.

Next, the stability of the complex mixture MR-379 was evaluated: the sample was kept in solution (either CH_3CN or DMSO) at room temperature for more than a month and the acquired chromatographic profile was compared with the profile of a freshly prepared solution of the MR-379 mixture. Qualitative and quantitative differences were not observed, demonstrating the mixture is a suitable candidate for further evaluation (Figure 6).

Table 2: Cytotoxicity and antiviral activity of mixture MR-379 on Influenza A and SARS-CoV-2

Cmpd	CC_{50}[a]	IC_{50}[b] Influenza A	CC_{50}	IC_{50} Influenza A	CC_{50}	IC_{50} SARS-CoV-2
	MDCK		A549		Caco-2	
MR-379	424	6.3	40	6.3	33.1	9.1

[a]CC_{50}: half-maximal cytotoxic concentration (µM); [b]IC_{50}: half-maximal inhibitory concentration (µM).

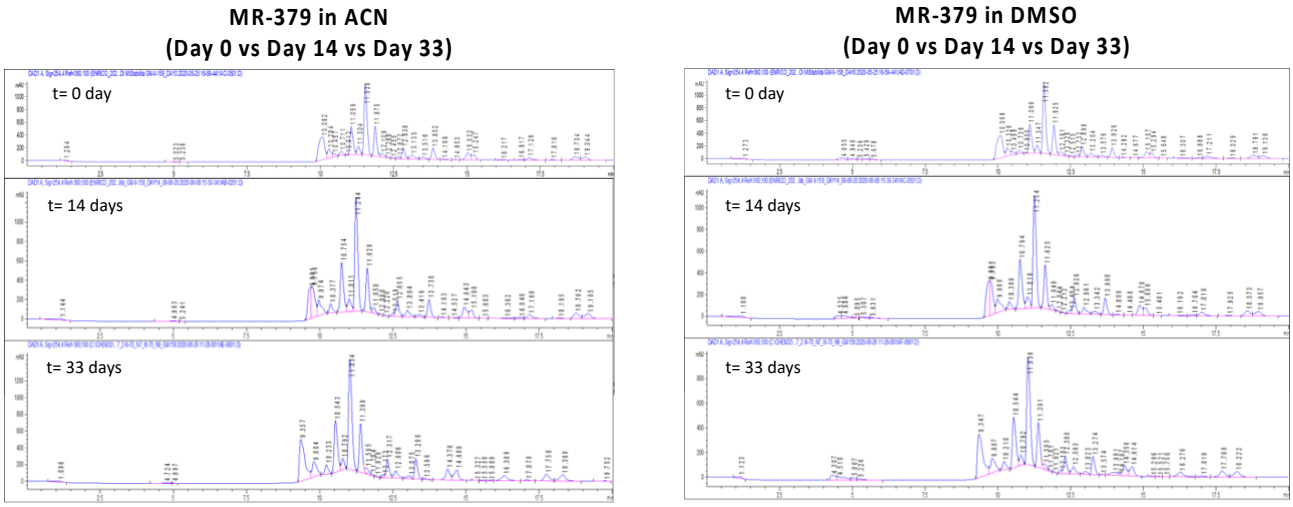

Figure 6. Chromatographic profile of MR-379 at different time-frames.

The LC-UV/MS analysis supported by the knowledge of the chemical reactivity the doping agent **2** allowed us to conduct a partial deconvolution of the complex mixture MR-379 and to identify the main component of the mixture (Figure 7)[65]. It should be also mentioned that both biological and analytical studies were conducted on those fractions of the prebiotic mixtures that were soluble in MeOH:H_2O 90:10. This choice was based on the fact the hydroalcoholic extracts may contain molecules with less solubility problems in the biological studies and easiest chromatographic analysis.

As predicted from collected information on the reactivity of furo[3,4-d]-pyrimidin-7-one scaffold, the microwave heating led mainly to opening of the lactone ring of the "doping agent" **2**, followed by the conversion into the corresponding pentyl ether derivatives. C2 substitution versus lactone opening seemed to be the more difficult to occur, as demonstrated by the fact that we identified only one compound C2 substituted in contrast to the many characterized by opening lactone ring.

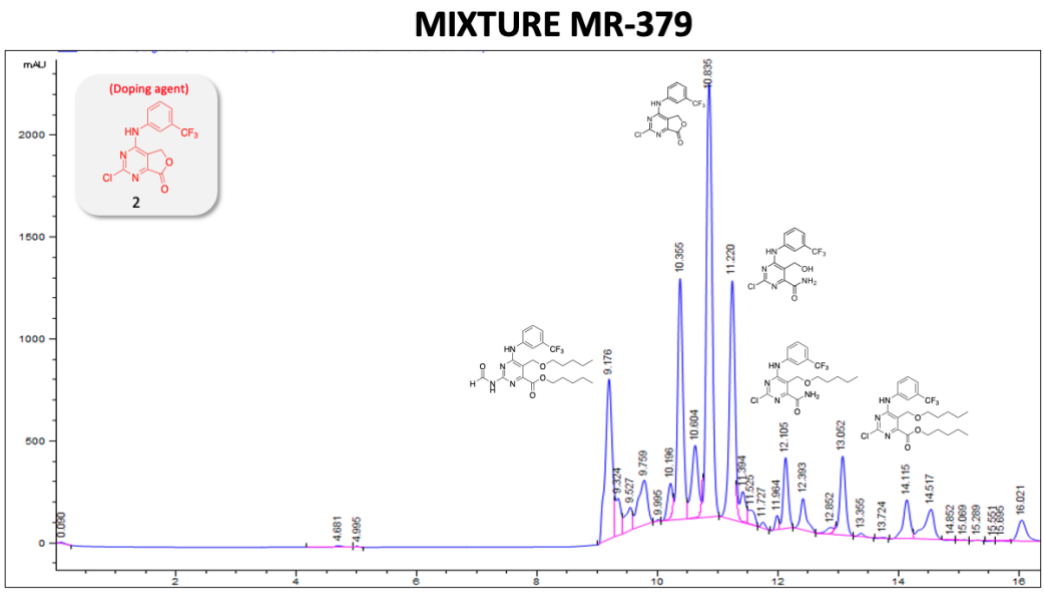

Figure 7. Partial deconvolution of MR-379 via LC-UV/MS

To identify which components of the mixture could be responsible for the antiviral activity in cell, apparent permeability and membrane retention were determined with the parallel artificial membrane permeability assay (PAMPA). MR-379 was solubilized in 1:1 DMSO:PBS 10 mm pH 7.4 at a concentration of 0.5 mM and incubated for 5 hours. After this time, the permeability of substances from a donor compartment into an acceptor compartment was determined, and the variation of the composition of the whole mixture was evaluated. PAMPA is characterized by a high degree of correlation with passive permeation across a variety of barriers. Although active transport is not envisaged from PAMPA, the assay may allow to define which component remains in the donor compartment and which component crosses the membrane, and the latter is more probable to contribute to the antiviral biological data in cell lines. As illustrated by Figure 8, the more permeable component was compound **4** (corresponding to peak C).

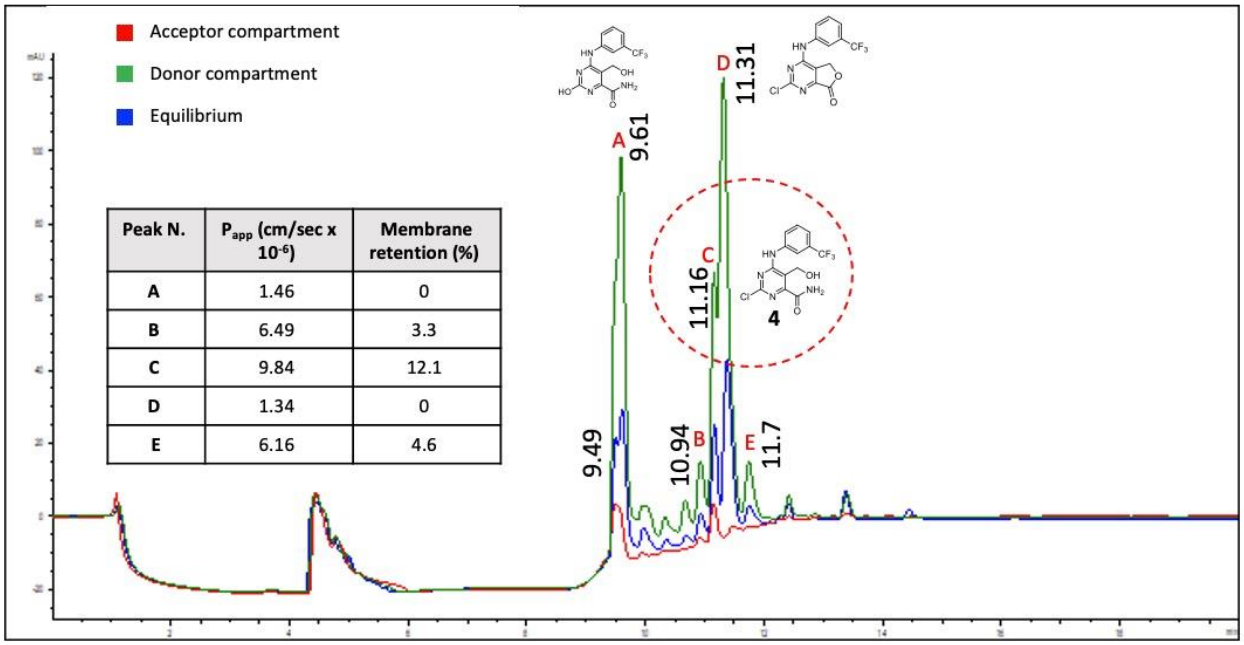

Peak N.	P_{app} (cm/sec x 10^{-6})	Membrane retention (%)
A	1.46	0
B	6.49	3.3
C	9.84	12.1
D	1.34	0
E	6.16	4.6

Figure 8: overlay of donator compartment (green), acceptor compartment (red) and equilibrium(blue) at 254 nm, P_{app} values and membrane retention values of each peak.

Considering the complexity of the reaction mixture, the isolation of the main components for a full characterization was considered quite challenging and time consuming. We decided therefore to fully characterize the more permeable component **4**, whose structure was hypothesized by partial deconvolution studies, and to use it as a reference to enrich the MR-379 mixture for chromatographic analysis. Compound **4** was easily synthesized by stirring the doping agent **2** in a solution of NH_4OH in methanol for 19h at room temperature (Scheme 2).

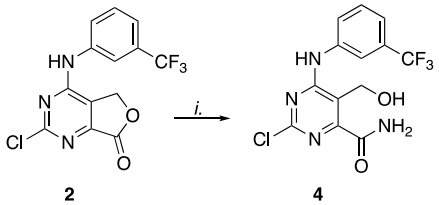

Scheme 2. *Reagents and conditions: i.* NH_4OH/CH_3OH, r.t., 19h.

Once we obtained compound **4**, the original mixture MR-379 was enriched with a small percentage of the synthesized compound to confirm that the latter corresponded to the predicted one (Figure 9). The original mixture MR-379 was compared with the new mixture, constituted from MR-379 enriched with the synthetized compound **4**. As evident from the overlay of two chromatograms in Figure 9, compound **4** corresponded to the peak of more permeable component of the original mixture MR-379.

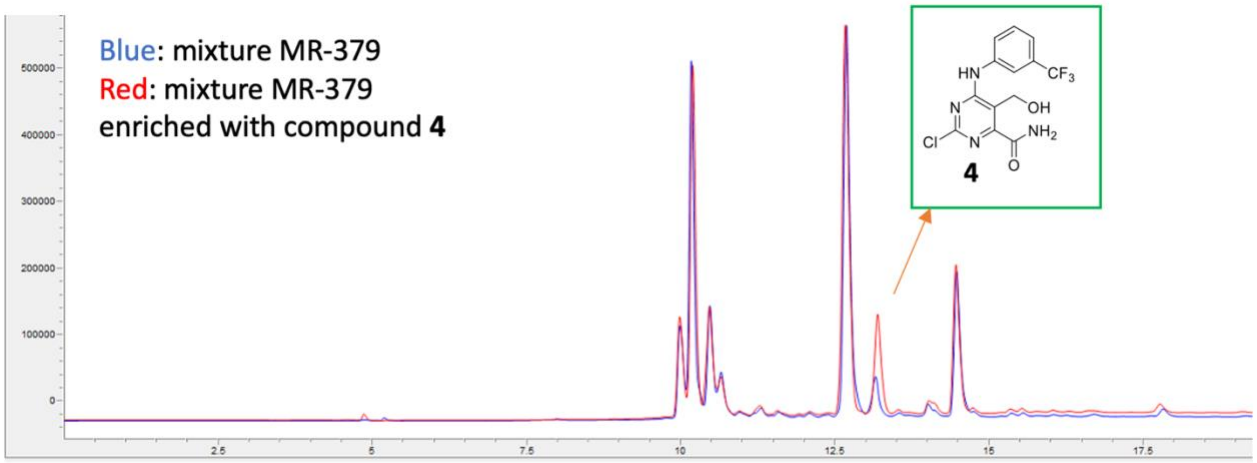

Figure 9: Overlay of mixture MR-379 (blue) and mixture MR-379 enriched with the synthesized compound **4** (red)

Once confirmed that compound **4** was the more permeable component of mixture MR-379, it was submitted to the same screening workflow of the prebiotic mixture: it was tested against Dengue Virus, West Nile Virus, HIV-1, and SARS-CoV-2. Unfortunately, despite this molecule did not show significative toxicity for the different cell lines used, it was devoid of any antiviral activity against all viruses that were inhibited by the mixture MR-379 (Table 3).

Table 3: Cytotoxicity and antiviral activity of the main component of the prebiotic mixture

	CC_{50} [a]	**IC_{50}** [b] **WNV**	**IC_{50} DENV**	**CC_{50}**	**IC_{50} HIV**	**CC_{50}**	**IC_{50} SARS-CoV-2**
Cmpd	**Huh7**			**H9**		**Caco-2**	
4	>200	NA[c]	NA	>100	NA	>200	NA
MR-379	160	7.95	15.7[d] 5[e]	65	NA	33.1	9.1

[a]CC_{50}: half-maximal cytotoxic concentration (µM); [b]IC_{50}: half-maximal inhibitory concentration (µM); [c]NA: not active; [d]IC_{50}: half-maximal inhibitory concentration calculated through DYRA (µM); [e]IC_{50}: half-maximal inhibitory concentration calculated through SYRA (µM).

As a different approach to identify the active component of the prebiotic mixture MR-379, it was subjected to a chromatographic separation into sub-fractions to be tested separately in order to simplifying the process of identification of the antiviral molecule. The mixture MR-379 was separated in first analysis in two sub-fractions (Fr1-Fr2) and in a second analysis in four sub-fractions (Fr3-Fr6). After passing each obtained sub-fraction in semipreparative column, the acquired UV

chromatograms allowed us to have a profile of each sub-fractions. Figure 10 shows the obtained sub-fractions starting from the original mixture MR-379.

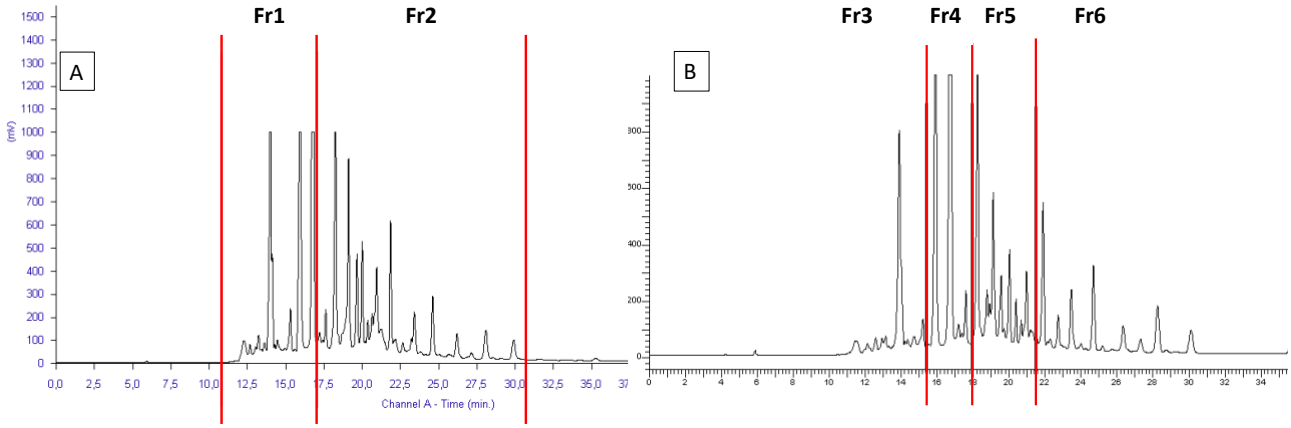

Figure 10: First separation of mixture MR-379 in sub-mixtures (A); second separation of mixture MR-379 in sub-mixtures (B).

Each fraction was then dried and submitted to biological evaluation. Most strikingly, no one of the simpler obtained sub-fractions showed activity in WNV, DENV, HIV, and SARS-CoV-2. Even more interestingly, when Fr3-6 were reunified (MR-379c) to restore the original prebiotic mixture, the broad-spectrum antiviral activity was restored, even if with a loss of activity against SARS-CoV-2 (Table 4).

Table 4. Cytotoxicity and antiviral activity of sub-fractions (Fr1-Fr6) obtained from different separations of the mixture MR-379.

	CC_5[a]	**IC_{50}[b] WNV (DYRA)**	**IC_{50} DENV (DYRA/SYRA)**	**CC_{50}**	**IC_{50} HIV**	**CC_{50}**	**IC_{50} SARS-CoV-2**
Cmpd	**Huh7**	**WNV**	**DENV**	**H9**		**Caco-2**	
Fr1	38	NA[c]	NA	84	NA	ND[d]	ND
Fr2	9	NA	NA	46	NA	ND	ND
Fr3	190	NA	NA	100	NA	170	NA
Fr4	95	NA	NA	<100	NA	75	NA
Fr5	25	NA	NA	40	NA	55	NA
Fr6	70	NA	NA	83	NA	55	NA
MR-379c	82.2	9	4.69	100	NA	47.7	NA
MR-379	160	7.95	15.7	60	NA	33.1	9.1

[a]CC_{50}: half-maximal cytotoxic concentration (µM); [b]IC_{50}: half-maximal inhibitory concentration (µM); [c]NA: not active; [d]ND: not determineted.

Although the obtained results were quite unexpected, this scenario (active mixture vs inactive components) is not surprising considering that this behavior is observable in some natural extracts

where the biological activity may be not due to a single constituent of the mixture [66,67]. Each natural mixture contains components with different molecular weights and at different concentrations, and each constituent takes part in the overall outcome and may modulate the effects of the others, and it is not possible to ascribe the biological effect to a single component, but it would be better to refer to a sort of complexity-activity relationships (CARs). What happens with the biological activity of some natural extracts might somehow explain why the main component or sub-fractions we tested, did not recapitulate the biological activity of the whole complex mixture.

2.1.5 Conclusion

In conclusion, the prebiotic formamide model was modified by addition of doping agents (chemical precursors of antiviral molecules), using microwave irradiation as energy source to generate different prebiotic mixtures. Biological evaluation of these mixtures in cells infected with different viruses allowed to identify a promising mixture (MR379), endowed with broad-spectrum antiviral activity. PAMPA analysis was then performed on MR379 to identify which components are able to passively cross the membrane and thus probably interfering with the intracellular viral replication. A rough deconvolution based on the known chemical reactivity of the doping agents and on the mass analysis allowed to identify the compounds (**4**) endowed with higher passive permeability, which was synthesized and biologically tested. Unfortunately, **4** did not show any antiviral activity against the selected viruses. Next, MR379 was subjected to a separation into sub-fractions with the purpose of simplifying the process of identification of the active component by testing each single sub-fraction. Unfortunately, none of the sub-fractions showed antiviral activity, which was however detected once the sub-fraction were reunified to restore the original prebiotic mixture MR379. Further studies and analysis should be performed but the results collected until now confirms that the chemical complexity of the mixture of molecules may contribute to its biological activity.

The identification of new antivirals from synthetic mixtures obtained by modifying prebiotic chemistry models is, to date, an unexplored field and our data suggest that these "synthetic extracts" may display a complexity-dependent biological activity similar to that shown by some plant extracts. Nevertheless, this approach turned out to be challenging and laborious because of difficult identification of every constituent, as well as time-consuming biological investigation aimed at elucidating the effects of different constituents of the complex antiviral mixture.

For this reason, we thought it would be convenient to move on the chemical optimization of antiviral purines previously identified in our lab.

2.2. Modified 2,6-Diaminopurines as Multi-Target BSAAs

2.2.1 Introduction

Most of the antiviral development in the past relied on the "one-drug-one virus" dogma by targeting specific viral proteins with a single drug, which has led to the approval of a limited number of antiviral drugs for the treatment of a few chronic viral infections, leaving the majority of known viral diseases without a readily available antiviral treatment[68].To overcome issues related to increasingly rapid epidemics as well as low availability of antiviral drugs, the strategy based on the dogma of "one drug-one virus" should be revised. A method that can expand the antivirals repertoire focuses the research on compounds that can target more than one virus, shifting away from the "one drug-one virus" paradigm and embracing the new "one drug-multiple viruses" paradigm, that targets viral proteins highly conserved among different viruses (e.g. RNA/DNA polymerases) or common infection pathways shared by multiple viruses.

Over the years, the shift from the dogma "one drug-one virus" has seen the exploration of different paradigms. "one-drug-multiple viruses", in combination with "host-targeting antivirals" paradigm, based on targeting host-proteins (e.g. CCR5 with Maraviroc), exploited by different viruses, becomes central in the battle against emerging and re-emerging viruses. This approach can definitely lead to the identification of BSAAs.

To further increase the efficiency of antiviral research of BSAAs, the paradigm "one drug-multiple viruses" has been joined by "one drug- multiple-targets" paradigm (polypharmacology). Multi-targets drugs have attached considerable attention in the last decade, as potential therapeutical solution to the complexity of the viral infection. Indeed, this latter approach takes into account the high of on-target and off-target interaction of the drug candidate and the presence of compensatory pathways that can reduce the efficiency of highly specific drugs[69,70]. Indeed, the above-mentioned scenario is not surprising considering that this behavior is observable in old antivirals, such as Ribavirin, for which new targets and mechanisms of action are found respect to the original one[71].

Thus, partial inhibition of multi-targets with a single drug should be more advantageous than full inhibition of a single target, because multitarget antivirals may retain activity in case of viral mutation and may be cheaper than a combination treatment.

Following to this new paradigm whereby a compound inhibiting multiple targets (both viral and host proteins) may lead to more potent and less resistance-prone antivirals, our group has previously reported the identification of new multitarget antivirals that inhibit DENV replication by targeting both host kinases c-Src/Fyn and an allosteric site on the thumb of viral NS5 required to form the functional NS5-NS3 replication complex[72]. These 2,6-diaminopurine derivatives were also able to

block the replication of both Zika virus and all serotypes of dengue virus (DENV 1–4) in infected cells[73].

Here, with the aim to identify new promising BSAAs endowed with an increased spectrum of action no longer focused exclusively on Flaviviruses, we submitted the 2,6-diaminopurine chemotype to a system-oriented optimization based on available structure-activity relationships (SARs) and phenotypic screening on cells infected with different viruses.

The efforts led to the identification of **12i**, a BSAA that is able to inhibit the replication of viruses belonging to different families (DENV, ZIKV, WNV, Influenza A, SARS-CoV-2), while the reference BSAA Ribavirin has a more limited spectrum of activity and lower potency[74,75].

2.2.2 Aim of the work

Our research group has recently identified a family of modified purine heterobases that are able to inhibit DENV replication by targeting an allosteric pocket on the thumb of viral NS5 polymerase and (thus blocking the NS5-NS3 interaction) and, at the same time, inhibiting the activity of host c-Src/Fyn kinases. First-generation compounds (e.g. **5**, **6**; Figure 11) were found active against DENV replication only[72], while second-generation compounds, opportunely modified to better fill the allosteric cavity B of DENV and ZIKV NS5, (e.g. **7**, Figure 11) were active against both DENV and ZIKV[73]. Unfortunately, the antiviral potency expected from the *in silico* predictions was not achieved with any of the second generation derivatives.

Considering the unsatisfactory results of the target-based optimization of these 2,6-diaminopurine derivative, we decided to attempt a hit-to-lead optimization by using a more holistic approach that may better exploit the multitarget nature of our molecules. The application of phenotypic screening on new derivatives, designed on the basis of available SARs, may lead to the identification of more potent and broad-spectrum antivirals whose activity may be due to the inhibition of different or a still-unknown targets. It is also known that viruses could induce oxidative stress in infected cells that is mediated by free radicals and is well recognized as a common trigger of exacerbation in diseases caused by different viruses, including Flavivirus, Coronavirus, and Influenza[76,77,78]. Thus, we also planned to implement to SAR-based modification of the 2,6-diaminopurine scaffold with the introduction of structural moieties that may confer additional antioxidant properties. A phenylhydrazino group in C6, chosen for the achievement of this purpose, may counteract the virus-induced oxidative stress converting the target molecules into stable azo-derivatives. Thus, C6 and C2 substitutions on purine core allowed us to obtain a set of multi-targets purine derivatives characterized by general structure Ⅰ.

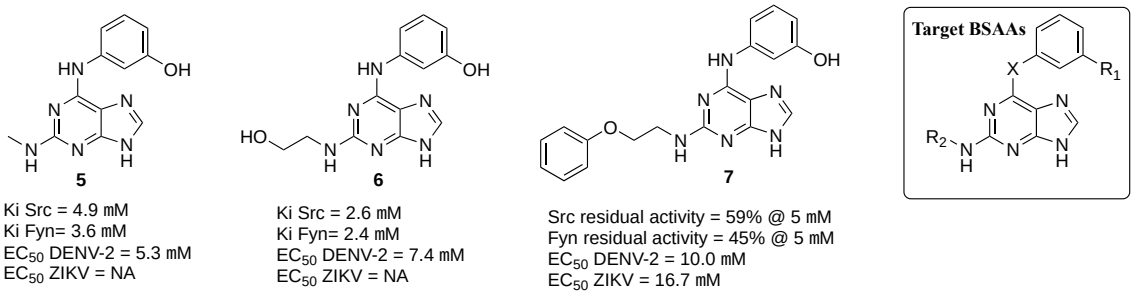

Figure 11. 2,6-diaminopurine-based antivirals **5-7**

2.2.3 Results and discussion

The first part of this work was dedicated to modifying the 2,6-diaminopurine hits based on available SARs: *i)* cyclic secondary amine in C2 lead to poorly active o inactive compounds (e.g. compounds **12c-e** from ref 73 *ii)* increasing of the length of the C2 substituent of the secondary amine increase the antiviral spectrum and allow to have a multitarget activity (reference compounds **6** and **7**); *iii)* position C6 of active purine may tolerate different substituent on aniline ring (Figure 12).

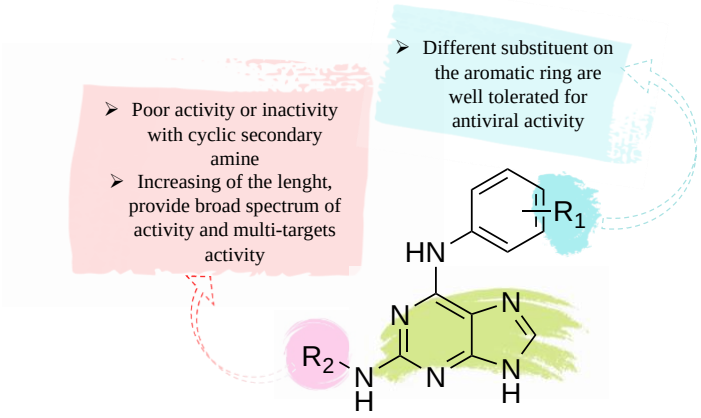

Figure 12. SARs of multi-targets purine derivatives

We synthesized a series of new derivatives by keeping in C2 the substituents of the more active compounds **5-7** and focusing on the substitution of C6 with different moieties. To do so, we used the two steps synthetic protocol previously developed in our laboratory (Scheme 3, Table 5).

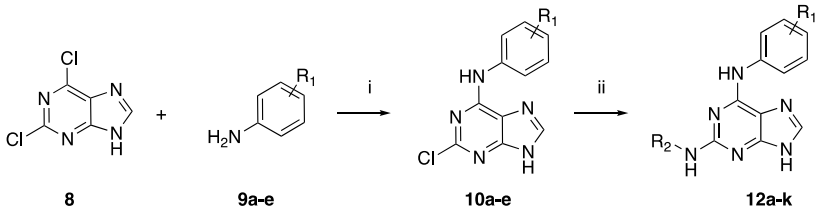

Scheme 3. *Reagents and conditions: i.* Et_3N, n-BuOH, 70-100 °C, 10-50 min, µW; *ii.* amines **11a-c**, n-BuOH, TFA, 150-170 °C, 40-70 min, µW.

Table 5: R_1 and R_2 of compounds **10a-e**, **12a-k**

Cpd.	**R^1**	**R^2**	**Cpds**	**R^1**	**R^2**
10a	3-F	-	**12d**	3-CO_2Me	Me-
10b	3-CO_2Me	-	**12e**	3-CO_2Me	HO$(CH_2)_2$-
10c	3-CF_3	-	**12f**	3-CO_2Me	PhO$(CH_2)_2$-
10d	3,4-OH	-	**12g**	3-CF_3	Me-

10e	3,4,5-OMe	-	**12h**	3-CF_3	$HO(CH_2)_2$-
12a	3-F	Me-	**12i**	3-CF_3	$PhO(CH_2)_2$-
12b	3-F	$HO(CH_2)_2$-	**12j**	3,4-OH	$PhO(CH_2)_2$-
12c	3-F	$PhO(CH_2)_2$-	**12k**	3,4,5-OMe	$PhO(CH_2)_2$-

The first step was a nucleophilic substitution of the chlorine atom in C6 with an excess of different aromatic amines (**9a-e**): this reaction was conducted in presence of a base (triethylamine) heating under microwave irradiation between 70°C and 100°C for 10-50 minutes to give the desired intermediates **10a-e**. Amine **9b** was synthesized through methylation of 3-aminobenzoic acid with thionyl chloride in MeOH at room temperature overnight. (Scheme 4).

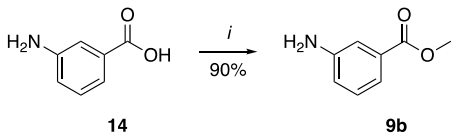

Scheme 4. *Reagent and conditions i.* $SOCl_2$, MeOH, r.t., overnight.

The second step for the synthesis of the final compounds **12a-j** consisted in the displacement of the chlorine atom in C2 with the three selected primary amines under more drastic conditions: methylamine **11a**, 2-phenoxyethylamine **11b**, and ethanolamine **11c**. The reaction proceeded in the presence of trifluoroacetic acid (TFA), heating under microwave irradiation at 150-170°C for a few minutes. In both steps, n-butanol (n-BuOH) was used as solvent.
Final compounds **13d** and **13f** were obtained from the hydrolysis of compounds **12d** and **12f** (Scheme 5)**.**

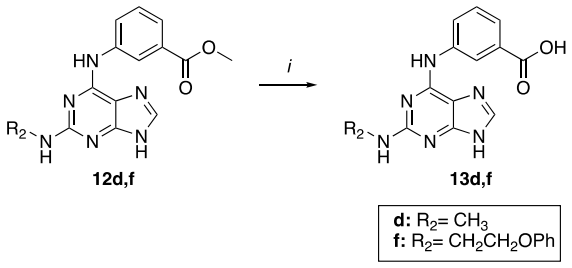

Scheme 5. *Reagent and conditions i.* LiOH, THF/MeOH, r.t., 24 h.

In addition, we also synthesized the "inverted analogues" of compounds **12i** and **12c** (**16a** and **16b**, respectively) where C2 and C6 substituents were exchanged following the synthetic approach described in Scheme 3. The first step was conducted at lower temperatures and for shorter times, while the second step with the aromatic amines, required longer times at the same temperature

(Scheme 6). The desired final product **12a-k**, **13d,e** and **16a,b** were obtained in moderate to good yields.

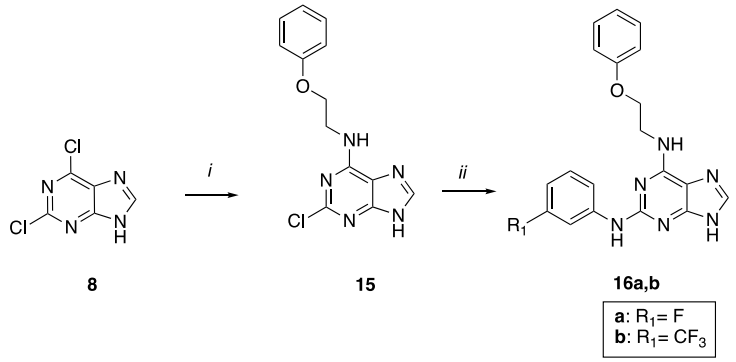

Scheme 6. *Reagents and conditions*: *i.* **11b,** n-BuOH, NEt_3, µW 70°C, 25 min; *ii.* **9a** (or **9c**), n-BuOH, TFA, µW 150-170°C, 140 min.

Next, in order to obtaining purine derivatives endowed with antioxidant activity, we decided to functionalize the C6 position with functionalized hydrazine moieties that may act as radical scavengers. The first step was a nucleophilic substitution of the chlorine atom in C6 of 2,6-dichloropurine with an excess of substituted phenylhydrazine **17a-e**. These reactions were heated under microwave irradiation at 70°C for 20 minutes, to give the desired intermediates **18a-e.** The second step consisted of the displacement of the chlorine atom in C2 with 2-phenoxyethylamine **11b** in the presence of trifluoroacetic acid (TFA), heating under microwave irradiation at 170°C for about 1 hour to give the desired products **19a-e** in moderate yields (Scheme 7). In both steps n-butanol (n-BuOH) was used as solvent. In addition, as a preliminary demonstration of the antioxidant potential of the hydrazine derivatives **19a-e**, we showed the that the chemotype **19** can be easily oxidized by atmospheric oxygen into the corresponding 6-azopurine analogue. Oxidized compounds **20a-d** were thus simply obtained by heating a methanolic solution of **19a-e** in an open flask under vigorous stirring (Scheme 7).

The nature of the substituent on the phenylhydrazine moiety plays an important role in the kinetics of oxidation. Compound **19b** was oxidized after approximately 96 hours of vigorous open air stirring, at 65 °C Compound **19c** required 96 hours. Compound **19d** was converted in its oxidized form after 48 hours and, also in this case, heating the reaction at 65 °C was necessary. Compound **19a**, without doubt, showed the lowest kinetic in the oxidation reaction, requiring almost 120 hours at room temperature to afford the corresponding azo-derivative **20a**. Differently from the other analogues, compound **19e** was oxidized very quickly and rapidly decomposed after 24 hours.

Since hydrazine derivative compounds are easily oxidized in the presence of atmosphere O_2, to avoid the oxidation before the obtainment of compounds **19a-e**, it was necessary, in the first step that led to

intermediates **18a-e**, to remove the oxygen from the microwave tube, before heating it. This was done by using Argon and removing the oxygen with the vacuum pump.

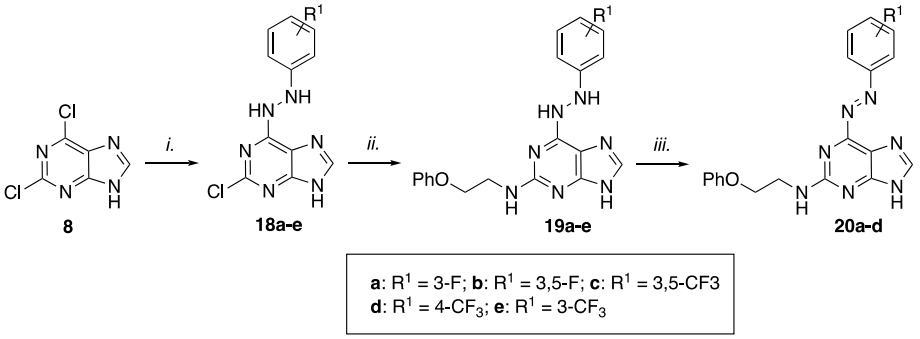

Scheme 7. *Reagents and conditions: i.* $R_1PhNHNH_2$ (**17 a-e)**, n-BuOH, Et_3N, µW, 70 °C, 20-40 min, µW; *ii.* phenoxyethylamine **11b**, n-BuOH, TFA, µW, 170 °C, 120 min, µW; *iii.* MeOH, air, r.t.- 65 °C, stirring, 48-120h.

2.2.4 Biological results

The antiviral activity of all final compounds was evaluated. Initially, compounds **12a-k**, **13d,f** and **16a,b** were analyzed for their anti-DENV and anti-ZIKV activity in a Huh7 hepatoma cell-based secondary yield reduction assay (SYRA) which quantifies infectious culture supernatants by immunodetection and by which antiviral effect at late steps of the virus life cycle can be measured. In Table 6, below, are listed the results of the biological evaluation of the synthesized compounds.

Table 6. DENV-2/ZIKV/WNV replication inhibitory effect.

		DENV-2		**ZIKV**		**WNV**	
Cpd.	**Huh7 CC_{50}**[a] (μM)	**IC_{50}**[b] (μM)	**SI**[c]	**IC_{50}** (μM)	**SI**	**IC_{50}** (μM)	**SI**
12a	84.0	9.3±4.2	9	14.7±5.7	6	ND	-
12b	136.0	29.8±0.3	5	8.9±0.9	15	ND	-
12c	200.0	12.0±0.2	17	2.9±0.9	68	ND	-
12d	200.0	18.0±12.2	11	8.0±1.5	25	ND	-
12e	200.0	17.5±7.3	11	6.2±2.5	32	ND	-
12f	100.0	NA[d]	-	8.2±1.5	12	ND	-
12g	200	3.5±4.0 (4.9±2.6)[f]	57	ND		ND (NA)[f]	-
12h	50.0	4.5±0.2	11	10.6±0.5	5	ND (1.9±2.9)[f] (1.5±1.3)[g]	- 26 33
12i	200.0	2.6±0.3 (NA)[f] (0.9±0.04)[g]	77 - 222	1.1±0.4 (0.8±0.3)[f] (0.5±0.32)[g]	182 250 400	ND (NA)[f] (3.9±0.67)[g]	- - 51
12j	200.0	NA	-	25.0±7.1	8	ND	-
12k	7.5	NA	-	ND	-	NA	-
13d	200.0	NA	-	33.5±7.6	6	ND	-
13f	200.0	28.2±3.9	7	29.0±4.8	7	ND	-
16a	8.0	ND[e]	-	ND	-	ND	-
16b	6.0	ND	-	ND	-	ND	-
Sofosbuvir	200.0	4.7±0.7 (4.6±1.4)[f]	42 43	3.2±0.7 (2.7±0.5)[f]	62 74	ND (1.7±0.5)[f]	- 117

		(3.8±1.1)[g]	53	(2.0±1.1)[g]	100	(1.2±0.3)[g]	166
Ribavirin	200.0	4.0±0.6	50	4.4±0.6	45	ND	
		(7.6±1.2)[f]	26	(3.8±0.6)[f]	53	(9.5±4.0)[f]	21
		(4.1±0.6)[g]	49	(2.2±0.6)[g]	91	(6.7±0.6)[g]	30

[a]CC_{50}: half-maximal cytotoxic concentration (μM); [b]IC_{50}: half-maximal inhibitory concentration calculated through SYRA; each value is the mean of three experiments ± standard deviation (SD); [c]SI: selectivity index (SI = CC_{50}/IC_{50}). [d]NA: not active; [e]ND: not determined; [f]IC_{50}: half-maximal inhibitory concentration calculated through DYRA; [g]IC_{50}: half-maximal inhibitory concentration calculated through PRA

Sofosbuvir and Ribavirin were used as reference compounds, since detained antiviral activity against all selected viruses selected for the antiviral evaluation of our compounds. All compounds tested, that didn't show toxicity in Huh7 cells, were endowed with promising antiviral activity against both DENV and ZIKV. Among the 3-F and 3-CF_3 series (compounds **12a-c** and **12g-i**, respectively), the selectivity index (SI) on both viruses increased with the length of the C2 side chain. The 3-CO_2Me series (compounds **12d-f**) was characterized by a similar potency on ZIKV and, surprisingly, the 2-phenoxyethylamino derivative **12f** did not show any activity on DENV. Compared to the 3-CO_2Me series, the series with a free acid portion (compounds **13d,f**) showed a reduced potency and opposite tendency since the 2-phenoxyethylamino derivative **13f** showed potency against both DENV and ZIKV (compared to **12f**) while the 2-methylamino derivative **12d** did not show any activity on DENV (compared to **13d**). Also the 3,4-OH derivative **12j** showed efficacy only against ZIKV, while the trimethoxy derivative **12k** was endowed with a quite low CC_{50}. It was also interesting to note that the two "inverted" compounds **16a,b**, analogues of the active compounds **12c** and **12i**, were not evaluated for antiviral potency, since showed high cytotoxicity. These observations allowed to draw additional SAR considerations: i) increasing the length of the C2 substituent increases the selectivity index and the antiviral spectrum; ii) different functional groups on the C6 aniline moiety are well tolerated for the antiviral activity, with a few exceptions (e.g. **12k**); iii) substituted anilines in C2 lead to cytotoxic compounds (e.g. **16a,b**).This first set of results showed that, among those 15 tested compounds, **12i** detained the most potent antiviral activity against ZIKV (SI 182), DENV (SI 77) with IC_{50} values in the low micromolar range, comparable to or sometimes even slightly better than those of the reference drugs Sofosbuvir and Ribavirin.

The compounds endowed with best antiviral activity against DENV and ZIKA (**12h,i**) and the reference molecules (Sofosbuvir and Ribavirin), were evaluated for their activity against another viruses belongs to Flaviviridae family, WNV, thought two different assays: direct yield reduction assay (DYRA), which allows measuring interference of the drug with the early steps of the virus life cycle; plaque reduction assay (PRA)[79,80,81]. The obtained values, reported in Table 7, showed that **12h**

inhibited the WNV replication in both DYRA and PRA, while **12i** endowed with antiviral activity only in PRA.

To better characterize the mechanism of action (MOA) of this multi-target class of compounds and to obtain preliminary information about what stage of viral replication the drug interferes, the IC_{50} values against DENV and ZIKA of the best compound **12i** were calculated through DYRA. Next, the IC_{50} values against DENV and ZIKA of **12i** and reference molecules, calculated through SYRA, were compared with DYRA data. As it is evident, compound **12i** showed promising activity against ZIKV, both in SYRA and DYRA assay, but it didn't show any activity against DENV and WNV in DYRA assay. These obtained results could demonstrate that compound **12i** exerts its activity in DENV and WNV not in the early step, being inactive in DYRA, and it has an inhibition effect of replication ZIKA on earlier phases of the viral life cycle. Lastly, the anti-Flavivirus efficacy of compound **12i** was confirmed by PRA giving an IC_{50} of 0.9 μM against DENV and an IC_{50} of 0.5 μM against ZIKA, demonstrating better activity with respect to the reference molecules Sofosbuvir and Ribavirin.

Testing of compounds **19a-e** and **20a-d** against Flavivirus showed that most derivatives, with the exception of **19a** and **20a**, were quite cytotoxic in Huh7 cells (Table 7). As a consequence, only **19a** and **20a** were evaluated for their antiviral activity against DENV, ZIKV, and WNV. It was interesting to note that both compounds **19a**, and its corresponding aza-derivative **20a** were able to inhibit the viral replication of DENV, ZIKV, and WNV, with a EC_{50} in low micromolar range, sustaining the idea that, within the cell, **19a** exerts an antiviral/antioxidant effect, and once converted into its oxidized form **20a**, still exerts its antiviral effect.

Table 7. Cytotoxicity and DENV-2/ZIKV/WNV replication inhibitory effect.

		DENV-2		**ZIKV**		**WNV**	
	Huh7						
Cpd.	**CC_{50}**[a] (μM)	**IC_{50}**[b] (μM)	**SI**[c]	**IC_{50}** (μM)	**SI**	**IC_{50}** (μM)	**SI**
19a	20.0	3.4±0.9	6	2.4±0.3	8	(1.1±1.5)[d]	18
19b	8.5	ND[e]	-	ND	-	ND	-
19c	5.0	ND	-	ND	-	ND	-
19d	8.0	ND	-	ND	-	ND	-
19e	7.5	ND	-	ND	-	ND	-
20a	18.5	4.0±1.02	5	2.8±0.8	7	(0.6±0.2)[d] (0.6±0.4)[f]	28 30
20b	12	ND	-	ND	-	ND	-

20c	7.5	ND	-	ND	-	ND	-
20d	8.0	ND	-	ND	-	ND	-
Sofosbuvir	200.0	4.7±0.7	42	3.2±0.7	62	(1.7±0.5)[d] (1.2±0.3)[f]	117 166

[a]CC_{50}: half-maximal cytotoxic concentration (μM); [b]IC_{50}: half-maximal inhibitory concentration calculated through SYRA, each value is the mean of three experiments ± standard deviation (SD); [c]SI: selectivity index (SI = CC_{50}/IC_{50}). [d]IC_{50}: half-maximal inhibitory concentration calculated through DYRA [e]ND: not determined; [f]IC_{50}: half-maximal inhibitory concentration calculated through PRA

To confirm that compound **19a** may possess an antioxidant effect that may contribute to its antiviral potency, we decided to experimentally evaluate its antioxidant effect in terms of "radical scavenging activity" (RSA), using the ABTS radical decolorization method. The results obtained for **19a** were compared with **20a**, **12i** and the potent antioxidant ascorbic acid. As shown in Figure 13, **19a** displayed a concentration-dependent radical scavenging activity, which was not found for compounds **20a** and **12i**.

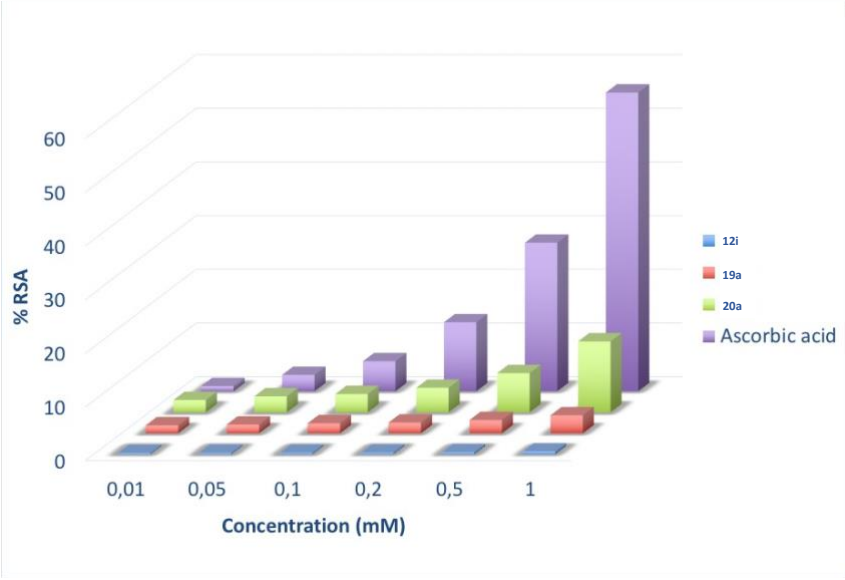

Figure 13. Radical scavenging activity of compounds **19a**, **20a** and **12i** expressed as % inhibition of the ABTS absorbance at 734 nm. The potent antioxidant ascorbic acid was used as a positive control.

To further explore the broad-spectrum antiviral activity of the most promising compounds **12c**, **12i**, and **19a,** they were tested against two different strains of Influenza A in MDCK and A549 cells using Ribavirin as reference compound[82]. (Table 8).

Table 8. Influenza-A virus replication inhibitory effect.

	Influenza A Puerto Rico 8/34/H1N1			**Influenza A Puerto Rico 8/34/H1N1 (PR8)**		
Cpd.	**MDCK**			**A549**		
	CC_{50}[a] (μM)	**IC_{50}**[b] (μM)	**SI**[c]	**CC_{50}** (μM)	**IC_{50}** (μM)	**SI**
12c	77.0	14.0	5.5	58.0	20.8	2.8
12i	77.0	5.3	14.5	106.0	9.9	11
19a	136.0	6.3	21.6	52.4	14.9	3.5
Ribavirin	(>50)	(9.50)[83]	(>5.26)	>50	37.37	>1.33

[a]CC_{50}: half-maximal cytotoxic concentration (μM); [b]IC_{50}: half-maximal inhibitory concentration, each value is the mean of three experiments ± standard deviation (SD) at 0.01 MOI; [c]SI: selectivity index (SI = CC_{50}/IC_{50}); Literature antiviral data for Ribavirin are reported in parenthesis

The selected compounds didn't show significative toxicity in both cell lines, with a selective index (SI) higher than Ribavirin. Once again, compound **12i** was the most interesting antiviral. For this reason, we decided to better study its mechanism of action: infected A549 cells were treated with compound **12i** at different times, 2 hours before infection (PRE), at 1 hour of viral adsorption (DUR), after 24 hours of infection (POST), or before, during, and after (PDP) infection for the following 24 h. Supernatants from infected cells were recovered at 24 h from infection and used to infect a fresh cell monolayer. Subsequently, the expression of viral protein Hemagglutinin (HA) was quantified as the percentage of relative fluorescence intensity (RFI). It's evident a reduction of 50 % of the percentage of HA when **12i** was added both during and post-infection (DUR and POST), and no effect on the percentage of HA when the compound **12i** was added before infection (PRE), as shown in Figure 14A. No differences between these treatments (DUR or POST) and with the long one (PDP) were noted.

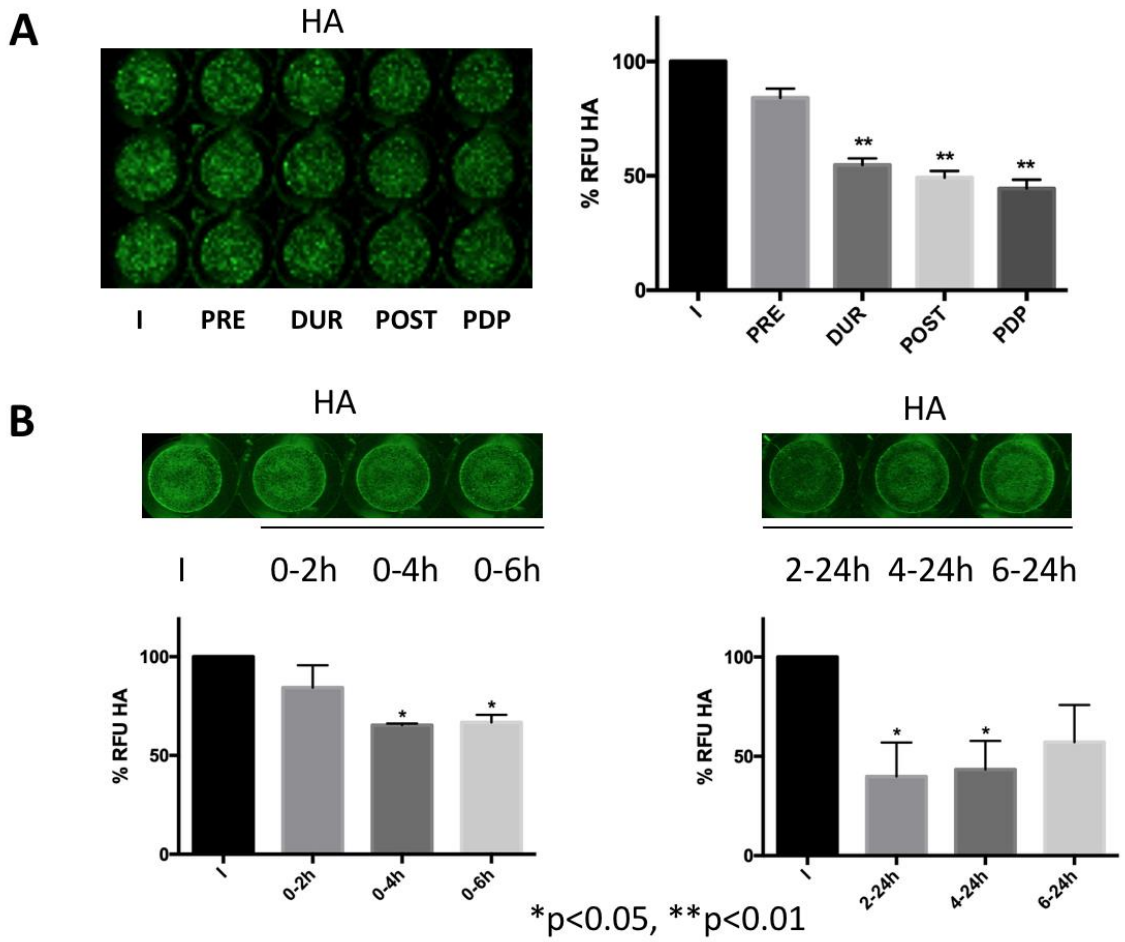

Figure 14. Before, during and after infection for the following 24 hrs (PDP). Compound **12i** interference with early steps of influenza virus replication. A549 cells were infected with PR8 and treated or not with **12i** (10 μM) at different phases of the virus life-cycle: A) the compound was added for 2 hrs before (PRE); during viral adsorption for 1 h (DUR); immediately after viral adsorption for 24 hrs (POST); before, during and for the following 24 hrs (PDP). B) left panel, the compound was added immediately after viral adsorption for 2 (0-2h), 4 (0-4h) or 6 (0-6h) hrs. Then cells were maintained up to 24 hrs in fresh medium plus 2% FBS; right panel, the compound was added after 2 (2-24h), 4 (4-24h) or 6 (6-24h) hrs infection and maintained until 24 hrs from infection. Untreated-infected cells (I) were used for comparison. The supernatants of treated or not treated infected cells were recovered and used to infect fresh MDCK monolayers for the following 24 hrs. The expression of hemagglutinin (HA) was analyzed by ICW, using LI-COR Image Studio Software, as described in Methods. The percentage of relative fluorescence units (RFU) was calculated in comparison to I (considered 100%). Values are the mean ± S.D. of two experiments, each performed in duplicate (n=4). Statistical significance of the data vs I was defined as *P < 0.05 and ** P < 0.01.

Next, two sets of experiments of time of addition were performed to evaluate specific steps of infection (early or late phases). The first one included the addition of **12i** immediately after infection for 2, 4 and 6 hours, and the infected monolayers were maintained in a fresh medium without the compound until 24 hours from infection, and the second one was performed by adding **12i** after 2, 4 and 6 hours from infection and maintained until 24 hours from infection. As shown in Figure 14B the infection was mostly inhibited when the compound **12i** was added after the 2 hours and within the 6

hours of infection. Indeed, if the compound was added after 6 hours, we did not find a significant inhibition, confirming the hypothesis that the early phases were compromised by **12i** addition.

Next, the activity of compound **12i** against other Influenza strains was evaluated. A549 cells were infected with the human PR8 H1N1, the human pandemic 2009H1N1 or the avian Ulster H7N1. To observe the expression of viral proteins on the infected monolayer at 24 hours was employed an anti-FLU antibody, able to recognize more viral proteins belonging to different strains. Also in this case, the conditions performed with the Puerto Rico 8/34/H1N1 strain were used (Figure 15).

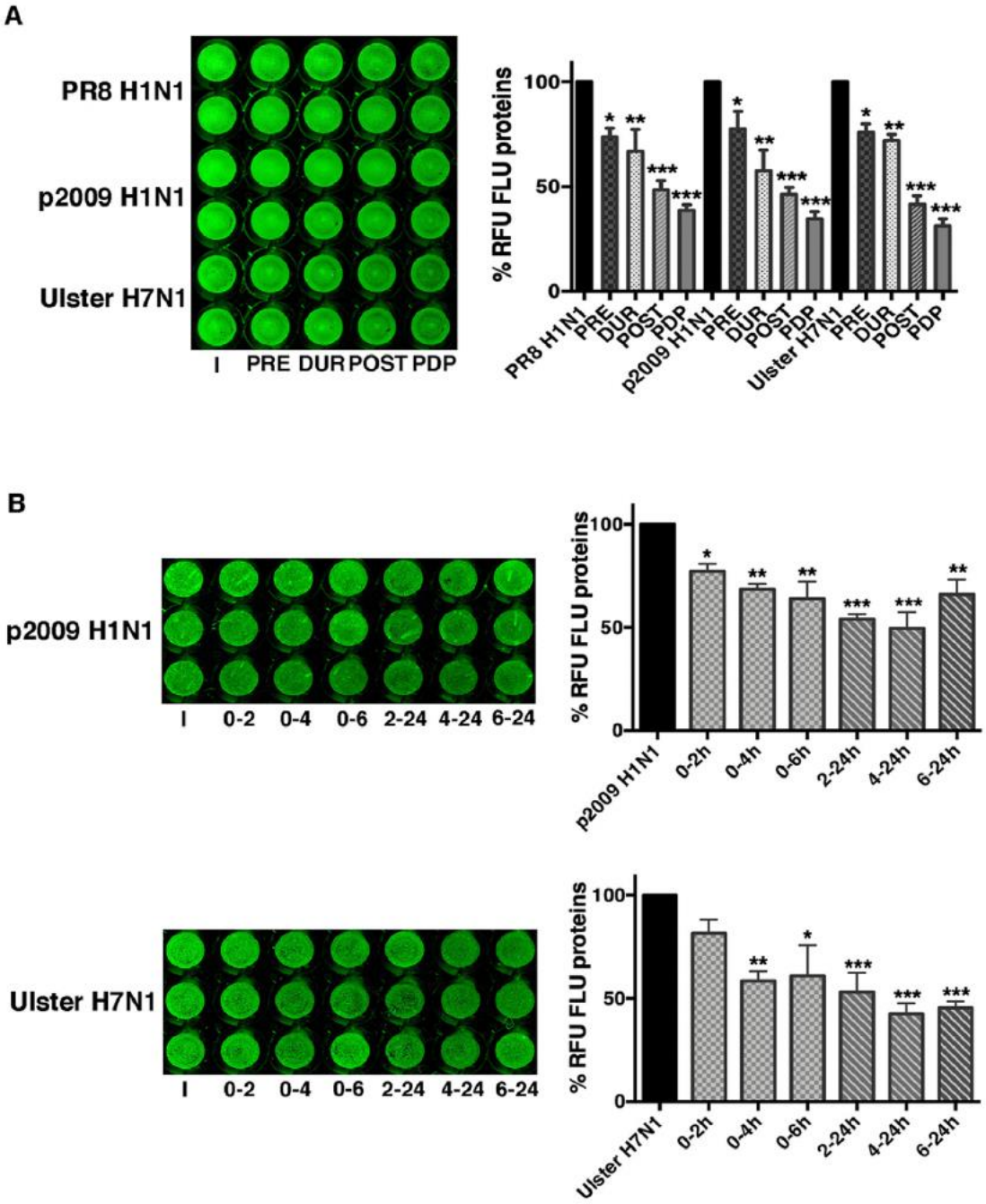

Figure 15. Compound **12i** is effective against different influenza A virus strains. A549 cells were infected with influenza A virus strains and treated or not with **12i** (20 μM) at different phases of the virus life-cycle: A) compound **12i** was added for 2 h before (PRE); during viral adsorption for 1 h (DUR); immediately after viral

adsorption for 24 h (POST); before, during and for the following 24 h (PDP). Infected treated cells were fixed and stained with anti-FLU antibodies as already described; B) compound **12i** was immediately added after viral adsorption for 2 (0-2 h), 4 (0-4 h) or 6 (0-6 h) hours. Then cells were maintained without the compound up to 24 h in fresh medium plus 2% FBS; the compound was added after 2 (2-24 h), 4 (4-24 h) or 6 (6-24 h) hours infection and maintained until 24 h from infection. The supernatants were recovered and used to infect fresh MDCK monolayers for 24 h.

The treatment with **12i** after infection (POST) and before, during and after infection (PDP) was the most effective, and especially **12i** was effective when added in the first 6 h from infection, thus suggesting an impairment in the early phases of the virus life-cycle, even if it cannot be excluded some effects on host membranes, considering the 20-26% inhibition during the pretreatment (PRE) of cell monolayers or some effects on the viral attach/entry, considering the 28-45% inhibition during the viral adsorption phase (DUR).

Finally, the most promising compound **12i** was selected for antiviral evaluation against the SARS-CoV-2 (Table 9). **12i** didn't show any major toxicity in all used cell lines (Huh7, Caco-2, Vero E6 and Calu-3). It was noteworthy to find that **12i,** at low micromolar concentrations, inhibited the replication of SARS-CoV-2 in all human cell lines tested. In analogy with Remdesivir, compound **12i** showed a significative reduction of efficacy in Vero E6 cells in comparison to Calu-3 cells, even if the efficacy was higher than that of Ribavirin.

Table 9. Cytotoxicity and SARS-CoV-2 replication inhibitory effect.

SARS-CoV-2												
Cpd.	**Huh7**			**Caco-2**			**Vero E6**			**Calu-3**		
	CC_{50}[a] (μM)	**IC_{50}**[b] (μM)	**SI**[c]	**CC_{50}** (μM)	**IC_{50}** (μM)	**SI**	**CC_{50}** (μM)	**IC_{50}** (μM)	**SI**	**CC_{50}** (μM)	**IC_{50}** (μM)	**SI**
12i	200	2.7±0.1	74	81.3	5.9± 1.8	14	200	53.4±1.1	4	120.0	4.3±2.4	28
Ribavirin	ND[d]	ND	-	ND	ND	-	(>400)	(109.5)[84]	-	ND	ND	-
Remdesivir	77	0.004± 0.005 (0.002)[85]	19250	80.0	0.01± 0.006 (0.38)[86]	8000	166.0	6.0±1.1 (26.9)[87]	28	97.0	0.11± 0.04 (0.28)[85]	882

[a]CC_{50}: half-maximal cytotoxic concentration (μM); [b]IC_{50}: half-maximal inhibitory concentration, each value is the mean of three experiments ± standard deviation (SD) at 0.01 MOI; [c]SI: selectivity index (SI = CC_{50}/IC_{50}); [d]ND: Not determined. Literature antiviral data for Remdesivir and Ribavirin are reported in parenthesis.

Overall, compound **12i** proved to be a promising BSAAs, inhibiting the replication of viruses belonging to different families at low micromolar concentrations. In addition, it can be obtained with a cheap and fast synthetic protocol and, therefore, we decided to further investigate its multitarget mechanism of action.

Considering its high SI against DENV and ZIKV *in vitro* selection experiments were performed to evaluate the genetic barrier to resistance. Different increasing concentrations of compound **12i** (starting from 15 μM up to 120 μM) were used to treat infected Huh7 cells with DENV and ZIKV. Untreated cells were used as a negative control to discriminate cytopathic effect (CPE) induced by cytotoxicity of **12i** and cytopathic effects of physiological cell death. 15-120 μM of **12i** delayed the viral growth, in fact the 80 % of CPE was reached after 5-9 days post infection (dpi), while the same effect was obtained at 2-4 day dpi with no-drug virus control (VC). In vitro selection experiments were stopped after a mean of 23.8 ± 1.5 dpi that correspond to the days in which the drug pressure was 133-fold and 240-fold higher than the IC_{50} of **12i** against DENV and ZIKV wild type, respectively. Since this multitarget family of compounds was initially designed to inhibit the viral NS3-NS5 interaction, all aminoacidic (aa) variations of both these proteins under **12i** pressure was analyzed and reported in Table 10.

Table 10. In vitro ZIKV and DENV resistance selection to **12i.**

		12i [15 μM]			**12i** [30 μM]			**12i** [60 μM]			**12i** [120 μM]		
Exp.	**VIRUS**	**dpi**[a]	**NS3 mutation**	**NS5 mutation**	**dpi**	**NS3 mutation**	**NS5 mutation**	**dpi**	**NS3 mutation**	**NS5 mutation**	**dpi**	**NS3 mutation**	**NS5 mutation**
1	DENV	6	none	none	7	none	E427E/K	5	R54R/P, M267M/I	none	5	none	none
2	DENV	6	none	K61K/E, E74E/K, P154P/T	7	none	none	4	none	none	9	T168T/S, **I600V**	N241N/H, T244T/P
3 (VC)[b]	DENV	3	none	none	3	none	none	3	none	none	2	none	none
4	ZIKV	8	L435L/R	T792T/P	5	none	D245A	5	none	D245D/A	5	none	D245D/A, M806M/I
5	ZIKV	8	none	D245D/A, D788D/	5	none	D245D/A	5	none	D245D/A, D788D/E	5	none	none

				G, **T860P**									
6 (VC)	ZIKV	6	none	none	4	L435L/R	none	3	L435R	none	2	L435R	D245D/A, V257V/G

[a]Dpi: days post infection; [b]VC: virus control. AA mutations emerging both in VC (in absence of **12i**) and under **12i** pressure are indicated in red. Unique AA variations (not mixed populations) are bolded.

It must be noted that some mutations are observed transiently or permanently also in absence of **12i**, indicating an adaptation of the viruses to the cell line. AA mutations emerging both in VC (in absence of **12i**) and under **12i** pressure are indicated in red. Both DENV and ZIKV escaped from **12i** pressure although mutations were then lost, increasing the drug concentration in later steps.

The 2 viral strains emerging at 120 µM (I600V in DENV NS3) and at 15 µM (T860P in ZIKV NS5) and the viral strains carrying the mixed aa profile selected in ZIKV NS5 at 60 µM **12i** (D245D/A combined with D788D/E) were not quantifiable by immunodetection assay. This means that these profiles selected by **12i** impair the viral fitness resulting in lack of CPE at subsequent infection rounds. In this context, CPE is probably caused not only by replicating viruses but also by the accumulation of viral transcripts and non-replication competent viruses.

Under **12i** drug pressure, the mixed and pure mutations were distributed in different NS5 domains for ZIKV and DENV, but at conserved sites among different flaviviruses[88]. Instead, DENV E427E/K and ZIKV D788D/G/E, were distributed in non-conserved site.

The distribution of different mutations is thus displayed: the majority of NS5 aa variations selected (D788D/G, D788D/E, T792T/P, M806M/I, T860P for ZIKV and E427E/K for DENV) were located in a specific region, the polymerase region (RdRp); none of them were located in the catalytic site.[89] Moreover, the E427 is located between the G and F motifs of DENV RdRp, involved in the interaction with the nascent RNA template. D788, T792, M806 and T860 are in the ZIKV priming loop which is involved in the correct positioning of nucleotides during polymerization. Interestingly, the T860P mutation, detected in ZIKV, is located in the allosteric RdRp cavity B and mutated residues located in this cavity near T860 (W859A, I863A in DENV) significantly reduced viral replication.[90] All the remaining mixed mutations (K61K/E, E74E/K, P154P/T, N241N/H and T244T/P) that emerged in DENV were located in the N terminal region of NS5 in the methyltransferase domain (MTase) which interacts with the C-terminal domain of NS3 involved in the unwinding of double-stranded RNA intermediate (ATPase/helicase activity) and in viral RNA 5'-capping reaction (triphosphatase).[91] Regarding mutation in NS3 protein, under **12i** drug pressure, no pure or mixed mutations were selected in ZIKV NS3. The mixed R54R/P substitution selected in DENV NS3 is located in the N terminal domain near the catalytic site (His53, Asp77 and Ser138) of the trypsin-like serine protease.[92] The mixed substitution M267M/I is located in the C terminal subdomain I of NS3; the

conserved motifs in subdomains I and II are key regions for binding to RNA to generate the ATP binding cleft.[93] It's important to underline that, the only pure aa variation I600V acquired in the presence of 120 uM **12i** by DENV is located in the subdomain 3 of the helicase region of the NS3 protein and between two α-helices (559 to 607 residues) α9 and α10.[94] Interestingly, the subdomain III (NS3 483-618 aa) contains the interaction site with the RdRP domain of NS5 (320-368 aa).[95,96] However, **12i** seems not to have a high genetic barrier, since the selected mutations were then lost, simply increasing the drug concentration in later steps. In addition, in the presence of **12i** was not visible an increase in the time of viral breakthrough with respect to VC. Nevertheless, the I600V mutation for DENV NS3 and the D788D/G/E alone or coupled with the T860P substitution for ZIKV NS5 reduced dramatically the viral fitness, and mutated viral strains were not capable to replicate in subsequent cycles in the presence of **12i.** Moreover, the viral profile reverted to wild type in the absence of **12i** (data not shown). Once again, these studies could support the idea that compound **12i** may interact between NS3 and NS5 as per our original design[72].

To further understand if one of the targets of our new 2,6-diaminopurine derivatives is represented by the viral NS5, the most promising compounds **12c**, **12i**, **19a** and **20a**, were evaluated for the inhibition of both MTase and polymerase enzymatic activity of DENV and ZIKV in cell free experiments (Table 11).

Table 11. IC_{50} values of compounds **12c**, **12i**, **19a** and **20a** against DENV/ZIKV polymerases and MTases.

Cpds.	IC_{50} (μM)[a]			IC_{50} (μM)	
	D2pol[b]	**D2 NS5**[c]	**Zika NS5**[d]	**DENV NS5-MTase**	**ZIKV NS5-MTase**
12c	31.2±7.8	>100	18.9±3.1	NA	NA
12i	20.8±5.7	43.7±12.0	12.8±2.2	112.0±51.5	NA
19a	>100	153.2±38.2	105± 24.3	NA	NA
20a	>100	>100	>100	226.1±107.4	NA
3'dATP control	0.27± 0.03	0.32±0.05	1±0.2	-	-
Sinefungin	-	-	-	(0.63±0.04)[97]	(1.18±0.05)[98]

[a]inhibition concentration 50%; [b]D2pol: polymerase domain of dengue 2 virus; [c]D2 NS5: full length DENV protein; [d]Zika NS5: full length ZIKV protein. Literature data for Sinefungin are reported in parenthesis.

Increasing concentrations of the selected compounds were incubated with the purified MTase or polymerase and then the residual enzymatic activity was determined. The IC_{50} values showed that compounds poorly inhibited the MTase activity, while **12c** and **12i** inhibit the polymerase of DENV and ZIKV at micromolar concentrations. The latter data are slightly higher than the corresponding

antiviral IC_{50}s in cell, which is not unexpected for a multitarget class of molecules blocking multiple steps of DENV/ZIKV replication.

According to these data, **12i** would interfere with the formation of the DENV replication complex. Thus, to further investigate the effect of **12i** on the formation of the DENV replication complex in whole-cell context, we conducted an immunofluorescence analysis. The intracellular localization of NS5 and NS3 proteins was followed with and without the presence of the drug (**12i** or Sofosbuvir). **12i** or Sofosbuvir a non-toxic concentration (50 and 100 μM, respectively) was added at 8, 12, 16 and 24 hours post infection.

The confocal microscopy analysis, treated with drug, revealed that compound **12i** significantly reduced the expression of NS3 ($p \leq 0.05$ at 12 hours) and NS5 ($p \leq 0.0001$ at 16 hours) proteins (Figure 16, panels B and C), and significantly protected cell viability at 24 hours ($p \leq 0.05$) (Figure 16, panel A). On the other hand, treatment with Sofosbuvir significantly reduced NS3 and NS5 proteins expression starting from 12 hours ($p \leq 0.05$ and $p \leq 0.01$, respectively) (Figure 16, panels B and C), however no complete recovery in the number of viable cells was observed.

Next, as evident from the immunofluorescence analysis, the untreated cell highlights that the NS3 protein has a large nuclear localization at 8h, and it moves in the cytoplasm within 24h. Otherwise, NS5 protein has mainly cytoplasmic localization at 8h and moves to the nucleus between 16h and 24h. The formation of the replication complex could be associated with a NS3:NS5 colocalization, that in this analysis occurred at 16h (Figure 16, panel D, merge line).

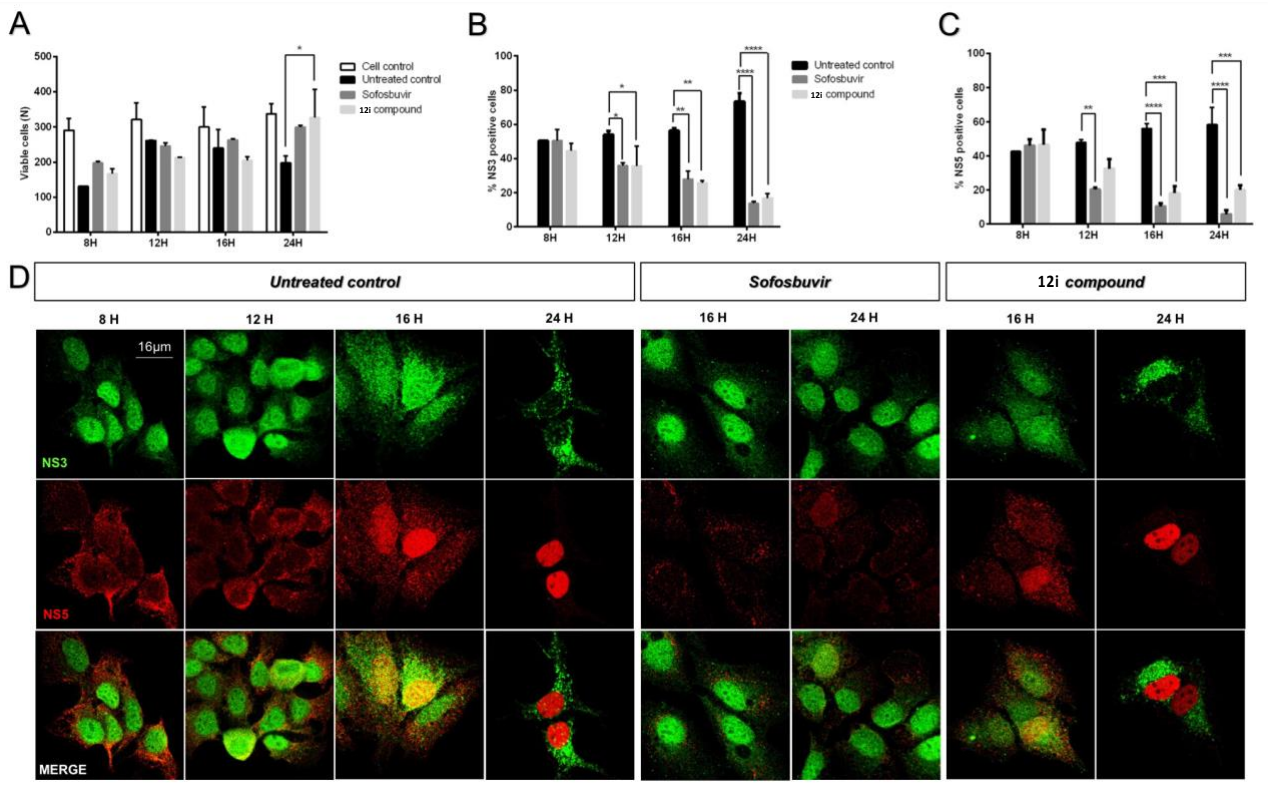

Figure 16. Immunofluorescence analysis. DENV-2 infected cells were treated with Sofosbuvir (100 µM) or **12i** compound (50 µM) and stained at different time points with DENV NS3 antibody (detected using AlexaFluor® 488 labeled secondary antibody) and DENV NS5 antibody (detected using AlexaFluor® 568 labeled secondary antibody), and examined by confocal microscopy. A) Cells stained with DAPI and counted at 40x magnification in 5 random fields per well (* $p \leq 0.05$). B) Expression of the viral NS3 protein in cells counted at 40x magnification in 5 random fields per well (* $p \leq 0.05$; ** $p \leq 0.01$; **** $p \leq 0.0001$). C) Expression of the viral NS5 protein in cells counted at 40x magnification in 5 random fields per well (** $p \leq 0.01$; *** $p \leq 0.001$; **** $p \leq 0.0001$). D) Individual antibody stained as well as merged images in untreated control, cells treated with Sofosbuvir, and cells treated with **12i** compound. Each experiment was repeated at least two times.

Examining the localization of NS5:NS3 in treated cells, both Sofosbuvir and **12i** seemed to abolish the formation of the replication complex, though to a greater extent for Sofosbuvir. In fact, NS5 translocation into the nucleus was reduced or absent while, at the same time, NS3 protein did not translocate into the cytoplasm (Figure 16, panel D, Sofosbuvir column and **12i** column).

Next, the NS3:NS5 colocalization reduction observed in **12i** treated cells was confirmed and quantified by colocalization analysis, with the greatest reduction observed at 16 hours (MCC NS3/NS5=0.404±0.106 and MCC NS5/NS3=0.397±0.101; Costes P=100%) compared to the untreated control (MCC NS3/NS5=0.726±0.135 and MCC NS5/NS3=0.752±0.125; Costes P=100%) ($p \leq 0.0001$) (Figure 17).

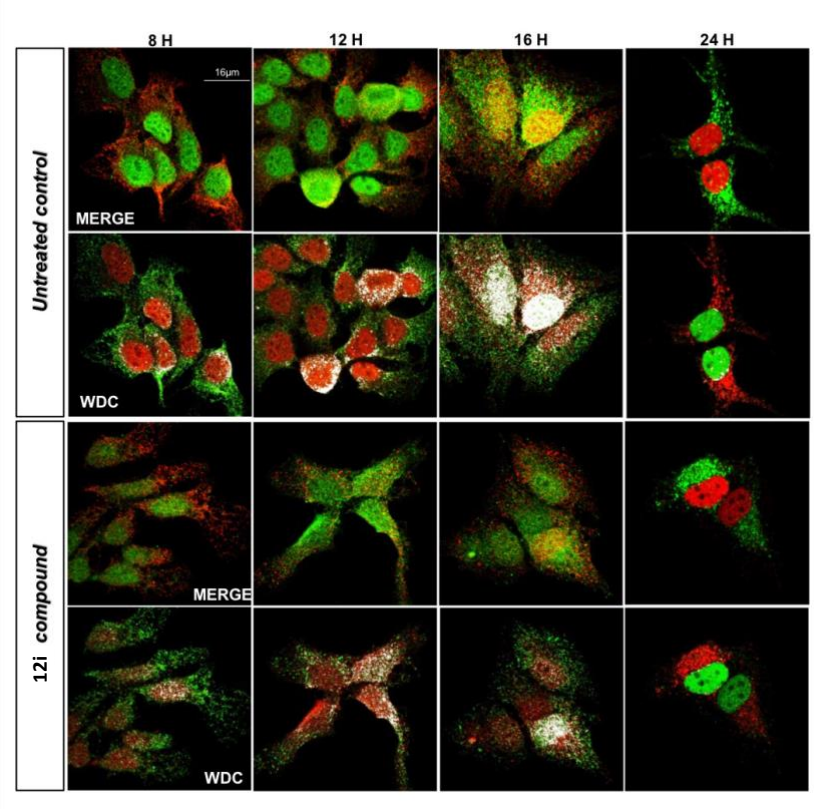

Figure 17. Immunofluorescence analysis. DENV-2 infected cells were treated with **12i** (50 µM) and stained at different time points with DENV NS3 antibody (detected using AlexaFluor® 488 labeled secondary antibody) and DENV NS5 antibody (detected using AlexaFluor® 568 labeled secondary antibody), and examined by confocal microscopy. NS3:NS5 stained cells merged images and white dots colocalization (WDC) images in untreated control (above) and treated with **12i** compound (below) are shown as indicated. Each experiment was repeated at least two times.

Table 12. Inhibitory effect of BSAAs **12c**, **12i**, **19a** and **20a** against selected kinases.

	Residual enzymatic activity (%)[b]				
Cpd.[a]	**Src**	**Abl**	**Fyn**	**PI3Kα**	**CDK9/cT1**
12c	45.0±20.0	54.0±4.0	NA[c]	69.0± 1.0	87.0±14.0
12i	47.0±20.0	70.0±10.0	NA	66.0±0.2	NA
19a	84.0±1.0	67.0±2.0	NA	77.0±3.2	88.0±10.0
20a	NA	NA	89.0±2.0	78.0±0.3	NA
7	59.0±9.4	65.0±5.6	45.0±6.9	ND	NA

[a]Each compound was tested at fixed 5µM concentration. Values for reference compound **7** reported from the literature. [b]Values are the mean ±SD of two independent experiments. [c]NA: residual enzymatic activity >98%.

In conclusion, **12i** and Sofosbuvir showed a reduction of NS5/NS3 expression over time, but they induced a completely different effect on the localization of the same proteins, which reflects the different mechanism of action of the two compounds.

Finally, to confirm the multi-target effect of the most interesting, synthesized compounds **12c**, **12i**, **19a** and **20a** were evaluated against a panel of host kinases that were reported to play a role in the replication of Flaviviruses, Influenza viruses, and Coronaviruses [33,99,100]. As reported in Table 12, selected compounds were tested at a fixed concentration corresponding to their median antiviral IC_{50} (5 μM) in comparison with the hit compound **7**.

Compound **12i** reduced the activity of Src, Abl and PI3Kα by roughly 50% at 5 μM, showing a moderate inhibitory effect on the selected kinases at micromolar concentration. Despite potent nanomolar kinase inhibitors with no antiviral activity have been reported among 2,6-diaminopurine derivatives[101], our compound has the advantage to lead a moderate inhibition of few host kinases together with an observed effect on NS5/NS3 and, possibly, this double inhibition of viral and/or host targets may contribute to the antiviral efficacy of these multi-target inhibitors.

2.2.5 Conclusion

Outbreaks of zoonotic viral diseases have increased in number, frequency, and variety over the last several decades. Enhanced globalization and climate changes have strongly contributed to the increase in the spreading of new and re-emerging viruses, which are no longer confined to geographically limited risk areas and represent a growing danger to global public health. To these points, we must also take into consideration the increase in viral co-infections, which make diagnosis difficult. Unfortunately, the effectiveness of approved antiviral drugs is limited to only a few among the known strains and the antiviral arsenal that is available to us is not yet profuse. Therefore, the development of broad-spectrum antiviral agents (BSAAs) represents the ideal option for prompt interevent to counteract the spreading of new and re-emerging different viruses and to deal with viral co-infections. Efforts should be placed on the development of cheap and easy to be produced drugs, with a broad-spectrum of activity to fight with a single drug, multiple viruses.

Considering the unsatisfactory results obtained with the target-based optimization of our hit compounds **5-7**, we decided to exploit the advantages of a phenotypic approach to conduct a hit-to-lead optimization. Starting from previously obtained SAR data, the first set of molecules, that we developed (**12a-k**; **13d,f**; **16a,b**), showed good inhibitory potency of replication of Flaviviruses (DENV-2, ZIKV, WNV). Next, we investigated the possibility to functionalize the 2,6-diaminopurine scaffold with a ROS-scavenging moiety to reduce the cellular oxidative stress generated by some viral infections. Unfortunately, only two derivatives (**19a** and **20a**) of this second set of molecules (**19a-e**; **20a-d**) were characterized by antiviral efficacy against selected Flaviviruses. The three most promising compounds obtained with a phenotypic approach (**12c**, **12i**, and **19a**) were then evaluated against Influenza A (subtype H1N1). **12i** was identified as the most potent and promising candidate and for this reason, it was also tested against the novel coronavirus SARS-CoV-2 proving to inhibit its replication at low micromolar concentration in all human cell lines evaluated. Overall, compound **12i** represents a very interesting BSAA capable of inhibiting the replication of DENV-2, ZIKV, WNV, Influenza A, and SARS-CoV-2 at low micromolar range and with high selectivity index. In comparison to the reference antiviral drugs used in this study (sofosbuvir, ribavirin, and remdesivir), compound **12i** is very simple/cheap to make (only two synthetic steps from commercial materials) and exhibits low micromolar antiviral efficacy in all infected cell lines, indicating broad-spectrum activity that none of these reference drugs have.

In vitro selection experiments were performed on DENV and ZIKV under **12i** pressure to confirm our original rationale, based on the contemporary inhibition of Src/Fyn host kinases and blockage of viral NS3:NS5 interaction, that led us to the development of the first-generation of 2,6-diaminopurine antivirals: although compound **12i** does not appear to have a high genetic barrier for resistance, a few

mutations in important functional sites of both NS5 and NS3, involved in NS3:NS5 interaction, dramatically reduced viral fitness; moreover, immunofluorescence experiments also revealed a significant reduction in NS5/NS3 colocalization in cells treated with **12i**, indicating that its inhibitory effect on DENV replication is directly related to inhibition of replication complex. Finally, the multi-target MOA of this class of 2,6-diaminopurine antivirals was also supported by the moderate activity of **12i** against ZIKV/DENV polymerase and against a small selection of kinases that are known to be involved in the replication of Flavivirus, Influenza A and SARS-CoV-2.

In summary, the concept of multi-target drugs of these compounds, for prompt aid in case of new and re-emerging viral emergences, is well described by the modest inhibition of numerous isolated targets combined with the low micromolar potency in cells infected with distinct viruses.

2.3 Nucleoside Derivatives

2.3.1 Introduction

Nucleosides or nucleotides are involved in many biochemical reactions and play an important role in cellular functions, such as DNA and RNA synthesis, cell signalling, enzyme regulation and metabolism. Chemically modified nucleoside analogs, that have been developed to mimic their physiological counterparts, are widely used as therapeutic drugs both in the treatment of cancer and viral infections[102]. The first antiviral nucleoside, edoxudine, was developed in the far 1969, and it is not used in clinic anymore. Currently, there are over 25 approved therapeutic nucleosides used for the therapy of viral infections of high medical importance, such as HIV/AIDS (tenofovir),[103,104] hepatitis B (lamivudine/entecavir),[105,106] hepatitis C (sofosbuvir),[107] or herpes infections (acyclovir).[108]

Nucleoside analogs may enter inside the cells through specific plasma membrane transporters or by passive permeation[109]. Once inside the cell, nucleosides are phosphorylated by cellular kinases resulting in the formation of nucleoside mono-, di-, and triphosphates, with the latter being the active form in the inhibition of virus replication. Considering that the first kinase phosphorylation is the rate-limiting step of the triphosphate conversion, different synthetic strategies have been developed to overcome the issue, mainly through the introduction of a phosphorylated group into the 5′ nucleoside position with the obtainment of monophosphate prodrug. This modified phosphate group includes protecting moieties to increase hydrophobicity and facilitate the cellular uptake of the prodrug. Through this strategy, the monophosphate prodrugs don't need membrane transporters to enter the cells and the protecting groups are then removed by phosphoramidases or esterases after cell penetration. The modified nucleoside triphosphate act by inhibiting cellular or viral enzymes, such as DNA/RNA polymerases, DNA methyltransferases kinases, ribonucleotide reductase, purine and pyrimidine nucleoside phosphorylase, etc. During DNA/RNA replication, nucleoside analogs are incorporated into nascent DNA or RNA chains resulting in the termination of nucleic acid synthesis or in the accumulation of mutations in viral genomes to suppress viral replication. However, the possibility of inhibiting other viral targets by nucleoside analogs cannot be excluded. In fact, some studies clearly show that the monophosphate prodrug approaches may fail to improve the activity of antiviral nucleosides in some specific cases[110,111], and one could speculate that this means that nucleosides might have other alternative mechanisms of action, which may not involve their activation through phosphorylation.

Mutations in the viral genomes cause resistance to currently used nucleoside and nucleotide analogs. Thus, the synthesis of nucleosides with different mechanisms of action is necessary to overcome resistance mechanisms. The most common nucleoside drugs belong to the category of sugar-modified

nucleosides[112,113,114,115]. However, base-modified nucleosides have also shown promising pharmacological activities and represents an attractive topic to synthetic organic and medicinal chemists. Ribavirin is an example of a base-modified purine nucleoside, endowed with a broad antiviral spectrum against DNA as well as RNA viruses. Other examples of base-modified nucleoside derivatives, that have been found to have various biological activity, such antiviral, antibacterial and anticancer, include didanosine (ddI) and abacavir (ABC) are both marketed anti-HIV drugs and contain a hypoxanthine and 2-amino-6-cyclopropylaminopurine as a nucleobase, respectively[116]; amdoxovir, with a 2,6-diaminopurine nucleobase, is a HIV reverse transcriptase inhibitor that underwent clinical trials[117,118]; 5-fluorouracil is the base moiety of the anticancer drug floxuridine[119]; 7-Deaza-2′-C-methyladenosine is an inhibitor of HCV replication[120] and 2′-Deoxy-2′-fluoro-β-D-arabinofuranosyl-5-methylcytosine (FMAC) is endowed with promising antiviral activity against herpes simplex virus[121]. Therefore, an extensive literature on base-modified nucleosides characterized by significant biological properties has been reviewed in recent years[122,123,124,125,126,127,128]. Considering that the modification of the nucleobase moiety has been shown to be a successful strategy in the discovery of biologically active nucleosides, a variety of strategies has been conceived to design effective and non-toxic base-modified nucleosides.

For what concern the sugar modifications, it has long been assumed that only nucleoside analogs having a natural D-configuration could exhibit biological activity, due to the stereospecificity of enzymes in living systems[129,130]. At the beginning of the 90s, L-nucleoside enantiomers emerged as a new class of antiviral agents. Although the first synthesis of an L-nucleoside was reported in 1964[131], little attention was paid to L-nucleoside analogs until the discovery of lamivudine, one of the most important drugs used in hepatitis B infection and in the treatment of AIDS. Since then, a large number of L-nucleoside analogs have been synthesized and their antiviral activities evaluated[132,133,134,135,136].

Moreover, it is important to emphasize the clinical relevance of co-infection, where one pathogen can affect the severity of infection by another pathogen, either directly or indirectly, resulting in enhanced disease severity. In fact, recent studies of viral-bacterial interactions demonstrated that virus-bacterial interactions may be pervasive and have serious implications for microbial pathogenesis[137]. Although the mechanisms of single infections by isolated pathogens have been studied considerably, little is known about the regulatory mechanisms of co-infections between them[138]. Data on the prevalence of bacterial and viral co-infections among patients with SARS-CoV-2 were collected. It was demonstrated that severe SARS-CoV-2 pneumonia might have a respiratory bacterial co-infection and the leading involved bacteria were methicillin-sensitive Staphylococcus aureus, Streptococcus pneumoniae, Haemophilus influenzae and Enterobacteriaceae[139]. This increasing phenomenon of co-

infection has created a need to develop new broad-spectrum antimicrobial agents that may inhibit the growth of both bacterial and viral infection.

In bacteria, the metabolism and mechanism of action of pyrimidine and purine analogs have significant differences[140]. Thus, nucleoside analogs are also used as effective therapeutics for a variety of bacterial infections[141,142,143]. Considering the growing problems connected with the antibiotic-resistance to common drugs, there is an urgent need for new antibiotics to treat those strains that have progressively become more prevalent in the community and nucleoside derivatives may play an important role[144,145].

2.3.2 Aim of the work

Under physiological conditions, nucleoside/nucleotide are subjected to catabolic pathways, such as deamination (oxidation) of heterocyclic base, hydrolysis or phosphorolysis of heterocyclic base, and hydrolysis of phosphomonoester bonds. Purine nucleosides undergo extensive metabolism and among the different metabolites, nucleobases represent one of the possible metabolites that can be generated by the cleavage of the glycosidic bond, under a reversible reaction catalyzed by purine nucleoside phosphorylase (PNP)[146,147,148,149]. This consideration may lead to a belief that an active nucleos(t)ide analog, constituted by a nucleobase endowed with antiviral activity and a sugar moiety, can generate a dual agent, as a consequence of metabolism, to which the nucleos(t)ide is subjected.

Considering the known metabolic fate of purine nucleosides and the availability of broad-spectrum purine antivirals (Chapter 2.2), we planned to develop new base-modified nucleosides built upon the most promising 2,6-diaminopurines in order to create prospective dual-acting drugs that inhibit the viral replication both directly through the nucleoside itself and indirectly through the antiviral nucleobase that might be generated after metabolic cleavage of the glycosidic bond.

Among the 2,6-diaminopurine derivatives developed within this PhD project, four compounds (**12a,c,g,i)** have shown promising antiviral activity against both DENV and ZIKV, and compound **12i** has turned out to be a BSAA active against all tested viruses (DENV, ZIKV, WNV, Influenza-A and SARS-CoV-2) in the submicromolar to low micromolar range and with high selectivity index (Figure 18). The next chapter will describe the development of different nucleoside derivatives base-modified, having as base our best 2,6-diamino purines, to further investigate the chemical and biological space around this class of 2,6-diaminopurine. Structures Ⅰ and ⅠⅠ (Figure 18) represent the general structures of target molecules, including nucleosides with natural D configuration, the prodrug ones on 5’ hydroxylic group, nucleosides with non-natural L configuration and acyclic derivatives. Next, during my secondment period at the Rega Institute for Medical Research in Leuven, I experimentally evaluated, with the use of on-line electrochemistry/electrospray ionization mass spectrometry (EC-ESI/MS) system, the hypothesis that *in vivo* may occur the cleavage of the glycosidic bond of β -D-, β -L nucleosides and a D-phosphoramidate prodrug of compound **12i**, with the release of the nucleobases, which allow us to obtain a single entity with dual activity.

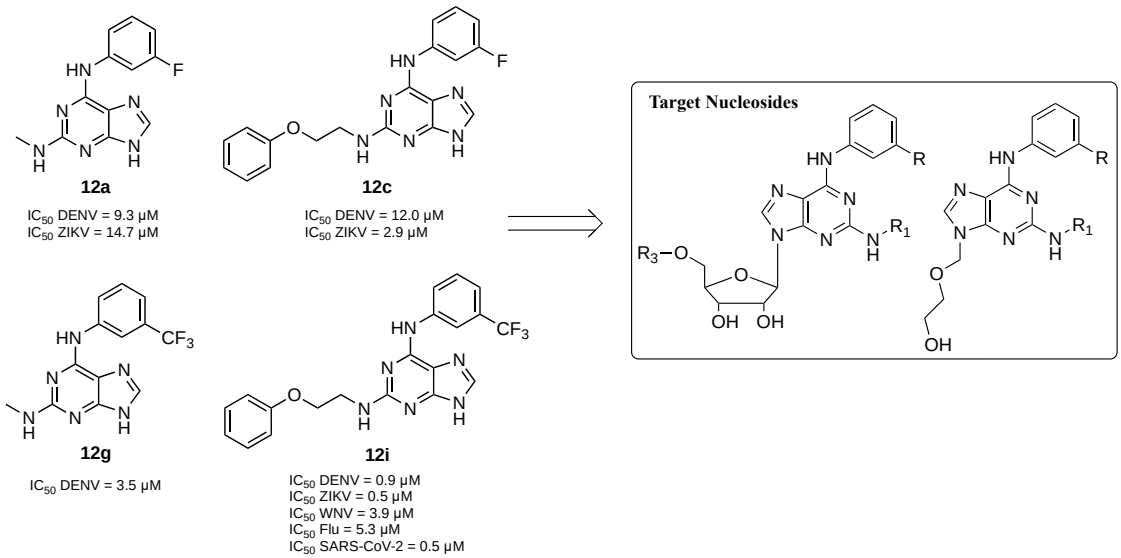

Figure 18: 2,6-Diaminopurine-based antiviral, their antiviral potency and target molecules

2.3.3 Results and discussion

For the purpose of our work, the first set of synthesized nucleosides was prepared keeping the natural ribose configuration (D). The first attempt at the synthesis of nucleoside analogs consisted in the direct coupling between selected 2,6-diaminopurine antivirals and the protected D-ribose (1,2,3,5 tetraacetyl-D- ribofuranose).

We tried to set up the synthetic protocol on the more interesting nucleobases with long chain in C2, previously identified in Chapter 2.2 (**12g or 12i)**. The nucleobases **12g** or **12i** were silylated with bis(trimethylsilyl)acetamide (BSA) and reacted with ß-D- tetra acetyl ribose in the presence of the Lewis acid trimethylsilyl trifluoro methanesulfonate. This reaction led thus to the obtainment of protected nucleosides **21a,b** with yields above 60 %. For the ribose deprotection, three different approaches were attempted to evaluate the one that allows the obtainment of a better yield. K_2CO_3 in methanol allowed a better yield than NaOMe, albeit with longer reactions times. A saturated solution of NH_3 in EtOH was the more convenient approach for the deprotection of the sugar moiety, which allowed the obtainment of final compounds **22a,b**, with yield of 54 % (Scheme 8).

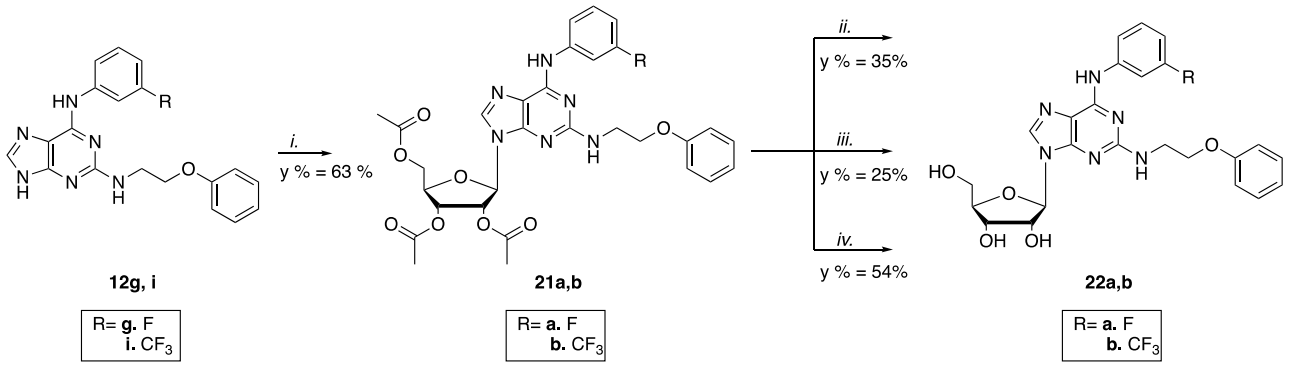

Scheme 8: *Reagents and conditions*: *i.* a) BSA, ACN dry, 1h, r.t.; b) TMSOTf, 1,2,3,5 tetraacetyl-D ribofuranose, 1h, reflux; *ii.* K_2CO_3, MeOH, r.t., 3h; *iii.* NaOMe, MeOH, r.t., 30'; *iv*. NH_3/EtOH, 1h, r.t.

However, with the application of the previous described synthetic protocol to the nucleobase **12g** with a short chain on C2, we didn't obtain compound **21c** (Scheme 9). In fact, surprisingly, the formed glycosidic bond between the nucleobase **12g** and protected ribose (1,2,3,5 tetraacetyl-D-ribofuranose) was not stable enough to obtain the desired protected nucleoside derivative **21c**, to be submitted to subsequent deprotection of the acetyl groups of ribose for the obtainment of final nucleoside.

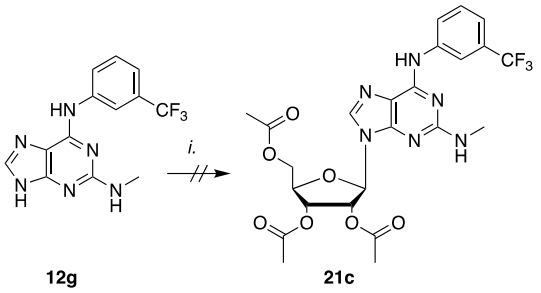

Scheme 9: *Reagents and conditions: i.* a) BSA, ACN dry, 1h, r.t.; b) TMSOTf, 1,2,3,5 tetraacetyl- D ribofuranose, 1h, reflux.

Given the failure of the latter synthesis, we decided to set up a synthetic protocol, applicable to all selected nucleobases, which foresaw the C2 substitution only after forming glycosidic bond between the 2-chloro-6-amino substituted-9*H*-purine derivatives and the protected ribose. Following Vorbruggen's glycosylation[150,151], the C6 substituted purine base **10c** was silylated with bis(trimethylsilyl)acetamide (BSA), and the silylated bases then reacted with a ß-D- tetra acetyl ribose in the presence of a Lewis acid catalyst trimethylsilyl trifluoro methanesulfonate (TMSOTf) to give the intermediate **23c** (Scheme 10). At first, the latter intermediate **23c** was isolated, but the yield was very low. Subsequently deprotection of acetyl groups of ribose in a saturated solution of NH_3 in EtOH allow us to obtain compound **24c**. C2 substitution at the microwave with 2-phenoxyethylamine **11b** or methylamine **11a** led to final compounds **22b,d** respectively, but with a low overall yield (< 2% over three steps).

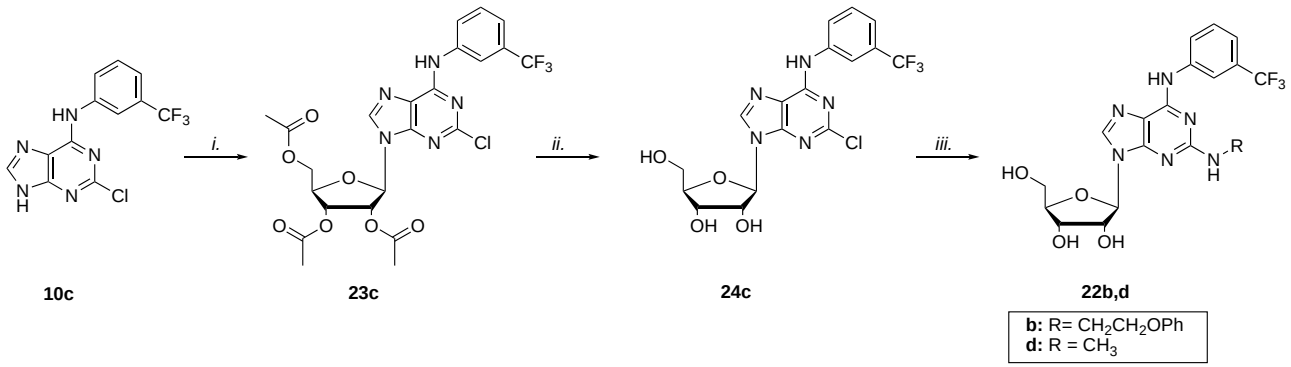

Scheme 10. *Reagents and conditions: i.* a) BSA, ACN dry, 1h, r.t.; b) TMSOTf, 1,2,3,5 tetraacetyl- D ribofuranose, 1h, reflux; *ii.* NH_3/EtOH, 1-3h, r.t.; *iii.* R_1NH_2 **11b** or **11a**, TFA, n-BuOH, 1-2h, μW 170 °C.

In the following attempt to optimize the synthetic protocol, compounds **23c** was not isolated but directly deprotected with a saturated solution of NH_3 in EtOH to give the desired compounds **24c**. The introduction of 2-phenoxyethylamine **11b** or methylamine **11a** in C6 position was accomplished through a microwave-assisted reaction in presence of TFA (Scheme 11). This simple protocol was

then applicable for the synthesis of all nucleosides of our selected nucleobases and so it afforded the final compounds **22a-d** with higher overall yield with respect to the first approach that used the 2,6-diaminopurines in the coupling reaction. Unexpectedly, it was observed that the treatment of intermediate **24a,c** with methylamine in presence of TFA, gave the desired compounds **22c,d** and the acylated ones on 5'OH **25c,d**, possibly due to traces of acetic acid in TFA (Scheme 11).

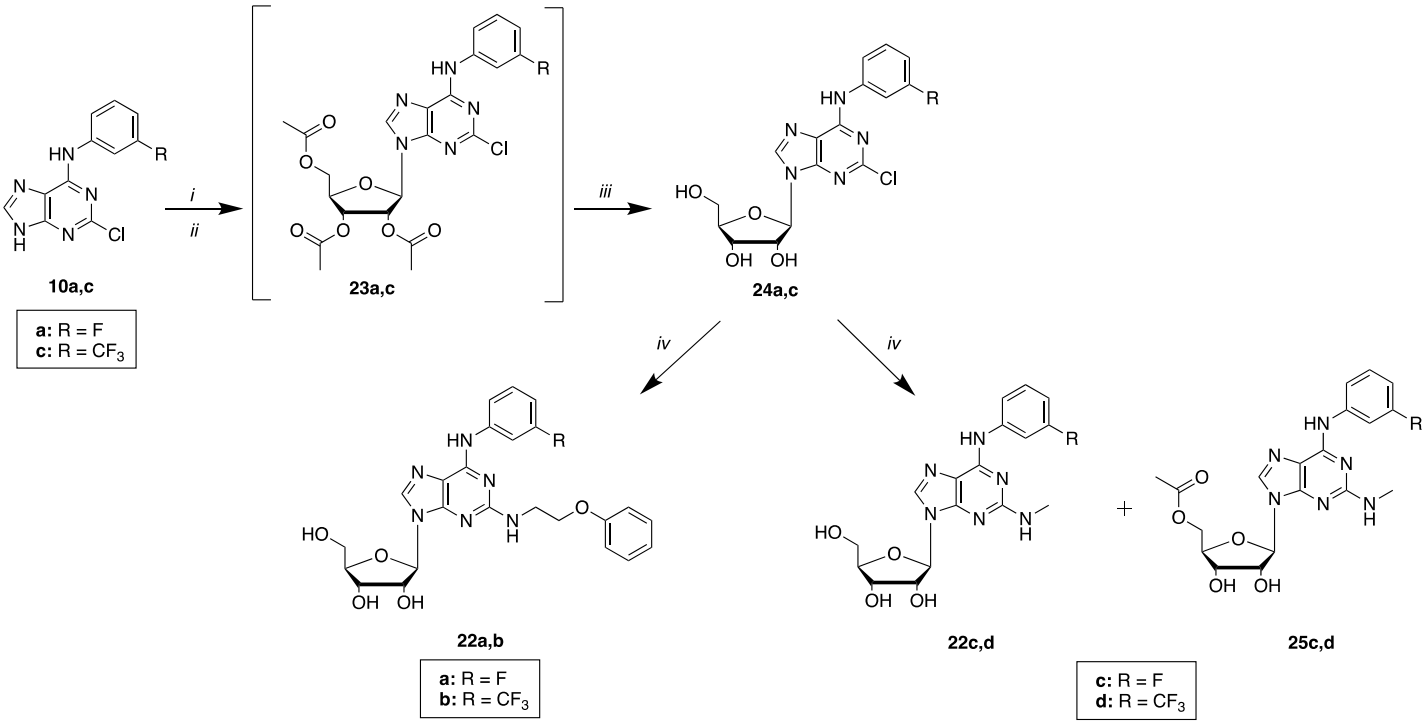

Scheme 11: *Reagents and conditions: i*. BSA, ACN dry, 1h, r.t.; *ii.* TMSOTf, 1,2,3,5 tetraacetyl- D ribofuranose, 1h, reflux; *iii*. NH_3/EtOH, 1-3h, r.t.; *iv*. R_1NH_2, TFA, n-BuOH, 1-2h, μW 170 °C.

Compounds **25c,d**, which can be considered as prodrugs of **22c,d**, may have a better passive permeation of the cell membrane and be converted to **22c,d** once inside the cell. For this reason, we decided to prepare other prodrugs by functionalizing the 5'- hydroxy group with an isobutyryl group (as in the antiviral Molnupiravir), and with a longer aliphatic chain (Scheme 12).

The 2'- and 3'- hydroxyls group of **22d** were first protected with acetonide to afford compound **26**, and then the 5'- hydroxy was converted to ester derivatives by reaction with opportune acyl chlorides (isobutyryl chloride or octanoyl chloride). Octanoyl chloride was quantitively obtained, starting from its corresponding acid, octanoic acid, by using thionyl chloride as chlorinating agent. Deprotection of **27a,b**, in aqueous acid condition, yielded the final compounds **28a,b** in moderate yields.

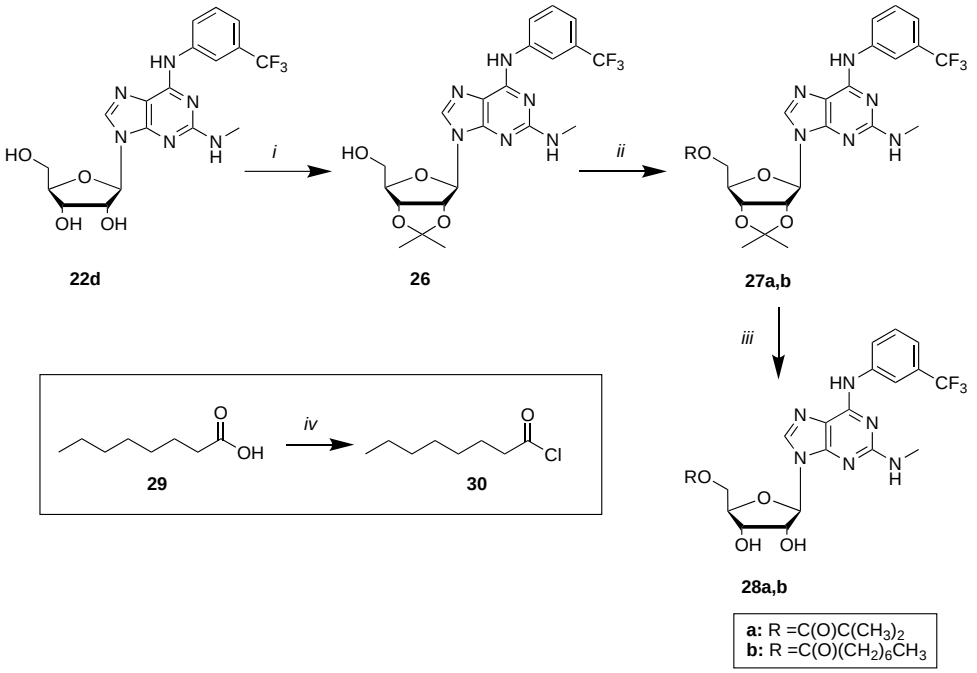

Scheme 12: *Reagents and conditions: i.* DMP, p-toluensulfonic acid, o.n., r.t.; *ii.* isobutyryl chloride or octanoyl chloride, DMAP, DCM, 2-16h, r.t.; *iii.* H_2O/TFA (2:1), 2-3h, r.t.; *iv*. $SOCl_2$, THF, 4h, r.t.-55 °C.

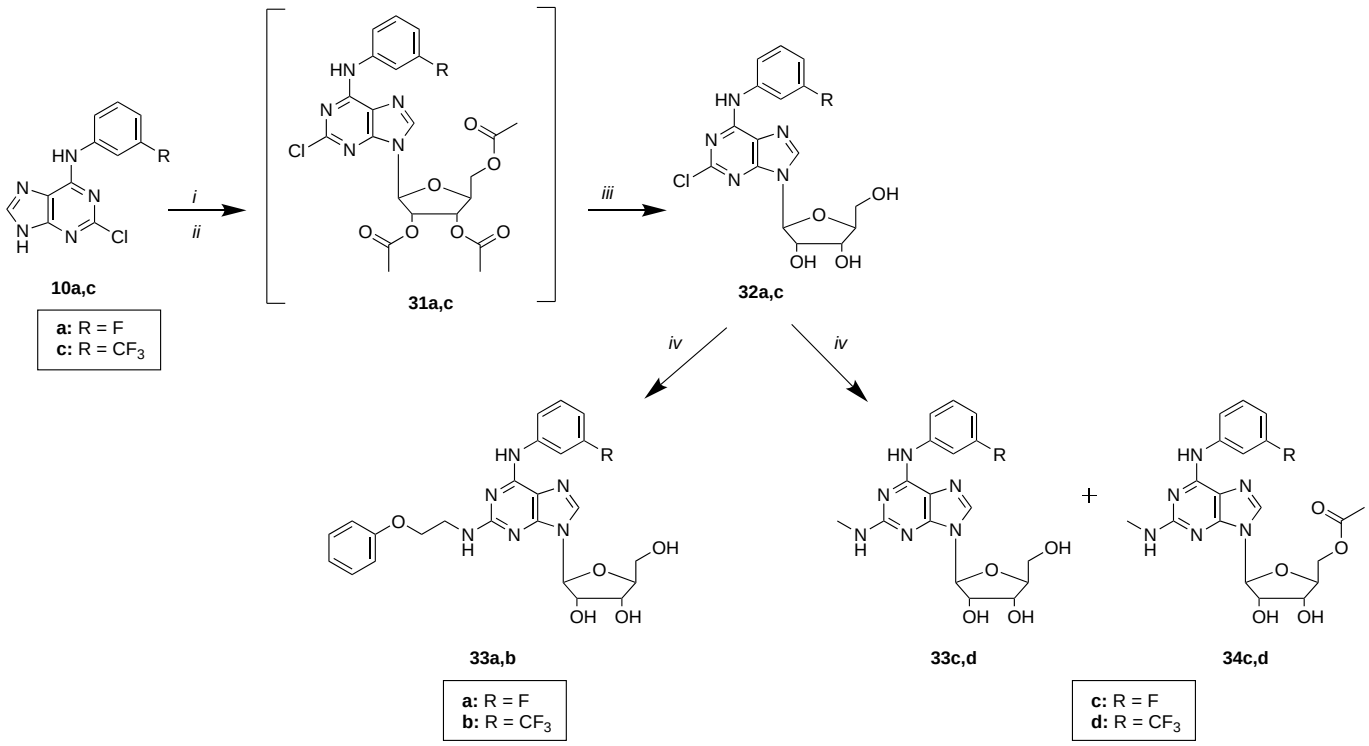

Scheme 13: *Reagents and conditions: i.* BSA, ACN dry, 1h, r.t.; *ii.* TMSOTf, 1,2,3,5 tetraacetyl- L ribofuranose, 1h, reflux; *iii*. NH_3/EtOH, 1-3h, r.t.; *iv*. R_1NH_2 (**11a** or **11b**), TFA, n-BuOH, 1-2h, μW 170 °C.

The synthetic approach applied for the synthesis of L-derivatives is the same used to prepare the above D-nucleosides (Scheme 13). Commercial ß-L- 1,2,3,5-tetra acetyl ribofuranose was used for

the coupling with 2-chloro-6-amino substituted-9*H*-purine derivatives **10a,c**, in presence of TMSOTf to direct the reaction to N9 regioisomer.

The prodrug approach has proven to be a powerful tool for enhancing the biological activity, via by-passing certain mechanisms of resistance and increasing lipophilicity, which lead to better delivery of the drugs inside the cells. One of the most widely used monophosphate masking approaches is the phosphoramidate prodrug (Protide)[152,153,154,155]. Thus, we first build the synthon **40**, bearing esterified L-alanine (L-Ala) as the amino acid, and an aryloxy group (Scheme 14). Compound **40** was thus prepared in quantitative yield, under argon atmosphere, starting from alanine isopropyl ester hydrochloride **38** and phenyl dichloro phosphate **39** in presence of triethylamine as shown in Scheme 14.

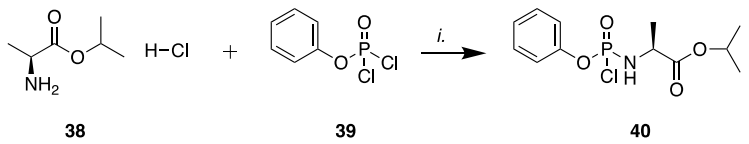

Scheme 14: *Reagents and conditions*: *i.* Et_3N, THF, N_2, r.t., 1h.

Next, nucleoside derivative **22b** was first protected on 2'- and 3'- hydroxyl groups with 2,2-dimethoxypropane to yield **35**, followed by coupling with **40**, using tert-Butyl MgCl. Final acid-catalyzed cleavage of protecting group of the compound **36** afforded phosphoramidate **37** as a mixture of two diastereomers in moderate yield (Scheme 15).

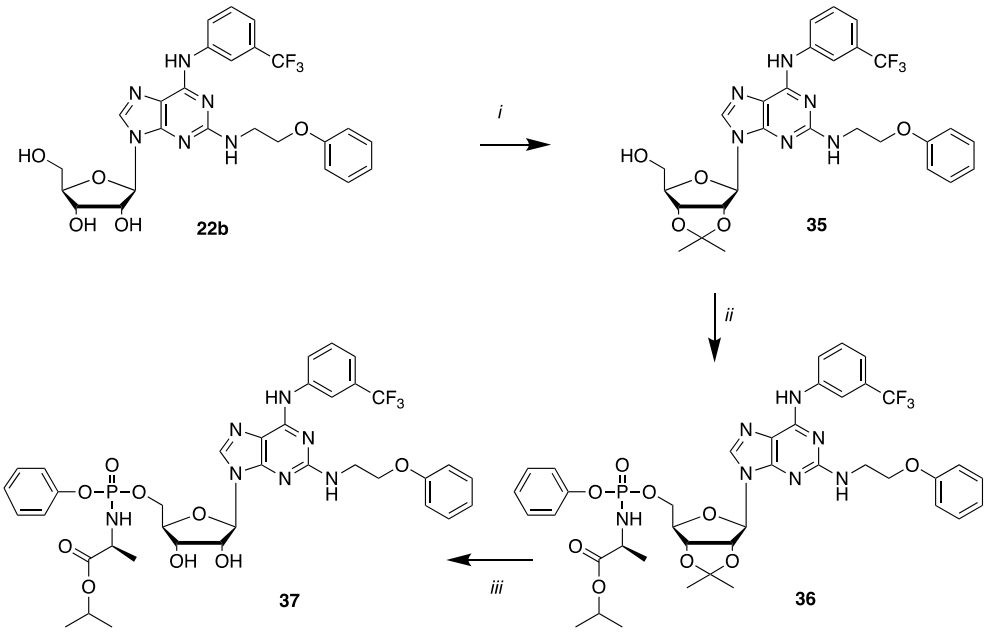

Scheme 15: *Reagents and conditions: i.* DMP, p-toluensulfonic acid, o.n., r.t.; *ii*. **40**, t-BuMgCl, THF, o.n., r.t.; *iii.* 90% TFA, 30', r.t.

Finally, we also decided to synthesize the acyclic nucleoside analog of the most promising BSAA **12i** by functionalizing N9 with the same acyclic chain of acyclovir. The synthesis of N9 substituted purine usually involves the alkylation of purine derivatives in the presence of an alkyl bromide or chloride and a base. However, the regioselectivity of the reaction is an issue to be overcome in order to obtain the functionalized N9 derivative. Thus, we decided to adopt the Vorbruggen reaction conditions in presence of Lewis acid catalyst. Following a reported protocol, we tried to synthetized the (2-acetoxyethoxy)methyl acetate to be used in the N9 functionalization (Scheme 16)[156]. Surprisingly, the reaction led to the formation of compound **43** instead of the expected (2-acetoxyethoxy)methyl acetate, as confirmed by NMR spectrum and mass analysis.

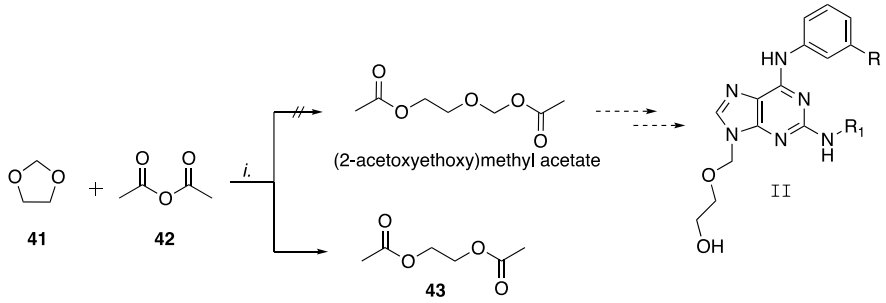

Scheme 16: *Reagents and conditions*: *i*. H_2SO_4, -5 °C-r.t, 12h

Despite we obtained this undesired product, we decided anyway to go ahead with the planned reaction to functionalize the purine N9. Running the coupling reaction between **8** and **43** (in place (2-acetoxyethoxy)methyl acetate) under standard conditions from the literature didn't give any product. However, reacting the silylated compound **8** with **43** under microwave-assisted conditions gave the N9-substituted compound **44** (Scheme 17)[157]. Functionalization of C6 and C2 with proper amines was achieved using our previously microwave-assisted protocol. The latter step, which required acidic conditions, also led to the contemporary C2 substitution and cleavage of the acetyl group, thus obtaining of the final compounds **46a-d** (Scheme 17).

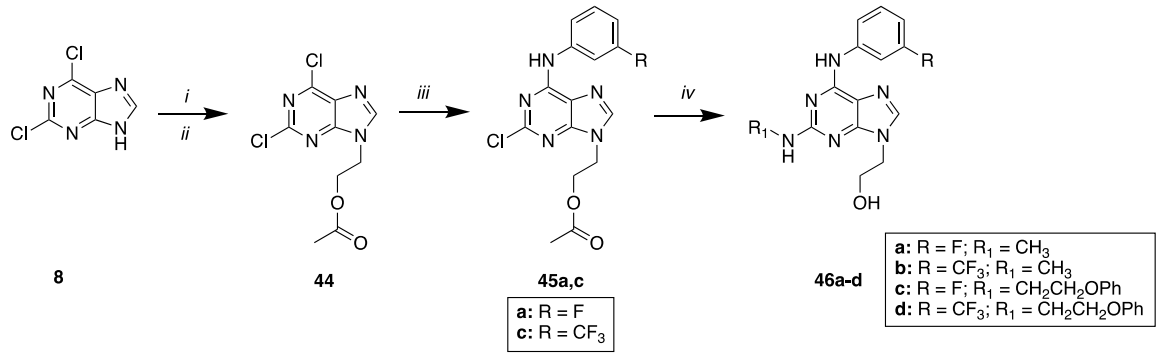

Scheme 17: *Reagents and conditions*: *i*. BSA, ACN dry, 1h, r.t.; *ii.* TMSOTf, **43**, 1h, μW 150 °C; *iii*. RNH_2 **9a** or **9c**, TEA, n-BuOH, 1h, μW 120 °C; *iv*. R_1NH_2 **11a** or **11b**, TFA, n-BuOH, 1h, μW 180 °C

2.3.4 Electrochemical/mass spectrometry studies

The online electrochemistry/electrospray ionization mass spectrometry (EC-ESI-MS) system is an alternative tool to emulate the oxidative metabolism of drug candidates, which is usually conducted in the liver cells by cytochrome P450 oxidation. The use of electrochemistry to mimic different phase I biologic reactions, such as aromatic hydroxylation, dehydrogenation, and O- and N-dealkylation, has been well documented and revised[158]. Moreover, in the last years, several studies have highlighted how electrochemistry successfully mimicked the oxidation reactions involving nucleic acids in biological systems. As pointed out above, our rationale behind the synthesis of nucleoside compounds was the achievement of a dual-acting agent able to have antiviral activity both as a single entity and, after likely metabolic cleavage of glycoside bond, as nucleobase.

In light of the above-mentioned scenario, with the use of the electrochemistry/mass spectrometry technique, we expected to provide insights into the plausible metabolic fate of the corresponding β-D-, β-L nucleosides and a D-phosphoramidate prodrug of the previously identified most promising broad-spectrum antiviral compound (**12i**), and to experimentally evaluate the hypothesis that the cleavage of the glycosidic bond of nucleosides may occur in vivo with the release of the nucleobases, which allows us to obtain a single entity with dual activity. Studzińska et al. have identified, with the use of the online electrochemistry/ mass spectrometry, different oxidation products of adenosine, detectable also with traditional in vitro/ in vivo studies[159]. During the investigation, they pointed out that the conditions applied influenced the obtained oxidation products: among the various oxidation products, adenine is detectable at pH 7 (ammonium acetate) in positive ionization mode. Therefore, we optimized the electrochemical conditions that led to the cleavage of the glycosidic bond with adenosine, and subsequently, the same conditions were applied to our compounds.

Electrochemical conversions were accomplished in an electrochemical cell (μ-PrepCell, Antec). The reactor cell consisted of a three-electrode arrangement including a working electrode, a counter electrode, and a reference electrode. As working electrode, a glassy carbon electrode was used. The inlet block of the cell was employed as counter electrode and the HyREF (Antec) electrode was used as reference electrode. Electrochemical potentials (E=0–2000mV) were applied using a potentiostat (ROXY Potentiostat, Antec). Sample solutions, prepared with 10 μM of adenosine, dissolved in 5mM of ammonium acetate, containing 50% of acetonitrile (v/v) were delivered through the electrochemical cell by a syringe pump with a flow rate of 10 μL/min. Eluting compounds were detected by electrospray ionization (ESI)-MS in positive ion mode. Accurate molecular mass measurements and MS/MS experiments were used to characterize the oxidation products: the adenine signal (m/z = 136 Da) was found in the mass spectrum with electrochemical cell ON, indicating the cleavage of the bond between the purine ring and the pentose molecule (Figure 19).

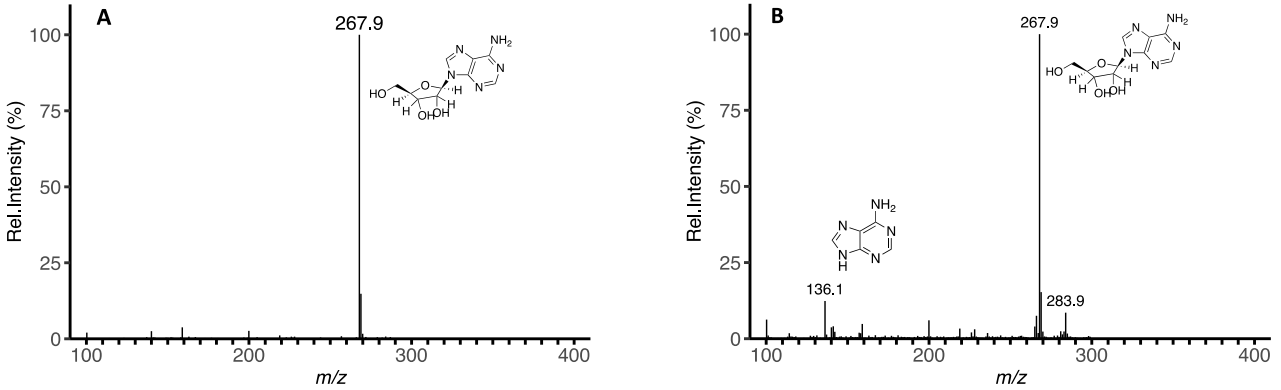

Figure 19: Mass spectra obtained of Adenosine at positive ionization mode with electrochemical cell OFF (panel A) and electrochemical cell ON (panel B)

Considering that these conditions led to the cleavage of the glycosidic bond, we applied the same conditions to our compounds. Unfortunately, the application of EC cell voltage to our compounds, under the above-described condition, suggested that the oxidation of C8 and aromatic hydroxylation metabolism might be the major biotransformation pathways, with no evidence of cleavage of the glycosidic bond since the peak of the nucleobase (m/z = 415) was not observable (Figure 20). Based on the mass fragmentation behaviors of the parent compounds and on the accurate masses of the respective ions, the HRMS technique was able to generate valuable structural information allowing to designate and identify the potential metabolites.

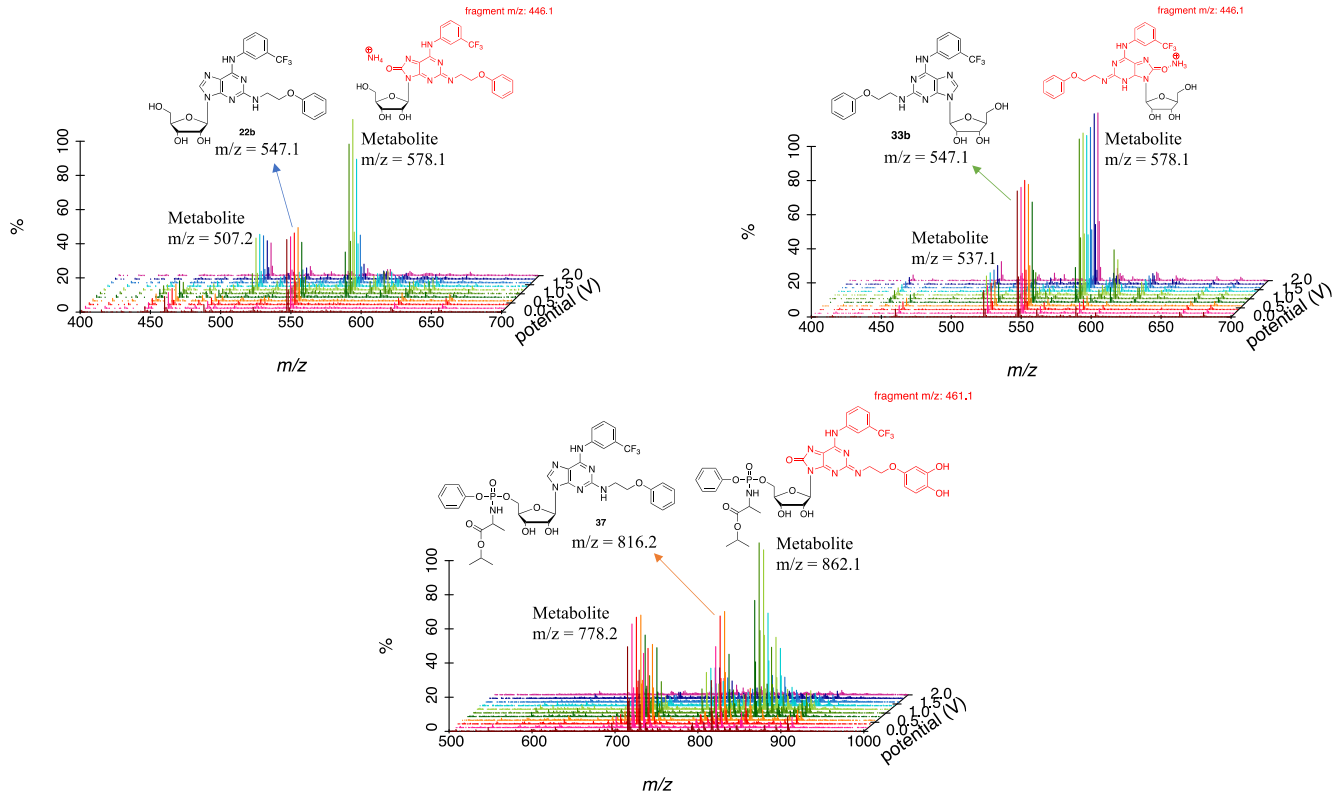

Figure 20: Voltammograms of oxidation products of D-nucleoside, L-nucleoside and protide, obtained under neutral conditions (ammonium acetate)

Since the synthesis of potential metabolites by electrochemistry depends on several parameters, we investigated different conditions, such as solvent and pH. However, no cleavage of the glycosidic bond was observed, and at low pH, multiple mass peaks, difficult to identify, were observed. Under conditions where the desired glycosidic cleavage is observed in adenosine, our products only give a number of oxidation derivatives.

Finally, the oxidative stability and generated metabolites observed with the EC-ESI-MS system were compared with the results of a traditional P450 study to evaluate if our compound were metabolically unstable or if the obtained results were due to drastically adopted electrochemically conditions. Human liver microsomes and rat liver microsomes were used for the experiment. Surprisingly, these results are divergent: an extensive adenosine metabolism was observed, although the found metabolites are not attributable to the free base, as assumed at the outset, and as observed for EC-MS experiment; while our compounds were characterized by high metabolic stability, with no evidence of metabolites, in contrast with the results obtained with EC-MS experiment. The discrepancy between EC/MS analysis and the results of a traditional P450 study clearly suggests that the molecules have low oxidative potential, but the oxidation processes occurring in the cells don't affect them.

2.3.5 Biological results

Initially, D-nucleoside derivatives, including the acetylated ones and the prodrugs, were evaluated for their potency against Flaviviruses[160]. Except for **22a** (CC_{50} > 200 μM), the first set of tested compounds showed borderline citoxicity on Huh7. Nevertheless, compounds **22a-d**, **25c,d** showed low micromolar activity against DENV and these values were comparable under DYRA and SYRA conditions. Instead, **28a,d** didn't show any activity against DENV.

Next, compounds **22a-d**, **25c,d** and **28a,d** were submitted to biological tests to evaluate anti-WNV activity in a Huh7 hepatoma cells under DYRA conditions[160]. Only the compounds **22b,c** and **25c** showed activity against WNV. To further explore the broad-spectrum antiviral activity of this first set of base-modified nucleosides, **22a-d**, **25c,d** and **28a,d** were tested against HIV[161] and SARS-CoV-2[160]. In H9 cell line only compounds **22b** and **25c** were able to inhibit HIV replication at low micromolar concentrations while, in Caco-2 cells, **22b** was characterized by interesting EC_{50}values against SARS-CoV-2. As evident in Table 13, only two compounds showed promising broad-spectrum activity: **22b** was active against DENV, HIV and SARS-CoV-2, whereas compound **25c** was active against DENV, WNV and HIV.

Table 13. Cytotoxicity and DENV-2/WNV/HIV and SARS-CoV-2 replication inhibitory effect.

		DENV-2		**WNV**	**HIV**		**SARS-CoV-2**	
Cpd.	**Huh7 CC_{50}**[a] (μM)	**IC_{50}**[b] DYRA (μM)	**IC_{50}**[c] SYRA (μM	**IC_{50}**[b] DYRA (μM)	**H9 CC_{50}** (μM	**IC_{50}** (μM)	**Caco-2 CC_{50}** (μM	**IC_{50}** (μM)
22a	>200	NA[d]	27.1	NA	60	NA	100	NA
22b	15.0	1.1	1.15	1.1	40	8.60	17	2.8
22c	25	6.05	3.9	10.2	37	NA	57	NA
22d	65	14.8	6.45	NA	45	NA	85	17.2
25c	26	4.8	5.0	9.0	40	6.35	54	NA
25d	60	17.5	6.75	NA	45	NA	55	NA
28a	26	NA	NA	NA	42	NA	35	NA
28d	18	NA	NA	NA	9	NA	32	NA

[a]CC_{50}: half-maximal cytotoxic concentration (μM); [b]IC_{50}: half-maximal inhibitory concentration calculated through DYRA, each value is the mean of three experiments ± standard deviation (SD); [c]IC_{50}: half-maximal inhibitory concentration calculated through SYRA; [d]NA: not active

Next, the second set of compounds, including L-nucleosides, protide, and acyclic nucleosides, were evaluated for their activity against DENV. For almost all compounds, the values of CC_{50} in Huh7 cell

line, as shown in Table 14, were higher in comparison to their counterpart D-nucleosides. Unfortunately, only compound **33a** showed low micromolar value of IC_{50}, and thus it was tested also against WNV, without obtaining interesting values. The other compounds, since were non active against DENV, were not tested against WNV.

The second set of compounds were evaluated also for their activity against SARS-CoV-2. Among the tested compounds, only compound **46d** was endowed with interesting activity against SARS-CoV-2 with a IC_{50} value of 1.4 μM.

Table 14. Cytotoxicity and DENV-2/WNV replication inhibitory effect.

		DENV-2	**WNV**	**SARS-CoV-2**	
Cpd.	**Huh7 CC_{50}**[a] (μM)	**IC_{50}**[b] DYRA (μM)	**IC_{50}** DYRA (μM)	**CACO-2 CC_{50}** (μM)	**IC_{50}**
33a	28.2	9.5 ± 3.5	NA[c]	24.5	NA
33b	16.5	NA	ND[d]	22.0	NA
33c	95.2	NA	ND	161.6	NA
33d	40.9	NA	ND	60.1	NA
34c	ND	ND	ND	ND	ND
34d	63.6	NA	ND	86.8	NA
37	7.7	NA	ND	8.3	NA
46a	20	NA	ND	62.4	NA
46b	139.9 ± 3.8	NA	ND	112.9	NA
46c	38.5 ± 2.8	NA	ND	181.9	NA
46d	74.1 ± 16.1	NA	ND	40	1.4

[a]CC_{50}: half-maximal cytotoxic concentration (μM); [b]IC_{50}: half-maximal inhibitory concentration calculated through DYRA, each value is the mean of three experiments ± standard deviation (SD); [c]NA: not active ; [d]ND: non determinated.

Finally, the D-nucleoside derivatives which showed activity against almost one virus, were evaluated against selected bacteria[162]. As shown in Table 15, **22a**, **22c**, **22d** were endowed with antibacterial activity against all tested Gram positive (MIC values 32 μg/mL). Also **25c** and **25d** presented antibacterial activity against almost one Gram positive. Next, given the lack of activity of tested compounds on Gram negative, their potential synergistic activity in the presence of sub-inhibitory concentration of colistin, a polymyxin well-known for its membrane permeabilization properties, were evaluated. Remarkably, in the presence of sub-inhibitory concentration of colistin, the D-nucleosides possess antibacterial activity against Gram negative, except for P.aeruginosa, (Table 16).

Thus, these compounds have the potential to be active on Gram-negative bacteria and their lack of activity, when used alone, is likely relying on poor diffusion through the outer membrane.

Table 15. In vitro antibacterial activity (MIC) of composts in reference strains.

	MIC/MBC (µg/ml)[a]							
	Bsu	Efa	Spy	Sau	Eco	Kpn	Aba	Pae
22a	32/>64	>64	32/>64	>64	>64	>64	>64	>64
22b	>64	>64	>64	>64	>64	>64	>64	>64
22c	32/>64	32/>64	32/>64	64/>64	>64	>64	>64	>64
22d	>64	>64	>64	>64	>64	>64	>64	>64
25c	>64	>64	32/>64	>64	>64	>64	>64	>64
25d	>64	>64	32/>64	>64	>64	>64	>64	>64

[a]Tested organisms: Gram-positive bacteria: Bacillus subtilis ATCC 6633 (Bsu), Enterococcus faecalis ATCC 29212 (Efa), Streptococcus pyogenes ATCC 12344 (Spy), Staphylococcus aureus ATCC 25923 (Sau); Gram-negative bacteria: Escherichia coli CCUGT (Eco), Klebsiella pneumoniae ATCC 13833 (Kpn), Acinetobacter baumannii ATCC 17978 (Aba), Pseudomonas aeruginosa ATCC 27853 (Pae).

Table 16. Synergistic antibacterial activity on Gram-negative bacteria with sub-inhibitory concentration of colistin

	MIC/MBC (µg/ml)[a] in the presence of 0.25 x MIC colistin[a]			
	Eco[b]	Kpn[c]	Aba[d]	Pae[e]
22a	8(>8)	16 (>4)	16 (>4)	>64
22b	8 (>8)	16 (>4)	32 (>2)	>64
22c	16 (>4)	32 (>2)	16 (>4)	64/>64
22d	64(>1)	>64	32(>2)	>64
25c	32 (>2)	16 (>4)	32(>2)	>64
25d	64(>1)	>64	64(>1)	>64

[a]Colistin concentration was 0.12 (Eco, Kpn) and 0.25 (Aba, Pae) µg/mL; [b]Escherichia coli CCUGT (Eco), [c]Klebsiella pneumoniae ATCC 13833 (Kpn), [d]Acinetobacter baumannii ATCC 17978 (Aba), [e]Pseudomonas aeruginosa ATCC 27853 (Pae).

2.3.6 Conclusion

We have prepared and tested a series of ribonucleosides and acyclic derivatives of the most interesting antiviral purines previously synthesized, together with a few prodrugs (comprising a phosphoramidate derivative). The aim was to investigate whether we can achieve an antiviral effect through base-modified nucleosides and at the same time if a metabolic cleavage of the glycosidic bond may lead to the release *in vivo* of the free nucleobases that we know to be endowed with antiviral activity. Considering that there is a huge literature that confirms that L-nucleoside analogs possess antiviral activity, we thought to synthetize also the L-nucleoside counterparts. The synthetised compounds were tested against DENV, WNV, HIV and SARS-CoV-2. We found that some of the synthetized D- nucleosides showed micromolar activities against ZIKV, WNV, DENV, and SARS-CoV-2 viruses, even if with a low selectivity index. Surprisingly, the protide did not shown any antiviral activity, although it is known from many previous studies that the monophosphate prodrugs of antiviral nucleosides are typically much more efficient [163,164,165,166,167,168,169]. Interestingly, we found that L- nucleosides and acyclic nucleosides didn't exert antiviral activity, except for the activity of **33a** on DENV-2 and **46d** on SARS-CoV-2.

We found that the most active D-nucleoside was the nucleoside **22b**, which inhibited the viral replication of DENV, WNV, HIV and SARS-CoV-2 at low micromolar range. To confirm our rationale of having an antiviral dual-acting agent both as a single entity and, after likely metabolic cleavage of glycoside bond, as nucleobase, we used the electrochemistry/mass spectrometry technique to experimentally evaluate the possible *in vivo* cleavage of the glycosidic bond with the release of the nucleobases. Under conditions where the desired glycosidic cleavage of adenosine is observed, our products only gave a few oxidation metabolites, without cleavage of the glycosidic bond. These results were partially confirmed by preliminary metabolic stability studies in Human Liver Microsomes (HLMs), which showed high stability under standard assay conditions (data not shown).

Finally, the more interesting D-nucleosides were selected for the evaluation of their activity against the selected bacteria. Surprising, they showed promising antibacterial activity on at least one tested Gram-positive organisms and on tested Gram-negative in the presence of sub-inhibitory concentration of colistin, except for **22b** which didn't exhibit antibacterial activity.

3. TARGET-BASED DRUG DISCOVERY

3.1 Purine Derivatives as Inhibitors of Viral and Host Helicases

3.1.1 Introduction

Both DNA and RNA helicases are considered enzymes that catalyze the separation of double-stranded nucleic acid. They utilize ATP, whose hydrolysis results in chemical energy needed to move along DNA or RNA, separating the double strands into their complementary single strands[170]. These enzymes perform a high variety of functions that are connected with nucleic acids. Currently, RNA helicases are divided into 6 superfamilies (named SF1-SF6). This classification is based on the characteristics of conserved motifs in primary sequences[171]. Superfamily 1 and 2 helicases have similar structural features, including two RecA-like domains where all conserved helicase motifs are located.

Viruses possess their own helicases that play critical roles in viral replication, transcription, and translation. Viral helicases belong to three out of the six currently recognized super-families: SF1, SF2, and SF3[172]. These key enzymes require in-depth study, not only because they play an essential role in the viral lifecycle, but also as targets for antiviral therapeutics, since helicases have been found in many viruses, responsible for threats to human health, including the novel coronavirus. The rapid global spread of SARS-CoV-2 has led to a focus on characterizing the viral genome. Previous outbreaks of SARS and MERS in 2002 and 2012 respectively, have led to the characterization of non-structural protein 13 (nsp13), which can unwind DNA or RNA in an NTP-dependent manner with a 5' to 3' polarity[173,174,175,176,177,178], demonstrating critical indispensable roles in replication-transcription complexes (RTC)[179] and thus in the life cycle of coronaviruses[180,181,182]. Subsequently, high homology with 99.8% sequence was detected between SARS-CoV-1 and SARS-CoV-2[183], making it a promising target for pan-coronavirus antiviral agents[184,185].

Nsp13 belongs to the SF1B superfamily and has two associated activities: RNA unwinding and a NTPase activity[186]. It consists of two canonical RecA ATPase domains, an N-terminal zinc-binding domain (ZBD), a stalk and 1B domain[187,188]. NSP13, and helicase in general, are not yet fully exploited as targets for antiviral drug discovery yet. Recently, however, some compounds have been reported to inhibit SARS-CoV-2 helicase activity, among these non-natural[189,190] and natural compounds such as flavonoids[191,192,193].

Although CoVs possess their own RNA helicases, they hijack multiple host factors, including cellular RNA helicases, to positively influence genome transcription and viral replication, and act as pro-viral effectors [194,195,196]. Among those, DEAD-box (DDX) RNA helicases have emerged as important players in the host-pathogen interaction network, by modulating innate immunity and viral replication in multiple ways. A number of viruses (e.g. HCV, HEV, HIV-1, SARS-CoV-2) hijack DDX3

helicase, to facilitate various steps of their replication cycles (reverse transcription, transcription, and nuclear export)[197,198,199,200,201]. In addition, comparative protein sequences analyses reveal structural similarity of SARS-CoV-2 Nsp13 with human DDX helicases, despite low sequence identity[202].

3.1.2 Aim of the work

Considering the high structural similarity between SARS-CoV-2 Nsp13 and host helicases[199], we thought that the target-based identification of novel Nsp13 inhibitors that may act as BSAAs by also inhibiting DDX3, a host factor that may be less prone to select drug resistance, may represent a promising approach to identify SARS-CoV-2 antivirals.

In the attempt of identifying new SARS-CoV-2 inhibitors, virtual screening studies have been carried out on our internal library of molecules: blind docking on the X-ray structure of SARS-CoV-2 Nsp13 (PDB code: 7NN0) has been employed to select those compounds able to binding the RNA bind site, which represents a conserved pocket among coronaviruses and is targeted by the known coronavirus helicase inhibitor SSYA10-001[182]. Top-ranking compounds (14 molecules belonging to different chemotypes) were then tested in vitro for their ability to inhibit both the helicase and ATPase activity of Nsp13 and positive hits were then evaluated for their ability to inhibit SARS-CoV-2 replication at 30 μM in VeroE6 cells (Figure 21). Surprisingly, compound MR333 (corresponding to the purine derivative **12i**) resulted in a specific inhibitor of Nsp13 helicase activity and the more potent antiviral among the selected compounds, further supporting the multitarget nature of this class of antivirals.

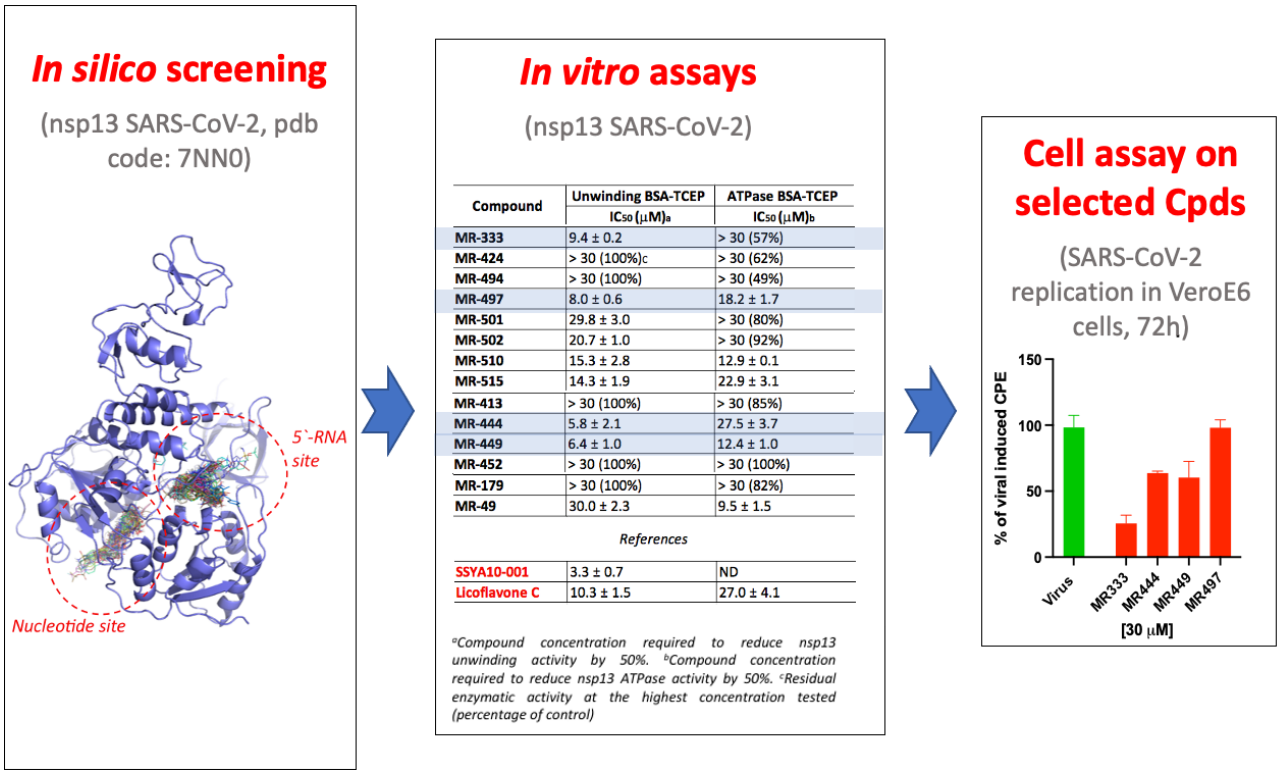

Compound	Unwinding BSA-TCEP IC50 (μM)a	ATPase BSA-TCEP IC50 (μM)b
MR-333	9.4 ± 0.2	> 30 (57%)
MR-424	> 30 (100%)c	> 30 (62%)
MR-494	> 30 (100%)	> 30 (49%)
MR-497	8.0 ± 0.6	18.2 ± 1.7
MR-501	29.8 ± 3.0	> 30 (80%)
MR-502	20.7 ± 1.0	> 30 (92%)
MR-510	15.3 ± 2.8	12.9 ± 0.1
MR-515	14.3 ± 1.9	22.9 ± 3.1
MR-413	> 30 (100%)	> 30 (85%)
MR-444	5.8 ± 2.1	27.5 ± 3.7
MR-449	6.4 ± 1.0	12.4 ± 1.0
MR-452	> 30 (100%)	> 30 (100%)
MR-179	> 30 (100%)	> 30 (82%)
MR-49	30.0 ± 2.3	9.5 ± 1.5
References		
SSYA10-001	3.3 ± 0.7	ND
Licoflavone C	10.3 ± 1.5	27.0 ± 4.1

aCompound concentration required to reduce nsp13 unwinding activity by 50%. bCompound concentration required to reduce nsp13 ATPase activity by 50%. cResidual enzymatic activity at the highest concentration tested (percentage of control)

Figure 21. Workflow and preliminary data on the identification of novel nsp13 inhibitors

Considering these interesting results, we decided to synthesize a new series of analogues of compound **12i** designed to better fill the Nsp13 RNA binding pocket and draw structure-activity relationships that may lead to the obtainment of more potent antivirals (Figure 22). To do this we have planned to

methylate one or more NH of the lead **12i** to evaluate the need of these hydrogen donor motif and eventually exploit the "magic methyl" concept.[203,204] We also planned to modify the C2 side chain by increasing the steric hindrance or including radical scavenging moieties to add an antioxidant effect.[205,206] Target compounds will be finally tested as Nsp13 inhibitors, and the more potent molecules will be also tested against the host helicase DDX3 to evaluate their pan-helicase or specific activity.

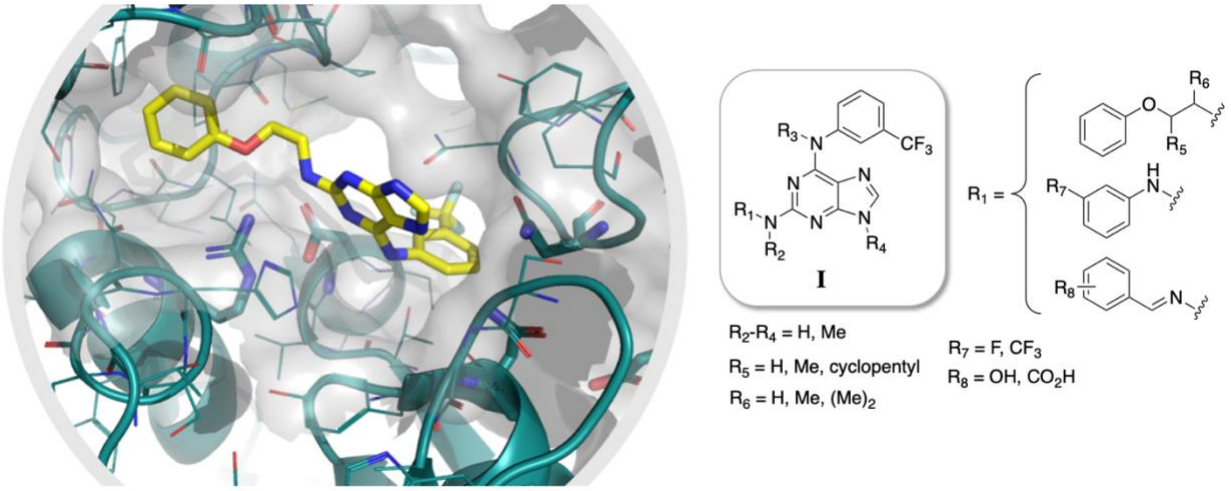

Figure 22. Docking pose of MR333 (**12i**) within the RNA binding pocket of SARS-CoV-2 Nsp13 and general structure (I) of the planned target compounds.

3.1.3 Results and discussion

In this first part of the work, we started with the synthesis of the NH methylated analogues of **12i**. In order to achieve this objective, it was necessary to synthesize the secondary amines (**51** and **52**) to be attached in position C2 and C6 of the purine core. In the synthesis of **51**, we started from 2-phenoxyethylamine **11b**, which was monoprotected with a Boc group to avoid the NH_2 double methylation (Scheme 18). The reaction was conducted under anhydrous conditions with anhydrous DCM for 3h at room temperature (r.t.). After obtaining the compound protected with Boc **49**, it was possible to proceed with the NH methylation. The protected intermediate **49** was solubilized in THF dry, treated with NaH, and finally, CH_3I was added. The reaction mixture was heated to 45 °C for 48 hours. The third step of the synthesis was the deprotection of the compound **50** with TFA to obtain the desired secondary amine **51**.

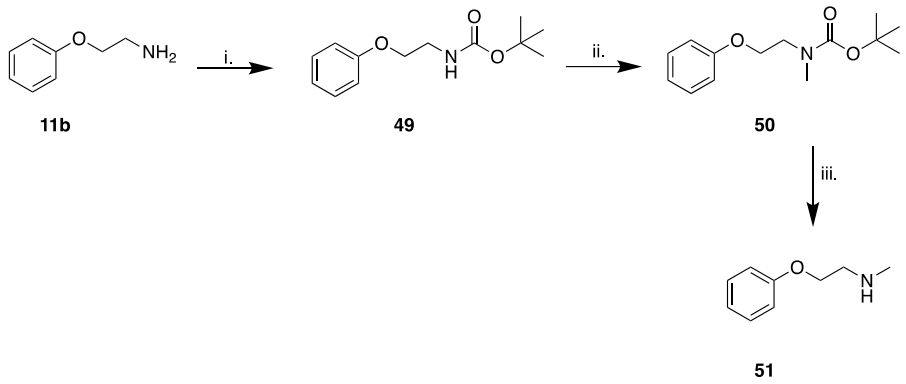

Scheme 18. *Reagents and conditions*: *i*. di-tertbutyl dicarbonate, Et_3N, DCM dry, r.t., 3h; *ii*. CH_3I, NaH, THF, 45 °C, o.n.; *iii*. DCM dry, TFA, r.t., 12 h.

For the synthesis of the secondary amine **52**, sodium methoxide was added to a solution of 3-trifluoromethylaniline **9c** in anhydrous MeOH. Paraformaldehyde was then added, and the reaction mixture was kept at r.t. for 2h. After this time, $NaBH_4$ was added, and the mixture was heated to 60 ºC until the starting material disappeared (Scheme 19).

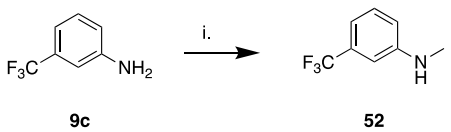

Scheme 19. *Reagents and conditions*: *i*. a) Na, MeOH, r.t. 1 h; b) $(CH_2O)_n$, r.t., 2 h; c) $NaBH_4$, 60°C, 6 h

Once the secondary amines were obtained, they were reacted with 2,6-dichloropurin **8a** and with the N9 methylated 2,6-dichloropurin **8b** (obtained according to Scheme 20) to obtain the target final products **54a-g**.

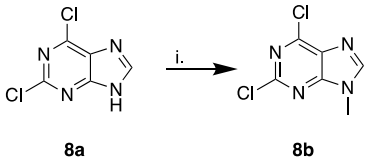

Scheme 20. *Reagents and conditions*: *i*. CH_3I, NaH, THF, 45 °C, 2h.

The first step for the synthesis of **54a-g** was a nucleophilic substitution reaction on 2,6-dichloropurine **8a,b** with intermediates **9c** or **52**. A solution of **8a** or **8b** in n-BuOH was treated with an excess of primary or secondary amine, **9c** or **52** respectively, in the presence of Et_3N. The mixture was microwave heated at 120 ºC for 30 min, thus obtaining the intermediated **53a-c** and **10c** (whose synthesis was already described in Chapter 2.2 in Scheme 3). Final compounds **54a-g** were finally obtained by heating **53a-c** or **10c** with 2-phenoxyethylamines **11b** or **51** at 170 °C-180 °C under microwave irradiation (Scheme 21). The different combination of reagents led also to the formation of **10c** in the first step and **12i** in the second step, that were not reported here since they already described in Chapter 2.2 (See Scheme 3).

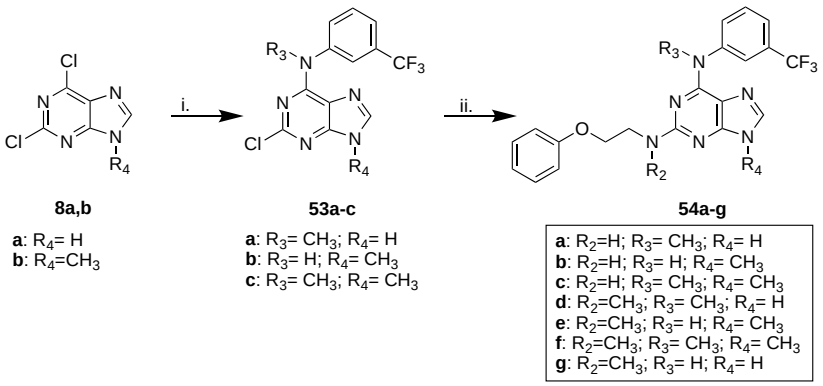

Schema 21. *Reagents e conditions*: *i.* **9c** or **52,** Et_3N, n-BuOH, µW, 120 °C, 30min; *ii*. **11b** or **51**, TFA, n-BuOH, µW, 170°C-180°C, 105-150 min.

Next, we focused our work on the functionalization of the C2 side-chain in of **12i**. To do this, we used a microwave-assisted synthetic protocol previously developed in our laboratory. In the first step, a nucleophilic substitution of the chlorine atom in C6 of **8a** with an excess of 3-(trifluoromethyl)aniline (**9c**) afforded the intermediate **10c** in presence of Et_3N at reflux overnight. The second step consisted in the displacement of chlorine atom in C2 with selected primary amines: 1-amino-2-propanol (**56a**), 2-amino-1-propanol (**56b**), 1-amino-2-methylpropan-2-ol (**56c**), 1-(aminomethyl)cyclopenanol (**56d**). The reaction proceeded in the presence of trifluoroacetic acid

(TFA), heating under microwave irradiation at 170°C for a few minutes, thus obtaining the key intermediates **57a-d** in moderate to good yields (Scheme 22). To obtain the desired final compounds, the OH group of latter intermediates must be converted in a PhO group.

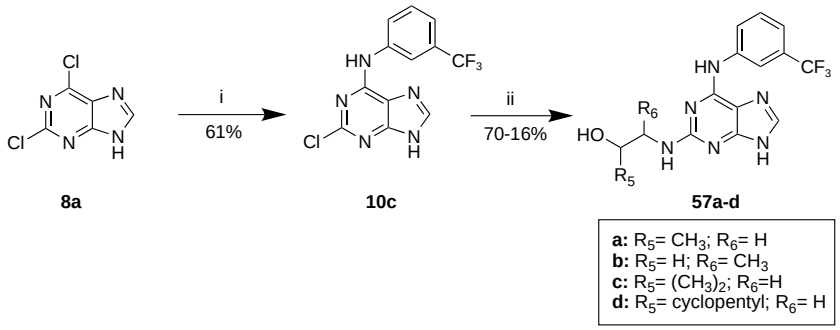

Scheme 22. Reagents and conditions: *i.* **9c**, Et_3N, n-BuOH, reflux, 24h; *ii*. **56a-d**, TFA, n-BuOH, mW 170°C, 30-120 min.

To set up a synthetic protocol that could lead us to these final compounds, **12h** was used as template molecules.

In a first attempt, compound **12h** was brominated with an excess of carbontetrabromide (CBr_4), in presence of triphenylphosphine (Ph_3P), using N,N-dimethylacetamide (DMA) as solvent, at room temperature for 24h to obtain the desired intermediate **58**. The last step was a coupling between intermediate **58** and mono-substituted phenols (salicylic acid **59a**; methyl p-hydroxy benzoate **59b**). This reaction was conducted in presence of potassium carbonate (K_2CO_3), using dimethylformamide as solvent, at room temperature for 24h. Unfortunately, this synthetic approach didn't allow us to obtain the desired products **60a,b** (Scheme 23).

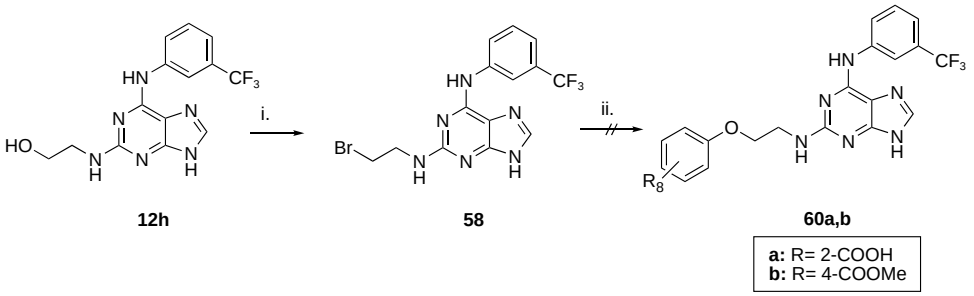

Scheme 23. *Reagents and conditions: i*. CBr_4, Ph_3P, DMA, r.t., 24h; *ii.* **59a** or **59b**, K_2CO_3, DMF, r.t., 24h.

Considering the failure of this synthetic approach, we decided to functionalize the C2 chain of compound **12h** by running a Mitsunobu reaction[207] with methyl p-hydroxy benzoate, as reported in Scheme 24. This reaction was conducted in the presence of triphenylphosphine,

diethylazadicarboxylate (DEAD), using tetrahydrofuran anhydrous as solvent. Also in this case, we didn't obtain the desired product **60b**, but surprisingly we obtained compound **61**, as confirmed by mass and NMR analysis. The reason for the formation of this side product should be due to the pKa value of OH group of methyl p-hydroxy benzoate, which was less acid than NH in the 9 position of the purine core.

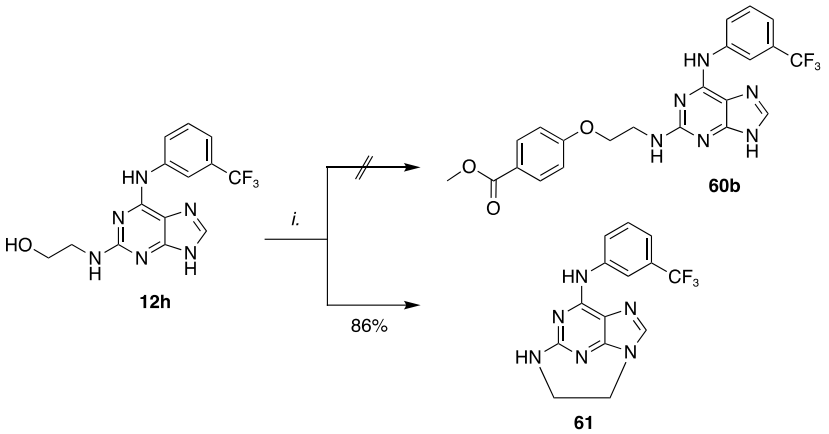

Scheme 24. *Reagents and conditions: i.* methyl p-hydroxybenzoate **59b**, DEAD, Ph_3P, THF dry, r.t., 28h.

To obtain the desired product **60b**, we decided to protect the NH groups before running the Mitsunobu reaction. The first attempt to protect the NH group with di-tert-butyl dicarbonate led to the protection of both NH and OH groups, and selective deprotection of the OH group to run Mitsunobu reaction was not possible (Scheme 25).

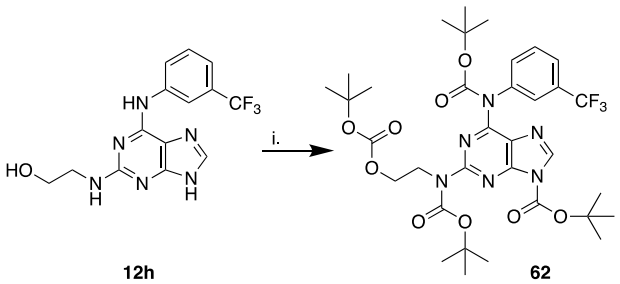

Scheme 25. *Reagents and conditions: i.* di-tertbutyl dicarbonate, Et_3N, DCM dry, r.t., 3h.

Thus, orthogonal protection of NH and OH groups was needed to obtain **60b**: after OH protection of **12h** with tertbutyldiphenylchlorosilane, the resulting intermediate **63** was reacted with di-tert-butyl dicarbonate leading to the fully protected compound **64**. Next, removal of tert-butyl diphenylsilane with TBAF led to the intermediate **65** but the following Mitsunobu reaction did not lead to the desired compound **60b** but, again, to the side product **61** (Scheme 26).

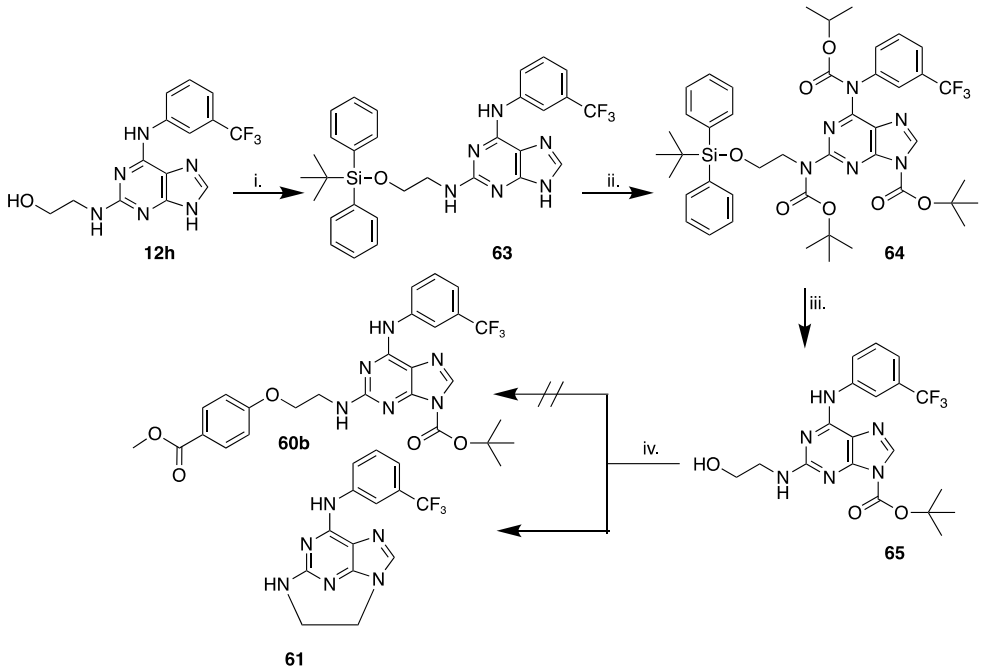

Scheme 26. *Reagents and conditions: i*. t-butyldiphenylchlorosilane, imidazole, DMF, 2h; *ii*. di-tert-butyl dicarbonate, Et_3N, DCM dry, r.t., 3h; *iii.* TBAF, DCM, r.t., 1h.; *iv*. methyl p-hydroxybenzoate, DEAD, Ph_3P, THF dry, r.t., 28h.

Considering the failure of the previous approached, we decided to synthesize the substituted 2-phenoxyethylamines **70a,b** to be used for the C2 nucleophilic substitution on the 2-chloropurine intermediate. The two chains were synthesized according to Scheme 27.

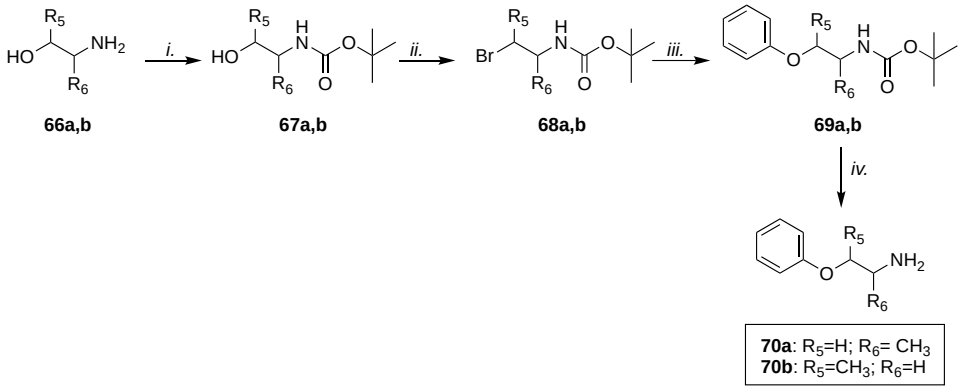

Scheme 27. *Reagents and conditions: i.* di-tertbutyl dicarbonate, Et_3N, DCM dry, r.t., 3h; *ii*. CBr_4, Ph_3P, DMA, r.t., 24h; *iii.* phenol, K_2CO_3, DMF, r.t., o.n.; *iv*. TFA, dry DCM, r.t., 1h.

Commercially available amines **66a,b** were protected on NH_2 with di-tert-butyl dicarbonate, followed by bromination of OH with CBr_4 and Ph_3P. A coupling reaction was performed with phenol to obtain compounds **69a,b**. Deprotection of NH_2 allowed the obtainment of the final amine **70a,b** to be reacted with intermediate **10c** in a microwave reaction, allowing the obtainment of derivatives of **12i** with a methyl group on the ethanolamine chain (Scheme 28).

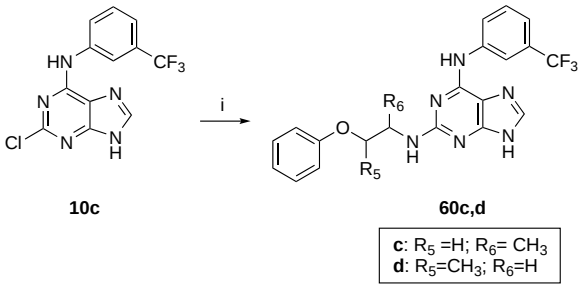

Scheme 28. Reagents and conditions: *i.* **70a,b**, TFA, n-BuOH, µW 170°C, 30-120 min.

A further functionalization consisted in the synthesis of 2,6-diaminopurine derivatives with a phenylhydrazine side chain in C2 to study the inhibition of Nsp13 and contemporary including an antioxidant function for the following cell-based assays. To do this, compound **10c** was reacted with substituted hydrazines to obtain the final compounds **71**. The choice of the substituted hydrazines was based on the previous results from C6 hydrazino-substituted derivatives with broad-spectrum antiviral activity and antioxidant activity (See Chapter 2.2). Thus, replacement of the chlorine atom in C2 of the intermediate **10c** with an excess of 3-fluoro-phenylhydrazine **17** or 3-trifluoromethyl-phenylhydrazine **17b** under microwave irradiation at 150 ºC in the presence of TFA, led to the desired final compounds **71a,b** (Scheme 29).

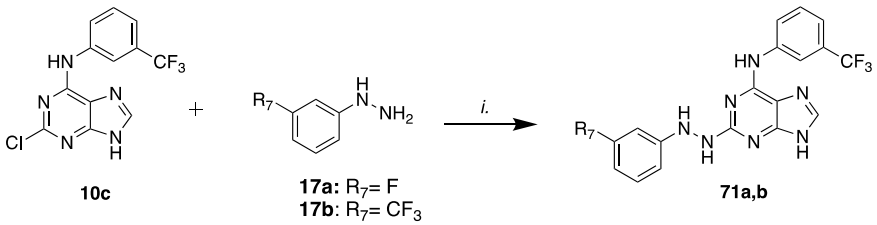

Scheme 29. *Reagents and conditions: i.* n-BuOH, TFA, µW, 150°C, 45 min.

The following final compounds were characterized a substituted phenylhydrazones chain in C2 of the purine core. To insert the hydrazone moiety, intermediate **10c** was initially reacted with hydrazine or methylhydrazine to give the key intermediates **72a,b** respectively. The reaction occurred in acid butanol by microwave heating at 170 C for 30 min. The hydrazine intermediates **72a,b** were finally condensed with substituted benzaldehydes to give the final compounds **74a-k** (Scheme 30, Table 17). The choice of the benzaldehydes substituents was based on literature data on radical scavenging hydrazones [203,208].

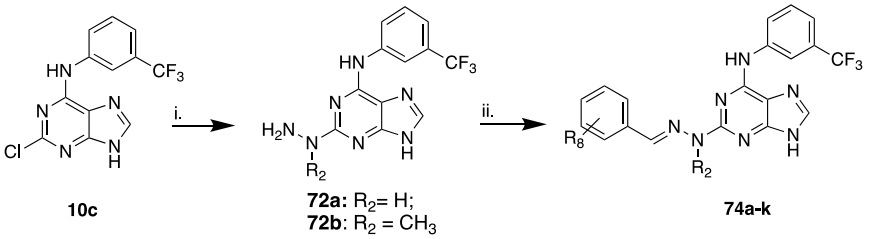

Scheme 30. *Reagents and conditions: i.* NH_2-NHR, n-BuOH, TFA, µW, 170°C, 30 min. *ii.* R_1PhCHO **73a-g**, CH_3COOH, EtOH; reflux, 12 h

Table 17. Substituents and yields of **74a-k** compounds

Cmp.	**R_2**	**R_8**	yields	Cmp.	**R_2**	**R_8**	yields
74a	H	2-OH	56%	**74h**	H	3-COOH	32%
74b	H	4-OH	56%	**74i**	H	2-COOH	30%
74c	H	3-OH	45%	**74l**	CH_3	4-COOH	43%
74d	CH_3	2-OH	64%	**74m**	CH_3	3-COOH	32%
74e	CH_3	4-OH	80%	**74n**	CH_3	2-COOH	56%
74f	CH_3	3-OH	67%	**74j**	H	H	38%
74g	H	4-COOH	36%	**74k**	CH_3	H	38%

Before conducting the biological evaluation of all synthesized compounds on Nsp13 and DDX3, we also synthesized two known DDX3 inhibitors to be used as reference compounds[196,197]. Reference molecules **47-48** with known activity, targeting the RNA binding pocket and the ATP binding pocket respectively (Figure 23).

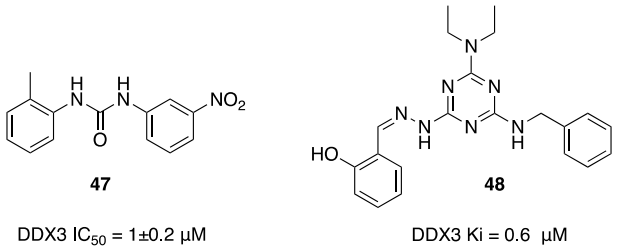

Figure 23: DDX3 inhibitors targeting the RNA binding pocket (compound **47**) and the ATP binding pocket (compound **48**)

Starting from the commercially available building block **75** and isocyanate **76**, the desired N,N'-diaryl urea **47**, an inhibitor of helicase activity was obtained in quantitative yield after stirring for 16 h at room temperature (Scheme 31). While for the synthesis of compound **48**, commercially available cyanuric chloride **77** was submitted by consecutive nucleophilic substitutions. The first chlorine of **77** was displaced with the moderately nucleophilic benzylamine **78** at −30 °C for 3h to give the

monosubstituted triazines **79**. Subsequent treatment with a more nucleophilic amine, Et_3N, provided the disubstituted triazine **80**. The remaining chlorine of disubstituted triazines was replaced by treatment with excess hydrazine at reflux to afford the corresponding 2,4,6-trisubstituted triazine intermediates **81**, which were finally allowed to react with salicylic aldehyde **82** to give the final compounds **48** (Scheme 32).

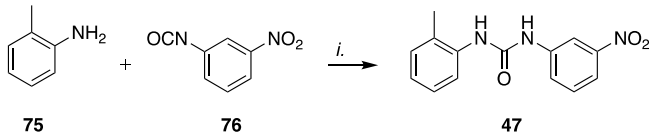

Scheme 31. *Reagents and conditions: i.* CH_2Cl_2, 16h, rt.

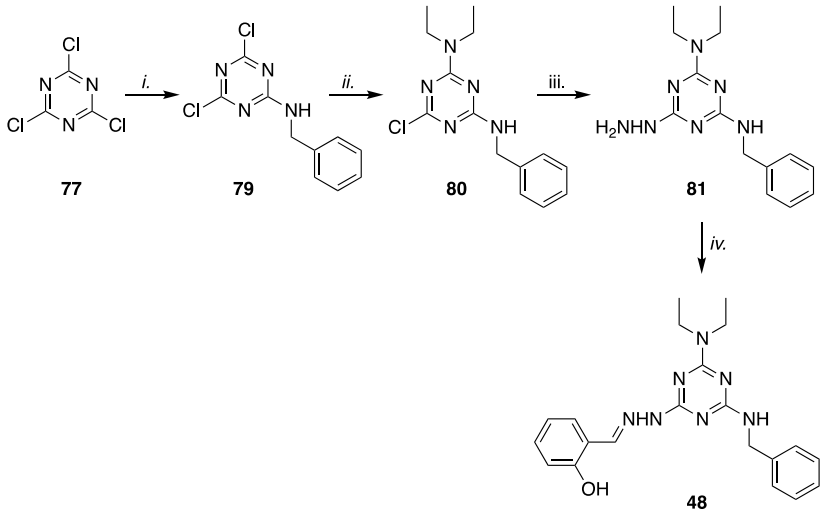

Scheme 32. *Reagents and conditions*: *i.* DME, −30 °C, $BnNH_2$ **78**, 3h; *ii.* CH_2Cl_2, Et_3N, r.t., 12h; *iii.* CH_2Cl_2, $NH_2NH_2{\cdot}H_2O$, reflux, 12h; *iv*. toluene, salicylaldehyde **82**, 3h, reflux, Dean–Stark.

3.1.4 Biological results

Compound SSYA10−00123 was used as the control, showing an IC_{50} value of 5.14 μM on SARS-CoV-2 nsp13 unwinding-associated activity, but it doesn't block the ATPase activity as previously reported for SARS-CoV[209]

Out of the 24 tested compounds, 16 inhibited the nsp13-associated unwinding activity, showing IC_{50} values below 30μM (Table 18), with values, many of which, comparable and sometimes better than reference compounds. Within the subset of active compounds, 5 were able to also inhibit the ATPase activity.

Table 18. Inhibition of SARS-CoV-2 nsp13 Helicase- Associated Activities

Cpds.	Unwinding BSA-TCEP IC_{50} (μM)[a]	ATPase BSA-TCEP IC_{50} (μM)[b]
54a	9.54 ± 0.48	>30 (85%)
54b	> 30 (60%)[c]	>30 (73%)
54c	> 30 (100%)	>30 (81%)
54d	5.18 ± 0.60	16.9 ± 0.705
54e	> 30 (100%)	>30 (87%)
54f	> 30 (73%)	>30 (69%)
54g	6.21 ± 1.54	4.9 ± 0.56
71a	7.07 ± 1.34	> 30 (57%)
71b	8.83 ± 1.61	> 30 (66%)
74a	2.91 ± 0.53	> 30 (89%)
74b	8.02 ± 0.08	11.43 ± 0.55
74c	29.8 ± 3.0	> 30 (80%)
74d	> 30 (85%)	> 30 (100%)
74e	16.06 ± 6.26	> 30 (92%)
74f	20.7 ± 1.0	> 30 (92%)
74g	> 30 (100%)	> 30 (49%)
74h	22.27 ± 0.74	30.56 ± 6.86
74i	2.56 ± 0.37	>30 (71%)
74l	8.0 ± 0.6	18.2 ± 1.7
74m	> 30 (70%)	> 30 (100%)

74n	> 30 (60%)	18.13 ± 0.2
74j	18.93 ± 1.25	>30 (83%)
74k	8.81 ± 0.81	>30 (80%)
SSYA10-001	5.14 ± 1.41	ND

[a]Compound concentration required to inhibit the SARS-CoV-2 nsp13-associated unwinding activity by 50%. [b]Compound concentration required to inhibit the SARS-CoV-2 nsp13-associated ATPase activity by 50%. [c]Residual enzymatic activity at the highest concentration tested

The compounds endowed with better results on nsp13 were selected for the evaluation of their inhibitory potency on human DDX3, but at this time we don't have the results of all tested compounds, since during the writing of this thesis, some of the biological tests have not been performed yet.

Table 19. Activity of selected compounds against helicase activity of DDX3

Cpds.[a]	Residual enzymatic activity
54a	NA[b]
54d	ND[c]
54g	74%
71a	ND
71b	ND
74a	49%
74b	40%
74e	ND
74h	NA
74i	52%
74l	NA
74n	48%
74j	ND
74k	ND
47	ND
48	ND

[a]Each compound was tested at 10 μM concentration; [b]NA: residual enzymatic activity > 98%; [c]ND: not determined.

The few obtained results are reported in Table 19, and among the eight tested compounds, four were able to reduce the enzymatic activity below 50%, demonstrating the highly advantageous potential of these molecules of targeting either viral or human helicases.

3.1.5 ABTS Assay

Considering that these molecules were drawn with a rationale to also have antioxidant activity, ABTS assay was performed to evaluate the experimental antioxidant activity (Figure 24).

From the obtained values from the first set of hydrazinic comopounds (Figure 24A), ascorbic acid was used as a reference molecule given its known antioxidant activity. Compound **19a**, synthetized in Chapter 2.2, became our reference compound in this set of plausible antioxidant compounds. It can be noted in Figure 24A that compound **71b** had values very similar to ascorbic acid. Moreover, the shift of the hydrazine substituent from C6 to C2, compared to compound **19a**, led to an increase in antioxidant ability; in fact, compound **71b** has a radical scavenger activity higher than the previous compound **19a** at the highest concentration used. Instead, the compound **71a** had lower activity of radical scavenger than the reference compound (ascorbic acid) and compound **71b**, but also had an antioxidant action that is promising, further supporting the potential antioxidant effect.

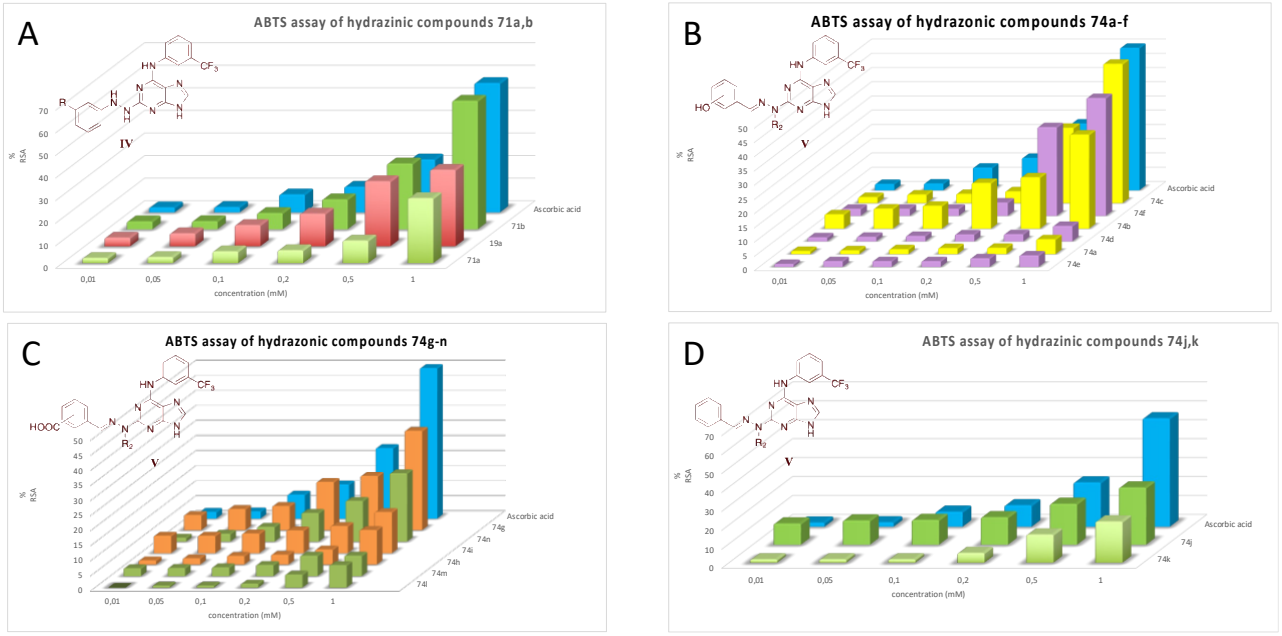

Figure 24. A) ABTS assay results of hydrazine compounds. In blue reference compound ascorbic acid; in red compound **19a**, synthetized in Chapter 2.2, in green compounds **71a,b**; **B)** ABTS assay data of hydrazonic compounds OH substituted. In blue ascorbic acid; in yellow compounds without methyl group in NH in C2; in purple compounds replaced with methyl group in NH in C2; **C)** ABTS assay data of hydrazonic compounds COOH substituted. In blue ascorbic acid; in orange compounds without methyl group in NH in C2; in green compounds replaced with methyl group in NH in C2; **D)** ABTS assay data of hydrazonic compounds **74i,k**. In blue ascorbic acid.

Figure 24B shows the data of the purinic scaffold replaced with hydrazonic groups in position C2 in turn replaced in ortho/para/meta position with hydroxyl group on aromatic group. The results show that 4-OH compounds substituted with not-methylated NH group C2 (**74b**) have a higher antioxidant

activity than NH methylated compounds in C2 (**74e)**. While the radical scavenger values for **74d** and **74a** are almost similar, as well as for **74c** and **74f**, with slightly radical scavenger value higher, once again, for the not-methylated compound. Similarly, compounds presenting a substituent COOH group on the hydrazone ring were compared: products with free NH in C2 had better antioxidant values than methylated compounds (Figure 24C). The same trend was shown for compounds **74j,k** without substituents on aromatic ring (Figure 24D). Examining all of the data collected, we can see that it is not only the position of the substituent on the aromatic ring of the hydrazonic group to influence the antioxidant activity, but also the functional group present. The -OH substituent has better radical scavenger results than the -COOH substituent. These results are in line with the studies in the literature that showed that the presence of a hydroxyl group on known scaffold antioxidants increases the activity of radical scavenger [202,203].

3.1.6 Conclusion

The COVID-19 pandemic brings out the urgent need for broad-spectrum antiviral drugs to face the present and future pandemics. Development of small molecules represents the most valid strategy due to low cost of production and achievable oral administration and chemical stability, allowing delivery under challenging climatic conditions and stockpile production. Optimal targets to be exploited include both viral-encoded proteins with high level of conservation among HCoVs, and host proteins essential for viral replication. SARS-CoV-2 helicase (nsp13) is considered an excellent target for the development of new antiviral drugs, being involved both in genome unwinding, and mRNA capping. Moreover, nsp13 is among the most conserved non-structural protein in CoVs, Instead, human DDX3X helicases is exploited by several viruses to facilitate various steps of their replication cycle.

Docking screening of the in-house collection of compounds has been performed on the structure of the SARS-CoV-2 nsp13 helicase focusing the selection of the compounds on the two druggable and highly conserved binding pockets: 1) the nucleotide binding pocket; and 2) the 5`-RNA site. From these docking simulations we obtained interesting results, who oriented us to the choice of a starting point for a structure-based optimization. In particular, **12i**, synthetized via a phenothypic approach in Chapter 2.2, resulted in the more interesting ones. Thus, we decided to design and synthetized some derivatives to explore the chemical space around these multi-target derivatives. Thus, we planned to modify the C2 side chain by increasing the steric hindrance or including radical scavenging moieties to add an antioxidant effect. The obtained compounds were evaluated for their ATPase and helicase-unwinding inhibitory properties on nsp13. The collection of these data allowed us to pursue in our workflow: non-toxic compounds and those found to inhibit nsp13 activity were selected to evaluate against human helicase DDX3. Unfortunately, we are still waiting for the whole set of the biological results concerning the inhibition of DDX3, and the complete overview of the functional and enzymatic information of all developed molecules may enable us to obtain enough information in order to optimize in a successive step the development of innovative BSAAs, targeting the nsp13 RNA helicase, highly conserved among different CoVs and the host RNA helicase (DDX3) exploited by different family of viruses for their replication.

This approach could represent an ideal, yet still underexplored, family of targets for the development of new pan-CoV antivirals.

3.2 Bithiazole Derivatives as Broad-Spectrum Antiviral Agents

3.2.1 Introduction

Host helicases are not the unique enzymes that viruses exploit for their replication. Because viruses are obligate parasites, they rely on the host protein kinases, enzymes that catalyze essential phosphorylation steps required for virus replication. Since kinase-dependent metabolic pathways are often redundant in eukaryotic cells and thus one kinase could be replaced by another one, targeting host kinases may represent a therapeutic window of opportunity, for the development of broad-spectrum antiviral agents. Recently, host factors have been considered attractive targets for antiviral drugs development because they present a high barrier to resistance and also because viruses belonging to different families, may exploit the same cellular pathways for replication. As has been shown previously, some kinase inhibitors block the replication of many viruses by interfering with different steps of the viral replication cycle[210,211].

In particular, the host phosphatidylinositol kinases (PIKs) have shown to have a pivotal role in the viral replication for various families' viruses, by forming replication organelles (ROs), specialized structures that support the replication of positive-sense ssRNA (+RNA) viruses infecting eukaryotes, and protect the viral genome from host defense since viruses may hide replication intermediates, facilitating the evasion of innate immune response[212,213,214,215]. In fact, viruses reorganize the composition of membrane lipids in their own interest since the viral replication machinery is assembled in a supramolecular complex on the cytosolic leaflet of these membranes. Thus, viruses often utilizing the host PI4K family of lipid kinases to generate membranes enriched with PI4P, which then they use as replication platforms to increase the rate of formation of the replication complexes. PI4Ps on these membranes allow the assembly of viral replication proteins and are involved in the regulation of viral replication[216,217].

Phosphatidylinositol 4-kinase type IIIβ (PI4KIIIβ) has been shown to be a key cellular protein in the viral replication of several families of plus-strand RNA viruses.[218] Most interesting, viruses, unrelated to each other, including noroviruses[219], picornaviruses[220], hepatitis C virus (HCV)[221], ZIKA virus, and coronaviruses such as SARS and MERS coronaviruses[222,223,224], exploit PI4Ks by different mechanisms.[225] Enteroviruses and rhinoviruses hijack the phosphatidylinositol 4-kinase type IIIβ (PI4KIIIβ) to accumulate phosphatidylinositol-4-phosphate (PI4P) on their ROs to facilitate viral replication.[226] Common studies on picornavirus replication highlighted the need for cholesterol and phosphatidylinositol 4-phosphate (PI4P) in their life cycle. In infected cells, type III phosphatidylinositol 4-kinases (PI4KIIIs) produce large amounts of PI4P, which is then exchanged for cholesterol during replication of organelles that forms at Golgi.

PI4P is also enriched in the ROs of Zika virus (ZIKV).[227] The SARS-CoV-2 was found to be dependent on PI4KIIIβ for spike-mediated cell entry. Lipid composition of the viral and host membranes influence the fusion process and PI4Ks seems to play opposite role in viral replication, varying the fluidity of the membrane; in fact, if on one side PI4KIIIβ enhances the membrane fluidity, PI4KIIIα has no effect and PI3KR1 regulates PI4P levels in the opposite direction [215]. The role of SARS-CoV-2 in viral replication was confirmed also by Yang H. et al., that showed that SARS-CoV-2 enter the cell via pH-dependent endocytosis and that PI4KIIIβ is required to enter the cell in a caveolae-independent manner.[228]

In conclusion, although some toxicity risks are to be expected when inhibiting a host factor, it should be kept in mind that most drugs currently used in therapy target host proteins with excellent therapeutic results and acceptable safety profiles.

3.2.2 Aim of the work

We recently reported a family of substituted bithiazoles that inhibit the lipid kinase PI4KIIIβ and block the replication of multiple viruses of the Enteroviruses family simultaneously also acting as correctors of the CFTR F508del folding defect in cystic fibrosis disease.[229,230]

Among the compounds previously identified, the bithiazole derivatives **83** and **84** (Figure 25) showed good potency against the targeted kinase and a broad-spectrum antiviral activity against multiple members of the Picornaviridae family.[227]

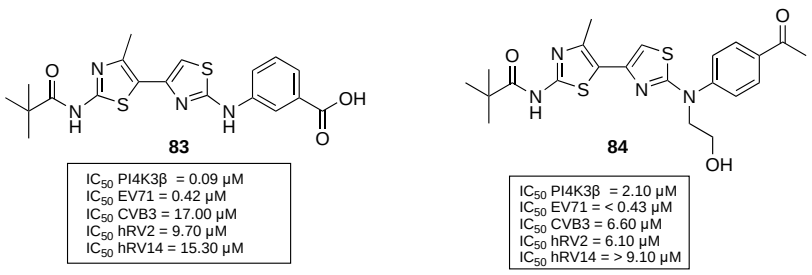

Figure 25. Structure and activity of bithiazole derivatives

Considering that it was demonstrated that viruses belonging to different families exploit PI4KIIIβ for their replication, with the aim to improve the spectrum of activity of these compounds, we investigated the chemical space around bithiazole derivatives through new sets of derivatives, designed on the basis of structure-activity relationships (SARs) for the inhibition of PI4KIIIβ collected so far for this family of compounds (Figure 26).

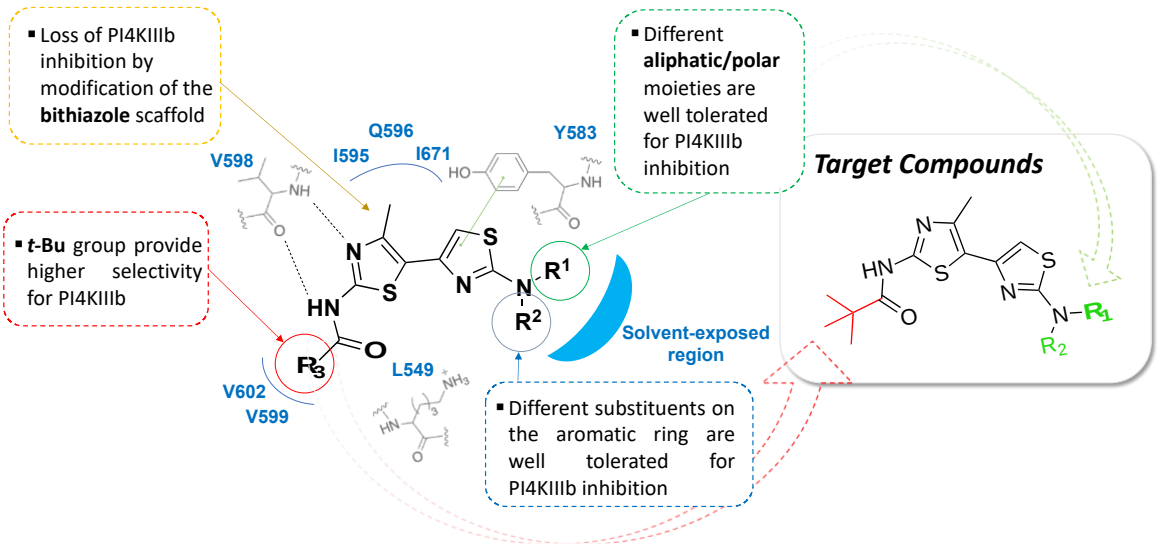

Figure 26. SARs of PI4KIIIβ-targeting bithiazole antivirals and Target compounds

The bithiazole scaffold is necessary since its modification led to a loss of activity. Considering the t-Bu group on the left side of the scaffold provides the higher selectivity for PI4IIIβ, the latter moiety

was maintained in all target molecules **I**. The planned modification was made on the right side of the scaffold, that is the solvent-exposed region, by changing the substituents on nitrogen. We synthesized a new set of derivatives, to evaluate if the chemotype, targeting PI4KIIIβ, could have a potential broad-spectrum of action.

3.2.3 Results and Discussion

All synthetical pathways of the final compounds included a step where a functionalized thiourea was coupled with a common intermediate, a 2-bromoacetyl derivate **89**. This compound was synthesized according to the synthetic procedure previously set up in our lab (Scheme 33)[226]. The first step was the reaction of commercially available thiourea **85** with 3-chloro-2,4-pentanedione **86** in refluxing ethanol to obtain intermediate **87**, in a quantitative yield. Pivaloyl chloride was added to the latter compound in order to obtain compound **88**. The amine in compound **87** serves as a nucleophilic group in a second-order nucleophilic substitution reaction with the aim to attach a t-Bu group to the thiazole scaffold which is of utmost importance to provide higher PI4KIIIβ selectivity. In order to be able to perform the coupling reaction with functionalized thioureas, compound **88** needed to undergo an α-bromination which was accomplished by the addition of bromine. This reaction afforded the 2-bromoacetyl derivate **89** with a low yield of 30% together with a higher percentage of a dibrominated side product **90**. The latter compound can be also reacted with functionalized thioureas to provide the final bithiazole compounds, thus overcoming the low yield issue in the preparation of the key intermediate **89**.

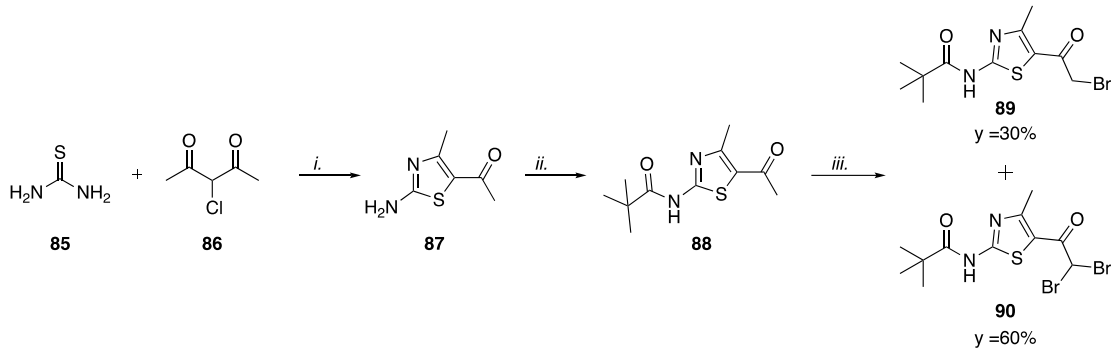

Scheme 33: *Reagents and conditions*: *i.* EtOH, reflux, 3h; *ii.* pivaloyl chloride, pyridine, dry THF, 0°C – reflux, 8h; *iii.* Br_2, 1,4-dioxane, r.t. 18h-reflux 5h

The key intermediate **89** already possesses some important structural features that have been shown to be important in the SARs of this family of compounds inhibiting PI4KIIIβ, such as the methylated thiazole, which will be part of the bithiazole scaffold, and the t-Bu. In order to generate the desired final compounds, a coupling reaction in refluxing ethanol was then conducted with functionalized thioureas, in turn prepared by corresponding amines

For the non-commercially available amines, it was necessary first to synthesize the secondary amines. Thus, the commercially available primary amines **91a-c** were converted into secondary amines **93a-l,** by reductive amination between the proper cycloketone **92a-e** and the aminoalcohols **91a-c,** using a mild reducing agent sodium borohydride ($NaBH_4$) (Scheme 34, Table 20).

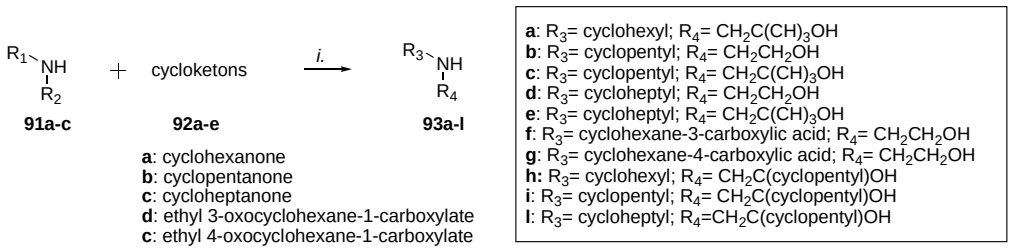

Scheme 34: *Reagents and conditions: i.* $NaBH_4$, EtOH, 0 °C-r.t., 4 h-o.n.

Table 20. Substituents of commercially amines **91a-e**

93a-e

Cmpds	R_1	R_2
91a	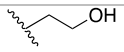	H
91b	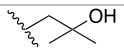	H
91c	H	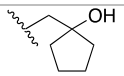
91d	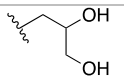	H
91e	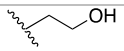	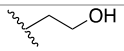

Commercially amines **91b-e** and secondary synthetized amine **93a-g** were converted in thioureas via a two steps protocol, consisting of a reaction with benzoyl isothiocyanate followed by deprotection with sodium methoxide (Scheme 35, Table 20).

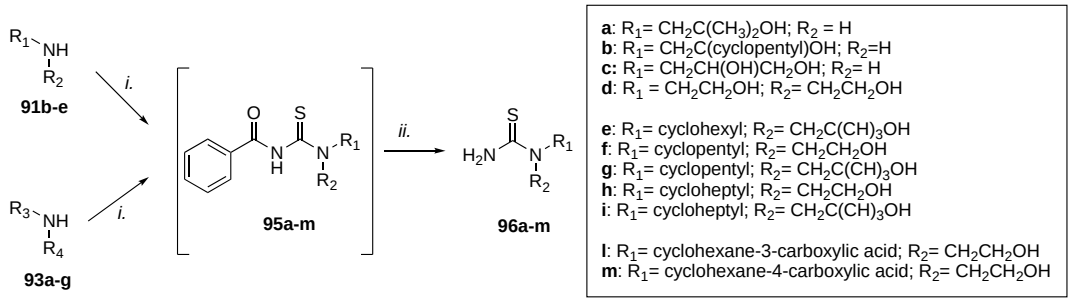

Scheme 35: *Reagents and conditions: i.* Benzoyl isothiocyanate **94**, DCM dry, 25 °C, 1–2 h; *ii.* MeOH dry NaOMe 25 °C, 2–19 h.

According the procedure of Scheme 35 the thioureas **96a-m** were prepared. Subsequently, for the synthesis of compounds **96n-p**, we tried to optimize the synthetic protocol in order to reduce the steps necessary to lead to final compounds. In this context, V. Golubev and colleagues have described a plausible mechanism for the preparation of 2-aminothiazoles, starting from a α-bromocarbonyl compound **97** and a secondary amine **100** (Scheme 36).[231] TMSNCS **98** is mixed with ethanol to obtain the acid HNCS, which is capable to react easily with **97** to form the respective thiocyanate **101**. Due to the high basicity of aliphatic amines, it is likely that all amine in the reaction mixture is protonated as a result of the formation of the thiocyanate **99**. An organic base, such as triethylamine, must be added for the reaction to be able to proceed. Golubev et al. established that **100** must be added last in order to avoid the unwanted formation of α-aminocarbonyl through the direct reaction of the secondary amine **100** and the α-bromocarbonyl compound **97**. The high nucleophilicity of the secondary amine causes this side product to form rapidly.

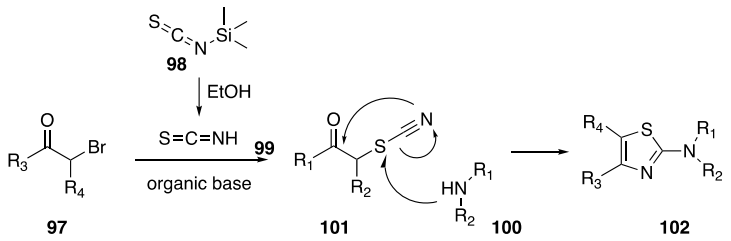

Scheme 36: Plausible mechanism for the multicomponent synthesis of 2-aminothiazoles by V. Golubev and colleagues

When R_3 and R_4 of compound **97** are considered the pivalamide-substituted methyl thiazole ring and hydrogen respectively, the 2-bromoacetyl derivate **89** can be equated to compound **97** in the reaction Scheme of V. Golubev and colleagues. Thus, this synthetic protocol was tried, reacting the 2-bromoacetyl derivate **89** and the secondary amine **93n**, in presence of TMSNCS and triethylamine in refluxing EtOH as solvent. However, although the two starting materials were ended, no aromatic protons were found in the ^{1}H NMR spectrum, which led to the conclusion that a non-aromatic product was obtained instead of the expected bithiazole (Scheme 37).

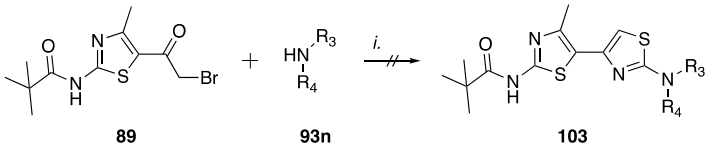

Scheme 37: *Reagents and conditions: i.* TMSNCS, Et_3N, EtOH, r.t.-reflux.

Thus, given the failure of the previous synthetic strategy, we decided to adopt TMSNCS to form the thioureas. The TMSNCS was first mixed with ethanol to allow the conversion into isothiocyanic acid (HNCS). Only after the formation of the acid, triethylamine, and the proper secondary amine **93h-l**

were added, resulting in the formation of the functionalized thioureas **96n-p** with yields ranging from 50-80%. Triethylamine was necessary for this second step of the formation of thiourea because of the high nucleophilicity of the secondary amines **93**. This property of **93** allowed them to be completely protonated during the formation of the acid, thus an organic base is necessary in this case to allow the reaction to proceed (Scheme 38).

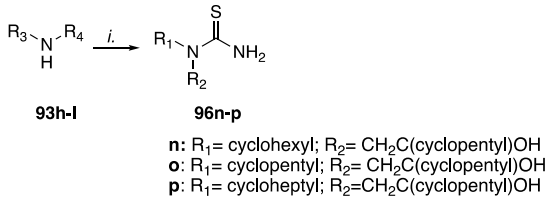

Scheme 38: *Reagents and conditions: i.* TMSCNS, Et_3N, EtOH, r.t., 4h- r.t.

Once obtained the corresponding thioureas, they were coupled with the common intermediate **89**. This coupling reaction was performed in refluxing ethanol (Scheme 39).

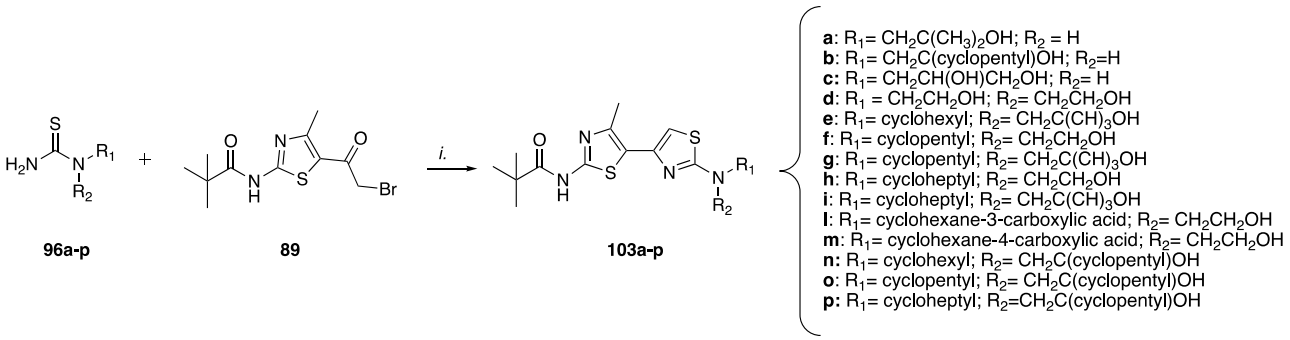

Scheme 39: *Reagents and conditions: i.* EtOH, reflux, 3h-o.n.

Our studies reported the identification of bithiazole chemotype with broad-spectrum antiviral agents (BSAAs) activity against human rhinoviruses (hRV), Zika virus (ZIKV) and SARS-CoV-2 at low micromolar and submicromolar concentrations, inhibiting host kinase PI4KIIIβ. Two of these were selected for the preparation of conjugates with the most interesting broad-spectrum antiviral purine **12i,** identified in Chapter 2.2 through a phenotypic approach, in order to obtain a probable synergistic effect from molecules acting with different mechanisms of action (Figure 27).

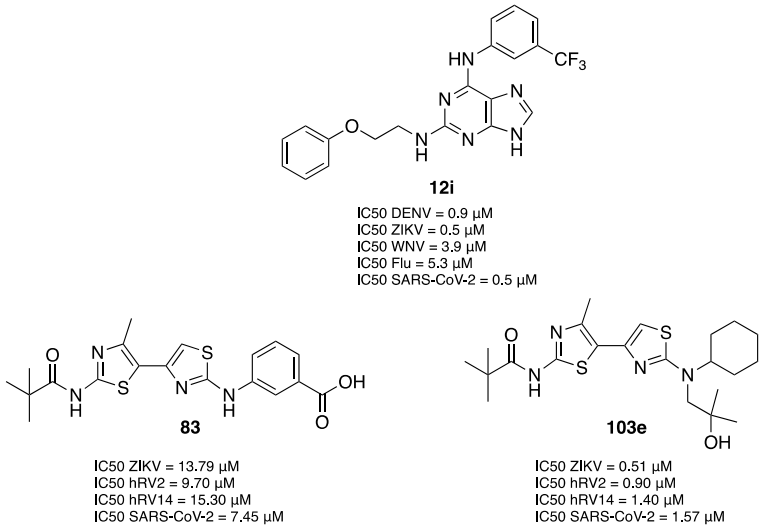

Figure 27: Target molecules for the synthesis of dual conjugate

Functionalization in N9 of compound **12i** was required to install a coupling chain for compound **83** and compound **103e**, thus we thought to exploit the N9 functionalization installed during the synthesis of acyclic compounds (See Chapter 2.3, compound **46d**).

The synthetic route of the compound **105** conjugate is illustrated in Scheme 40. The acid portion of compound **83** was converted into an acylic chloride **104**. The conjugate was obtained after forming a bond between the acyclic chloride and the hydroxylic group of the compound **46d**, in the presence of Et_3N.

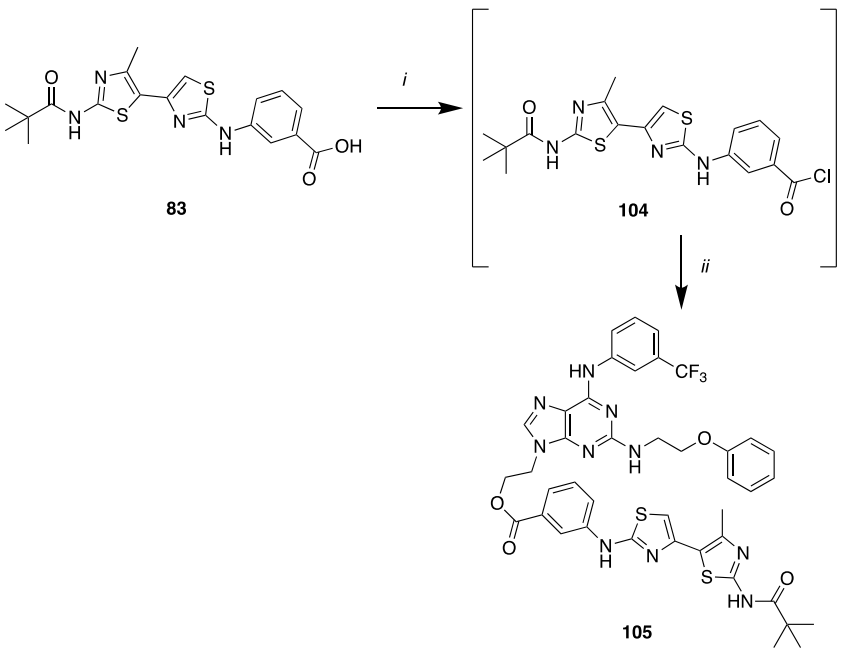

Scheme 40: *Reagents and conditions: i.* $SOCl_2$, THF dry, 30'., r.t.; *ii*. **46d**, Et_3N, THF, 9h, reflux.

Instead, compound **103e** and compound **46d** were conjugated by hydrolyzable linkers through a carbonate bond. The imidazole carboxylic ester **106** was formed via the reaction of CDI on primary

alcohol **46d**, in THF, in the presence of a catalytic amount of KOH. The bithiazole derivative **103e** was dissolved in acetonitrile and added to the reaction. After refluxing the reaction mixture o.n., we obtained the final compound **107** (Scheme 41).

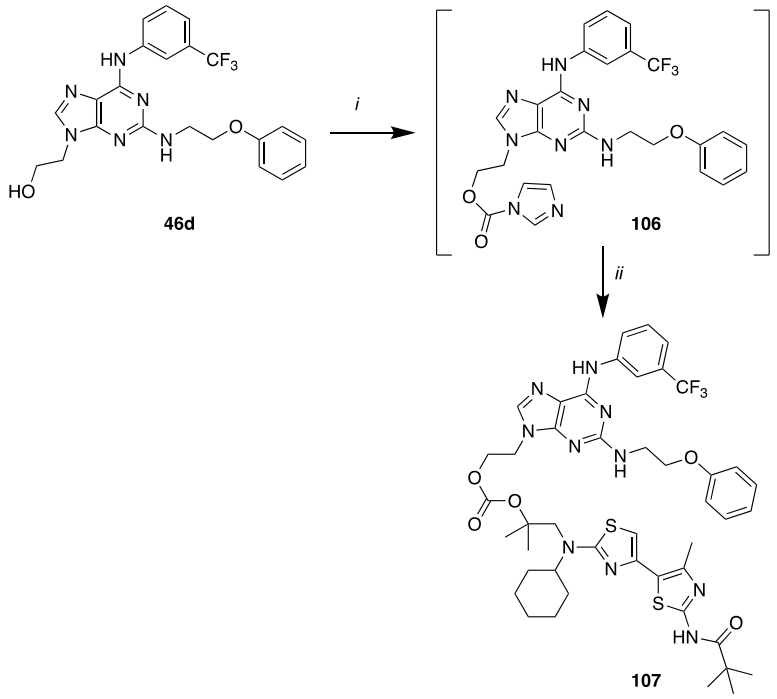

Scheme 41: *Reagents and conditions: i.* CDI, KOH, THF dry, 4h, 45 °C; *ii*. **103e**, DBU, ACN, o.n., 60 °C.

3.2.4 Biological results

The compounds that were initially evaluated for their effect on the enzymatic activity of the lipid kinases PI4KIIIβ, and for their antiviral effect included **103a,c,d,e**, compounds characterized by substituents with different lipophilicity to evaluate if different lipophilicity could influence the antiviral effect and the effect on PI4KIIIβ. As reported in Table 21, compounds **103a,c,d,e** inhibited the PI4KIIIβ activity at low micromolar concentrations, with no effect on PI3KR1. The assay was performed as previously described in ref. [232]

Table 21. Activity of bithiazole derivatives against selected lipid kinases and RNA viruses

ID	**PI4KIIIβ**	**PI3KR1**	**SARS-CoV-2**		**ZIKV**		**hRV2**	**hRV14**		**Human Lymphocytes**
	Calu-3				Huh7		HeLa			
	IC_{50} (μM)[a]		IC_{50} (μM)[b]	CC_{50} (μM)[c]	IC_{50} (μM)	CC_{50} (μM)	IC_{50} (μM)	IC_{50} (μM)	CC_{50} (μM)	Viability[d] @50uM
83[e]	0.09	NA[f]	7.45	45	13.79±	110	9.70	15.30	36	94.1
84[e]	2.10±0.17	NA	3.95±1.48	40	1.00 ±0.10	16	6.10	>9.10	17	94.5
103a	0.89 ±0.20	NA	NA	>100	0.83 ±0.31	37	0.39 ±0.01	0.48 ± 0.14	>30	98.3
103c	0.29 ±0.08	NA	NA	>100	46.50 ±2.96	>200	1.77 ± 0.62	2.32 ± 1.54	>30	96.0
103d	0.24 ±0.05	NA	NA	>100	5.00 ±1.20	125	1.37 ± 1.31	2.07 ± 1.45	>30	92.6
103e	1.97 ±0.79	NA	1.57±0.38 (0.37 ±0.08)	17	0.51 ±0.05	4	0.90 ± 0.72	1.40 ± 1.20	23.8 ± 1.7	94.8
RMD	ND[g]	ND	0.11 ±0.04	97	ND	ND	ND	ND	ND	ND
CMT	ND	ND	0.82 ± 0.32 (0.04 ±0.01)	200	ND	ND	ND	ND	ND	ND
SOF	ND	ND	ND	ND	2.70 ±0.50	200	ND	ND	ND	ND
BF738735	ND	ND	ND	ND	ND	ND	0.39 ± 0.36	0.59 ± 0.28	>30	ND

[a] Values are the mean of at least three independent experiments; [b] IC_{50}: half-maximal inhibitory concentration calculated with the DYRA protocol ± standard deviation (SD); data for active compounds under ENTRY-DYRA conditions are reported in parenthesis; [c] CC_{50}: half-maximal cytotoxic concentration; [d] Expressed as percentage of viable human lymphocytes with respect to vehicle (DMSO 0.5%); [e] hRV02 and hRV14 data have been taken from ref. 227; [f] NA: Not active; [g] ND: Not determined.

This set of PI4KIIIβ inhibitors was evaluated against viruses from different virus families. As positive controls for virus replication inhibitors, Remdesivir (RMD), Camostat (CMT), Sofosbuvir (SOF) and the PI4KIIIβ inhibitor BF738735 were used.

Initially, the new compounds **103a,c,d,e**, were evaluated for their antiviral activity against rhinoviruses hRV2 and hRV14 as previously described in ref. [233]. All compounds inhibited hRV2/hRV14 replication at low micromolar concentrations, with a potency comparable to that of the reference BF738735[234]. Successively, target compounds were evaluated for their anti-ZIKV activity, according to the protocol reported in ref. [237]. They showed to inhibit ZIKV replication, whose replication is known to be attenuated by PI4KIIIβ inhibitors such as IN-9[235], at low micromolar concentrations, with IC_{50} comparable (**103d**) or even five-times lower (**103a**, **103e**) than that of the reference compound SOF[236]. Next, we evaluated the efficacy of compounds **103a,c,d,e**, on SARS-CoV-2 replication as previously described in ref. [237]. Pulmonary Calu-3 cells were used as cell line because they better mimic lung infection. Interestingly compound **103e** was significantly less potent against PI4KIIIβ but did, in addition to ZIKV and RVs, also inhibit SARS-CoV-2 virus entry and replication, as demonstrated from the activity in direct yield reduction assay (DYRA) and a variation of the DYRA protocol (ENTRY-DYRA) protocol, while **103a,c,d** did not show any significant inhibition.

DYRA protocol foresees the incubation of infected cells and inhibitors for 72 hours, while ENTRY-DYRA is tailored for the evaluation of entry inhibitors, which foresees the incubation of cells and compounds for 1h, followed by virus adsorption, removal of inhibitors/viruses and incubation for 72 hours[232]. Compound **103e** was effective under ENTRY-DYRA conditions, indicating an inhibitory effect in the early phases of SARS-CoV-2 cell entry. As in the case of CMT, the effect of **103e** in the entry phase of SARS-CoV-2 is further supported by the lower efficacy of both compounds under DYRA conditions (Table 21). Considering the low values of CC_{50}, it was necessary to evaluate that the antiviral effect was not due to the cytotoxicity. Viability higher than 95% demonstrated the antiviral effect was not related to the cytotoxic effect. Primary human lymphocytes were incubated with a 50 μM concentration of each compound as described in ref. [232]. In all cases, as reported in Table 21, cell viability higher than 90% was found, showing a lower toxicity profile in primary cells than in specific immortalized cell lines used for virus amplification. In conclusion, the anti-ZIKV and anti-hRV activity of all compounds are in line with the effect on PI4KIIIβ. Antiviral activity against SARS-CoV-2 does not seem to be connected to PI4KIIIβ inhibition. In fact, submicromolar PI4KIIIβ inhibitors **103a,d** did not show any effect on SARS-CoV-2 replication under both experimental protocols (DYRA and ENTRY-DYRA protocol), while **103e** inhibited SARS-CoV-2 replication even if it is the less potent PI4KIIIβ inhibitor.

A few in vitro ADME properties of the synthetized compounds were analyzed to evaluate if different lipophilicity could influence the antiviral effect and the effect on PI4KIIIβ. The analyzed ADME properties, which are contained in Table 22, included aqueous solubility[232], membrane apparent permeability (Papp)[238], stability in human plasma[239], and stability in medium/serum at different times[232]. Compounds' lipophilicity (cLogP) was theoretically calculated and exhibited values in line with the experimental aqueous solubility. All compounds showed high stability in plasma, except for compound **103a** which showed some time-dependent decomposition in medium/serum. The conditions used for the membrane's apparent permeability with PAMPA assay simulated the ENTRY-DYRA protocol. As demonstrated by previous results, only **103e** showed good membrane permeability and high membrane retention after 5 hours of incubation at room temperature, and this may somehow explain its peculiar effect on the inhibition of SARS-CoV-2 entry.

Table 22. ADME properties of bithiazole derivatives **83, 84** and **103a,c,d,e**

Cpd	**cLogP**	**Aqueous Solubility[a] (mg/mL)**	**P_{app} 10^{-6} cm/sec (%MR[b])**	**Plasma Stability[c] (%)**	**Stability in Medium/Serum[d] (%)**	
					24 h	**48 h**
83	4.96	0.21	0.052 (<0.1)	99.1	96.4	93.1
84	4.39	0.05*	1.1*	>99*	98.5	90.4
103a	3.34	0.32	0.323 (<0.1)	92.3	77	67.3
103c	2.01	5.26	0.008 (<0.1)	99.4	99.0	97.5
103d	2.59	0.28	0.021 (0.94)	90.2	91.4	84.9
103e	5.77	0.01	11.729 (18.05)	92.4	93.3	85.7

*previously published in ref. 227. [a]In buffer solution at pH 7.4 (25 mM Hepes, 140 mM NaCl). [b]Membrane Retention (%MR) expressed as percentage of compound unable to reach the acceptor compartment. [c]After 24 h of incubation in human plasma solution. [d]Incubation in EMEM, 2 mM L-glut, 1% FBS, 1% Pen/Strep.

Subsequently, compounds **103b,f-p** were evaluated for their ability to inhibit PI4KIIIβ (Table 23). All tested compounds inhibited the activity of PI4KIIIβ, strangely except for compound **103f**. Unfortunately, results of PI4KIIIβ inhibition of compounds **103g** and **103n-p** are not yet available.

Table 23. Activity of bithiazole derivatives **103** against selected lipid kinases and hRV16 and EVD68

ID	**PI4KIIIβ**	**hRV16**	**EVD68**	
		HeLa		
	IC_{50} (μM)[a]	IC_{50} (μM)[b]	IC_{50} (μM)	CC_{50} (μM)[c]
103b	0.27	0.1449	0.4114	>50
103f	>50	0.3605	0.8993	8.283
103g	ND[d]	0.1887	0.5406	ND
103h	1.18	1.604	2.14	30.65
103i	1.69	1.057	2.537	29.35
103l	3.56	NA	NA	36.95
103m	0.4	1.414	3.217	ND
103n	ND	0.2846	0.8409	ND
103o	ND	0.1677	0.5178	ND
103p	ND	0.2047	0.8845	ND

[a] Values are the mean of at least three independent experiments; [b] IC50: half-maximal inhibitory concentration; [c] CC_{50}: half-maximal cytotoxic concentration; [d] ND: Not determined.

Like for the first set of derivatives, compounds **103b** and **103f-p** were evaluated for their antiviral activity against rhinovirus hRV16, and enterovirus EVD68. Immunostaining protocol with pan-rhinovirus antibody and pan-enterovirus antibody respectively was used. Culture supernatants were collected at 48hpi (48 h post-infection). As it is evident from Table 23, the compounds **103b** and **103f-p** showed values of rhinoviruses inhibition comparable and sometimes better than the first set including **103a,c,d,e**. The second set of tested compounds showed borderline cytotoxicity on HeLa cells.

Successively, compounds **103b** and **103f-p** were tested for their ability to inhibit ZIKV and SARS-CoV-2 replication in plaque assay on Vero cells (Figure 28), with compounds addition in the medium plus methylcellulose for ZIKV and avicel for SARS-CoV-2.

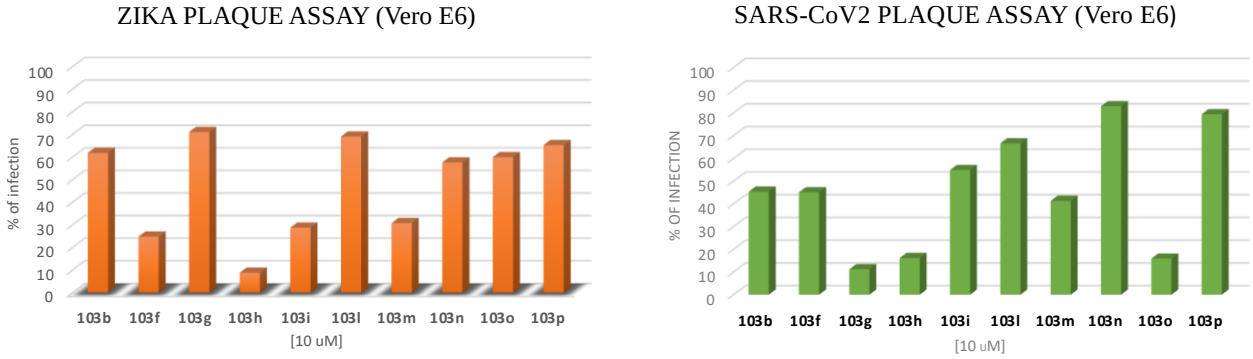

Figure 28. Plaque assay in Vero E6 for Zika and SARS-CoV-2 evaluated for compounds **103b** and **103f-p** at10 μM

At a 10 μM concentration, all compounds showed a slight activity against Zika, with more interesting results for compounds **103f,h,i,m**. All tested compound showed an inhibitory effect also on SARS-CoV-2 replication, with significant inhibition of viral replication for compounds **103g,h,o**.

Lastly, conjugate derivatives **105** and **107** were tested against Dengue Virus, HIV-1, and SARS-CoV-2, according to the protocols reported in ref. [161] for HIV-1 and [232] for Dengue Virus and SARS-CoV-2. Unfortunately, compound **105** showed toxicity in Huh7, but it was devoid of toxicity in H9 and Caco-2 cell lines. It showed antiviral activity against DENV-2 and Sars-CoV-2 and slight antiviral activity against HIV. Compound **107** showed toxicity in Huh7 and Caco-2 and it did not endow with activity against the already-mentioned viruses, as shown in Table 24. The high toxicity of each compound was demonstrated also by low values of CC_{90}, that is the drug concentration allowing at least the 90% of cell viability.

Table 24. Cytotoxicity and activity of conjugate derivatives against selected viruses

	DENV-2			**HIV**			**SARS-CoV-2**		
	Huh7			**H9**			**Caco-2**		
Cpd.	**CC_{50}**[a] (μM)	**CC_{90}**[b] (μM)	**IC_{50}**[c] (μM)	**CC_{50}** (μM)	**CC_{90}** (μM)	**IC_{50}** (μM)	**CC_{50}** (μM)	**CC_{90}** (μM)	**IC_{50}** (μM)
105	6.6	2.5	2.0	>100	40	21.6	>243	15.5	8.5
107	8.1	1.4	ND[d]	76	10	2.0	11.2	1.9	NA[e]

[a]CC_{50}: half-maximal cytotoxic concentration (μM); [b] CC_{90}: drug concentration allowing at least the 90% of cell viability; [c]IC_{50}: half-maximal inhibitory concentration; [d]ND: non determinated; [e]NA: not active

3.2.5 Conclusion

Considering the increasing diversity in the viruses causing severe human diseases and the enormous pool of potentially human-infecting viruses yet to be discovered, there is a great need for broad-spectrum antiviral treatments. The recent lockdowns imposed by the COVID-19 pandemic have affected every single individual worldwide, both financially and emotionally. To date, there are no known treatments available for several viral diseases, and the arsenal of available antiviral drugs is limited. Antiviral therapies have been primarily focused on the targeting of viral proteins, and thus specific for one particular virus. Moreover it is well known that viruses, especially RNA viruses, are prone to mutation and need to infect host cells to replicate themselves and thus survive. This parasitic characteristic leads to the conclusion that viruses require some components of the cells they have infected in order to proceed with their replication. It may be necessary to reconsider the current dominating antiviral strategy, where viral proteins are targeted. Many viruses exploit the same set of host proteins to replicate, leading to the opportunity for broad-spectrum antiviral agents to be developed by targeting these host proteins. When these common exploited host proteins are targeted in antiviral therapy, it becomes possible to inhibit multiple families of viruses with only one compound.

Recently, in our lab, bithiazole inhibitors of the host lipid kinase PI4KIIIβ block the replication of multiple viruses of the Enteroviruses family, and other families of viruses are also dependent on PI4KIIIβ for their replication. Thus, we decided to improve the spectrum of activity of these compounds, investigating the chemical space around bithiazole derivatives. We synthesized a new set of derivatives, designed on the basis of structure-activity relationships (SARs) for the inhibition of PI4KIIIβ collected so far for this family of compounds. Among the first set of synthesized compounds, anti-ZIKV and anti-rhinovirus activity of compounds **103a,c,d,e**, may be in line with the effect on PI4KIIIβ. However, the inhibition of SARS-CoV-2 entry seems to relate to an additional unknown target, since the less potent inhibitor of PI4KIIIβ, compound **103e**, turned out the most active against SARS-CoV-2. To better understand if the surprising biological result of the latter compound could be its higher lipophilicity or the interaction with an additional, still unknown, target exploited by SARS-CoV-2 for its entry and replication, bithiazole derivatives were synthesized, attaching more lipophilic substituents to the right side of bithiazole derivatives. The biological evaluation of antiviral activity against ZIKV, Enteroviruses, Rhinoviruses, and SARS-CoV-2 of the newly synthesized compounds is not complete and is currently ongoing. The general framework could allow us to better understand their mechanism of action.

4. EXPERIMENTAL PART

4.1 Chemistry

General. All commercially available chemicals were purchased from Merck or Fluorochem and, unless otherwise noted, used without any previous purification. Solvents used for work-up and purification procedures were of technical grade. TLC was carried out using Merck TLC plates (silica gel on Al foils, SUPELCO Analytical). Where indicated, products were purified by silica gel flash chromatography on columns packed with Merck Geduran Si 60 (40-63 μm). ^{1}H and ^{13}C NMR spectra were recorded on BRUKER AVANCE 300 MHz and BRUKER AVANCE 400 MHz spectrometers. Chemical shifts (δ scale) are reported in parts per million relative to TMS. ^{1}H-NMR spectra are reported in this order: multiplicity and number of protons; signals were characterized as: *s* (singlet), *d* (doublet), *dd* (doublet of doublets), *ddd* (doublet of doublet of doublets), *t* (triplet), *qt* (quintet), *m* (multiplet), *bs* (broad signal). Low resolution mass spectrometry measurements were performed on quattromicro API tandem mass spectrometer (Waters, Milford, MA, USA) equipped with an external APCI or ESI ion source. ESI-mass spectra are reported in the form of (*m/z*). Melting points were taken using a Gallenkamp melting point apparatus and were uncorrected. Elemental analyses were performed on a PerkinElmer PE 2004 elemental analyzer. The FDA-approved anti-HCV drugs sofosbuvir (MCE® cat. HY-15005), remdesivir (MCE® cat. HY-104077) and ribavirin (MCE® cat. HY-B0434) used as reference compounds, were supplied as powder and dissolved in 100% dimethyl sulfoxide (DMSO). All final compounds were screened for PAINS using the Free ADME-Tox Filtering Tool (FAF-Drugs4) program (http://fafdrugs4.mti.univ-paris-diderot.fr/): as expected, the azo-derivatives **20a-d** were flagged as potential PAINS. All final compounds showed chemical purity ≥95% as determined by elemental analysis data for C, H, and N (within 0.4% of the theoretical values). Optical rotations of nucleoside derivatives were measured in a 1 cm cell with a Perkin-Elmer Model 341 polarimeter at 20 °C.

Microwave Irradiation Experiments. Microwave reactions were conducted using a CEM Discover Synthesis Unit (CEM Corp., Matthews, NC). The machine consists of a continuous focused microwave power delivery system with an operator-selectable power output from 0 to 300 W. The temperature inside the reaction vessel was monitored using a calibrated infrared temperature control mounted under the reaction vessel. All experiments were performed using a stirring option whereby the reaction mixtures were stirred by means of a rotating magnetic plate located below the floor of the microwave cavity and a Teflon-coated magnetic stir bar in the vessel.

Evolution-inspired Synthesis of Antivirals

General Procedure for the Synthesis of Mixtures:

In a microwave tube, selected "doping agent" **1-3** (50 mg) were suspended in pure pentanol (1.5 mL) for mixtures MR-379, MR-380, and MR-430; water (1.5 mL) for MR-382 and MR-432; H_2O/n-pentanol (1 mL:1 mL) for MR-381, MR-428, MR-429 and MR-433; formamide (1 mL) for MR-385, MR-427, MR-431. Formamide (10 eq) was added when it was not used as solvent. The tube was heated to the microwave for 5' for MR-382, MR-385, MR-427, MR-431, MR-432; for 15' for MR-428, MR-429 and MR-433; for 30' for MR-381; and 1 hour for MR-379, MR-380 and MR-430 at 180 °C, except for MR-385, MR-427 and MR-431, which were heated at 140 °C. After this time, H_2O and EtOAc were added and the organic phases were washed with H_2O (x5) and brine (x3). The organic layers were dried over Na_2SO_4 and concentrated under vacuum.

General Procedure for the Synthesis of Compound 2-chloro-5-(hydroxymethyl)-6-((3-(trifluoromethyl)phenyl)amino)pyrimidine-4-carboxamide 4

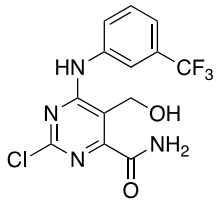

Compound 2-chloro-4-((3(trifluoromethyl)phenyl)amino) furo[3,4-*d*]pyrimidin-7(5*H*)-one **2** (50 mg; 0.16 mmol) was solubilized in MeOH (1mL). A solution of NH_4OH (1 mL) was added and the reaction mixture was stirred at r.t. for 19h. After checking with TLC the end of the starting materials, the solvents were evaporated and the mixture was extracted with EtOAc. The combined organic layers were washed with brine, dried over anhydrous Na_2SO_4, filtered and concentrated. The crude material was purified by silica gel chromatography, using 99:1 DCM:MeOH as eluent. **Yield**: 53 %; **MS** (ESI) $[M+H]^+$: 347.05 m/z. **^{1}H NMR** ($CDCl_3$ +CD_3OD, 400 MHz): δ 5.12 (s, 2H); 6.13 (bs, 1H); 7.40 (d, 1H, J = 8 Hz); 7.51 (t, 1H, J = 8 Hz); 7.71 (bs, 2H); 7.88 (s, 1H); 7.90 (s, 1H); 9.28 (bs, 1H).

Modified 2,6-Diaminopurines as Multi-Target BSAAs

General Procedure for the Synthesis of Compound methyl 3-aminobenzoate 9b

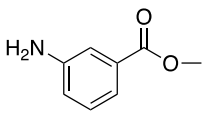

A solution of 3-aminobenzoic acid (1 g; 7.28 mmol) in MeOH dry (20 mL) was cooled to 0° at nitrogen atmosphere, followed by a dropwise addition of thionyl cloride (1.33 mL; 18.2 mmol). The mixture was stirred at room temperature overnight. After evaporation of the solvent and neutralization by addiction of $NaHCO_3$, the mixture was extracted with EtOAc. The combined organic layers were washed with brine, dried over anhydrous Na_2SO_4, filtered and concentrated. The crude material was purified used for the next step without further putification. **Yield**: 90%; **^{1}H NMR** ($CDCl_3$, 400 MHz): δ 3.91 (s, 3H); 6.93 (dd, 1H, J = 4 Hz, J = 8 Hz); 7.25 (t, 1H, J = 8 Hz); 7.42 (s, 1H); 7.48 (d, 1H, J = 8 Hz).

General Procedure for the Synthesis of intermediate 10a-e: In a microwave tube 2,6-dichloro-9*H*-purine **8** (100mg; 0.53mmol) and the proper amine (2.645 mmol) were suspended in *n*-BuOH (3 mL). NEt_3 (258 µL; 1.852 mmol) was added, and the tube was heated at 70-120 °C until the starting material was consumed (max µW power input: 100 W; ramp time: 1 min; power max: off; maximum pressure: 260 psi). At the end of irradiation, the solid obtained was isolated by filtration over a Buchner funnel after the addiction of cold *n*-hexane and ethyl acetate. In a few cases (**10b**, **10d**), at the end of irradiation, the reaction mixture was concentrated under vacuum, dissolved with ethyl acetate, and washed with $NaHCO_3$. The combined organic were washed with brine, dried over anhydrous Na_2SO_4, filtered and concentrated. The crude material was purified by silica gel chromatography, using the proper eluent: **10b**: CH_2Cl_2/MeOH 99:1-96:4; **10d**: CH_2Cl_2/Formic Acid/MeOH 93:3:4.

2-chloro-N-(3-fluorophenyl)-9H-purin-6-amine 10a:

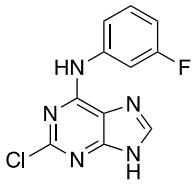

1st Irradiation cycle: 20 min, 100 °C; 2nd Irradiation cycle: 35 min, 120 °C. **Yield**: 67%. **MS** (ESI) $[M+H]^+$: 264.14 m/z. **^{1}H-NMR** (DMSO-d_6, 400 MHz): δ 5.37 (s, 1H); 6.29 (m, 1H); 6.99 (dd, 1H, *J* = 15.4, 7.9 Hz); 7.39 (d, 1H, *J* =7.4 Hz); 7.88 (d, 1H, *J* = 12.1 Hz); 8.34 (s, 1H); 10.44 (s, 1H).

Methyl 3-((2-chloro-9H-purin-6-yl)amino)benzoate 10b:

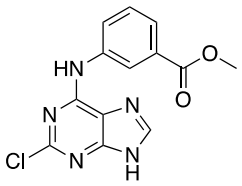

1st Irradiation cycle: 20 min, 70 °C; 2nd Irradiation cycle: 15 min, 100 °C. **Yield**: 25%. **MS** (ESI) $[M+H]^+$: 304.12 m/z. **^{1}H-NMR** (DMSO-*d*$_6$, 400 MHz): δ 3.87 (s, 3H); 7.51 (m, 1H); 7.66 (m, 1H); 8.14 (m, 1H); 8.33 (s, 1H); 8.54 (s, 1H); 10.42 (s, 1H); 13.36 (s, 1H).

2-chloro-N-(3-(trifluoromethyl)phenyl)-9H-purin-6-amine 10c:

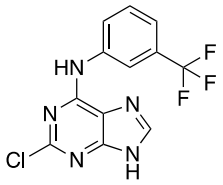

1st Irradiation cycle: 15 min, 100 °C. Yield: 96%. **MS** (ESI) $[M+H]^+$: 314.23 m/z. **^{1}H-NMR** (DMSO-*d*$_6$, 400 MHz): δ 7.42 (d, 1H, *J* = 8 Hz); 7.60 (t, 1H, *J* = 8 Hz); 8.15 (d, 1H, *J* = 8 Hz); 8.36 (s, 1H); 8.39 (s, 1H); 10.54 (s, 1H); 13.34 (s, 1H).

4-((2-chloro-9H-purin-6-yl)amino) benzene-1,2-diol 10d:

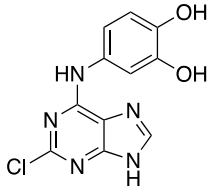

1st Irradiation cycle: 20 min, 70 °C; 2nd Irradiation cycle: 15 min, 120 °C. **Yield**: 29%. **^{1}H-NMR** (DMSO-*d*$_6$, 400 MHz): δ 6.71 (d, 1H, *J* = 8 Hz); 7.02 (d, 1H, *J* = 8 Hz); 7.22 (s, 1H); 8.33 (s, 1H); 9.90 (s, 1H).

2-chloro-N-(3,4,5-trimethoxyphenyl) -9H-purin-6-amine 10e:

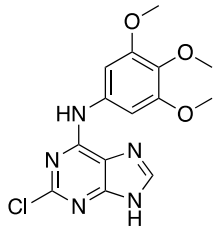

1st Irradiation cycle: 20 min, 70 °C. **Yield**: 70%. **^{1}H-NMR** (DMSO-*d*$_6$, 400 MHz): δ 3.65 (s, 3H); 3.78 (s, 3H); 7.40 (s, 2H); 8.30 (s, 1H); 10.12 (s, 1H); 13.33 (s, 1H).

General Procedure for the Synthesis of Compound 12a-m: In a microwave tube **10a-e** (0.19 mmol) and the proper amine (0.570 mmol) were suspended in *n*-BuOH (3 mL). TFA (0.19 mmol) was added and the tube was heated under microwave irradiation at 150-170 °C for 40-70 min (max µW power input: 300 W; ramp time: 1 min; power max: off; maximum pressure: 260 psi). The reaction mixture was concentrated under vacuum, dissolved with EtOAc and washed with $NaHCO_3$. The combined organic phases were washed with brine, dried over anhydrous Na_2SO_4, and evaporated to dryness. The crude material was purified by silica gel flash chromatography, using the proper eluent: **12a, 12c,**

12d, 12f, 12i: CH_2Cl_2/Formic Acid/MeOH 96:3:1; **12b, 12e**: CH_2Cl_2/Formic Acid/MeOH 92:3:5; **12g**: CH_2Cl_2/MeOH 96:4; **12h** CH_2Cl_2/MeOH 9:1 plus 1% of formic acid; **12j** CH_2Cl_2/Formic Acid/MeOH 95:3:2-96:1:3; **12k** CH_2Cl_2/MeOH/Formic Acid 96:3:1.

N6-(3-fluorophenyl)-N2-methyl-9H-purine-2,6-diamine 12a:

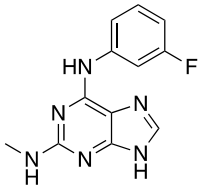

1st Irradiation cycle: 10 min, 170 °C; 2nd Irradiation cycle: 30 min, 150 °C. **Yield**: 20%. **Mp:** 266-267 °C. **MS** (ESI) $[M+H]^+$: 259.17 m/z. **^{1}H-NMR** (DMSO-d_6, 400 MHz): δ 2.83 (d, 3H, J = 2 Hz); 6.74 (s, 1H); 6.77 (t, 1H, J = 4 Hz); 7.29 (q, 1H, J = 15.2, 8 Hz); 7.76 (d, 1H, J = 8.4 Hz); 7.88 (s, 1H); 8.17 (m, 1H); 9.70 (s, 1H); 12.64 (bs, 1H). **^{13}C-NMR** (DMSO-d_6, 100 MHz): δ 28.89; 107.03; 108.44; 115.94; 130.24; 137.25; 142.79; 151.85; 153.34; 159.84; 161.43; 163.48. Anal. ($C_{12}H_{11}FN_6$) C, H, N.

2-((6-((3-fluorophenyl)amino)-9H-purin-2-yl)amino)ethan-1-ol 12b:

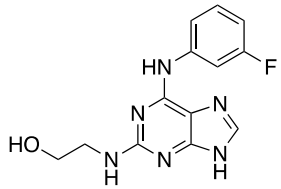

1st Irradiation cycle: 10 min, 170 °C; 2nd Irradiation cycle: 30 min, 150 °C. **Yield**: 27%. **MS** (ESI) $[M+H]^+$: 289.12 m/z. **^{1}H-NMR** (DMSO-d_6, 400 MHz): δ 3.36 (m, 2H); 3.56 (m, 2H); 6.59 (s, 1H); 6.75 (m, 1H); 7.28 (q, 1H J = 8 Hz); 7.78 (d, 1H, J = 4 Hz); 7.84 (s, 1H); 8.10 (s, 1H); 9.62 (s, 1H); 12.50 (s, 1H). **^{13}C-NMR** (DMSO-d_6, 100 MHz): δ 44.49; 60.55; 106.65; 106.92; 108.13; 115.86; 130.15; 130.25; 142.71; 142.83; 159.51; 161.43; 163.81. Anal. ($C_{13}H_{13}FN_6O$) C, H, N.

N6-(3-fluorophenyl)-N2-(2-phenoxyethyl)-9H-purine-2,6-diamine 12c:

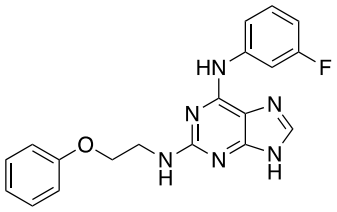

1st Irradiation cycle: 10 min, 170 °C; 2nd Irradiation cycle: 30 min, 150 °C. **Yield**: 28%. **Mp**: 217-219 °C. **MS** (ESI) $[M+H]^+$: 365.20 m/z. **^{1}H-NMR** (DMSO-d_6, 400 MHz): δ 3.67 (q, 2H, J = 6.32 Hz); 4.14 (t, 2H, J = 6.32 Hz); 6.75 (t, 1H, J = 10.84 Hz); 6.94 (m, 4H); 7.27 (m, 3H); 7.77 (d, 1H, J = 10.12 Hz); 7.87 (s, 1H); 8.13 (s, 1H); 9.64 (s, 1H); 12.54 (s, 1H). **^{13}C-NMR** (DMSO-d_6, 100 MHz): δ 41.11; 66.50; 106.77; 107.03; 108.48; 114.86; 115.96; 120.98; 129.97; 137.23; 142.61; 142.72; 152.02; 158.97; 159.22; 161.43; 163.51; 163.81. Anal. ($C_{19}H_{17}FN_6O$) C, H, N.

Methyl 3-((2-(methylamino)-9H-purin-6 yl)amino)benzoate 12d:

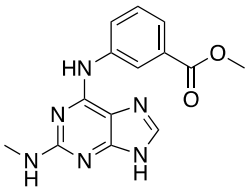

1st Irradiation cycle: 10 min, 170 °C; 2nd Irradiation cycle: 40 min, 150 °C. **Yield**: 55%. **Mp**: 255-257 °C. **MS** (ESI) $[M+H]^+$: 299.29 m/z. **^{1}H-NMR** (DMSO-*d*$_6$, 400 MHz): δ 2.86 (d, 3H, *J* = 4.4 Hz); 3.84 (s, 3H); 6.49 (q, 1H, *J* = 8 Hz); 7.41 (m, 1H); 7.55 (d, 1H, *J* = 8 Hz); 7.84 (s, 1H); 8.13 (s, 1H); 8.22 (s, 1H); 9.66 (s, 1H); 12.42 (bs, 1H). **^{13}C-NMR** (DMSO-*d*$_6$, 100 MHz): δ 28.99; 52.51; 120.97; 122.61; 124.75; 129.09; 130.28; 141.40; 152.01; 153.63; 160.06; 160.15; 163.52; 166.94. Anal. ($C_{14}H_{14}N_6O_2$) C, H, N.

Methyl 3-((2-((2-hydroxyethyl)amino)-9H-purin-6-yl)amino)benzoate 12e:

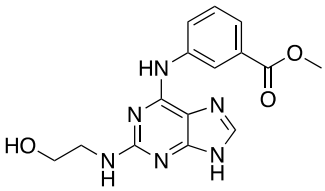

1st Irradiation cycle: 10 min, 170 °C; 2nd Irradiation cycle: 30 min, 150 °C. **Yield**: 45%. **Mp**: 250-252 °C. **MS** (ESI) $[M+H]^+$: 329.36 m/z. **^{1}H-NMR** (DMSO-*d*$_6$, 300 MHz): δ 3.41 (m, 2H); 3.56 (d, 2H, *J* = 3 Hz); 3.86 (s, 3H); 6.35 (t, 1H, *J* = 3 Hz); 7.42 (t, 1H, *J* = 9 Hz); 7.56 (d, 1H, *J* = 6 Hz); 7.84 (s, 1H); 8.25 (s, 1H); 8.71 (s, 1H); 9.65 (s, 1H); 12.45 (bs, 1H). **^{13}C NMR** (DMSO-*d*$_6$, 75 MHz): δ 44.59; 52.53; 60.61; 120.97; 122.65; 124.87; 129.12; 130.27; 137.10; 141.33; 152.10; 159.51; 163.57; 166.91. Anal. ($C_{15}H_{16}N_6O_3$) C, H, N.

Methyl 3-((2-((2-phenoxyethyl)amino)-9H-purin-6-yl)amino)benzoate 12f:

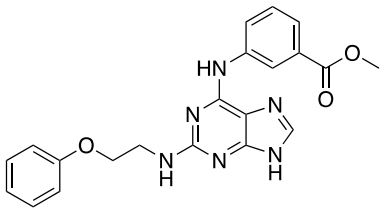

1st Irradiation cycle: 10 min, 170 °C; 2nd Irradiation cycle: 30 min, 150 °C. **Yield**: 32%. **Mp:** 209-211 °C. **MS** (ESI) $[M+H]^+$: 405.36 m/z. **^{1}H-NMR** (DMSO-*d*$_6$, 400 MHz): δ 3.71 (d, 2H, *J* = 5.6 Hz); 3.84 (s, 3H); 4.14 (t, 2H, *J* = 4 Hz); 6.71 (t, 1H, *J* = 4 Hz); 6.92 (m, 3H); 7.26 (t, 2H, *J* = 8 Hz); 7.39 (t, 1H, *J* = 8 Hz); 7.55 (d, 1H, *J* = 7.6 Hz); 7.85 (s, 1H); 8.26 (s, 1H); 8.73 (s, 1H); 9.70 (s, 1H); 12.44 (s, 1H). **^{13}C-NMR** (DMSO-*d*$_6$, 100 MHz): δ 41.21; 52.52; 66.72; 114.87; 120.95; 121.06; 122.73; 124.94; 129.12; 129.95; 130.30; 137.09; 141.27; 152.30; 159.03; 159.34; 163.51; 166.89. Anal. ($C_{21}H_{20}N_6O_3$) C, H, N.

N2-methyl-N6-(3-(trifluoromethyl)phenyl)-9H-purine-2,6-diamine 12g:

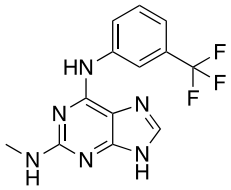

1st Irradiation cycle: 10 min, 170 °C; 2nd Irradiation cycle: 20 min, 170 °C. **Yield**: 40%. **^{1}H NMR** (DMSO-*d*$_6$, 400 MHz): δ 2.83 (d, 3H, *J* = 4.8); 6.59 (d, 1H, *J* = 4.4); 7.28 (d, 1H, *J* = 7.6 Hz); 7.50 (t, 1H, *J* = 8 Hz); 7.86 (s, 1H); 8.26 (s, 1H); 8.67 (s,1H); 9.79 (s, 1H); 12.44 (s, 1H). **^{13}C NMR** (DMSO-*d*$_6$, 100

MHz): δ 28.90; 113.91; 116.32; 117.96; 123.53; 123.62; 126.23; 129.78; 136.98; 141.86; 152.07; 153.45; 160.08. Anal. ($C_{13}H_{11}F_3N_6$) C, H, N.

2-((6-((3-(trifluoromethyl)phenyl)amino)-9H-purin-2-yl)amino)ethan-1-ol 12h:

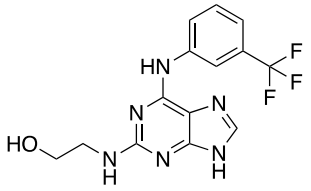

1st Irradiation cycle: 10 min, 170 °C; 2nd Irradiation cycle: 20 min, 150 °C. **Yield**: 35%. **^{1}H NMR** (DMSO-d_6, 400 MHz): δ 3.39 (t, 2H, J = 8 Hz); 3.57 (t, 2H, J = 4 Hz); 6.41 (t, 1H, J = 5.2 Hz); 7.28 (d, 1H, J = 8 Hz); 7.50 (t, 1H, J = 8 Hz); 7.87 (s, 1H); 8.15 (s, 1H); 8.32 (s, 1H); 8.49 (s, 1H); 12.44 (bs, 1H). **^{13}C NMR** (DMSO-d_6, 100 MHz): δ 31.16; 60.48; 116.27; 118.05; 118.07; 123.46; 123.64; 126.17; 129.44; 129.76; 129.84; 137.13; 141.75; 152.01; 159.44. Anal. ($C_{14}H_{13}F_3N_6O$) C, H, N.

N^2-(2-phenoxyethyl)-N^6-(3-(trifluoromethyl)phenyl)-9H-purine-2,6-diamine 12i:

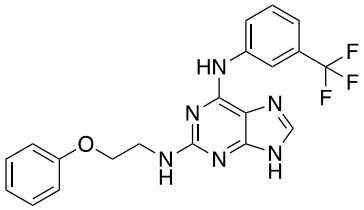

1st Irradiation cycle: 10 min, 170 °C; 2nd Irradiation cycle: 50 min**,** 150°C;. **Yield**: 56%. **Mp:** 180-181 °C. **MS** (ESI) $[M+H]^+$: 415.21 m/z. **^{1}H-NMR** (DMSO-d_6, 400 MHz): δ 3.68 (q, 2H, J = 6 Hz); 4.12 (t, 2H, J = 6 Hz); 6.78 (t, 1H, J = 6 Hz); 6.90 (m, 3H); 7.26 (t, 3H, J = 7.6 Hz); 7.48 (t, 1H, J = 8 Hz); 7.87 (s, 1H); 8.29 (s, 1H); 8.48 (s, 1H); 9.81 (s, 1H); 12.48 (bs, 1H). **^{13}C-NMR** (DMSO-d_6, 100 MHz): δ 41.16; 66.59; 114.83; 116.35; 118.19; 120.97; 123.73; 126.17; 129.50; 129.81; 129.86; 129.97; 141.71; 159.00; 159.30. Anal. ($C_{20}H_{17}F_3N_6O$) C, H, N.

4-((2-((2-phenoxyethyl)amino)-9H-purin-6-yl)amino)benzene-1,2-diol 12j:

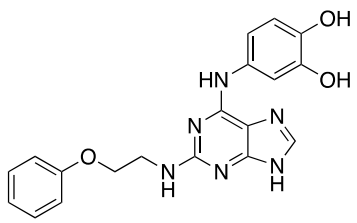

1st Irradiation cycle: 10 min, 170 °C; 2nd Irradiation cycle: 60 min, 150 °C. **Yield**: 39%. **Mp**: 170-172 °C. **MS** (ESI) $[M+H]^+$: 379.39 m/z. **^{1}H-NMR** (DMSO-d_6, 300 MHz): δ 3.63 (q, 2H, J = 6 Hz); 4.11 (t, 2H, J = 6 Hz); 6.44 (t, 1H, J = 6 Hz); 6.61 (d, 1H, J = 9 Hz); 6.95 (m, 3H); 7.26 (m, 3H); 7.77 (s, 1H); 8.20 (s, 1H); 8.93 (s, 1H); 12.42 (bs, 1H). **^{13}C-NMR** (DMSO-d_6, 100 MHz): δ 41.10; 66.67; 109.87; 112.38; 114.88; 115.48; 120.94; 129.97; 132.68; 141.06; 145.18; 159.02; 159.47; 163.91. Anal. ($C_{19}H_{18}N_6O_3$) C, H, N.

N2-(2-phenoxyethyl)-N6-(3,4,5-trimethoxyphenyl)-9H-purine-2,6-diamine 12k:

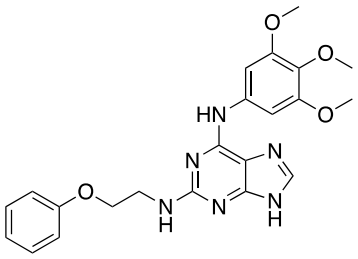

1st Irradiation cycle: 30 min, 170 °C; 2nd Irradiation cycle: 30 min, 170 °C. **Yield**: 52%. **MS** (ESI) $[M+H]^+$: 437.47 m/z. **^{1}H-NMR** (DMSO-*d*$_6$, 400 MHz): δ 3.62 (s, 3H); 3.72 (m, 2H); 3.78 (s, 6H); 4.12 (t, 2H, *J* = 6.4 Hz); 6.93 (m, 3H); 7.27 (m, 2H); 7.43 (s, 1H); 7.89 (s, 1H); 8.14 (s, 1H); 9.27 (s, 1H); 12.63 (m, 1H). **^{13}C-NMR** (DMSO-*d*$_6$, 100 MHz): δ 41.08; 56.20; 60.55; 66.45; 98.22; 114.02; 115.06; 121.01; 121.73; 129.98; 133.01; 136.69; 151.90; 152.97; 158.21; 158.88; 163.49. Anal. ($C_{22}H_{24}N_6O_4$) C, H, N.

General Procedures for the Synthesis of compounds 13d,f: Compound **13d** (45 mg; 0.151 mmol) or **13f** (33mg; 0.082 mmol) were dissolved in a 1:1 mixture of THF/MeOH (1.53 mL), treated with 2N aqueous solution of LiOH (0.30 mL) was added and the resulting mixtures were stirred for 24 hours at room temperature. At the end of reaction, the solvent was evaporated under vacuum. The crude material was purified by silica gel flash chromatography using the proper eluent: **13d**: CH_2Cl_2/NEt_3/MeOH 82:3:15; **13f**: CH_2Cl_2/Formic Acid/MeOH 95:3:2.

3-((2-(methylamino)-9H-purin-6-yl)amino)benzoic acid 13d:

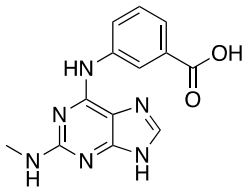

Yield: 16%. Mp: 211-213 °C. **MS** (ESI) $[M+H]^+$: 285.26 m/z. **^{1}H-NMR** (DMSO-*d*$_6$, 300 MHz): δ 2.85 (d, 3H, *J* = 4.5 Hz), 6.42 (d, 1H, *J* = 3 Hz), 7.38 (t, 1H, *J* = 8.1 Hz); 7.53 (d, 1H, *J* = 7.2 Hz); 7.82 (s, 1H); 8.24 (m, 1H); 8.65 (s, 1H); 9.58 (s, 1H); 12.38 (bs, 1H). **^{13}C-NMR** (DMSO-*d*$_6$, 100 MHz): δ 28.70; 113.88; 121.41; 122.89; 124.52; 128.85; 131.61; 136.80; 141.18; 152.24; 158.44; 160.18; 168.06. Anal. ($C_{13}H_{12}N_6O_2$) C, H, N.

3-((2-((2-phenoxyethyl)amino)-9H-purin-6-yl)amino)benzoic acid 13f:

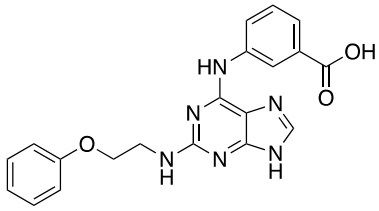

Yield: 91%. **Mp**: 209-211 °C. **MS** (ESI) $[M+H]^+$: 391.46 m/z. **^{1}H-NMR** (DMSO-*d*$_6$, 300 MHz): δ 3.70 (q, 2H, *J* = 4.2, 8.7 Hz); 4.14 (t, 2H, *J* = 4.2 Hz); 6.68 (t, 1H, *J* = 3.6 Hz); 6.92 (m, 2H); 7.27 (t, 1H, *J* = 7.2 Hz); 7.38 (t, 1H, *J* = 8 Hz); 7.55 (d, 1H, *J* = 8 Hz); 7.85 (s, 1H); 8.27 (s, 1H); 8.62 (s, 1H); 9.63 (s, 1H); 12.43 (s, 1H). **^{13}C-NMR** (DMSO-*d*$_6$, 100 MHz): δ 41.20; 66.78; 114.88; 120.96; 123.08; 124.65; 128.99; 129.97; 131.48; 136.98; 141.00; 159.02; 159.35; 168.00. Anal. ($C_{20}H_{18}N_6O$) C, H, N.

Synthesis of 2-chloro-*N*-(2-phenoxyethyl)-9*H*-purin-6-amine 15:

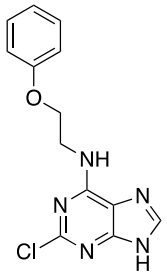

In a microwave tube 2,6-dichloro-9*H*-purine **8** (100 mg; 0.53 mmol) and 2-phenoxyethylamine (1.06 mmol) were suspended in n-BuOH (3 mL). NEt_3 (258 µL; 1.852 mmol) was added and the tube was heated at 70 °C for 30 min (max µW power input: 100 W; ramp time: 1 min; power max: off; maximum pressure: 260 psi). At the end of irradiation, the solid obtained was isolated by filtration over a Buchner funnel and washed with MeOH and EtOAc. **Yield**: 85%. **^{1}H-NMR** (DMSO-*d*$_6$, 300 MHz): δ 3.21 (t, 2H, *J* = 3 Hz); 4.17 (t, 2H, *J* = 6 Hz); 6.96 (m, 3H); 7.30 (m, 2H); 8.15 (s, 1H); 8.30 (s, 1H); 9.00 (bs, 1H).

General Procedures for the Synthesis of compounds 16a,b: In a microwave tube **15** (50 mg; 0.173 mmol) and 3-fluoroaniline or 3-trifluoromethylaniline (0.865 mmol) were suspended in *n*-BuOH (2mL). TFA (0.259 mmol) was added and the tube was heated under microwave irradiation for two consecutive cycles: 1st Irradiation cycle: 10 min, 170 °C; 2nd Irradiation cycle: 40 min, 150 °C (max µW power input: 300 W; ramp time: 1 min; power max: off; maximum pressure: 260 psi). The reaction mixture was concentrated under vacuum, diluted with ethyl acetate, and washed with $NaHCO_3$. The combined organic were washed with NH_4Cl, brine, dried over anhydrous Na_2SO_4, filtered and concentrated. The crude material was purified by silica gel flash chromatography using the proper eluent: **16a**: CH_2Cl_2/Formic Acid/MeOH 95:3:2; **16b**: CH_2Cl_2/Formic Acid/MeOH 96.5:3:0.5.

N2-(3-fluorophenyl)-N6-(2-phenoxyethyl)-9H-purine-2,6-diamine 16a:

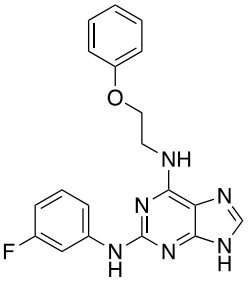

Yield: 33%. **Mp:** 208-210 °C. **MS** (ESI) $[M+H]^+$: 365.38 m/z. **^{1}H-NMR** (DMSO-*d*$_6$, 400 MHz): δ 3.89 (s, 2H); 4.20 (m, 2H); 6.25 (m, 1H); 6.93 (m, 3H); 7.20 (m, 1H); 7.30 (m, 2H); 7.48 (d, 1H, *J* = 1.2 Hz); 7.63 (s, 1H); 7.87 (s, 1H); 7.95 (d, 1H, *J* = 13.2 Hz); 9.15 (s, 1H); 12.54 (s, 1H). **^{13}C-NMR** (DMSO-*d*$_6$, 100 MHz): δ 40.66; 66.31; 104.65; 104.91; 106.34; 106.55; 114.20; 114.87; 121.06; 129.98; 130.07; 137.47; 144.10; 144.22; 156.26; 158.89; 161.71; 163.49; 164.08. Anal. ($C_{19}H_{17}FN_6O$) C, H, N.

N^6-(2-phenoxyethyl)-N^2-(3 (trifluoromethyl) phenyl)-9H-purine-2,6-diamine 16b:

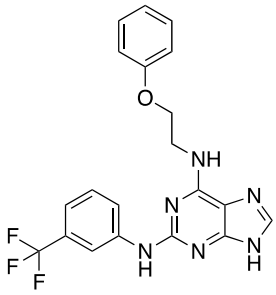

Yield: 42%. **Mp**: 211-213 °C. **MS** (ESI) $[M+H]^+$: 415.39 m/z. **^{1}H-NMR** (DMSO-*d*$_6$, 400 MHz): δ 3.89 (s, 2H); 4.20 (m, 2H); 6.91 (m, 3H); 7.15 (d, 1H, *J* = 8 Hz); 7.27 (m, 2H); 7.41 (t, 1H, *J* = 8 Hz); 7.68 (s, 1H); 7.88 (s, 1H); 7.97 (s, 1H); 8.42 (s, 1H); 9.30 (s, 1H); 12.53 (bs, 1H). **^{13}C-NMR** (DMSO-*d*$_6$, 100 MHz): δ 40.66; 66.39; 114.23; 114.85; 116.41; 121.06; 121.81; 123.64; 126.35; 129.52; 129.69; 129.83; 129.98; 143.06; 156.21; 158.91; 163.50. Anal. ($C_{20}H_{17}F_3N_6O$) C, H, N.

General Procedures for the Synthesis of intermediates 18a-e: In a microwave tube 2,6-dichloropurine (100 mg; 0,529 mmol) and the proper phenylhydrazine **17a-e** (2,645 mmol) were suspended in *n*-BuOH (3 mL). NEt_3 (221 µL; 1,587 mmol) was added and the tube was heated under microwave irradiation at 70 °C for 20-40 min. (max µW power input: 100W; ramp time: 1 min; power max: off; maximum pressure: 260 psi). When the reaction ended, the mixture was concentrated under vacuum, diluted with ethyl acetate, and washed with NH_4Cl. The combined organic were washed with NH_4Cl, brine, dried over anhydrous Na_2SO_4, filtered and concentrated under vacuum. The crude material was purified by silica gel flash chromatography using the proper eluent: **18a**: CH_2Cl_2/MeOH 96:4; **18b-d**: hexane/acetone 1:1; **18e**: CH_2Cl_2/MeOH 97:3.

(E)-2-chloro-6-(2-(3-fluorophenyl)hydrazinyl)-9H-purine 18a:

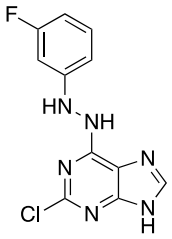

1st Irradiation cycle: 10 min, 70 °C; 2nd Irradiation cycle: 10 min, 70 °C. **Yield**: 60%. **^{1}H-NMR** (DMSO-*d*$_6$, 400 MHz): δ 6.58 (m, 2H); 6.30 (m, 1H); 6.18 (m, 1H); 7.83 (s, 1H); 8.14 (s, 1H); 9.56 (s, 1H); 12.41 (m, 1H).

(E)-2-chloro-6-(2-(3,5-difluorophenyl) hydrazinyl)-9H-purine 18b:

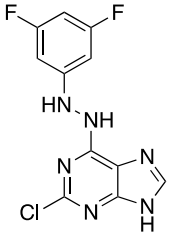

1st Irradiation cycle: 10 min, 70 °C; 2nd Irradiation cycle: 10 min, 70 °C; 3rd Irradiation cycle: 20 min, 70 °C. **Yield**: 37%. MS (ESI) $[M+H]^+$: 297.13 m/z. **^{1}H NMR** (DMSO-*d*$_6$, 400 MHz): δ 6.47 (m, 3H); 8.23 (s, 1H); 8.72 (s, 1H); 9.99 (s, 1H); 12.88 (m, 1H).

(E)-6-(2-(3,5-bis(trifluoromethyl)phenyl) hydrazinyl)-2-chloro-9H-purine 18c:

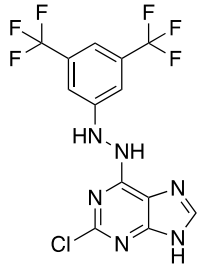

1st Irradiation cycle: 10 min, 70 °C; 2nd Irradiation cycle: 10 min, 70 °C. **Yield**: 73%. **MS** (ESI) $[M+H]^+$: 397.06 m/z. **^{1}H NMR** (DMSO-*d*$_6$, 400 MHz): δ 7.28 (m, 2H); 7.42 (m, 2H); 8.28 (s, 1H); 9.11 (m, 1H); 10.02 (m, 1H); 10.25 (m, 1H); 12.99 (m, 1H).

(E)-2-chloro-6-(2-(4-(trifluoromethyl)phenyl) hydrazinyl)-9H-purine 18d:

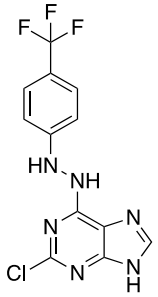

1st Irradiation cycle: 10 min, 70 °C; 2nd Irradiation cycle: 10 min, 70°C. **Yield**: 68%. **MS** (ESI) $[M+H]^+$= 331.20 m/z. **^{1}H NMR** (DMSO-*d*$_6$, 400 MHz): δ 6.86 (d, 2H, *J* = 8 Hz); 7.48 (d, 2H, *J* = 7.6 Hz); 8.23 (s, 1H); 8.79 (s, 1H); 10.09 (s, 1H); 12.9 (m, 1H).

2-chloro-6-(2-(3-(trifluoromethyl)phenyl) hydrazinyl)-9H-purine 18e:

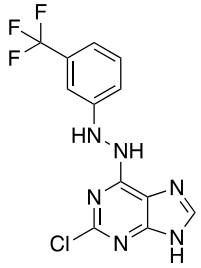

1st Irradiation cycle: 10 min, 70 °C; 2nd Irradiation cycle: 10 min, 70 °C. **Yield**: 54%. **MS** (ESI) $[M+H]^+$: 328.69 m/z. **^{1}H-NMR** (DMSO-*d*$_6$, 400 MHz): δ 7.14 (m, 4H); 8.24 (m, 1H); 8.63 (m, 1H); 10.00 (m, 1H); 12.97 (m, 1H).

General procedures for the Synthesis of compounds 19a-e: In a microwave tube **18a-e** and the proper amine (2.5 equivalent) were suspended in n-BuOH (2mL). TFA (1 equivalent) was added and the tube was heated at 170 °C for 4 consecutive cycles of 30 min each (max μW power input: 300W; ramp time: 1 min; power max: off; maximum pressure: 300 psi). The reaction mixture was concentrated under vacuum. Products were purified by silica gel flash chromatography, using the proper eluent: **19a**: hexane/acetone 3:7 plus 1% of formic acid; **19b**: hexane/acetone 3:7; **19c**: hexane/acetone 4:6 plus 1% of formic acid; **19d**: hexane/acetone 2:8 plus 1% of formic acid; **19e**: $CHCl_3$/MeOH 94:4 plus 1% of formic acid.

6-(2-(3-fluorophenyl) hydrazinyl)-N-(2-phenoxyethyl)-9H-purin-2-amine 19a:

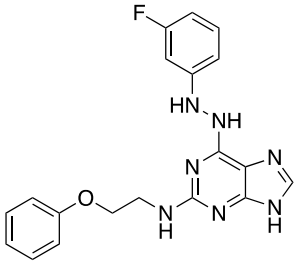

Yield: 46%. **MS** (ESI) $[M+H]^+$= 380.29 m/z. **^{1}H NMR** (DMSO-d_6, 300 MHz): δ 3.50 (s, 2H); 3.91 (s, 2H); 6.43 (m, 3H); 6.58 (d, 1H, J = 9 Hz); 6.90 (m, 3H); 7.13 (q, 1H, J = 9 Hz); 7.25 (t, 2H, J = 9 Hz); 7.77 (s, 1H); 8.06 (s, 1H); 9.17 (s, 1H). **^{13}C NMR** (DMSO-d_6, 100 MHz): δ 40.97; 66.42; 99.15; 104.41; 108.69; 114.76; 114.86; 120.84; 120.93; 121.23; 129.88; 130.56; 130.70; 153.10; 155.45; 158.98; 159.47; 162.42; 164.84. Anal. ($C_{19}H_{18}FN_7O$) C, H, N.

6-(2-(3,5-difluorophenyl) hydrazinyl)-N-(2-phenoxyethyl)-9H-purin-2-amine 19b:

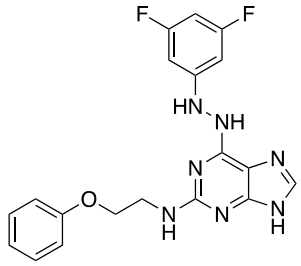

Yield: 42%. **MS** (ESI) $[M+H]^+$= 398.30 m/z. **^{1}H NMR** (DMSO-d_6, 300 MHz): δ 3.50 (d, 2H, J = 6); 3.92 (m, 2H); 6.31 (m, 3H); 6.51 (m, 1H); 6.87 (m, 3H); 7.24 (q, 2H, J = 6, 11.2 Hz); 7.76 (s, 1H); 8.35 (s, 1H); 9.30 (s, 1H); 12.36 (s, 1H). **^{13}C NMR** ($CDCl_3$+CD_3OD, 75 MHz): δ 41.24; 66.42; 92.89; 94.99; 95.25; 114.75; 114.94; 120.87; 129.91; 153.97; 155.27; 158.98; 159.28; 162.44; 162.60; 163.50; 164.84; 165.00. Anal. ($C_{19}H_{17}F_2N_7O$) C, H, N.

6-(2-(3,5-bis(trifluoromethyl)phenyl) hydrazinyl)-N-(2- phenoxyethyl)-9H-purin-2-amine 19c:

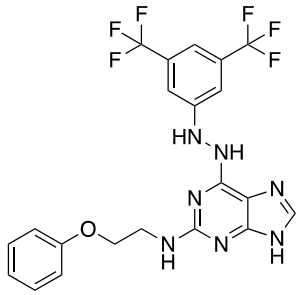

Yield: 38%. **MS** (ESI) $[M+H]^+$= 498.29 m/z. **^{1}H NMR** (DMSO-d_6, 400 MHz): δ 3.58 (q, 2H, J = 8 Hz); 3.97 (t, 2H, J = 8 Hz); 6.18 (t, 1H, J = 4 Hz); 6.89 (m, 3H); 7.19 (s, 1H); 7.24 (t, 2H, J = 4 Hz); 7.32 (s, 1H); 7.73 (s, 1H); 8.14 (s, 1H); 8.54 (s, 1H). **^{13}C NMR** (DMSO-d_6, 100 MHz): δ 40.91; 66.23; 106.69; 111.65; 114.62; 114.64; 120.85; 122.64; 125.36; 128.07; 129.87; 131.11; 131.43; 137.14; 137.76; 158.88; 163.55. Anal. ($C_{21}H_{17}F_6N_7O$) C, H, N.

N-(2-phenoxyethyl)-6-(2-(4-(trifluoromethyl)phenyl) hydrazinyl)-9H-purin-2- amine 19d:

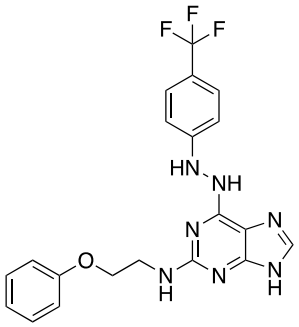

Yield: 41%. **MS** (ESI) $[M+H]^+$= 430.36 m/z. **^{1}H NMR** (DMSO-*d*$_6$, 300 MHz): δ 3.76 (q, 2H, *J* = 6 Hz); 4.15 (t, 2H, *J* = 6 Hz); 6.89 (t, 2H, *J* = 9 Hz); 6.96 (d, 2H, *J* = 9 Hz); 7.26 (m, 2H); 7.37 (bs, 1H); 7.68 (s, 1H); 8.03 (s, 1H); 8.05 (s, 1H); 8.25 (s, 1H); 8.28 (s, 1H); 8.37 (s, 1H). **^{13}C NMR** (DMSO-*d*$_6$, 75 MHz): δ 49.12; 66.38; 111.87; 114.73; 114.92; 120.83; 121.00; 124.33; 126.54; 127.37; 129.87; 129.96; 154.56; 158.95; 159.47; 159.88. Anal. ($C_{20}H_{18}F_3N_7O$) C, H, N.

N-(2-phenoxyethyl)-6-(2-(3- (trifluoromethyl)phenyl) hydrazinyl)-9H-purin-2- amine 19e:

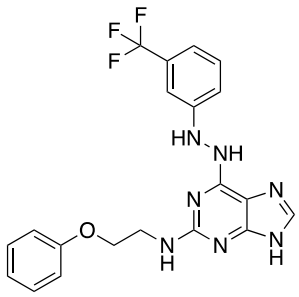

Yield: 21 %. **MS** (ESI) $[M+H]^+$= 430.15 m/z. **^{1}H NMR** (DMSO, 400 MHz) δ 3.50 (*m*, 2H); 3.89 (*m*, 2H); 6.46 (*bs*, 1H); 6.90 (*t*, 1H, *J* = 8 Hz); 6.99 (*m*, 4H); 7.28 (*m*, 4H); 7.76 (*s*, 1H); 8.21 (*s*, 1H); 9.28 (*bs*, 1H); 12.34 (*bs*, 1H). **^{13}C NMR** (DMSO-*d*$_6$, 100M Hz) δ 41.10; 66.30; 114.81; 114.93; 120.94; 121.00; 122.88; 125.56; 129.97; 130.62; 130.73; 131.05; 131.54; 131.55; 143.09; 158.97; 163.55. Anal. ($C_{20}H_{18}F_3N_7O$) C, H, N.

General procedures for synthesis of compounds 20a-d: Compounds **19b-e** (20 mg each) were dissolved in MeOH and stirred at room temperature under air atmosphere for 96 h. The corresponding oxidized compounds **21a-d** were obtained as pure products in quantitative yields.

6-((3-fluorophenyl)diazenyl)-N-(2-phenoxyethyl)-9H-purin- 2-amine 20a:

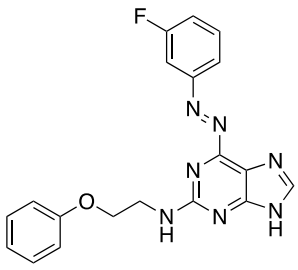

MS (ESI) $[M+H]^+$: 378.28 m/z. **^{1}H NMR** ($CDCl_3$, 400 MHz): δ 4.00 (m, 2H); 4.21 (m, 2H); 6.11 (bs, 1H); 6.94 (m, 3H); 7.27 (m, 3H); 7.50 (q, 1H, *J* = 8 Hz); 7.73 (s, 1H); 7.89 (d, 1H, *J* = 4 Hz); 8.24 (s, 1H). ^{13}C NMR ($CDCl_3$ +CD_3OD, 100 MHz): δ 41.22; 66.45; 108.88; 109.18; 114.46; 119.95; 120.93; 121.34; 129.45; 130.47; 130.58; 153.87; 158.58; 159.78; 161.50; 164.81. Anal. ($C_{19}H_{16}FN_7O$) C, H, N.

6-((3,5-difluorophenyl)diazenyl)-N-(2-phenoxyethyl)-9H-purin-2-amine 20b:

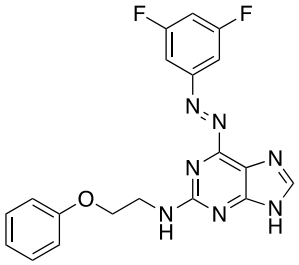

MS (ESI) $[M+H]^+$: 396.22 m/z. **^{1}H NMR** ($CDCl_3$+CD_3OD, 400 MHz): δ 3.93 (t, 2H, J = 4 Hz); 4.19 (t, 2H, J = 4 Hz); 6.91 (m, 3H); 7.02 (q, 1H, J = 4 Hz); 7.25 (t, 2H, J = 8 Hz); 7.28 (s, 1H); 7.70 (d, 2H, J = 4 Hz); 8.12 (s, 1H); 13.65 (s, 1H). **^{13}C NMR** ($CDCl_3$+CD_3OD, 100 MHz): δ 41.23; 66.41; 106.91; 107.18; 107.72; 107.98; 108.21; 114.45; 120.96; 129.46; 154.23; 158.58; 159.71; 162.02; 164.38. Anal. ($C_{19}H_{15}F_2N_7O$) C, H, N.

6-((3,5-bis(trifluoromethyl)phenyl)diazenyl)-N-(2-phenoxyethyl)-9H-purin-2-amine 20c:

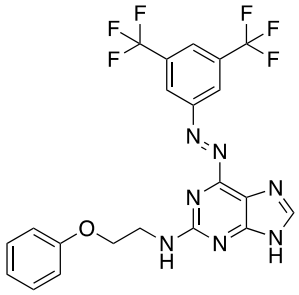

MS (ESI) $[M+H]^+$**:** 496.34 m/z. **^{1}H NMR** ($CDCl_3$, 400 MHz): δ 4.02 (m, 2H); 4.23 (m, 2H); 6.13 (bs, 1H); 6.95 (m, 3H); 7.28 (m, 2H); 8.08 (s, 1H); 8.26 (s, 1H); 8.56 (s, 1H). **^{13}C NMR** ($CDCl_3$+CD_3OD, 100 MHz): δ 41.51; 66.42; 114.45; 121.09; 121.38; 123.76; 124.09; 125.98; 129.53; 132.58; 132.92; 133.26; 133.60; 152.48; 158.50; 159.93. Anal. ($C_{21}H_{15}F_6N_7O$) C, H, N.

N-(2-phenoxyethyl)-6-((4- (trifluoromethyl)phenyl)diazenyl)-9H-purin-2-amine 20d:

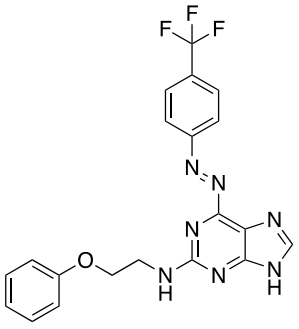

MS (ESI) $[M+H]^+$: 428.15 m/z. **^{1}H NMR** ($CDCl_3$, 400 MHz): δ 4.01 (t, 2H, J = 4 Hz); 4.22 (t, 2H, J = 4 Hz); 6.09 (s, 1H); 6.94 (m, 3H); 7.27 (m, 2H); 7.81 (d, 2H, J = 8 Hz); 8.15 (d, 2H, J = 8 Hz); 8.24 (s, 1H); 13.65 (bs, 1H). ^{13}C NMR ($CDCl_3$+CD_3OD, 100 MHz): δ 45.12; 70.29; 118.35; 118.39; 124.84; 126.19; 127.89; 128.90; 130.42; 133.35; 137.92; 138.24; 158.23; 162.54; 162.59; 163.67. Anal. ($C_{20}H_{16}F_3N_7O$) C, H, N.

Nucleoside Derivatives

General Procedure for the Synthesis of Compounds 23a,c and 31a,c: To a solution of intermediate **10a,c** (100 mg) in dry acetonitrile, synthesized according to the procedure reported in Rif. 150, was added BSA (1.5 eq.), under N_2. The reaction mixture was stirred for 1 hour. After this time, a clear solution was formed and TMSOTf (2 eq.) was added. The reaction was heated at reflux and D 1,2,3,5-tetra acetyl ribose or L-1,2,3,5-tetra acetyl ribose (1 eq.) respectively were added. The solution was stirred at reflux for 1,5 hours. The obtained reaction solution was cooled to r.t., saturated $NaHCO_3$ and EtOAc were added and the extraction was performed three times. The obtained organic layers were washed with brine, dried over Na_2SO_4, and concentrated under vacuum. The product was obtained in quantitative yield and used for the next step without further purification.

General Procedure for the Synthesis of Compounds 24a,c and 32a,c: Compound **23a,c** or **31a,c** were dissolved in NH_3/EtOH. The reaction mixture was stirred for 1 h at r.t. After this time, the solvent was removed under reduced pressure and the residue was purified on silica gel chromatography in 95:5 CH_2Cl_2/MeOH as eluent.

β-D-(2*R*,3*R*,4*S*,5*R*)-2-(2-chloro-6-((3-fluorophenyl)amino)-9*H*-purin-9-yl)-5 (hydroxymethyl)tetrahydrofuran-3,4-diol 24a:

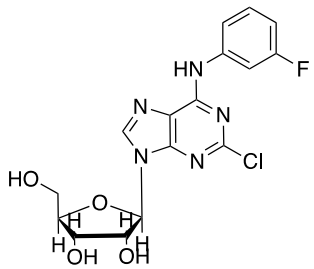

Yield: 100%; **^{1}H-NMR** (DMSO-d_6 400 MHz): δ 4.13 (m, 1H); 4.22 (m, 2H); 4.33 (m, 1H); 4.55 (t, 1H, J = 8 Hz); 4.62 (m, 1H); 5.44 (d, 1H, J = 8 Hz); 5.65 (m, 1H); 5.94 (m, 1H); 6.93 (td, 1H, J = 1.6 Hz, J = 8 Hz); 7.41 (q, 1H, J = 4 Hz); 7.72 (d, 1H, J = 4 Hz); 7.72 (td, 1H, J = 4 Hz; J = 8 Hz); 8.57 (s, 1H); 10.60 (s, 1H).

β-D-(2*R*,3*R*,4*S*,5*R*)-2-(2-chloro-6-((3-(trifluoromethyl)phenyl)amino)-9*H*-purin-9 yl)-5-(hydroxymethyl)tetrahydrofuran-3,4-diol 24c:

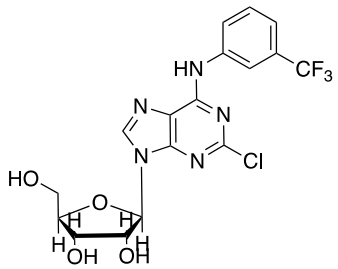

Yield: 100%; **^{1}H-NMR** (DMSO-d_6 400 MHz): δ 3.59 (m, 1H); 3.69 (m, 1H); 3.98 (m, 1H); 4.16 (m, H); 4.56 (q, 1H, J = 8 Hz); 5.07 (t, 1H, J = 4 Hz); 5.25 (d, 1H, J = 4 Hz); 5.55 (d, 1H; J = 4 Hz); 5.92 (d, 1H, J = 4 Hz); 7.45 (m, 1H); 7.62 (t, 1H, J = 12 Hz); 8.16 (d, 1H, J = 8 Hz); 8.39 (m, 1H); 8.59 (s, 1H); 10.70 (s, 1H).

β-L-(2*S*,3*S*,4*R*,5*S*)-2-(2-chloro-6-((3-fluorophenyl)amino)-9*H*-purin-9-yl)-5 (hydroxymethyl)tetrahydrofuran-3,4-diol 32a:

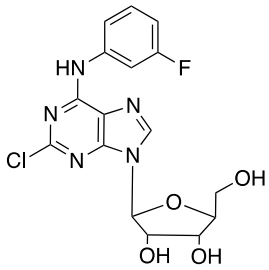

Yield: 100%; **^{1}H-NMR** (DMSO-*d_6* 400 MHz): δ 3.19 (m,1H); 4.24 (m, 2H); 4.35 (m, 1H); 4.65 (t, 1H, J = 8 Hz); 4.63 (q, 1H, J = 4 Hz); 5.45 (d, 1H, J = 4 Hz); 5.66 (d, 1H, J = 4 Hz); 5.94 (d, 1H, J = 4 Hz); 6.94 (m, 1H); 7.40 (q, 1H, J = 4 Hz); 7.71 (dt, 1H, J = 2 Hz, J = 4 Hz); 7.84 (s, 1H); 10.60 (s, 1H).

β-L-(2*S*,3*S*,4*R*,5*S*)-2-(2-chloro-6-((3-(trifluoromethyl)phenyl)amino)-9*H*-purin-9 yl)-5-(hydroxymethyl)tetrahydrofuran-3,4-diol 32c:

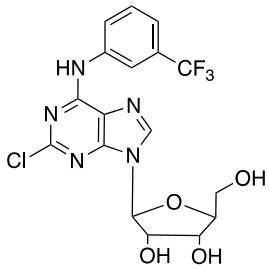

Yield: 100%; **^{1}H-NMR** (DMSO-*d_6* 400 MHz): δ 3.17 (d, 1H, J = 4 Hz); 4.11(m, 1H); 4.25 (m, 1H); 4.31 (m, 1H); 4.63 (m, 1H); 5.45 (d, 1H, J = 4 Hz); 5.66 (d, 1H, J = 8 Hz); 5.95 (d, 1H, J = 4 Hz); 7.45 (d, 1H, J = 8 Hz); 7.60 (t, 1H, J = 8 Hz); 8,16 (d, 1H, J = 8 Hz); 8.37 (t, 1H, J = 8 Hz); 8.59 (s, 1H); 10.73 (s, 1H).

General Procedure for the Synthesis of Compounds 22a-d and 25c-d, and 33a-d and 34c,d: In a microwave tube **24a,c** or **32a,c** (0.19 mmol) and the proper amine (0.570 mmol) were suspended in n-BuOH (3 mL). TFA (0.19 mmol) was added, and the tube was heated under microwave irradiation at 150-170 °C for 40-70 min (max mW power input: 300 W; ramp time: 1 min; power max: off; maximum pressure: 260 psi). The reaction mixture was concentrated under vacuum, dissolved with EtOAc, and washed with $NaHCO_3$. The combined organic phases were washed with brine, dried over anhydrous Na_2SO_4, and evaporated to dryness. The crude material was purified by silica gel flash chromatography, using the proper eluent:

β-D-(2*R*,3*R*,4*S*,5*R*)-2-(6-((3-fluorophenyl)amino)-2-((2-phenoxyethyl)amino)-9*H*-purin-9-yl)-5-(hydroxymethyl)tetrahydrofuran-3,4-diol 22a:

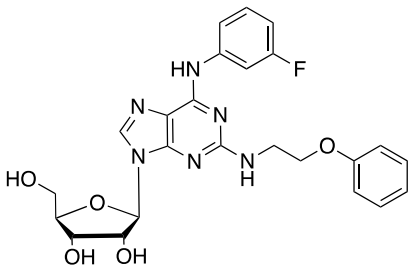

Yield: 75%; **MS** (ESI) $[M+H]^+$: 497.19 m/z. $[\alpha]^{20}_D$ = - 50 °C (c= 0.01, ACN); **^{1}H-NMR** (DMSO-*d_6* 400 MHz): δ 3.58 (m, 1H); 3.67 (m, 1H); 3.94 (t, 1H, J = 4 Hz); 4.14 (m, 4H); 4.50 (d, 1H, J = 4Hz); 5.08 (t, 1H; J = 4 Hz); 5.24 (d, 1H, J = 4 Hz); 5.51 (d, 1H, J = 4 Hz); 5.84 (d, 1H; J = 4 Hz); 6.77 (t, 1H, J = 8 Hz); 6.92 (t, 1H, J = 8 Hz); 6.98 (m, 3H); 7.28 (m, 3H); 7.80 (d, 1H, J = 8 Hz); 8.11 (bs, 1H); 8.13 (s, 1H); 9.78 (bs, 1H).

^{13}C-NMR (DMSO-*d*$_6$ 100 MHz): δ 42.51; 61.61; 66.50; 70.60; 73.49; 85.86; 87.93; 113.53; 119.76; 123.06; 130.08; 130.15; 139.99; 143.09; 148.54; 152.30; 155.44; 160.95; 163.37.

β-L-(2*S*,3*S*,4*R*,5*S*)-2-(6-((3-fluorophenyl)amino)-2-((2-phenoxyethyl)amino)-9*H*-purin-9-yl)-5-(hydroxymethyl)tetrahydrofuran-3,4-diol 33a:

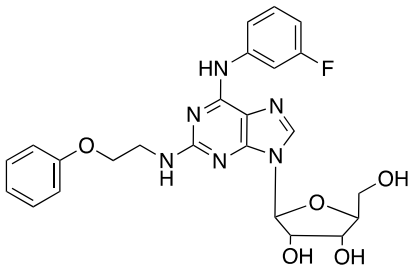

Yield: 25%; **MS** (ESI) [M+H]$^+$: 497.19 m/z; [α]$^{20}_D$ = + 50 °C (c= 0.012, ACN); **^{1}H-NMR** (DMSO-*d*$_6$ 400 MHz): δ 3.55 (m, 1H); 3.67 (m, 3H); 3.93 (t, 2H; J = 8Hz); 4.14 (m, 3H); 4.62 (bs, 1H); 5.17 (bs, 1H); 5.42 (d, 1H, J = 8 Hz); 5.83 (d, 1H, J = 8 Hz); 6.77 (t, 1H, J = 8 Hz); 6.95 (m, 5H); 7.29 (m, 3H); 7.80 (d, 1H, J = 8 Hz); 8.13 (s, 1H); 9.75 (s, 1H). **^{13}C-NMR** (DMSO-*d*$_6$ 100 MHz): δ 43.40; 61.24; 66.50; 68.55; 71.08; 73.70; 85.84; 87.35; 107.00; 108.68; 109.91; 114.89; 114.96; 116.18; 120.99; 130.00; 130.03; 137.74; 142.65; 152.44; 159.00; 159.27.

β-D-(2*R*,3*S*,4*R*,5*R*)-2-(hydroxymethyl)-5-(2-((2-phenoxyethyl)amino)-6-((3-(trifluoromethyl)phenyl)amino)-9*H*-purin-9-yl)tetrahydrofuran-3,4-diol 22b:

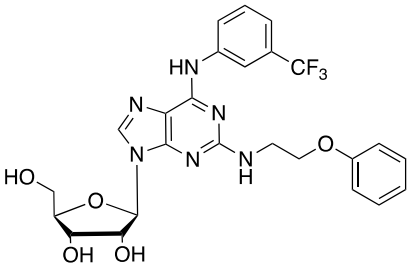

Yield: 73%; **MS** (ESI) [M+H]$^+$: 547.19 m/z; [α]$^{20}_D$ = - 150 °C (c= 0.004, ACN); **^{1}H-NMR** (DMSO-*d*$_6$ 400 MHz): δ 3.48 (m, 1H); 3.58 (m, 1H); 3.71 (q, 1H, J = 8 Hz); 4.07 (q, 1H, J = 4 Hz); 4.14 (m, 4H); 4.35 (t, 1H, J = 8 Hz); 6.20 (d, 1H, J = 8 Hz); 6.93 (m, 4H); 7.28 (m, 3H); 7.48 (t, 1H, J = 8 Hz); 8.14 (s, 1H); 8.26 (s, 1H); 9.93 (bs, 1H). **^{13}C-NMR** (DMSO-*d*$_6$ 100 MHz): δ 42.60; 61.63; 66.59; 70.63; 73.54; 87.97; 119.79; 123.61; 123.69.; 125.64; 128.96; 129.30; 131.32; 140.08; 141.54; 148.58; 152.33; 154.43.

β-L-(2*S*,3*R*,4*S*,5*S*)-2-(hydroxymethyl)-5-(2-((2-phenoxyethyl)amino)-6-((3-(trifluoromethyl)phenyl)amino)-9*H*-purin-9-yl)tetrahydrofuran-3,4-diol 33b:

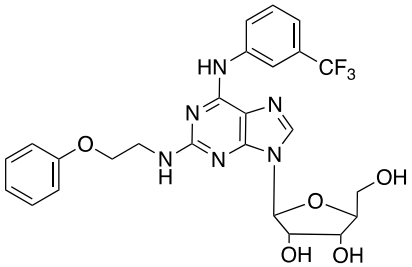

Yield: 41%; **MS** (ESI) [M+H]$^+$: 547.19 m/z; [α]$^{20}_D$ = + 220 °C (c= 0.005, DMSO); **^{1}H-NMR** (DMSO-*d*$_6$ 400 MHz): δ 3.56 (m; 1H); 3.68 (m, 3H); 3.93 (d, 2H, J = 4 Hz); 4.14 (m, 3H); 4.59 (bs, 1H); 5.08 (bs, 1H); 5.17 (d, 1H; J = 4 Hz); 5.42 (d, 1H, J = 8 Hz); 5.83 (d, 1H, J = 8 Hz); 6.92 (m, 5 H); 7.29 (m, 3H); 7.49 (t, 1H, J = 8 Hz); 8.10 (s, 1H); 8.15 (s, 1H); 9.93 (s, 1H). **^{13}C-NMR** (DMSO-*d*$_6$ 100 MHz): δ 43.41; 61.10; 66.54;

71.04; 73.73; 79.65; 85.82; 87.28; 114.83; 116.57; 116.59; 118.43; 120.98; 123.96; 129.49; 129.87; 129.98; 134.22; 137.87; 141.50; 152.33; 158.90; 159.20.

β-D-(2*R*,3*R*,4*S*,5*R*)-2-(6-((3-fluorophenyl)amino)-2-(methylamino)-9*H*-purin-9-yl)-5-(hydroxymethyl)tetrahydrofuran-3,4-diol 22c:

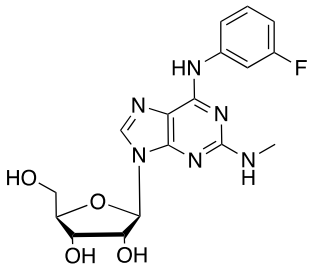

Yield: 50%; **MS** (ESI) $[M+H]^+$: 391.15 m/z; $[\alpha]^{20}_D$ = - 38.46 °C (c= 0.013, ACN); **^{1}H-NMR** (DMSO-*d*$_6$ 400 MHz): δ 2.84 (s, 3H); 3.56 (m, 1H); 3.66 (m, 1H); 3.91 (m, 1H); 4.15 (q, 1H, J= 4); 4.63 (bs, 1H); 5.08 (bs, 1H); 5.18 (d, 1H, J=4); 5.43 (d, 1H, J = 8); 5.81 (d, 1H, J = 8); 6.78 (m, 2H); 7.30 (q, 1H, J = 8); 7.79 (dd, 1H, J = 4); 8.10 (s, 1H); 8.15 (dt, 1H, J = 4, J = 12); 9.74 (s, 1H). **^{13}C-NMR** (DMSO-*d*$_6$ 100 MHz): δ 28.90; 61.66; 70.50; 73.70; 87.40; 97.30; 107.03; 108.44; 115.94; 130.24; 137.25; 142.79; 151.85; 153.34; 159.84; 161.43; 163.48.

β-L-(2*S*,3*S*,4*R*,5*S*)-2-(6-((3-fluorophenyl)amino)-2-(methylamino)-9*H*-purin-9-yl)-5-(hydroxymethyl)tetrahydrofuran-3,4-diol 33c:

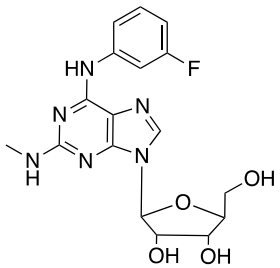

Yield: 41%; **MS** (ESI) $[M+H]^+$: 391.15 m/z; $[\alpha]^{20}_D$ = + 40 °C (c= 0.015, DMSO);**^{1}H-NMR** (DMSO-*d*$_6$ 400 MHz): δ 2.84 (d, 3H, J = 4 Hz); 3.56 (q, 1H, J = 4 Hz); 3.65 (m, 1H); 3.92 (m, 1H); 4.16 (d, 1H, J = 4 Hz); 4.43 (m, 1H); 4.64 (d, 1H, J = 4 Hz); 5.06 (d, 1H, J = 4 Hz); 5.15 (d, 1H, J = 4 Hz); 5.40 (d, 1H, J = 4 Hz); 5.81 (d, 1H, J = 4 Hz); 6.78 (m, 1H); 7.30 (q, 1H, J = 8 Hz); 7.79 (d, 1H, J = 8 Hz); 8.09 (s, 1H); 8.15 (d, 1H, J = 12 Hz); 9.71 (s, 1H). **^{13}C-NMR** (DMSO-*d*$_6$ 100 MHz): δ 30.97; 62.19; 71.13; 73.51; 85.86; 87.42; 106.81; 107.18; 108.51; 116.09; 130.22; 137.67; 142.73; 152.34; 160.01; 161.89.

β-D-(2*R*,3*S*,4*R*,5*R*)-2-(hydroxymethyl)-5-(2-(methylamino)-6-((3-(trifluoromethyl)phenyl)amino)-9*H*-purin-9-yl)tetrahydrofuran-3,4-diol 22d:

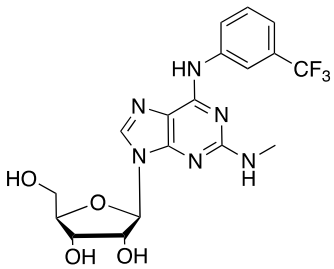

Yield: 59%; **MS** (ESI) $[M+H]^+$: 441.46 m/z; $[\alpha]^{20}_D$ = - 100 °C (c= 0.005, ACN); **^{1}H-NMR** (DMSO-*d*$_6$ 400 MHz): δ 2.85 (*d*, 3H, J=4), 3.55 (*m*, 1H), 3.66 (*m*, 1H), 3.91 (q, 1H; *J*=4), 4.15 (m, 1H), 4.61 (bs, 1H), 5.11 (bs, 1H), 5.18 (d, 1H, *J*=4); 5.43 (d, 1H, J = 8); 5.81 (d, 1H, *J* = 8); 6.73 (q, 1H, J = 8); 7.31 (d, 1H, J = 4); 7.51 (t, 1H, J = 8); 8.13(s, 1H); 8.24

(bs, 1H); 9.93 (bs, 1H). **^{13}C-NMR** (DMSO-*d*$_6$ 100 MHz): δ 28.91; 61.20; 70.37; 73.51; 87.86; 97.42; 113.91, 116.32, 117.96, 123.53, 126.23, 129.78, 136.98, 141.86, 152.07, 153.45, 160.09.

β-L-(2*S*,3*R*,4*S*,5*S*)-2-(hydroxymethyl)-5-(2-(methylamino)-6-((3-(trifluoromethyl)phenyl)amino)-9*H*-purin-9-yl)tetrahydrofuran-3,4-diol 33d:

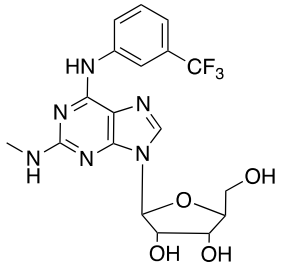

Yield: 43%; **MS** (ESI) [M+H]$^+$: 441.46 m/z; [α]$^{20}_D$ = - 75 °C (c= 0.003, DMSO); **^{1}H-NMR** (DMSO-*d*$_6$ 400 MHz): δ 3.55 (m, 1H); 3.66 (m, 1H); 3.92 (q, 1H, J = 4Hz); 4.16 (q, 1H, J= 4 Hz); 4.60 (m, 1H); 5.08 (m, 1H); 5.16 (d, 1H, J = 4 Hz); 5.42 (d, 1H, J = 4 Hz); 5.81 (d, 1H, J = 4 Hz); 6.70 (m, 1H); 7.30 (d, 1H, J = 8 Hz); 7.51 (t, 1H, J = 8 Hz); 8.10 (s, 1H); 8.39 (bs, 1H); 9.90 (s, 1H). **^{13}C-NMR** (DMSO-*d*$_6$ 100 MHz): δ 28.91; 64.60; 70.95; 73.02; 81.81; 87.99; 114.52; 116.09; 130.12; 130.21; 137.71; 142.62; 142.73; 152.36; 159.87 160.04; 161.39; 163.77.

β-D-((2*R*,3*S*,4*R*,5*R*)-5-(6-((3-fluorophenyl)amino)-2-(methylamino)-9*H*-purin-9-yl)-3,4-dihydroxytetrahydrofuran-2-yl)methyl acetate 25c:

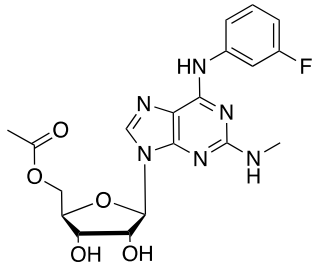

Yield: 10%; **MS** (ESI) [M+H]$^+$: 433.22 m/z; **^{1}H-NMR** (DMSO-*d*$_6$ 400 MHz): δ 2.02 (s; 3H), 2.84 (d, 3H, J=4); 4.05 (m, 1H); 4.18 (m, 1H); 4.33 (dd, 1H; J = 4 Hz; J = 8 Hz); 4.69 (bs, 1H); 5.37 (d, 1H, J = 8 Hz); 5.56 (d, 1H, J = 8 Hz); 5.77 (s, 1H); 5.83(d, 1H, J = 8 Hz); 6.78 (ddd, 1H, J = 8 Hz, J = 16 Hz); 6.85(bs, 1H); 7.78 (m,1H); 8.07(s, 1H); 8.15 (dt, 1H, J = 4 Hz; J = 12 Hz); 9.73(bs, 1H). **^{13}C-NMR** (DMSO-*d*$_6$ 100 MHz): δ 21.06; 28.86; 30.96; 64.60; 70.95; 73.02; 81.81; 107.18; 108.50; 114.52; 116.09; 130.21; 137.71; 142.62; 152.36; 160.05; 161.39; 163.77; 170.67.

β-L-((2*S*,3*R*,4*S*,5*S*)-5-(6-((3-fluorophenyl)amino)-2-(methylamino)-9*H*-purin-9-yl)-3,4-dihydroxytetrahydrofuran-2-yl)methyl acetate 34c:

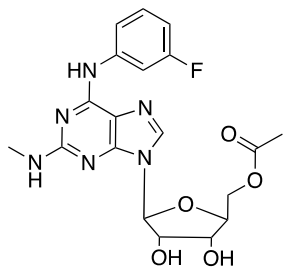

Yield: 17%; **MS** (ESI) [M+H]$^+$: 433.22 m/z; **^{1}H-NMR** (DMSO-*d*$_6$ 400 MHz): δ 2.01 (s, 3H); 2.82 (d, 3H, J = 8 Hz); 4.06 (q, 1H, J = 8 Hz); 4.18 (m, 1H); 4.34 (m, 1H); 4.39 (t, 1H, J = 8 Hz); 4.69 (bs, 1H); 5.34 (d, 1H, J = 8 Hz); 5.52 (t, 1H, J = 8 Hz); 5.83 (t, 1H, J = 8 Hz); 6.78 (t, 1H, J = 8 Hz); 6.83 (m, 1H); 7.30 (q, 1H, J = 12 Hz); 7.78 (d, 1H, J = 8 Hz); 8.06 (s, 1H); 8.15 (d, 1H, J = 12 Hz); 9.70 (s, 1H). **^{13}C-NMR** (DMSO-*d*$_6$ 100 MHz): δ 21.06; 28.86; 64.60; 70.95; 73.02;

81.81; 107.18; 108.50; 114.52; 116.09; 130.21; 137.71; 142.62; 152.36; 160.05; 161.39; 163.77; 170.67.

β-D-((2*R*,3*S*,4*R*,5*R*)-3,4-dihydroxy-5-(2-(methylamino)-6-((3-(trifluoromethyl)phenyl)amino)-9*H*-purin-9-yl)tetrahydrofuran-2-yl)methyl acetate 25d:

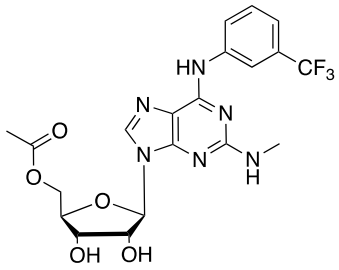

Yield: 22%; **MS** (ESI) $[M+H]^+$: 483.22 m/z; **^{1}H-NMR** (DMSO-*d_6* 400 MHz): δ 2.02 (s, 3H); 2.85 (d, 3H, J = 4 Hz); 4.05 (m, 1H); 4.19 (m, 1H); 4.28 (bs, 1H); 4.34 (dd, J = 4 Hz, J = 12 Hz); 4.66 (bs, 1H); 5.36 (d, 1H, J= 4 Hz); 5.56 (d, 1H, J= 4 Hz); 5.83 (d, 1H, J= 4 Hz); 6.79 (q, 1H, J = 4 Hz); 7.30 (d, 1H, J = 8 Hz); 7.51 (t, 1H, J = 8 Hz); 8.10 (s, 1H); 8.31 (bs, 1H); 9.92(bs, 1H). **^{13}C-NMR** (DMSO-*d_6* 100 MHz): δ 21.05; 28.82; 62.19; 71.13; 73.51; 85.86; 91.42; 106.81; 107.18; 108.51; 116.09; 130.22; 137.67; 142.73; 152.34; 161.01; 161.80.

β-L-((2*S*,3*R*,4*S*,5*S*)-3,4-dihydroxy-5-(2-(methylamino)-6-((3-(trifluoromethyl)phenyl)amino)-9*H*-purin-9-yl)tetrahydrofuran-2-yl)methyl acetate 34d:

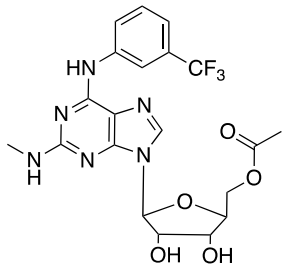

Yield: 27%; **MS** (ESI) $[M+H]^+$: 483.22 m/z; **^{1}H-NMR** (DMSO-*d_6* 400 MHz): δ 2.02 (s, 3H); 2.86 (d, 3H, J = 4 Hz); 4.07 (m, 1H); 4.18 (m, 1H); 4.25 (m, 1H); 4.34 (m, 1H); 4.66 (bs, 1H); 5.34 (d, 1H; J = 4 Hz); 5.54 (d, 1H, J = 4 Hz); 5.83 (d, 1H); 6.77 (d, 1H, J = 8 Hz); 7.30 (d, 1H, J = 8 Hz); 7.51 (t, 1H, J = 8 Hz); 8.02 (s, 1H); 8.09 (s, 1H); 8.26 (bs, 1H); 9.89 (s, 1H). **^{13}C-NMR** (DMSO-*d_6* 100 MHz): δ 20.06; 28.82; 66.19; 71.13; 73.51; 85.86; 87.42; 106.80; 107.20; 108.50; 116.10; 130.22; 137.67; 142.73; 152.34; 160.01; 161.89.

General Procedure for the Synthesis of Compounds 26 and **35:** To compound **22c** (260 mg; 0.59 mmol) or **22b** (150 mg; 027 mmol) respectively and p-toluene sulfonic acid monohydrate (1.2 eq.) were added 4 mL of 2,2'-dimethoxypropane (4 mL). The reaction mixture was stirred at r.t. for 15h. After 15h, the reaction mixture was neutralized with $NaHCO_3$. After that, the water phase was extracted several times with EtOAc. The combined organic phases were extracted once with brine, dried over Na_2SO_4, and evaporated under reduced pressure in vacuo. The product was purified by silica gel chromatography in 98:2 CH_2Cl_2/MeOH as eluent.

β-D-((3a*R*,4*R*,6*R*,6a*R*)-2,2-dimethyl-6-(2-(methylamino)-6-((3-(trifluoromethyl)phenyl)amino)-9*H*-purin-9-yl)tetrahydrofuro[3,4-*d*][1,3]dioxol-4-yl)methanol 26:

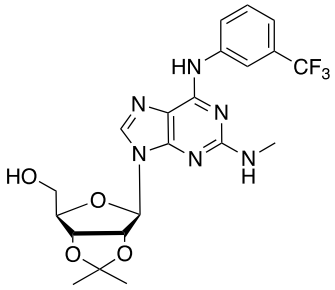

Yield: 92%; **MS** (ESI) $[M+H]^+$: 481.18 m/z; **1H-NMR** (DMSO-d_6 400 MHz): δ 1.33 (s, 3H); 1.54 (s, 3H); 2.86 (d, 3H, J = 4 Hz); 3.54 (dd, 2H, J = 4 Hz; J = 8 Hz); 4.15 (m, 1H); 5.04 (dd, 1H, J = 4 Hz, J = 8 Hz); 5.39 (m, 1 H); 6.07 (d, 1H, J = 1.6 Hz); 6.81 (d, 1H, J = 8 Hz); 7.30 (d, 1H, J = 8 Hz); 7.51 (t, 1H, J = 8 Hz); 8.10 (s, 1H); 8.24 (bs, 1H); 9.92 (s, 1H).

β-D-((3a*R*,4*R*,6*R*,6a*R*)-2,2-dimethyl-6-(2-((2-phenoxyethyl)amino)-6-((3 (trifluoromethyl)phenyl)amino)-9*H*-purin-9-yl)tetrahydrofuro[3,4 *d*][1,3]dioxol-4-yl)methanol 35:

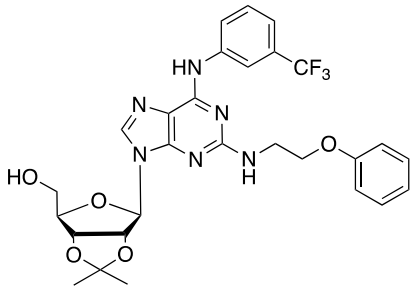

Yield: 76%; **MS** (ESI) $[M+H]^+$: 587.22 m/z; **^{1}H-NMR** (DMSO-d_6 400 MHz): δ 1.35 (s, 3H); 1.56 (s, 3H); 3.55 (m, 2H); 3.69 (m, 2H); 4.15 (m, 3H); 4.98 (dd, 1H, J = 4 Hz, J = 8 Hz); 5.35 (dd, 1H, J = 4 Hz, J = 8 Hz); 6.15 (d, 1H, J = 4 Hz); 6.94 (m, 4H); 7.23 (m, 3H), 7.46 (t, 1H, J = 8 Hz); 8.12 (s, 1H); 8.58 (s, 1H); 9.93 (bs, 1H).

General Procedure for the Synthesis of Compounds 27a,b: To a solution of **26** (50 mg) and DMAP (3 eq.) in anhydrous CH_2Cl_2 (2 mL) was added isobutyryl chloride (0.16 mmol; 1.5 eq.) for obtaining compound **27a** or octanoyl chloride (0.33 mmol; 3 eq.) for obtaining compound **27b**, and the reaction mixture was stirred at r.t. for 1h. The reaction mixture was then diluted with CH_2Cl_2 and washed with water for three times and brine. The organic layer was separated, dried over Na_2SO_4, and evaporated to dryness. **27a** was used for the next step without further purification. **27b** was purified by silica gel flash chromatography, using 99:1 CH_2Cl_2/MeOH as eluent.

((3a*R*,4*R*,6*R*,6a*R*)-2,2-dimethyl-6-(2-(methylamino)-6-((3-(trifluoromethyl)phenyl)amino)-9*H*-purin-9-yl)tetrahydrofuro[3,4-*d*][1,3]dioxol-4-yl)methyl isobutyrate 27a:

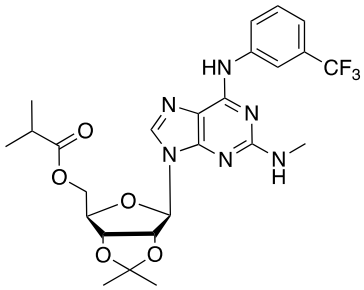

Yield: 100%; **^{1}H-NMR** (DMSO-d_6 400 MHz): 1.04 (dd, 1H, J = 1 Hz, J = 6.8 Hz); 1.35 (s, 3H); 1.55 (s, 3H); 2.85 (d, 3H; J = 4 Hz); 4.16 (m, 1H); 4.28 (m, 2H); 5.18 (m, 1H); 5.45 (m, 1H); 5.76 (s, 1H); 6.16 (s, 1H, J = 4 Hz); 6.88 (m, 1H); 7.31 (d, 1H, J = 8 Hz); 7.51 (t, 1H, J = 8 Hz); 8.06 (s, 1H); 8.25 (bs, 1H); 9.92 (bs, 1H).

((3a*R*,4*R*,6*R*,6a*R*)-2,2-dimethyl-6-(2-(methylamino)-6-((3-(trifluoromethyl)phenyl)amino)-9*H*-purin-9-yl)tetrahydrofuro[3,4-*d*][1,3]dioxol-4-yl)methyl octanoate 27b:

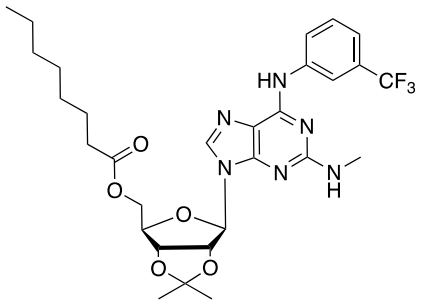

Yield: 64%

General Procedure for the Synthesis of Compounds 28a,b: To compounds **27a,b** was slowly added at 0 °C a mixture of water and TFA (2:1), and then the mixture was stirred at r.t. for 2h. The reaction mixture was neutralized with $NaHCO_3$ and extracted with CH_2Cl_2. The organic layer was separated, dried over Na_2SO_4, and concentrated under vacuum. The product was purified by silica gel chromatography in 95:5 CH_2Cl_2:MeOH.

β-D-((2*R*,3*S*,4*R*,5*R*)-3,4-dihydroxy-5-(2-(methylamino)-6-((3-(trifluoromethyl)phenyl)amino)-9*H*-purin-9-yl)tetrahydrofuran-2-yl)methyl isobutyrate 28a:

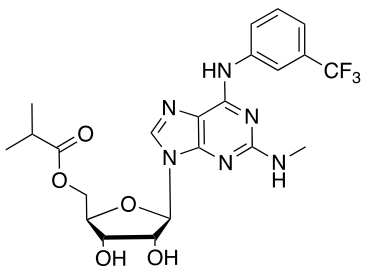

Yield: 28%; **MS** (ESI) $[M+H]^+$: 511.19 m/z; **^{1}H-NMR** (DMSO-d_6 400 MHz): δ 1.08 (d, 6H, J = 4 Hz); 2.86 (d, 3H, J = 4 Hz); 4.07 (m, 1H); 4.19 (m, 1H); 4.28 (bs, 1H); 4.36 (m, 1H); 4.64 (s, 1H); 5.33 (d, 1H; J = 4 Hz); 5.55 (d, 1H, J = 4 Hz); 5.84 (d, 1H, J = 4 Hz); 6.76 (d, 1H, J = 8 Hz); 7.30 (d, 1H, J = 8 Hz); 7.51 (t, 1H, J = 8 Hz); 8.07 (s, 1H); 8.26 (bs, 1H); 9.89 (s, 1H). **^{13}C-NMR** (DMSO-d_6 100 MHz): δ 28.89; 29.70; 34.14; 60.74; 61.90; 68.24; 82.40; 91.44; 111.06; 112.33; 113.92; 116.78; 119.25; 122.51; 124.94; 129.78; 135.38; 137.17; 152.73; 153.70; 176.84.

β-D-((2*R*,3*S*,4*R*,5*R*)-3,4-dihydroxy-5-(2-(methylamino)-6-((3-(trifluoromethyl)phenyl)amino)-9*H*-purin-9-yl)tetrahydrofuran-2-yl)methyl octanoate 28b:

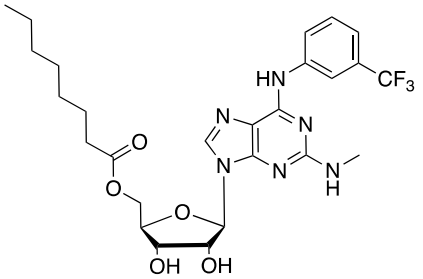

Yield: 59%; **MS** (ESI) $[M+H]^+$: 567.25 m/z; **^{1}H-NMR** (DMSO-*d_6* 400 MHz): δ 0.83 (m, 3H); 1.19 (m, 6H); 1.25 (m, 2H); 1.45 (m, 2H); 2.27 (m, 2H); 2.86 (s, 3H); 4.21 (m, 4H); 4.35 (m, 2H); 4.68 (s, 1H); 5.84 (d, 1H, J = 4 Hz); 7.31 (d, 1H, J = 8 Hz); 7.51 (t, 1H, J = 8 Hz); 8.09 (s, 1H); 8.25 (bs, 1H); 8.52 (bs, 1H); 9.91 (s, 1H). **^{13}C-NMR** (DMSO-*d_6* 100 MHz): δ 14.06; 22.59; 24.84; 28.91; 29.70; 31.64; 34.00; 63.39; 71.21; 72.43; 80.91; 91.10; 101.32; 106.83; 108.11; 123.93; 129.47; 131.16; 131.48; 135.25; 136.42; 173.28; 173.95; 177.79.

General Procedure for the Synthesis of Compound 40:

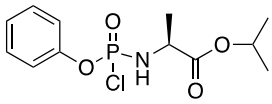

267 mg (3.4 mmol; 1 eq.) of isopropyl alaninate hydrochloride **38** were dissolved in 7 mL anhydrous CH_2Cl_2 at -78 °C. After adding 0.11 mL (3.4 mmol; 1 eq.) of phenyl phosphorodichloridate **39**, 0.21 mL (6.8 mmol; 2 eq.) of anhydrous triethylamine in CH_2Cl_2 were added dropwise. The solution was stirred at -78 °C for 30 min and subsequently at room temperature for 1 h. After evaporating the CH_2Cl_2, 8.6 mL anhydrous tetrahydrofuran were added, the suspension filtrated under N_2 atmosphere, and tetrahydrofuran was finally removed in vacuo to give a colorless oil, quantitative, that was used for the next step without purification because of its instability. **Yield**: 100%; **^{31}P-NMR** (DMSO-*d_6* 121 MHz): δ 7.68; 8.05.

General Procedure for the Synthesis of isopropyl β-D-((((3a*R*,4*R*,6*R*,6a*R*)-2,2-dimethyl-6-(2-((2-phenoxyethyl)amino)-6-((3-(trifluoromethyl)phenyl)amino)-9*H*-purin-9-yl)tetrahydrofuro[3,4-*d*][1,3]dioxol-4-yl)methoxy)(phenoxy)phosphoryl)alaninate 36:

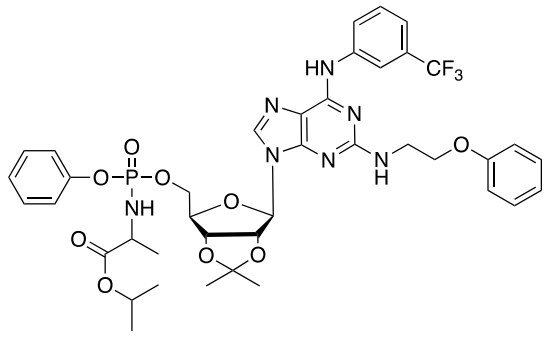

200 mg (0.6 mmol; 1 eq.) of the protected nucleoside **35** were dissolved in 8 mL anhydrous tetrahydrofuran and 1.3 mL (1.2 mmol; 2 eq.) of t-BuMgCl were added dropwise. After stirring at room temperature for 30 minutes, 849 mg (2.4 mmol; 4 eq.) isopropyl(chloro(phenoxy)phosphoryl)alaninate **40** in 8 mL anhydrous tetrahydrofuran were added dropwise with a cannula under inert gas, and the mixture stirred at room temperature overnight. Afterward, the

reaction was quenched with NH_4Cl, and the product was extracted with EtOAc. The combined organic phases were dried over Na_2SO_4, and the product was concentrated in vacuo to yield **36.**

Yield: 45%; **MS** (ESI) $[M+H]^+$: 856.30 m/z; **^{1}H-NMR** (DMSO-*d*$_6$ 600 MHz): δ δ 1.10 (s, 6H); 1.17(s, 3H); 1.35 (s, 3H); 1.56 (s, 3H); 3.70 (m, 3H); 4.27 (m, 4H); 4.41 (m, 1H); 4.80 (m, 2H); 5.38 (d, 1H, J = 6 Hz); 5.95 (d, 1H, J = 6 Hz); 6.91 (m, 3H); 7.13 (m, 2H); 7.30 (m, 5H); 7.45 (m, 1H); 7.61 (t, 1H, J = 12 Hz); 8.14 (m, 1H); 8.36 (m, 1H); 8.53(s, 1H); 10.72 (s, 1H).**^{31}P-NMR** (DMSO-*d*$_6$ 121 MHz): δ 3.52; 3.73.

General Procedure for the Synthesis of isopropyl β-D-((((2*R*,3*S*,4*R*,5*R*)-3,4-dihydroxy-5-(2-((2-phenoxyethyl)amino)-6-((3-(trifluoromethyl)phenyl)amino)-9*H*-purin-9-yl)tetrahydrofuran-2-yl)methoxy)(phenoxy)phosphoryl)alaninate 37:

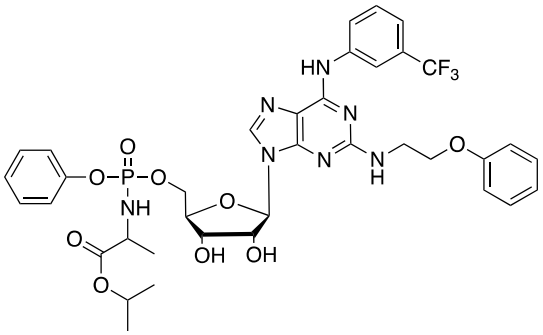

276 mg (0.4 mmol) of the protected protide **36** were dissolved in 5 mL 90% trifluoracetic acid and stirred at room temperature for 1h. The reaction was quenched with MeOH which was then co-evaporated with TFA. The crude product was dissolved in CH_2Cl_2 and purified by silica gel flash chromatography, using 98:2 CH_2Cl_2:MeOH as eluent.

Yield: 100%; **MS** (ESI) $[M+H]^+$: 816.27 m/z; **^{1}H-NMR** (DMSO-*d*$_6$ 600 MHz): δ 1.12 (s, 6H); 1.21(s, 3H); 3.72 (m, 2H); 4.20 (m, 5H); 4.59 (m, 1H); 4.80 (m, 1H); 5.48 (d, 1H, J = 6 Hz); 5.69 (d, 1H, J = 6 Hz); 5.95 (d, 1H, J = 6 Hz); 6.03 (m, 2H); 6.91 (m, 1H); 7.25 (m, 6H); 7.44 (m, 1H); 7.60 (t, 1H, J = 12 Hz); 8.15 (m, 1H); 8.37 (d, 1H, J = 6 Hz); 8.70 (s, 1H); 8.97 (s, 1H); 10.75 (s, 1H). **^{13}C-NMR** (DMSO-*d*$_6$ 151 MHz): δ 17.73; 19.82; 21.46; 21.50; 29.15; 50.03; 68.09; 70.29; 73.41; 79.63; 82.97; 87.43; 87.62; 104.81; 114.46; 120.28; 124.60; 124.69; 129.64; 129.69; 129.74; 129.90; 131.54; 133.55; 139.07; 139.77; 141.25; 146.75; 148.94; 150.76; 151.01; 152.31; 152.45; 153.11; 154.72; 172.78. **^{31}P NMR** (DMSO-*d*$_6$ 121 MHz): δ 3.74

Acyclic Derivatives

General Procedure for the Synthesis of Compound ethane-1,2-diyl diacetate 43:

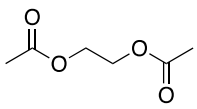

To a stirred and cooled (-5 °C) solution of 1,3-dioxolane **41** (1 mL, 1.49 mmol) and acetic anhydride **42** (1 mL, 1.09 mmol), conc. H_2SO_4 (98 %, d = 1.84 g/mL, 0.008 mmol) was added dropwise. The reaction mixture was stirred at r.t. for 12 h, then sat. aqueous $NaHCO_3$ was added, and the mixture was extracted with DCM (x3). The organic layers were dried over anhydrous Na_2SO_4, the solvent was evaporated, and the residue was distilled under reduced pressure. **Yield**: 52 %; **MS** (ESI) $[M+H]^+$: 147.06 m/z; **^{1}H NMR** ($CDCl_3$, 400 MHz): δ 2.02 (s, 6H); 4.18 (s, 4H).

General Procedure for the Synthesis of 2-(2,6-dichloro-9*H*-purin-9-yl)ethyl acetate 44:

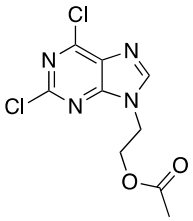

In a microwave tube compound **8** (100 mg; 0.53 mmol) was suspended in dry ACN. BSA (0.80 mmol; 1.5 eq.) was added and the reaction mixture was stirred until a clear solution was formed (about 1h). TMSOTf (0.26 mmol; 0.5 eq.) and ethylene glycol diacetate (0.80 mmol; 1.5 eq.) were added and the tube was heated at 150 °C for 30 minutes. The solvent was evaporated, and the reaction mixture was then diluted with CH_2Cl_2 and washed with water for three times and brine. The organic layer was separated, dried over Na_2SO_4, and concentrated under vacuum. The product was purified by silica gel chromatography in 98:2 CH_2Cl_2: MeOH with 0.5 % of formic acid as eluent. **Yield**: 48%; **MS** (ESI) $[M+H]^+$: 275.01 m/z; **^{1}H-NMR** (DMSO-*d_6* 400 MHz): δ 2.06 (s; 3H); 4.47 (m; 2H); 4.54 (m; 2H); 8.16 (s; 1H).

General Procedure for the Synthesis of Compounds 45a,c: In a microwave tube 2,6-dichloropurine **8** (mg; mmol) and the proper amine (3-fluoroaniline **9a** or 3-(trifluoromethyl)aniline **9c**) (2.645 mmol) were suspended in n-BuOH (3 mL). NEt_3 (258 mL; 1.852 mmol) was added, and the tube was heated at 120 °C for 1h (max mW power input: 100W; ramp time: 1 min; power max: off; maximum pressure: 260 psi). At the end of irradiation, the reaction mixture was concentrated under vacuum, dissolved with EtOAc, and washed with $NaHCO_3$. The combined organic layers were washed with brine, dried over anhydrous Na_2SO_4, filtered, and evaporated to dryness. The crude material was purified by silica gel chromatography, using 98:2 DCM/MeOH as eluent.

2-(2-chloro-6-((3-fluorophenyl)amino)-9*H*-purin-9-yl)ethyl acetate 45a:

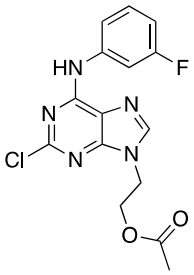

Yield: 45%; **MS** (ESI) $[M+H]^+$: 350.08 m/z; **^{1}H-NMR** (DMSO-d_6 400 MHz): δ 1.97 (s, 3H); 4.40 (m, 2H); 4.45 (m, 2H); 6.91 (td, 1H, J = 4 Hz, J = 8 Hz); 7.39 (q, 1H, J = 8 Hz); 7.71 (d, 1H, J = 8 Hz); 7.86 (dt, 1H; J = 4 Hz, J = 12 Hz); 8.38 (s, 1H); 10.52 (s, 1H).

2-(2-chloro-6-((3-(trifluoromethyl)phenyl)amino)-9*H*-purin-9-yl)ethyl acetate 45c:

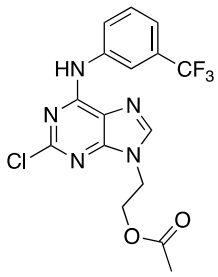

Yield: 41%; **MS** (ESI) $[M+H]^+$: 400.08 m/z; **^{1}H-NMR** (DMSO-d_6 400 MHz): δ 1.97 (s, 3H); 4.45 (m, 4H); 7.44 (d, 1H, J = 8 Hz); 7.61 (t, 1H, J = 8 Hz); 8.16 (d, 1H, J = 8 Hz); 8.38 (s, 1H); 8.40 (s, 1H); 10.65 (s, 1H).

General Procedure for the Synthesis of Compound 46a-d In a microwave tube **24a,c:** (0.19 mmol) and the proper amine (0.570 mmol) (methylamine **11a** or 2-phenoxyethylamine **11b**) were suspended in n-BuOH (3 mL). TFA (0.19 mmol) was added, and the tube was heated under microwave irradiation at 180 °C for 2h (max mW power input: 300 W; ramp time: 1 min; power max: off; maximum pressure: 260 psi). The reaction mixture was concentrated under vacuum, dissolved with EtOAc, and washed with $NaHCO_3$. The combined organic phases were washed with brine, dried over anhydrous Na_2SO_4, and evaporated to dryness. The crude material was purified by silica gel flash chromatography, using using 98:2 DCM/MeOH as eluent.

2-(6-((3-fluorophenyl)amino)-2-(methylamino)-9*H*-purin-9-yl)ethan-1-ol 46a:

Yield: 46%; **^{1}H-NMR** (DMSO-d_6 400 MHz): δ 2.85 (d, 3H, J = 4 Hz); 4.30 (m, 2H); 4.39 (t, 2H, J = 4 Hz); 6.77 (m, 1H); 7.29 (d, 1H, J = 8 Hz); 7.78 (d, 1H, J = 8Hz); 7.89 (s, 1H); 8.15 (m, 1H); 9.65 (s, 1H). **^{13}C-NMR** (DMSO-d_6 100 MHz): δ 28.83; 53.64; 59.40; 106.83; 108.21; 114.40; 129.95; 130.11; 139.56; 142.66; 142.76; 152.29; 158.97; 159.17.

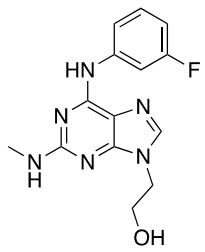

2-(2-(methylamino)-6-((3-(trifluoromethyl)phenyl)amino)-9*H*-purin-9-yl)ethan-1-ol 46b:

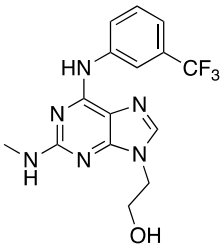

Yield: 80%; **^{1}H-NMR** (DMSO-d_6 400 MHz): δ 2.86 (s, 3H); 4.31 (m, 2H); 4.38 (m, 2H); 6.8 (bs, 1H); 7.30 (d, 1H, J = 8 Hz); 7.51 (t, 1H, J = 8 Hz); 7.96 (s, 1H); 8.20 (bs, 1H); 8.71 (bs, 1H); 9.90 (s, 1H). **^{13}C-NMR** (DMSO-d_6 100 MHz): δ 28.90, 54.64; 60.40; 113.91, 116.32, 117.96, 123.53, 123.62, 126.23, 129.78, 136.98, 141.86, 152.07, 153.45, 160.08.

2-(6-((3-fluorophenyl)amino)-2-((2-phenoxyethyl)amino)-9*H*-purin-9-yl)ethan-1-ol 46c:

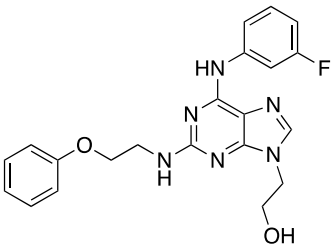

Yield: 90%; **^{1}H-NMR** (DMSO-d_6 400 MHz): δ 3.69 (q, 2H, J = 8 Hz); 3.76 (q, 2H, J = 8 Hz); 4.10 (t, 2H, J = 8 Hz); 4.16 (t, 2H, J =8 Hz); 5.01 (t, 1H, J = 8 Hz); 6.76 (td, 1H, J = 4 Hz, J = 8 Hz); 6.92 (t, 2H, J = 8 Hz); 6.98 (d, 2H, J = 8 Hz); 7.28 (m, 3H); 7.79 (dd, 1H, J = 4 Hz, J = 8 Hz); 7.86 (s, 1H); 8.09 (d, 1H, J = 12 Hz); 9.68 (s, 1H). **^{13}C-NMR** (DMSO-d_6 100 MHz): δ 30.88; 45.86; 59.64; 66.40; 106.83; 107.10; 108.21; 114.40; 114.84; 116.02; 120.95; 129.95; 130.11; 139.56; 142.66; 142.76; 152.29; 158.97; 159.17.

2-(2-((2-phenoxyethyl)amino)-6-((3-(trifluoromethyl)phenyl)amino)-9*H*-purin-9-yl)ethan-1-ol 46d:

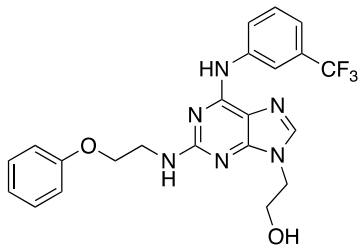

Yield: 52%; **MS** (ESI) $[M+H]^+$: 459.17 m/z; **^{1}H-NMR** (DMSO-d_6 400 MHz): δ 3.73 (m, 4H); 4.12 (m, 4H); 5.03 (t, 1H, J = 4Hz); 6.93 (m, 4H); 7.27 (m, 3H); 7.48 (t, 1H, J = 8 Hz);7.87 (s, 1H); 8.28 (bs, 1H); 8.53 (bs, 1H); 9.87 (s, 1H). **^{13}C-NMR** (DMSO-d_6 100 MHz): δ 41.16, 54.64; 60.40; 66.59, 114.83, 116.35, 118.19, 120.97, 123.73, 126.17, 129.50, 129.81, 129.86, 129.97, 141.71, 159.00, 159.30.

Purine Derivative as Inhibitors of Viral and Host Helicase

General Procedure for the Synthesis of *Tert*-butyl (2-phenoxyethyl)carbamate 49:

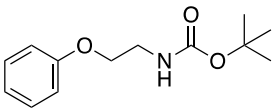

To a solution of 2-phenoxyethylamine **11b** (477.1µL, 3.64 mmol) in dry DCM (4 ml), 2 eq. of Et_3N (74µL, 7.28 mmol) were added at 0 °C. A di-tert-butyl-carbamate solution (863.24 mg; 3.64 mmol) in dry DCM (4 ml) was made and added to the reaction mixture. The mixture was stirred for 3h at r.t. The reaction mixture was quenched with NH_4Cl. The product was extracted with EtOAc(x3). The combined organic phases were washed with brine, dried over anhydrous Na_2SO_4, and evaporated to dryness. The product was used for the next step without further purification.

Yield: 80%; **^{1}H-NMR** ($CDCl_3$; 400 MHz): δ 1.5 (s, 9H), 3.56 (q, 2H, J = 4 Hz), 4.05 (t, 2H, J= 8 Hz), 5.05 (bs, 1H), 6.92 (d, 2H, J= 8 Hz), 6.99 (t, 1H, J= 4 Hz), 7.31 (t, 2H, J= 8 Hz).

General Procedure for the Synthesis of *tert*-butyl methyl(2-phenoxyethyl)carbamate 50:

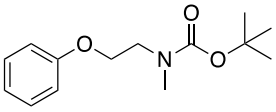

The intermediate **49** (2.6 g, 10.96 mmol) was solubilized in anhydrous THF (25 ml). NaH (0.39g, 16.4 mmol) was added to the reaction mixture. Finally, CH_3I (2.1 ml; 32.9 mmol) was added to the solution. The reaction was heated at 45 °C. 2 eq of CH_3I and 0.5 eq. of NaH were added. The reaction mixture was stirred o.n. After this time water was added to the reaction mixture and the product was extracted with EtOAc (x3). The combined organic phases were washed with brine, dried over anhydrous Na_2SO_4, and evaporated to dryness. The product was used for the next step without further purification. **Yield**: 100%; **^{1}H-NMR** ($CDCl_3$, 400MHz):δ 1.49 (s, 9H), 3.01 (s, 3H;), 3.62 (m, 2H), 4.11 (m, 2H), 6.91 (d, 2H, J = 8 Hz), 6.97 (t, 1H, J = 8 Hz), 7.31 (d, 1H, J = 4 Hz), 7.33 (m, 1H).

General Procedure for the Synthesis of *N*-methyl-2-phenoxyethan-1-amine 51:

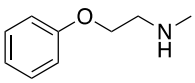

The intermediate **50** (313 mg; 1.25 mmol) was dissolved in dry DCM (4 ml). TFA (574.2 L; 1.87 mmol) was added to the solution. The reaction was stirred at r.t. o.n. The reaction mixture was neutralized with NaOH. The product was extracted with EtOAc (x3). The combined organic phases were washed with brine, dried over anhydrous Na_2SO_4, and evaporated to dryness. The product was used for the next step without further purification. **Yield**: 100%; **^{1}H-NMR** ($CDCl_3$, 400MHz):δ 2.53 (s, 3H), 3.00 (t, 3H, J=4 Hz), 4.10 (t, 2H, J = 4 Hz), 6.94 (m, 3H), 6.99 (m, 1H), 7.31 (m, 1H).

General Procedure for the Synthesis of *N*-methyl-3-(trifluoromethyl)aniline 52:

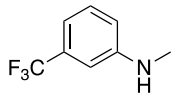

3-(trifluoromethyl)aniline **9a** (1.5 ml; 0.012 mmol) and paraformaldehyde (0.54 g; 0.018 mmol) were added to a solution in MeOH (70 ml) of metallic sodium (1.94 g; 0.084 mmol). The reaction was stirred at r.t. for 2 h. At the end of this time $NaBH_4$ (1.13 g; 0.03 mmol) was added. The reaction was heated at 60 ºC. When the starting material ended, the reaction mixture was washed with H_2O and NH_4Cl. The product was extracted with EtOAc (x3). The combined organic phases were washed with brine, dried over anhydrous Na_2SO_4, and evaporated to dryness. The product was used for the next step without further purification. **Yield**: 84%; **^{1}H-NMR** ($CDCl_3$; 400 MHz): δ 2.89 (s, 3H), 6.77 (d, 1H, J = 4 Hz), 6.81 (s, 1H), 6.90 (d, 1H, J = 4 Hz), 7.3 (t, 1H, J = 8 Hz).

General Procedure for the Synthesis of 2,6-dichloro-9-methyl-9*H*-purine 8b:

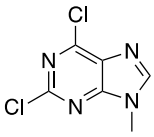

2,6-dichloropurine (2.0 g, 10.58 mmol) was solubilized in anhydrous THF (25 ml). NaH (0.38 g, 15.87 mmol) was added to the reaction mixture. Finally, CH_3I (1.975 ml; 31.74 mmol) was added to the solution. The reaction was heated at 45 °C for xh. The reaction mixture was quenched with NH_4Cl. The product was extracted with EtOAc(x3). The combined organic phases were washed with brine, dried over anhydrous Na_2SO_4, and evaporated to dryness. The product was purified by silica gel chromatography with 98:2 DCM: MeOH as eluent. **Yield**: 51%; **^{1}H-NMR** ($CDCl_3$; 400 MHz): 3.81 (s, 3H) 7.7 (m, 3H) 7.8 (s, 1H) 12.25 (bs, 1H).

General Procedure for the Synthesis of Compounds 53a-c:

In a microwave tube, 2,6-dichloropurine **8a** (100 mg; 0.529 mmol) or N9 methylated 2,6-dichloropurine **8b** was solubilized in n-BuOH (1 mL). 3-(trifluoromethyl)aniline **9a** or intermediate **52** (3 eq) were added. Then Et_3N (3 eq) were added. The reaction mixture was heated in the microwave at 120 ºC for 30 min (max µw power input: 100 W; ramp time: 1 minute; power max: off; maximum pressure: 260 psi). At the end of the radiation, the reaction mixture was collected in a balloon flask and washed with NH_4Cl. The product was extracted with EtOac (x3). The combined organic phases were washed with brine, dried over anhydrous Na_2SO_4, and evaporated to dryness. The product was purified with silica gel chromatographic column using the proper eluent: 98:2 $CDCl_3$: MeOH for **53a** and **53c**, 99:1 $CDCl_3$: MeOH for **53b**.

2-chloro-*N*-methyl-*N*-(3-(trifluoromethyl)phenyl)-9*H*-purin-6-amine 53a:

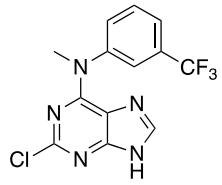

Yield: 53%; **^{1}H-NMR** (DMSO; 400 MHz):δ 3.81 (s, 3H); 7.67 (m, 3H); 7.71 (m, 1H); 8.10 (s, 1H); 13.25 (bs, 1H).

2-chloro-9-methyl-*N*-(3-(trifluoromethyl)phenyl)-9*H*-purin-6-amine 53b:

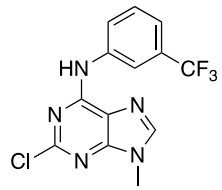

Yield: 98%; **^{1}H-NMR** (DMSO; 400 MHz):δ 3.78 (s, 3H); 7.42 (d, 1H, J = 8 Hz); 7.61 (t, 1H, J = 8 Hz); 8.15 (d, 1H, J = 8 Hz); 8.33 (s, 1H); 8.39 (s, 1H); 10.62 (s, 1H).

2-chloro-*N*,9-dimethyl-*N*-(3-(trifluoromethyl)phenyl)-9*H*-purin-6-amine 53c:

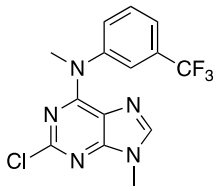

Yield: 53%; **^{1}H-NMR** (DMSO; 400 MHz):δ 3.83(s, 3H); 8.68 (s, 1H).

General Procedure for the Synthesis of Final Compounds 54a-g:

To the solution of the intermediate **53a-c** or **10c** (for **54f**) in n-BuoH, 3.5 equivalents of 2-phenoxyethylamine **11b** or **51** were added (except for **54a** for which 7eq of **11b** and **54d** for which 5eq of **51** were used). Then 1 eq. of TFA was added to the reaction mixture. The reaction mixture was heated to the microwave between 170 and 180 ºC for 1h- 1h 45min. When the starting material ended the reaction mixture was neutralized with $NaHCO_3$. The product was extracted with EtOAc (x3). The combined organic phases were washed with brine, dried over anhydrous Na_2SO_4, and evaporated to dryness. The product was purified with silica gel chromatographic column using the proper eluent: 98:2 DCM: MeOH for **54a**,**b**,**d**,**e,g** and 98:2 DCM: MeOH plus 0.5 % of formic acid for **54c**,**f.**

N^6-methyl-N^2-(2-phenoxyethyl)-N^6-(3-(trifluoromethyl)phenyl)-9*H*-purine-2,6-diamine 54a:

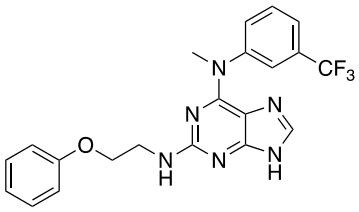

1st Irradiation cycle: 1h, 180 °C; 2nd Irradiation cycle: 1h, 180 °C, 3rd Irradiation cycle: 30 min, 180 °C. **Yield**: 33%; **^{1}H-NMR** (DMSO; 400MHz): δ 3.00 (s, 3H), 3.58 (m, 2H), 4.12 (m, 2H), 6.50 (t, 1H; J = 8 Hz), 6.92 (m, 3H), 7.29 (m, 2H), 7.53 (d, 1H; J = 8 Hz), 7.57 (t, 1H, J = 8 Hz), 7.66 (m, 1H), 7.75 (s, 1H), 8.10 (s, 1H), 12.46 (s, 1H). **^{13}C-NMR** (DMSO; 100 MHz): δ 41.16, 49.07; 66.59, 114.83, 116.35, 118.19, 120.97, 123.73, 126.17, 129.50, 129.81, 129.86, 129.97, 141.71, 159.00, 159.30.

9-methyl-N^2-(2-phenoxyethyl)-N^6-(3-(trifluoromethyl)phenyl)-9*H*-purine-2,6-diamine 54b:

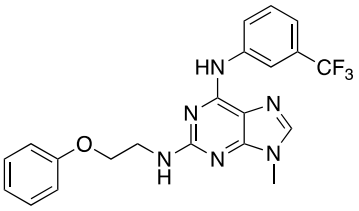

1st Irradiation cycle: 15 min, 170 °C; 2nd Irradiation cycle: 15 min, 170 °C, 3rd Irradiation cycle: 10 min, 170 °C. **Yield**: 76%; **^{1}H-NMR** (DMSO; 400MHz): δ 3.64 (s, 1H); 3.72 (q, 2H, J = 4 Hz); 4.15 (t, 2H, J = 4 Hz); 6.93 (m, 4H); 7.27 (t, 3H, J = 8 Hz); 7.48 (t, 1H, J = 8 Hz); 7.89 (s, 1H); 8.24 (bs, 1H); 8.54 (bs, 1H); 9.85 (s, 1H). **^{13}C-NMR** (DMSO; 100 MHz): δ 30.51; 41.16; 66.59; 114.83; 116.35; 118.19; 120.97; 123.73; 126.17; 129.50; 129.81; 129.86; 129.97; 141.71; 159.00; 159.30.

N^6,9-dimethyl-N^2-(2-phenoxyethyl)-N^6-(3-(trifluoromethyl)phenyl)-9*H*-purine-2,6-diamine 54c:

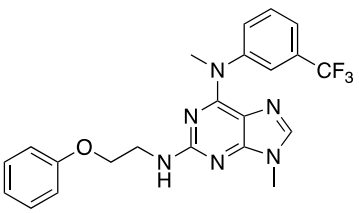

1st Irradiation cycle: 30 min, 170 °C; 2nd Irradiation cycle: 30 min, 170 °C, 3rd Irradiation cycle: 15 min, 170 °C. **Yield**: 25%; **^{1}H-NMR** (DMSO-d_6 400 MHz): δ 3.56 (s, 3H); 3.63 (q, 2H, J = 4 Hz); 3.87 (s, 3H); 4.11 (t, 2H, J = 4 Hz); 6.43 (t, 1H, J = 8 Hz); 6.92 (t, 2H, J = 8 Hz); 6.97 (d, 3H, J = 8 Hz); 7.28 (t, 3H, J = 8 Hz); 7.69 (s, 1H). **^{13}C-NMR** (DMSO; 100 MHz): δ 30.37; 41.16; 49.09; 66.59; 114.83; 116.35; 118.19; 120.97; 123.73; 126.17; 129.50; 129.81; 129.86; 129.97; 141.71; 159.00; 159.30.

N^2,N^6-dimethyl-N^2-(2-phenoxyethyl)-N^6-(3-(trifluoromethyl)phenyl)-9*H*-purine-2,6-diamine 54d:

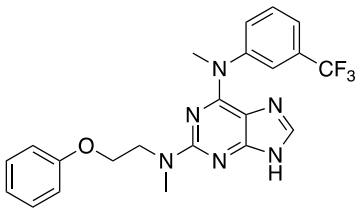

1st Irradiation cycle: 30 min, 170 °C; 2nd Irradiation cycle: 30 min, 180 °C, 3rd Irradiation cycle: 30 min, 180 °C. **Yield**: 21%; **^{1}H-NMR** (DMSO; 400 MHz) δ 3.07 (s, 3H), 3.78 (m, 2H), 3.87 (s, 3H), 4.02 (m, 2H), 6.87 (d, 2H, J = 8 Hz), 6.93 (t, 1H, J = 8 Hz), 7.27 (t, 2H, J = 8 Hz), 7.52 (d, 1H, J = 8 Hz), 7.57 (t, 1H, J = 8 Hz), 7.66 (m, 1H), 7.75 (s, 1H), 8.10 (s, 1H), 12.46 (s, 1H). **^{13}C-NMR** (DMSO; 100 MHz): δ 36.91; 49.07; 48.89; 65.81; 114.77; 120.96; 120.97; 121.93; 123.49; 123.50; 125.97; 129.37; 129.69; 129.95; 130.42; 136.78; 146.73; 153.61; 158.05; 158.90.

N^2,9-dimethyl-N^2-(2-phenoxyethyl)-N^6-(3-(trifluoromethyl)phenyl)-9*H*-purine-2,6-diamine 54e:

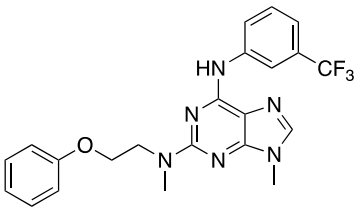

1st Irradiation cycle: 15 min, 170 °C; 2nd Irradiation cycle: 15 min, 170 °C. **Yield**: 90%; **^{1}H-NMR** (DMSO-d_6 400 MHz): δ 3.24 (s, 3H); 3.64 (s, 3H); 4.01 (t, 2H, J = 4 Hz); 4.19 (t, 2H, J = 4 Hz); 6.93 (m, 3H); 7.26 (m, 3H); 7.49 (t, 1H, J = 8 Hz); 7.91 (s, 1H); 8.08 (d, 1H, J = 8 Hz); 8.72 (s, 1H); 9.90 (s, 1H). **^{13}C-NMR** (DMSO; 100 MHz): δ 30.17; 37.40; 55.37; 65.82; 114.80; 118.21; 118.25; 121.02; 123.52; 123.73; 126.23; 129,45; 129.76; 129.84; 129.96; 141.60; 158.75; 158.92.

N^2,N^6,9-trimethyl-N^2-(2-phenoxyethyl)-N^6-(3-(trifluoromethyl)phenyl)-9*H*-purine-2,6-diamine 54f:

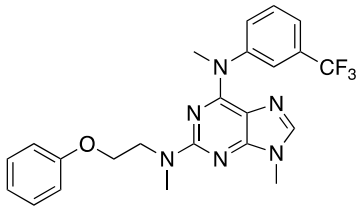

1st Irradiation cycle: 1h, 170 °C. **Yield**: 22%; **^{1}H-NMR** (DMSO-d_6 400 MHz): δ 3.07 (s, 3H); 3.64 (s, 3H); 3.78 (t, 2H, J = 4 Hz); 4.02 (t, 2H, J = 4 Hz); 6.88 (d, 2H, J = 8 Hz); 6.92 (d, 1H, J = 8 Hz); 7.26 (t, 2H, J = 8 Hz); 7.54 (m, 1H); 7.57 (t, 1H, J = 8 Hz); 7.67 (d, 1H, J = 8 Hz); 7.75 (s, 1H). **^{13}C-NMR** (DMSO; 100 MHz): δ **^{13}C-NMR** (DMSO; 100MHz): δ 30.51; 37.40; 49.07; 55.37; 65.82; 114.80; 118.21; 118.25; 121.02; 123.52; 123.73; 126.23; 129.45; 129.76; 129.84; 129.96; 141.60; 158.75; 158.92.

N^2-methyl-N^2-(2-phenoxyethyl)-N^6-(3-(trifluoromethyl)phenyl)-9*H*-purine-2,6-diamine 54g:

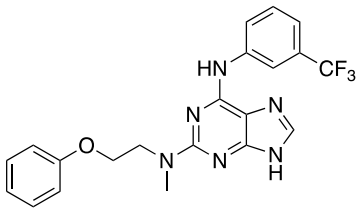

1st Irradiation cycle: 30 min, 170 °C; 2nd Irradiation cycle: 15 min, 170 °C, 3rd Irradiation cycle: 15 min, 180 °C. **Yield**: 55%; **^{1}H-HMR** (DMSO; 400MHz): δ 3.24 (s, 3H), 4.00 (t, 2H, J. = 4 Hz), 4.20 (t, 2H, J = 4 Hz), 6.91 (m, 3H) 7.27 (m, 3H) 7.49 (t, 1H, J = 16 Hz) 7.91 (s, 1H) 8.08 (d, 1H, J = 8 Hz); 8.72 (s, 1H); 9.90 (s, 1H); 12.56 (s, 1H). **^{13}C-NMR** (DMSO; 100MHz): δ 37.40; 55.37; 65.82; 114.80; 118.21; 118.25; 121.02; 123.52; 123.73; 126.23; 129.45; 129.76; 129.84; 129.96; 141.60; 158.75; 158.92.

General Procedures for the Synthesis of final compounds 57a-d:

In a glass vial equipped with a small magnetic stirring bar, the intermediate 2-chloro-N-(3-(trifluoromethyl)phenyl)-9H-purin-6-amine **10a** (100 mg, 0.32 mmol, 1 eq) was suspended in n-BuOH (2 mL). Then the proper amine **56a-d** (3 eq for compound **57a,c**, 4eq for compound **57b** and 5eq for compound **57d**) and trifluoroacetic acid (25μL, 0.32mmol, 1 eq) were added to the mixture. The reaction mixture was heated under microwave irradiation at 170 °C for 30-120 min (max μW power input: 100 W; ramp time: 1 minute; power max: off; maximum pressure: 260 psi). After check through TLC the end of the starting material, the reaction mixture was concentrated under vacuum and extracted with ethyl acetate. The organic layers were washed with brine and dried under sodium sulphate. The products were purified by silica gel flash chromatography using DCM: MeOH as eluent (98:2 for compounds **57a,d,e** and 95:5 for compounds **57b,c**).

1-((6-((3-(trifluoromethyl)phenyl)amino)-9H-purin-2-yl)amino)propan-2-ol 57a:

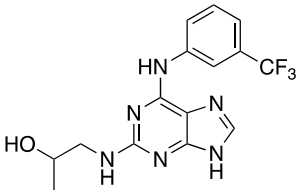

1st Irradiation cycle: 95 min, 170 °C. **Yield**: 66%; **^{1}H-NMR** (DMSO-d_6, 400 MHz): δ 1.09 (d, 3H, J = 6 Hz); 3.18 (m, 1H); 3.84 (s, 1H); 4.71 (s, 1H); 6.36 (m, 1H); 7.29 (d, 1H, J = 7.6 Hz); 7.51 (t, 1H, J = 7.6 Hz); 7.86 (s, 1H); 8.35 (m, 1H); 8.39 (bs, 1H); 9.78 (s, 1H); 12.43 (s, 1H). **^{13}C-NMR** (DMSO-d_6, 100 MHz): δ 21.76; 49.85; 65.72; 114.09; 116.38; 118.09; 123.75; 126.20; 129.45; 129.83; 137.09; 141.76; 152.09; 153.32; 159.54.

2-((6-((3-(trifluoromethyl)phenyl)amino)-9H-purin-2-yl)amino)propan-1-ol 57b:

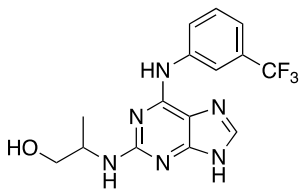

1st Irradiation cycle: 75 min, 170 °C. **Yield:** 51%; **^{1}H-NMR** (DMSO-d_6, 400 MHz): δ 1.16 (d, 3H, J = 8 Hz); 3.35 (m, 1H); 3.41 (m, 1H); 3.98 (m, 1H); 6.18 (d, 1H, J = 8 Hz); 7.28 (d, 1H, J = 8Hz); 7.50 (t, 1H, J = 8Hz);

7.85 (s, 1H); 8.33 (m, 1H); 8.38 (bs, 1H); 9.75 (s, 1H); 12.43 (bs, 1H). **^{13}C-NMR** (DMSO-d_6, 100 MHz): δ 17.99; 49.03; 65.10; 114.03; 116.29; 118.04; 123.70; 129.45; 129.85; 137.03; 140.84; 141.80; 152.12; 153.35; 159.02.

2-methyl-1-((6-((3-(trifluoromethyl)phenyl)amino)-9H-purin-2-yl)amino)propan-2-ol 57c:

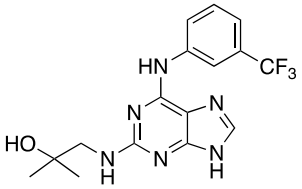

1st Irradiation cycle: 30 min, 170 °C. **Yield:** 52%; **^{1}H-NMR** (DMSO-d_6, 400 MHz): δ 1.14 (d, 6H, J = 12 Hz); 3.34 (m, 1H); 4.62 (m, 1H); 6.11 (d, 1H, J = 8 Hz); 7.30 (d, 1H, J = 8 Hz); 7.51 (t, 1H, J = 8 Hz); 7.85 (s, 1H); 8.25 (m, 1H); 8.57 (bs, 1H); 9.79 (s, 1H); 12.41 (s, 1H). **^{13}C-NMR** (DMSO-d_6, 100 MHz): δ 27.89; 53.03; 70.04; 114.15; 116.45; 118.20; 123.53; 123.85; 129.42; 129.87; 137.21; 141.72; 141.73; 152.09; 159.91.

1-(((6-((3-(trifluoromethyl)phenyl)amino)-9*H*-purin-2-yl)amino)methyl)cyclopentan-1-oln 57d:

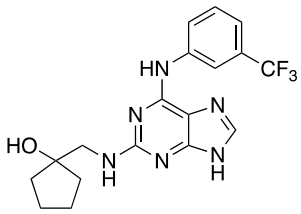

1st Irradiation cycle: 120 min, 170 °C. **Yield:** 16%; **^{1}H-NMR** (DMSO-d_6, 400 MHz): δ 1.60 (m, 4H); 1.70 (m, 2H); 3.43 (d, 1H, J = 6 Hz); 4.60 (m, 1H); 6.12 (m, 1H); 7.29 (d, 1H, J=8 Hz); 7.51 (t, 1H, J= 8Hz); 7.86 (s, 1H); 8.25 (m, 1H); 8.60 (bs, 1H); 9.79 (s, 1H); 12.42 (s, 1H). **^{13}C-NMR** (DMSO-d_6, 100 MHz): δ 24.15, δ 37.95, 81.34, 114.12, 116.41, 118.13, 123.79, 129.84, 137.16, 137.17, 141.70, 152.06, 153.22, 159.85, 161.26.

General Procedures for the Synthesis of Compound *N*^{2}-(2-bromoethyl)-*N*^{6}-(3-(trifluoromethyl)phenyl)-9*H*-purine-2,6-diamine 58:

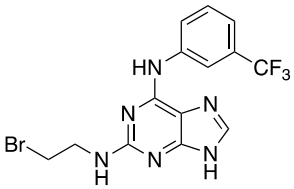

Yield: 63 %; **^{1}H-NMR** (DMSO-d_6, 400 MHz): δ 3.84 (t, 2H, J = 8 Hz), 4.44 (t, 2H, J = 8 Hz), 7.45 (d; 1H J = 8 Hz), 7.60 (t; 1H; J=8 Hz), 7.84 (s, 1H), 8.14 dd, 1H, J = 4 Hz, J = 8 Hz), 8.28 (s, 1H), 8.75 (bs; 1H).

_N_-(3-(trifluoromethyl)phenyl)-4,5-dihydro-3_H_-2,9-(azenometheno)imidazo[1,5-_a_][1,3,5]triazepin-10-amine 61:

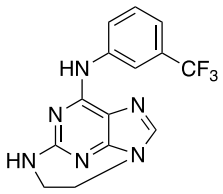

In a two neck round bottomed flask, methyl p-hydroxy benzoate (1.1 eq; 18.26 mg), diethyl azodicarboxylate (DEAD; 2.1 eq; 36 µL), triphenylphosphine (2.0 eq; 57.5 mg) were solubilized in THF anhydrous (6 mL).

Then 2 ((6 ((3-(trifluoromethyl)phenyl)amino)-9*H*-purin-2-yl)amino)ethan-1-ol (1 eq; 37.5 mg) was added to reaction mixture. The reaction was stirred at room temperature under argon conditions and for 24 hours. Other DEAD (2.1 eq; 36 µL) and triphenylphosphine (2.0 eq; 57.5 mg) were added and the reaction proceeded at reflux at 100 °C for other 4 hours. The clear orange solution was concentrated under vacuum and extracted with ethyl acetate. The organic phase was washed with brine, dried over sodium sulphate anhydrous to delete the remnants of aqueous phase. The product was purified by silica gel flash chromatography using DCM:MeOH 95:5. **Yield:** 86%; **MS** (ESI) $[M+H]^+$: 321,28 m/z; **^{1}H-NMR** (DMSO-d_6, 400 MHz): δ 3.80 (t, 2H, J = 8 Hz); 4.41 (t, 2H, J = 8Hz); 7.38 (d, 1H, J = 8Hz); 7.55 (t, 1H, J = 8Hz); 7.58 (s, 1H); 8.18 (dd, 1H, J = 8Hz, J = 4Hz); 8.22 (bs, 1H); 8.31 (s, 1H).

The same product was obtained following the Scheme 25.

General Procedures for the Synthesis of *tert*-butyl 2-((*tert*-butoxycarbonyl)(2-((*tert*-butoxycarbonyl)oxy)ethyl)amino)-6-((*tert*-butoxycarbonyl)(3-(trifluoromethyl)phenyl)amino)-9*H*-purine-9-carboxylate 62:

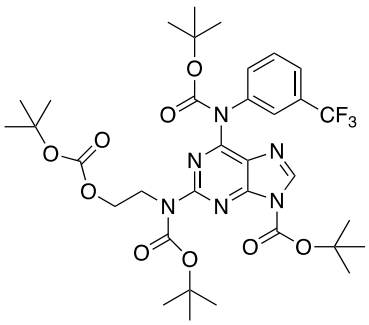

Yield: 100% **^{1}H-NMR** (DMSO-d_6, 400 MHz): δ 1.29 (s, 18H); 1.38 (s, 9H); 1.48 (s, 9H); 3.98 (t, 2H, J = 4 Hz); 4.14 (t, 2H, J = 4 Hz); 7.52 (m, 2H); 7.65 (m, 2H); 8.83 (s, 1H).

General Procedures for the Synthesis of N^2-(2-((*tert*-butyldiphenylsilyl)oxy)ethyl)-N^6-(3-(trifluoromethyl)phenyl)-9*H*-purine-2,6-diamine 63:

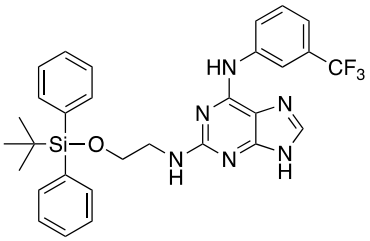

Compound **12c** (100mg, 0.29 mmol) was dissolved in dry DMF. Imidazole (0.58 mmol, 2eq) was added, and the reaction mixture was cooled to 0 °C. Tert-bytyldiphenylsylil chloride (TBDPSiCl) (0.35 mmol, 1.2 eq) was added dropwise and the reaction mixture was leave to reach r.t. After 2 h the reaction ended. The reaction mixture was concentrated under vacuum and extracted with ethyl acetate (x3). The organic layers were washed with an aqueous solution of LiCl (%5) and brine and dried under sodium sulphate. The product was purified by silica gel flash chromatography using DCM: MeOH (98:2) as eluent. **Yield:** 96% **^{1}H-NMR** (DMSO-d_6, 400 MHz): δ 0.97 (s, 9H); 3.55 (q, 2H, J = 6 Hz); 3.78 (t, 2H, J = 6 Hz); 6.52 (t, 1H, J = 4 Hz); 7.27 (d, 1H, J = 8 Hz); 7.33 (m, 4H); 7.39 (d, 3H, J = 4 Hz); 7.42 (t, 1H, J = 8 Hz); 7.59 (d, 4H, J = 8 Hz); 7.86 (s, 1H); 9.77 (s, 1H); 12.42 (bs, 1H).

General Procedures for the Synthesis of *tert*-butyl 2-((*tert*-butoxycarbonyl)(2-((*tert*-butyldiphenylsilyl)oxy)ethyl)amino)-6-((*tert*-butoxycarbonyl)(3-(trifluoromethyl)phenyl)amino)-9*H*-purine-9-carboxylate 64:

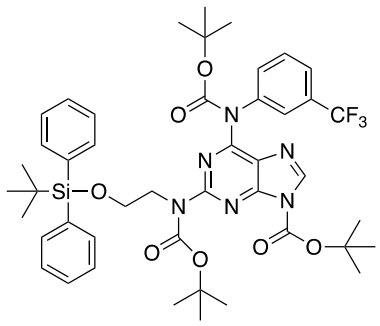

Compound **63** (160 mg, 0.28 mmol) was dissolved in dry THF. Tert-butyl dicarbonate (1.11 mmol, 4 eq) solubilized in dry THF was added. 1.5 eq of Et_3N (0.42 mmol) were added and the reaction mixture was stirred o.n. at r.t. After check through TLC the end of the starting material, the reaction mixture was concentrated under vacuum and extracted with ethyl acetate (x3). The organic layers were washed with brine and dried under sodium sulphate. The product was used for the next step without further purification. **Yield:** 66% **^{1}H-NMR** (DMSO-d_6, 400 MHz): δ 0.96 (s, 9H); 1.47 (s, 18H); 1.66 (s, 9H); 3.57 (t, 2H, J = 4 Hz); 3.79 (t, 2H, J = 4 Hz); 7.38 (m, 8H); 7.59 (m, 6H); 8.68 (s, 1H):

General Procedures for the Synthesis of *tert*-butyl 2-((2-hydroxyethyl)amino)-6-((3-(trifluoromethyl)phenyl)amino)-9*H*-purine-9-carboxylate 65:

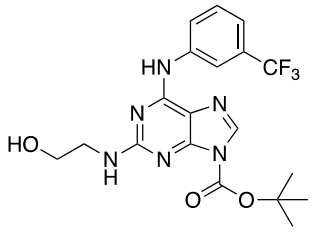

To a solution of compound **64** (100mg, 0.11 mmol) in THF/pyridine (2:1), HF • pyridine (125 µL) was added. The reaction mixture was stirred at r.t. for 30 min. After dried the solvent, the reaction mixture was diluted in EtOAc and H_2O. The organic layer was washed several time with H_2O (x7) to remove pyridine. The organic phase was washed with brine, dried over anhydrous Na_2SO_4, and evaporated to dryness. The product was purified with silica gel chromatographic column using the proper eluent: 98:2 DCM: MeOH. **Yield:** 63% **^{1}H-NMR** (DMSO-d_6, 400 MHz): δ 1.44 (s, 9H); 3.42 (m, 2H); 3.57 (q, 2H, J = 4 Hz); 4.68 (bs, 1H); 6.90 (m, 1H); 7.32 (d, 1H, J = 8 Hz); 7.47 (m, 2H); 8.23 (s, 1H); 8.32 (bs, 1H); 9.93 (bs, 1H).

General Procedures for the Synthesis of final compounds 71a,b:

A suspension of the intermediate **10a** (100mg; 0.319mmol) n-BuOH (2ml) was placed in a microwave tube. To the suspension, 3 eq. of phenylhydrazine for **17a** and 4eq for **17b** were added. 1 eq. of TFA in the microwave tube. The reaction mixture was heated at the microwave at a temperature of 150 ºC for a reaction time of 35 min. (max µw power input: 300 W; ramp time: 1 minute; power max: off; maximum pressure: 260 psi). At the end of the radiation the reaction was quenched with $NaHCO_3$. The reaction product was extracted with EtOAc (x3). The combined organic phases were washed with brine, dried over anhydrous Na_2SO_4, and evaporated to dryness. The product was purified with silica gel chromatographic column using DCM:MeOH 96:4.

General synthesis for the Synthesis of Compound 67a,b

In a round bottomed flask, commercial compounds **66a,b** (1 mL, 11 mmol) were solubilized in dry DCM. Et_3N (14.3 mmol, 1.3 eq) and tertbutyl decarbonate (13.2 mmol, 1.2 eq) were added. The reaction mixture was stirred for 1h under argon atmosphere at r.t. The reaction product was extracted with DCM (x3). The combined organic phases were washed with brine, dried over anhydrous Na_2SO_4, and evaporated to dryness. The products were used for the next step without further purification.

***tert*-butyl (1-hydroxypropan-2-yl)carbamate 67a:**

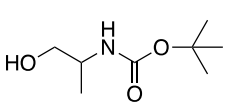

Yield: 100%; **^{1}H-NMR** ($CDCl_3$, 400MHz):δ 1.19 (d, 3H, J = 4 Hz); 1.29 8(s, 9H); 3.52 (dd, 1H, J = 8 Hz, J = 4 Hz); 3.67 (dd, 1H, J = 8 Hz, J = 4 Hz); 3.79 (m, 1H); 5.32 (bs, 1H).

1-((*tert*-butoxymethyl)amino)propan-2-ol 67b:

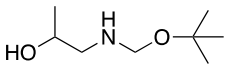

Yield: 100%; **^{1}H-NMR** ($CDCl_3$, 400MHz):δ 1.18 (d, 3H, J = 4 Hz); 1.46 (s, 9H); 3.53 (m, 1H); 3.66 (m, 1H); 3.79 (m, 2H); 4.64 (bs, 1H).

General synthesis for the Synthesis of Compound 68a,b:

In a round bottomed flask, compound **67a** or **67b** (1 gr, 5.3 mmol) triphenylphosphine (5.83 mmol, 1.1 eq), carbon tetrabromide (5.83 mmol, 1.1 eq) were solubilized in dimethylacetamide (1 mL). The reaction was conducted in dry condition and stirred for two hours under nitrogen. At the end of the radiation the reaction was quenched with H_2O. The reaction product was extracted with DCM (x3). The combined organic phases were washed with brine, dried over anhydrous Na_2SO_4, and evaporated to dryness. the products were used for the next step without further purification.

***tert*-butyl (1-bromopropan-2-yl)carbamate 68a:**

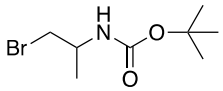

Yield: 70%; **^{1}H-NMR** ($CDCl_3$, 400MHz):δ 1.28 (d, 1H, J = 4 Hz); 3. 93 (dd, 1H, J = 8 Hz, J = 4 Hz); 4.02 (qt, 1H, J = 4 Hz); 4.48 (t, 1H, J = 8 Hz); 6.63 (bs, 1H).

***tert*-butyl (2-bromopropyl)carbamate 68b:**

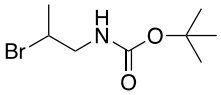

Yield: 88%; **^{1}H-NMR** ($CDCl_3$, 400MHz):δ 1.25 (s, 9H); 1.67 (d, 3H, J = 4 Hz); 3.31 (m, 1H); 3.53 (m, 1H); 4.19 (m, 1H); 5.03 (bs, 1H).

General procedure for the synthesis of compounds 69a,b:

Compound **68a** or **68b** (100 mg, 0.42 mmol) and phenol (0.63 mmol, 1.5 eq) were dissolved in dry DMF (1 mL). Anhydrous K_2CO_3 (0.63 mmol, 1.5 eq) was added and the reaction was stirred at r.t. o.n. Then the reaction was heated at 90-100 °C and stirred for 24 h. After check through TLC the end of the starting material, the reaction mixture was concentrated under vacuum and extracted with ethyl acetate (x3). The organic layers were washed with brine and dried under sodium sulphate. The product was used for the next step without further purification.

***tert*-butyl (1-phenoxypropan-2-yl)carbamate 69a:**

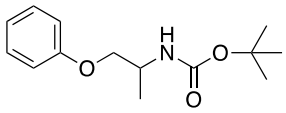

Yield: 38%; **^{1}H-NMR** ($CDCl_3$, 400MHz):δ 1.51 (s, 9H); 1.67 (d, 3H, J = 6 Hz); 3.33 (m, 1H); 3.57 (m, 1H); 4.20 (m, 1H); 5.23 (bs, 1H); 6.94 (m, 3H); 7.25 (m, 2H).

***tert*-butyl (2-phenoxypropyl)carbamate 69b:**

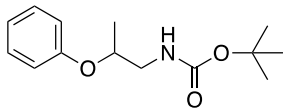

Yield: 41%; **^{1}H-NMR** ($CDCl_3$, 400 MHz): δ 1.52 (s, 9H); 1.67 (d, 3H, J = 4 Hz); 3.35 (m, 1H); 3.58 (m, 1H); 4.20 (m, 1H); 5.22 (bs, 1H); 6.93 (m, 3H); 7.25 (m, 2H).

General procedure for the synthesis of compounds 70a,b:

Compound **69a** or **69b** (260 mg, 1.03 mmol) were solubilized in dry DCM. TFA (10eq, 10.3 mmol) was added and the reaction mixture was stirred o.n. at r.t. After check through TLC the end of the starting material, the reaction mixture was concentrated under vacuum and extracted with ethyl acetate (x3). The organic layers were washed with brine and dried under sodium sulphate. The product was used for the next step without further purification.

1-phenoxypropan-2-amine 70a:

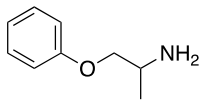

Yield: 100% **^{1}H-NMR** (DMSO-d_6, 400 MHz): δ 1.13 (d, 3H, J = 8 Hz); 3.78 (m, 1H); 3.85 (m, 1H); 4.33 (t, 1H, J = 8 Hz); 6.73 (t, 1H, J = 8 Hz); 6.80 (d, 2H, J = 8 Hz); 7.06 (bs, 2H); 7.10 (t, 2H, J = 8 Hz).

2-phenoxypropan-1-amine 70b:

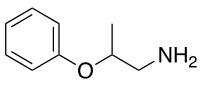

Yield: 100%; **^{1}H-NMR** (Ac_2O, 400 MHz): δ 1.39 (d, 2H, J = 4 Hz); 3.17 (m, 1H); 3.69 (m, 1H); 4.72 (m, 1H); 6.75 (m, 1H); 6.98 (m, 2H); 7.09 (t, 1H, J = 4 Hz); 7.29 (m, 1H).

General procedure for the synthesis of Compounds 60c,d:

To the solution of the intermediate **10c** in n-BuoH, 3 equivalents of **70a** or 5 eqivalent of **70b** were added**.** Then 1 eq. of TFA was added to the reaction mixture. The reaction mixture was heated to the microwave at 170 ºC for 1h. When the starting material ended the reaction mixture was neutralized with $NaHCO_3$. The product was extracted with EtOAc (x3). The combined organic phases were

washed with brine, dried over anhydrous Na_2SO_4, and evaporated to dryness. The product was purified with silica gel chromatographic column using the proper eluent: 98:2 DCM: MeOH plus 0.5 % of formic acid.

N^2-(1-phenoxypropan-2-yl)-N^6-(3-(trifluoromethyl)phenyl)-9*H*-purine-2,6-diamine 60c:

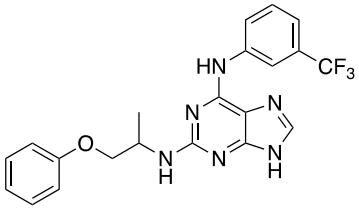

Yield: 30%. **^{1}H-NMR** (DMSO-d_6, 400 MHz): δ 1.27 (d, 2H, J = 8 Hz); 3.59 (m, 1H); 4.65 (q, 2H, J = 8 Hz); 6.88 (t, 1H, J = 8 Hz); 7.26 (m, 5H); 7.47 (m, 3H); 8.35 (s, 1H); 8.40 (s, 1H); 9.87 (s, 1H); 12.48 (bs, 1H). **^{13}C-NMR** (DMSO-d_6, 100 MHz): δ 17.41; 57.16; 66.59; 114.83; 116.35; 118.19; 120.97; 123.73; 126.17; 129.50; 129.81; 129.86; 129.97; 141.71; 144.00; 152.10; 152.71; 159.30.

N^2-(2-phenoxypropyl)-N^6-(3-(trifluoromethyl)phenyl)-9*H*-purine-2,6-diamine 60d:

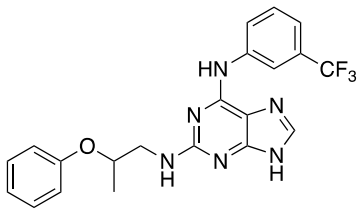

Yield: 32%. **^{1}H-NMR** (DMSO-d_6, 400 MHz): δ 1.38 (d, 2H, J = 6 Hz); 3.60 (m, 1H); 4.28 (q, 2H, J = 6 Hz); 6.78 (t, 1H, J = 6 Hz); 6.97 (m, 3H); 7.28 (t, 3H, J = 7.6 Hz); 7.51 (t, 1H, J = 8 Hz); 7.88 (s, 1H); 8.14 (s, 1H); 8.33 (s, 1H); 9.88 (s, 1H); 12.48 (bs, 1H). **^{13}C-NMR** (DMSO-d_6, 100 MHz): δ 19.61; 52.59; 79.20; 114.83, 116.35, 118.19, 120.97, 123.73, 126.17, 129.50, 129.81, 129.86, 129.97, 141.71, 152.10; 152.71; 159.00.

General procedure for the synthesis of Compounds 71a,b:

A suspension of the intermediate **10a** (100mg; 0.319mmol) in n-BuOH (2ml) was placed in a microwave tube. To the suspension 4 eq. of phenylhydrazine **17a** for **71a** and **3 eq.** of phenylhydrazine **17b** for **71b** were added. 1 eq. of TFA was added in the microwave tube. The reaction mixture was heated to the microwave at 150 ºC for a reaction time of 35 min for **71a** and 90 min for **71b**. (max µw power input: 300 W; ramp time: 1 minute; power max: off; maximum pressure: 260 psi). At the end of the irradiation the reaction was quenched with $NaHCO_3$. The reaction product was extracted with EtOAc (x3). The combined organic phases were washed with brine, dried over anhydrous Na_2SO_4, and evaporated to dryness. The product was purified with silica gel chromatographic column, using 96:4 DCM:MeOH as eluent mixture.

2-(2-(3-fluorophenyl)hydrazineyl)-N-(3-(trifluoromethyl)phenyl)-9H-purin-6-amine 71a:

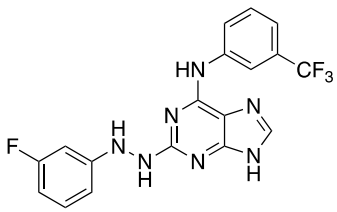

1st Irradiation cycle: 30 min, 150 °C; 2nd Irradiation cycle: 5 min, 150 °C. **Yield**: 77%; **^{1}H-NMR** (DMSO, 400MHz): δ 6.39 (t, 1H, J = 12 Hz); 6.49 (d, 1H, J = 12 Hz); 6.62 (d, 1H, J = 12 Hz); 7.13 (q, 1H, J = 8 Hz); 7.26 (d, 1H, J = 8 Hz); 7.36 (m, 1H); 7.9 (s, 1H); 8.0 (s, 1H); 8.19 (s, 1H); 8.44 (m, 1H); 8.58 (s, 1H); 9.88 (s, 1H); 12.64 (s, 1H). **^{13}C-NMR** (DMSO, 100MHz): δ 98.42; 98.67; 103.83; 104.04; 108.27; 115.23; 116.47; 118.13; 123.90; 129.71; 130.66; 137.83; 141.48; 152.20; 153.06; 160.18; 162.57; 164.95.

***N*-(3-(trifluoromethyl)phenyl)-2-(2-(3(trifluoromethyl)phenyl)hydrazineyl)-9*H*-purin-6-amine 71b:**

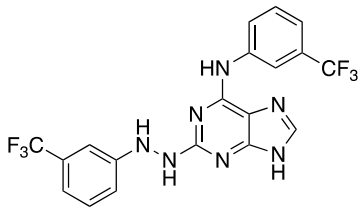

1st Irradiation cycle: 1 h, 150 °C; 2nd Irradiation cycle: 15 min, 150 °C, 3rd Irradiation cycle: 15 min, 150 °C. **Yield**: 33%; **^{1}H NMR** (DMSO; 400MHz): δ 6.93 (d, 1H, J = 8 Hz); 7.03 (d, 2H, J = 8 Hz); 7.25 (d, 1H, J = 8 Hz); 7.33 (t, 2H, J = 8 Hz); 7.94 (s, 1H); 8.18 (s, 1H); 8.20 (s, 1H); 8.39 (m,1H); 8.64 (s, 1H); 9.90 (s, 1H); 12.64 (s,1H). **^{13}C-NMR** (DMSO, 100MHz): δ 98.42; 98.67; 103.83; 104.04; 108.27; 115.23; 116.47; 118.13; 123.90; 129.71; 130.66; 137.83; 141.48; 152.20; 153.06; 160.18; 162.57; 164.95.

General Procedures for the Synthesis of intermediates 72a,b:

In a glass vial equipped with a small magnetic stirring bar, the intermediate **10a** (100mg, 0.32mmol) was suspended in n-BuOH (1ml). Then the proper hydrazine (78 µL; 1.6mmol) and TFA (24.5 µL; 0.32mmol) were added to the mixture. The reaction mixture was heated under microwave irradiation at 170 °C for 30 min (max µW power input: 100 W; ramp time: 1 minute; power max: off; maximum pressure: 260 psi). The solution was concentrated under vacuum and $NaHCO_3$ was utilized to neutralize the TFA, and ethyl acetate was used as organic phase to extract the product. The product was purified by silica gel flash chromatography using DCM: MeOH 9:1 for **72a** and with 8:2 with 0.5% of formic acid for **72b**.

2-hydrazineyl-*N*-(3-(trifluoromethyl)phenyl)-9*H*-purin-6-amine 72a:

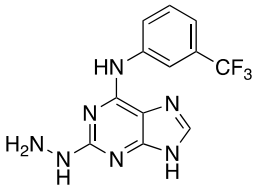

Yield: 35%; **^{1}H-NMR**: (DMSO, 400 MHz) δ 6.06 (s, 1H), 7.27 (d, 1H, J = 8 Hz); 7.50 (t, 1H, J = 8 Hz); 7.85(s, 1H); 8.14 (s, 2H); 8.32 (s, 1H); 8.47 (d, 1H, J = 8 Hz); 9.70 (s, 1H).

2-(1-methylhydrazineyl)-*N*-(3-(trifluoromethyl)phenyl)-9*H*-purin-6-amine 72b:

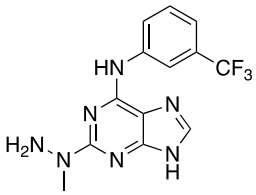

Yield: 53%; **^{1}H-NMR** (MeOD, 400MHz) δ 2.04 (s, 3H); 2.11 (s, 2H); 7.36 (d, 1H, J = 8 Hz); 7.55 (t, 1H, J = 8 Hz); 7.92 (s, 1H); 8.23 (d, 1H, J = 8 Hz); 8.27 (s, 1H); 9.71 (s, 1H).

General Procedures for the Synthesis of final compounds 74a-k:

In a round bottomed flask 1-2 eq of several benzaldehydes differently substituted was added to a solution of **72a,b** (1eq) in EtOH. Then 2-3 drops of CH_3COOH were added to the reaction mixture that was left at reflux overnight. At the end of the reaction, the precipitate obtained was filtrated under vacuum and washed with methanol. The precipitate was dried under vacuum.

(*E*)-2-((2-(6-((3-(trifluoromethyl)phenyl)amino)-9*H*-purin-2-yl)hydrazineylidene)methyl)phenol 74a:

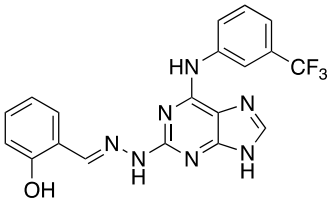

Yield: 56%; **^{1}H-NMR** (DMSO; 400MHz): δ 6.90 (s, 1H); 6.92 (s, 1H); 7.23 (t, 1H, J = 8 Hz); 7.3 (dd, 2H, J = 24 Hz, J = 8 Hz); 7.59 (t, 1H, J = 8 Hz); 8.05 (s, 1H); 8.23 (s, 1H); 8.32 (s, 1H); 8.66 (d, 1H, J = 8 Hz); 10.04 (s, 1H); 11.10 (s, 1H); 11.68 (s, 1H); 11.97 (s, 1H); 12.83 (s, 1H). **^{13}C-NMR** (DMSO; 100MHz): δ 116.66; 118.65; 119.56; 119.84; 123.41; 124.08, 126.12; 129.43; 129.66; 130.12; 130.18; 138.66; 141.37; 141.99; 152.21; 152.84; 155.69; 157.36; 172.50.

(*E*)-4-((2-(6-((3-(trifluoromethyl)phenyl)amino)-9*H*-purin-2-yl)hydrazineylidene)methyl)phenol 74b:

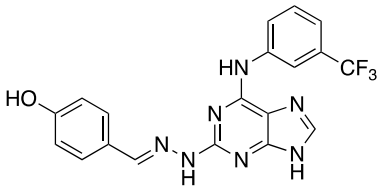

Yield: 56%; **^{1}H-NMR** (DMSO; 400MHz): δ 6.82 (d, 2H, J = 8 Hz); 7.34 (d, 2H, J = 8 Hz); 7.53 (m, 3H); 8.00 (s, 1H); 8.04 (s, 1H); 8.50 (s, 1H); 8.63 (d, 1H, J = 8 Hz); 9.76 (bs, 1H); 9.97 (bs, 1H); 10.63 (s, 1H); 12.71 (bs, 1H). **^{13}C-NMR** (DMSO; 100MHz): δ 115.84; 116.43; 118.49; 123.50; 124.01; 126.26; 129.59; 129.90; 130.14; 130.62; 138.49; 138.52; 138.69; 140.29; 141.67; 152.22; 152.84; 152.86; 156.05; 167.55.

(*E*)-3-((2-(6-((3-(trifluoromethyl)phenyl)amino)-9*H*-purin-2-yl)hydrazineylidene)methyl)phenol 74c:

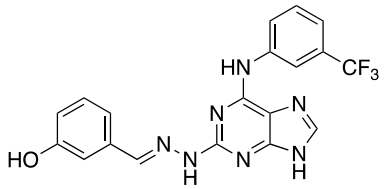

Yield: 45%; **^{1}H-NMR** (DMSO; 400MHz): δ 6.76 (d, 1H, J = 8 Hz); 7.10 (s, 1H); 7.13 (t, 1H; J = 8 Hz); 7.22 (t, 1H, J = 8 Hz); 7.34 (d, 1H, J = 8 Hz); 7.58 (t, 1H, J = 8 Hz); 8.02 (s, 1H); 8.05 (s, 1H); 8.37 (s, 1H); 8.80 (d, 1H, J = 8 Hz); 9.49 (s, 1H); 10.00 (s, 1H); 10.80 (s, 1H); 12.74 (s, 1H). **^{13}C-NMR** (DMSO;100MHz): δ 113.00; 115.61; 116.23; 116.51; 117.68; 118.35; 123.94; 129.91; 130.08; 137.44; 138.27; 140.40; 141.79; 152.21; 152.97; 156.31; 158.08.

(*E*)-2-((2-methyl-2-(6-((3-(trifluoromethyl)phenyl)amino)-9*H*-purin-2-yl)hydrazineylidene)methyl)phenol 74d:

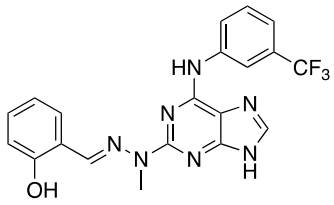

Yield: 63%**; ^{1}H-NMR** (DMSO, 400MHz): 3.70 (s, 3H); 7.37 (d, 1H, J = 8 Hz); 7.46 (t, 1H, J = 8 Hz); 7.50 (t, 1H, J = 8 Hz); 7.68 (t, 1H, J = 8 Hz); 7.90 (d, 1H, J = 4 Hz); 8.11 (s, 1H); 8.20 (d, 1H, J = 8 Hz); 8.32 (s, 1H); 8.61 (s, 1H); 8.90 (d, 1H, J = 8 Hz); 10.21 (s, 1H); 12.90 (s, 1H). **^{13}C-NMR** (DMSO; 100MHz): δ 28.90; 113.88; 114.02; 116.30; 116.32; 117.98; 118.02; 120.80; 123.51; 123.59; 126.20; 129.43; 129.74; 129.80; 130.05; 136.99; 137.01; 141.84; 152.07; 153.46; 160.07.

(*E*)-4-((2-methyl-2-(6-((3-(trifluoromethyl)phenyl)amino)-9*H*-purin-2-yl)hydrazineylidene)methyl)phenol 74e:

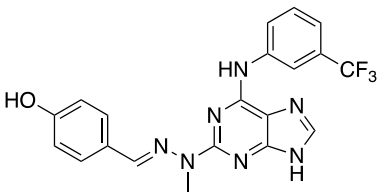

Yield: 80%; **^{1}H-NMR** (DMSO;400 MHz): 3.73 (s, 3H); 7.42 (d, 1H, J = 8 Hz); 7.61 (t, 1H, J = 8 Hz); 7.90 (t, 3H, J = 12 Hz); 8.03 (d, 2H, J= 8 Hz); 8.12 (s, 1H); 8.32 (s, 1H); 8.90 (d, 1H, J = 8 Hz); 10.21 (s, 1H); 12.93 (s, 1H). **^{13}C-NMR** (DMSO; 100 MHz): δ 28.90; 113.91; 116.31; 116.35; 117.98; 118.02; 123.51; 123.59; 126.21; 129.43; 129.80; 136.99; 141.85; 152.06; 153.48; 160.07.

(*E*)-3-((2-methyl-2-(6-((3-(trifluoromethyl)phenyl)amino)-9*H*-purin-2-yl)hydrazineylidene)methyl)phenol 74f:

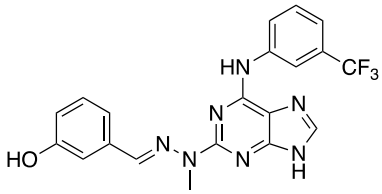

Yield: 67%; **^{1}H-NMR** (DMSO; 400MHz): δ 3.69 (s, 1H); 6.78 (m, 1H); 7.27 (s, 2H); 7.35 (d, 1H, J = 8 Hz); 7.67 (t, 1H, J = 8 Hz); 7.82 (s, 1H); 8.09 (s, 1H); 8.13 (s, 1H); 9.02 (d, 1H, J = 8 Hz); 9.51 (s, 1H); 10.14 (s, 1H); 12.88 (bs, 1H). **^{13}C-NMR** (DMSO;100MHz): δ 32.20; 116.50; 118.49; 123.47; 123.96; 126.18; 127.55; 129.12; 129.44; 129.83; 130.16; 136.37; 137.09; 141.58; 156.57.

(*E*)-4-((2-(6-((3-(trifluoromethyl)phenyl)amino)-9*H*-purin-2-yl)hydrazineylidene)methyl)benzoic acid 74g

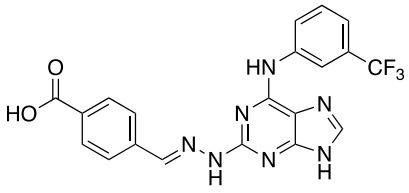

Yield: 36%; **^{1}H-NMR** (DMSO; 400MHz): δ 7.37 (d, 1H, J = 8 Hz); 7.59 (t, 1H, J = 8 Hz); 7.81 (d, 2H, J = 8 Hz); 7.99 (d, 2H, J = 8 Hz); 8.05 (s, 1H); 8.18 (s,1H); 8.52 (s, 1H); 8.66 (d, 1H, J = 8 Hz); 10.09 (s, 1H); 11.12 (s, 1H); 12.83 (s, 1H); 12.93 (s, 1H). **^{13}C-NMR** (DMSO; 100MHz): δ 115.84; 116.43; 118.49; 123.50; 124.01; 126.26; 129.59; 129.90; 130.14; 130.62; 138.49; 138.52; 138.69; 140.29; 141.67; 152.22; 152.86; 156.05; 167.55.

(*E*)-3-((2-(6-((3-(trifluoromethyl)phenyl)amino)-9*H*-purin-2-yl)hydrazineylidene)methyl)benzoic acid 74h:

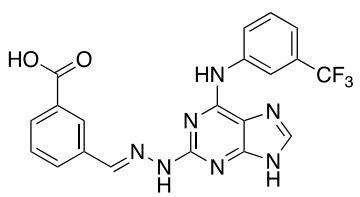

Yield: 32%; **^{1}H-NMR** (DMSO;400MHz) :δ 7.32 (d, 1H, J = 8 Hz), 7.52 (t, 1H, J = 8 Hz); 7.66 (d, 1H, J = 8 Hz); 7.90 (m, 3H); 8.2 (s, 1H); 8.03 (s, 1H); 8.19 (s, 1H); 8.33 (s, 1H); 10.0 (s, 1H); 10.02 (s,

1H); 10.96 (s, 1H); 12.85 (s, 1H). **^{13}C-NMR** (DMSO;100MHz): δ 116.52; 118.50; 123.47; 123.96; 126.18; 127.55; 129.12; 129.44; 129.83; 130.16; 136.40; 138.10; 141.58; 156.57.

(*E*)-2-((2-(6-((3-(trifluoromethyl)phenyl)amino)-9*H*-purin-2-yl)hydrazineylidene)methyl)benzoic acid 74i:

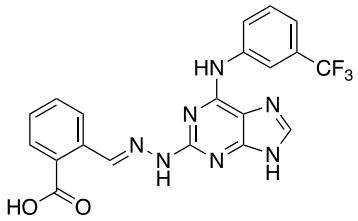

Yield:30%; **^{1}H-NMR** (DMSO; 400MHz) δ 7.33 (d, 1H, J = 8 Hz); 7.43 (t, 1H, J = 8 Hz); 7.55 (d, 2H, J = 8 Hz); 7.61 (t, 1H, J = 8 Hz); 7.86 (d, 1H, J = 8 Hz); 8.03 (s, 1H); 8.19 (d, 1H, J = 8 Hz); 8.46 (s, 1H), 8.75 (s, 1H); 8.87 (s, 1H); 10.02 (s, 1H); 11.13 (s, 1H); 12.79 (s, 1H). **^{13}C-NMR** (DMSO;100MHz): δ 116.49; 118.50; 123.61; 123.95; 126.19; 127.50; 129.13; 129.45; 129.80; 130.16; 135.20; 135.36; 136.05; 140.15; 141.57; 151.70; 151.80; 157.60; 169.90; 172.50.

(*E*)-4-((2-methyl-2-(6-((3-(trifluoromethyl)phenyl)amino)-9*H*-purin-2-yl)hydrazineylidene)methyl)benzoic acid 74l:

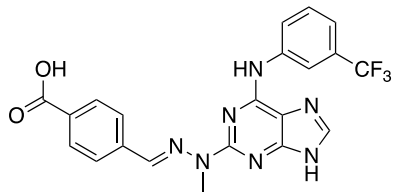

Yield: 43%**; ^{1}H-NMR** (DMSO; 400 MHz): δ 3.72 (s, 3H); 7.42 (d, 1H, J = 8 Hz); 7.62 (t, 1H, J = 8 Hz); 7.92 (d, 3H, J = 8 Hz); 7.96 (s, 1H); 8.02 (d, 2H, J = 8 Hz); 8.12 (s, 1H); 8.37 (s, 1H); 8.90 (d, 1H, J = 8 Hz); 10.20 (s,1H); 12.97 (s, 1H). **^{13}C-NMR** (DMSO; 100MHz): δ 32.13; 115.97; 116.66; 118.76; 123.47; 124.08; 126.55; 130.18; 135.43; 139.30; 141.08; 141.57; 151.84; 152.82; 156.42; 167.68.

(*E*)-3-((2-methyl-2-(6-((3-(trifluoromethyl)phenyl)amino)-9*H*-purin-2-yl)hydrazineylidene)methyl)benzoic acid 74m:

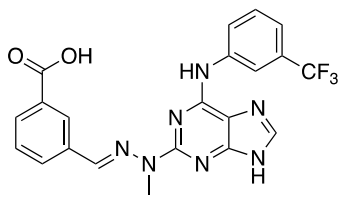

Yield : 32%; **^{1}H-NMR** (DMSO; 400MHZ): δ 3.37 (s, 3H); 7.35 (d, 1H, J = 8 Hz); 7.57 (t, 1H, J = 8 Hz); 7.66 (t, 1H, J = 8 Hz); 7.94 (d, 1H, J = 8 Hz); 8.00 (s, 1H); 8.03 (d, 1H, J = 8 Hz); 8.11 (s, 1H); 8.38 (s, 2H); 8.84 (d, 1H, J = 8 Hz); 10.24 (bs, 1H); 13.01 (bs, 1H). **^{13}C-NMR** (DMSO; 100 MHz): δ 32.20; 116.50; 118.49; 123.47; 123.96; 126.18; 127.55; 129.12; 129.44; 129.83; 130.16; 136.37; 137.09; 141.58; 156.57.

(*E*)-2-((2-methyl-2-(6-((3-(trifluoromethyl)phenyl)amino)-9*H*-purin-2-yl)hydrazineylidene)methyl)benzoic acid 74n:

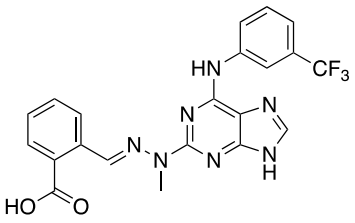

Yield: 56%; **^{1}H-NMR** (DMSO; 400 MHz): δ 3.99 (s, 3H); 7.37 (d, 1H, J = 8 Hz); 7.47 (t, 1H, J = 8 Hz); 7.56 (d, 1H, J = 8 Hz); 7.68 (t, 1H, J = 8 Hz); 7.93 (d, 1H, J = 7.2 Hz); 8.13 (s, 1H); 8.28 (d, 1H, J = 8 Hz); 8.35 (s, 1H); 8.63 (s, 1H); 8.91 (d, 1H, J = 8 Hz); 10.18 (s, 1H); 12.93 (s, 1H). **^{13}C-NMR** (DMSO; 100 MHz): δ 31.91; 115.82; 116.58; 118.60; 123.43; 124.07; 126.14; 126.38; 128.40; 129.91; 131.01; 132.20; 135.36; 137.05; 139.15; 141.57; 151.76; 152.80; 156.58; 168.93; 172.50.

(*E*)-2-(2-benzylidenehydrazineyl)-*N*-(3-(trifluoromethyl)phenyl)-9*H*-purin-6-amine 74j:

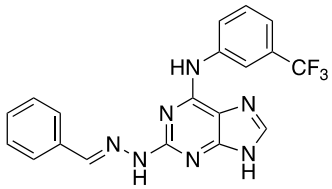

Yield : 38%; **^{1}H-NMR** (DMSO; 400 MHz): δ 7.35 (t, 2H, J = 4 Hz); 7.46 (t, 2H, J = 4 Hz); 7.57 (t, 1H, J = 8 Hz); 7.71 (d, 2H, J = 8 Hz); 8.04 (s, 1H); 8.13 (s, 1H); 8.52 (s, 1H); 8.67 (d, 1H, J = 8 Hz); 10.01 (s, 1H); 10.89 (s, 1H); 12.90 (s, 1H). **^{13}C-NMR** (DMSO; 100MHz): δ 21.52; 115.64; 116.42; 118.41; 123.96; 126.48; 129.10; 129.85; 136.10; 138.31; 140.09; 141.76; 152.22; 152.93; 156.33; 172,48.

(*E*)-2-(2-benzylidene-1-methylhydrazineyl)-*N*-(3(trifluoromethyl)phenyl)-9*H*-purin-6-amine 74k:

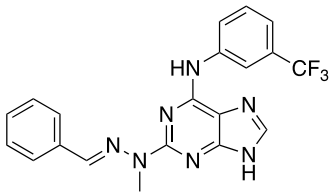

Yield: 38%; **^{1}H-NMR** (DMSO;400MHz): δ 3.71 (s, 3H); 7.37 (d, 2H, J = 8 Hz); 7.48 (t, 2H, J = 8 Hz); 7.60 (t, 2H, J = 8 Hz); 7.85 (d, 1H, J = 8 Hz); 7.91(s, 1H); 8.10 (s, 1H); 8.34 (s, 1H); 8.99 (d, 1H, J = 8 Hz); 10.20 (s, 1H); 12.80 (s, 1H). **^{13}C-NMR** (DMSO; 100MHz): δ 31.89; 116.50; 118.53; 123.46; 123.99; 126.16; 126.73; 128.72; 129.08; 129.56; 129.90; 136.48; 136.91; 139. 33; 141.69; 151.52; 156.62; 172.70.

General synthesis of 1-(3-nitrophenyl)-3-(*o*-tolyl)urea 47:

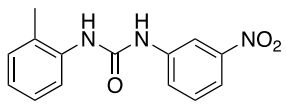

2-amino toluene **75** (100 mg, 100 µL, 0.93 mmol, 1 eq.) was added to a solution of 3-nitrophenyl isocyanate **76** (150 mg, 0.93 mmol, 1 eq.) in anhydrous DCM (3 mL). The solution was stirred for 2 hours at room temperature under a nitrogen atmosphere. The white precipitate was filtered, washed with petroleum

ether and dried under high vacuum. The product was purified by silica gel chromatography in 98:2 DCM/MeOH as eluent. Yield: 90 %; ^{1}H NMR (400 MHz, MeOD): δ 2.33 (s, 3H); 7.08 (t, 1H, J = 8 Hz); 7.23 (m, 2H); 7.53 (t, 1H, J = 8 Hz); 7.65 (d, 1H, J = 8 Hz); 7.76 (d, 1H, J = 8 Hz); 7.88 (d, 1H, J = 8 Hz); 8.53 (t, 1H, J = 8 Hz).

General synthesis of *N*-benzyl-4,6-dichloro-1,3,5-triazin-2-amine 79:

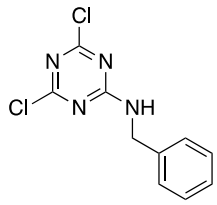

To a stirred solution of cyanuric chloride **77** (1 g, 5.42 mmol) in dimethoxyethane (35 mL) at r.t., benzylamine **78** (1 equiv) was added dropwise. The reaction mixture was vigorously stirred for 3 h at r.t. After this time, the reaction mixture was washed with 3N HCl, H_2O, and brine. The organic phase was dried over anhydrous Na_2SO_4 and then evaporated to dryness. The resulting white residue was dissolved in a minimum amount of DCM. Finally, by addition of petroleum ether, the final compound was precipitated and collected by filtration. **Yield**: 85%; **^{1}H NMR** (400 MHz, $CDCl_3$): δ 4.69 (s, 2H, J = 8 Hz); 7.30-7.43 (m, 5H).

General synthesis of N^2-benzyl-6-chloro-N^4,N^4-diethyl-1,3,5-triazine-2,4-diamine 80:

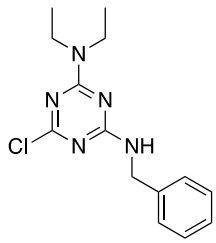

To a suspension of the intermediate **79** (100 mg, 0.39 mmol, 1 equiv) in DCM, triethylamine (109 μL, 0.78 mmol, 2 equiv) was added dropwise. The reaction mixture was stirred at rt for 12 h and then washed with 3N HCl, H_2O, and brine. The organic phase was dried over anhydrous Na_2SO_4 and evaporated to dryness. The resulting white residue was dissolved in a minimum amount of DCM. Finally, by addition of petroleum ether, the final compound precipitated and was collected by filtration. **Yield** 75 %; **^{1}H NMR** (400 MHz, $CDCl_3$): δ 1.17 (m, 6H); 3.56 (m, 2H); 3.92 (q, 2H, J = 8 Hz); 4.62 (m, 2 H); 7.35 (m, 5H).

General synthesis of 2-((2-(4-(benzylamino)-6-(diethylamino)-1,3,5-triazin-2-yl)hydrazineylidene)methyl)phenol 48:

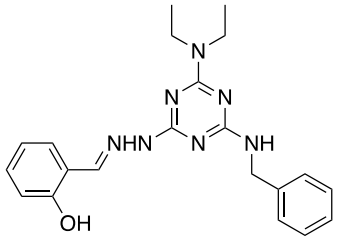

To a solution of the appropriate intermediate **80** (50 mg, 0.17 mmol, 1 equiv) in DCM, hydrazine (4 equiv) was added and the resulting mixture was heated at reflux for 12 h. After cooling down to r.t., the mixture was washed with H_2O and brine. The organic phase was dried over anhydrous Na_2SO_4 and evaporated to dryness. The formed

intermediate N2-benzyl-N4,N4-diethyl-6-hydrazineyl-1,3,5-triazine-2,4-diamine **81** was dissolved in toluene and reacted with aldehyde salicylic **82** (2 equiv). The reaction mixture was heated at reflux for 3 h using a Dean–Stark apparatus for azeotropical removal of H_2O. The reaction mixture was evaporated to dryness and the resulting residue was dissolved in a minimum amount of DCM. Upon subsequent addition of petroleum ether, the desired compounds **48** precipitated and were collected by filtration. **Yield** 74 %; **^{1}H NMR** (400 MHz, $CDCl_3$): δ 1.15 (t, 6H, J = 8 Hz); 3.55 (q, 4H, J = 8 Hz); 4.59 (d, 2H, J = 4 Hz); 7.00 (t, 1H, J = 8 Hz); 7.07 (d, 1 H, J = 8 Hz); 7.25 (m, 1H); 7.36 (m, 8H); 8.75 (s, 1 H); 11.42 (s, 1H).

Bithiazole Derivatives as Broad-Spectrum Antiviral Agents

Synthesis of 1-(2-amino-4-mathylthiazol-yl)ethan-1-one 87:

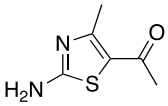

In a round-bottomed flask, commercially available thiourea **85** (2.000 g; 26.275 mmol) and 3- chloropentane-2,4-dione **86** (3.534 g; 26,274 mmol), solubilized in ethanol (20 mL), were stirred at reflux for three hours. The progress of the reaction was monitored by TLC. At the end of the reaction, a precipitate was formed. The reaction mixture was filtered, causing the precipitate to separate from the solution of the residual starting reagents in EtOH, and washed with Et_2O. **Yield**: 97%; **^{1}H NMR** (DMSO-*d6*, 400 MHz): δ 2.44 (s, 3H); 2.54 (s, 3H); 9.33 (s, 2H).

Synthesis of N-(5-acetyl-4-methylthiazol-2-yl)pivalamide 88:

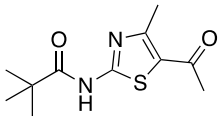

In a round-bottomed flask, compound **87** (2.000 g; 12.8 mmol) was suspended in dry THF (32 mL) and the mixture was cooled to 0°C. Pyridine (2 mL) was added and the mixture was stirred for a few minutes. Next, pivaloyl chloride (5,3 mL; 43,295 mmol) was added dropwise. The mixture was allowed to warm to room temperature and then was heated at reflux for 8h. The progress of the reaction was monitored by TLC. At the end of the reaction, equal parts of H_2O and ethyl acetate were added, and the aqueous phase was extracted three times with ethyl acetate. The combined organic phases were washed with a saturated aqueous solution of NH_4Cl and brine, dried over Na_2SO_4, and concentrated under vacuum. **Yield**: 52%; **^{1}H NMR** (DMSO-d_6, 400 MHz): δ 1.12 (s, 9H); 2.48 (s, 3H); 2.58 (s, 3H); 12.16 (s, 1H).

Synthesis of N-(5-(2-bromoacetyl)-4-methylthiazol-2-yl)pivalamide 89:

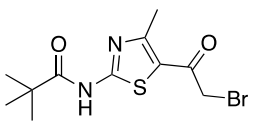

A solution of Br_2 (0.42 mL; 8.321 mmol) in 1,4-dioxane (10 mL) was added dropwise to a round- bottomed flask, containing a stirred solution of **88 (**1.600 g; 6,657 mmol) in 1,4-dioxane (8 mL). The mixture was allowed to react for 18 hours at room temperature and then was heated at reflux for 5 hours. The progress of the reaction was monitored by TLC. At the end of the reaction, equal parts of saturated $NaHCO_3$ aqueous solution and ethyl acetate were added and the aqueous phase was extracted three times with ethyl acetate. The combined organic phases were washed with brine, dried over Na_2SO_4, and concentrated under vacuum. The crude was purified by silica gel chromatography using hexane/ethyl acetate (from 9:1 to 7:3) as eluent mixture. **Yield**: 30%; **^{1}H NMR** ($CDCl_3$, 400 MHz): δ 1.38 (s, 9H); 2.69 (s, 3H); 4.24 (s, 2H); 9.10 (s, 1H).

General procedure for the synthesis of secondary amines 93a-m:

A solution of the proper primary amine **91a-c**, in EtOH was formed. The proper cycloketone **92a-e** (2 equivalents) was added to the mixture and it was stirred under N_2. After 10 minutes $NaBH_4$ (2.5 equivalents) was added at a temperature of 0 °C. The reaction was allowed to reach room temperature and then stirred overnight. The progress of the reaction was monitored by TLC. At the end of the reaction, the resultant reaction mixture was quenched by water, filtered through the Celite reagent, then solvents were evaporated. The residue was dissolved in HCl 1N and extracted one time with ethyl acetate. The pH of the aqueous layer was adjusted to 8 using saturated sodium bicarbonate solution. The compound was extracted 6 times with ethyl acetate and 2 times with chloroform. The organic phase was dried over sodium sulphate and concentrated under vacuum. The product was used in the next step without further purification.

1-(cyclohexylamino)-2-methylpropan-2-ol 93a:

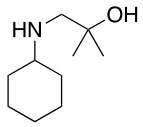

Yield: 64%. **^{1}H-NMR** ($CDCl_3$ 400 MHz): δ 1.01 -1.10 (m, 2H); 1.16 (s, 6H); 1.20 - 1.31 (m, 3H); 1.60 - 1.65 (m; 1H); 1.72 - 1.76 (m, 2H); 1.89 - 1.93 (m, 2H); 2.37 - 2.44 (m, 1H); 2.55 (s, 2H).

2-(cyclopentylamino)ethan-1-ol 93b:

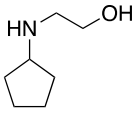

Yield:85 %; **^{1}H NMR** ($CDCl_3$, 400 MHz): δ 1.65 (m, 5H); 1.88 (m, 1H); 2.10 (m, 3H); 2.81 (t, 2H, J = 4 Hz); 3.67 (t, 2H; J = 4 Hz).

1-(cyclopentylamino)-2-methylpropan-2-ol 93c:

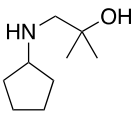

Yield: 82%; **^{1}H NMR** ($CDCl_3$, 400 MHz): δ 1.14 (s, 6H); 1.25-1.35 (m, 2H); 1.49-1.55 (m, 2H); 1.64-1.69 (m, 2H); 1.76-1.83 (m,2H); 2.49 (s, 2H); 3.03-3.12 (m, 1H); 3.43-3.45 (d,1H).

2-(cycloheptylamino)ethan-1-ol 93d:

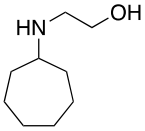

Yield: 87%; **^{1}H-NMR** ($CDCl_3$, 400 MHz): δ 1.13 (m, 4H); 1.33 (m, 4H); 1.59 (m, 4H); 2.43 (t, 2H, J = 8 Hz); 3.37 (t, 2H, J = 8 Hz); 3.51 (qt, 1H, J = 8 Hz).

1-(cycloheptylamino)-2-methylpropan-2-ol 93e:

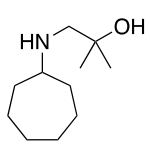

Yield: 100%; **^{1}H-NMR** ($CDCl_3$, 400 MHz): δ 1.13 (m, 4H); 1.14 (s, 6H); 1.34 (m, 4H); 1.59 (m, 4H); 3.37 (t, 2H, J = 8 Hz); 3.40 (qt, 1H, J = 8 Hz).

ethyl 3-((2-hydroxyethyl)amino)cyclohexane-1-carboxylate 93f:

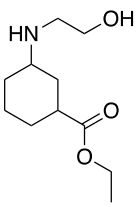

Yield: 61%; **^{1}H-NMR** ($CDCl_3$, 400 MHz): δ 1.23 (m, 7H); 1.53 (m, 3H); 2.51 (t, 3H, J = 4 Hz); 3.33 (q, 2H, J = 4 Hz); 3.45 (m, 2H); 4.55 (m, 2H).

ethyl 4-((2-hydroxyethyl)amino)cyclohexane-1-carboxylate 93g :

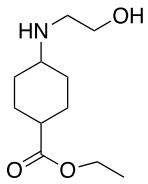

Yield: 66%; **^{1}H NMR** ($CDCl_3$, 400 MHz): δ 1.23-1.26 (t, 3H); 1.43-1.69 (m, 4H); 1.98-2.24 (m, 6H); 2.75-2.81 (m, 1H); 3.60-3.66 (m, 2H); 4.09-4.16 (m, 2H).

1-((cyclohexylamino)methyl)cyclopentan-1-ol 96h:

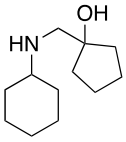

Yield: 90%; **^{1}H NMR** ($CDCl_3$, 400 MHz): δ 1.02-1.30 (m, 8H); 1.43-1.49 (m, 1H); 1.53-1.92 (m, 9H); 2.37-2.43 (m, 1H); 2.66 (s, 2H).

1-((cyclopentylamino)methyl)cyclopentan-1-ol 96i:

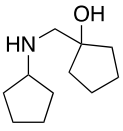

Yield: 56%; **^{1}H NMR** ($CDCl_3$, 400 MHz): δ 1.19-1.28 (m, 2H); 1.35-1.51 (m, 6H); 1.53-1.61 (m, 4H); 1.69-1.77 (m, 4H); 2.55 (s, 2H); 2.96-3.02 (m, 1H).

1-((cycloheptylamino)methyl)cyclopentan-1-ol 96l:

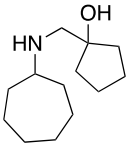

Yield: 77%; **^{1}H NMR** ($CDCl_3$, 400 MHz): δ 1.18-1.28 (m, 4H); 1.30-1.54 (m, 12H); 1.65-1.78 (m,4H); 2.48 (s, 2H); 3.61-3.66 (m, 1H).

General Procedure for the Synthesis of compounds 95a-m:

Benzoyl isothiocyanate (302 μL; 2.25 mmol) was added dropwise to a solution of the proper amine (**91b-e** and **93a-g**) (2.25 mmol) in dichloromethane (7.29 mL). The mixture was stirred at room temperature for 1-2 h. The crude was used for the next step without further purifications (for **95f,i,l**), except for **95a-d,** that were purified by flash chromatography using using the proper eluent: **a,b**: petroleum ether/ethyl acetate 85:15-7:3; **c**: CH_2Cl_2/MeOH 99:1-98:2; **d**: CH_2Cl_2/MeOH 98:2-97:3. Instead for **95e,g,h,m,** extraction with CH_2Cl_2 was performed (x3).

N-((2-hydroxy-2-methylpropyl)carbamothioyl)benzamide 95a:

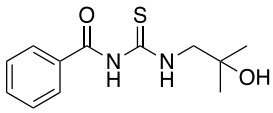

Yield: 77%; **MS** (ESI) $[M+H]^+$ = 253,33 m/z; **^{1}H-NMR** (DMSO-d_6 400 MHz): δ 1.17 (s, 6H); 3.55 (d, 2H, *J* = 4 Hz); 4.88 (s, 1H); 7.48-7.52 (m, 2H); 7.64 (td, 1H, *J* = 4 Hz, *J* = 8 Hz); 7.91-7.94 (m, 2H); 11.11 (t, 1H, *J* = 8 Hz); 11.31 (s, 1H).

***N*-(((1-hydroxycyclopentyl)methyl)carbamothioyl)benzamide 95b:**

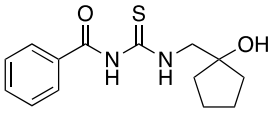

Yield: 54%.

N-((2,3-dihydroxypropyl)carbamothioyl)benzamide 95c:

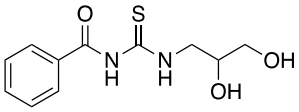

Yield: 44%; **^{1}H-NMR** ($CDCl_3$ 400 MHz): δ 3.65-3.69 (m, 1H); 3.76-3.86 (m, 2H); 3.98-4.08 (m, 2H); 7.52 (t, 2H, *J* = 8 Hz); 7.63 (t, 1H, *J* = 8 Hz); 7.85 (m, 2H); 9.17 (s, 1H); 11.02 (m, 1H).

N-(bis(2-hydroxyethyl)carbamothioyl)benzamide 95d:

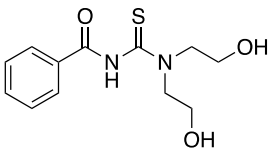

Yield: 87%; **^{1}H-NMR** (MeOD 400 MHz): δ 3.89 (s, 4H), 4.00 (m, 2H); 4.10 (m, 2H); 7.50-7.53 (m, 2H); 7.60-7.62 (td, 1H, *J* = 4 Hz, *J* = 8 Hz); 7.91-7.93 (m, 2H).

N-(cyclohexyl(2-hydroxy-2-methylpropyl)carbamothioyl)benzamide 95e:

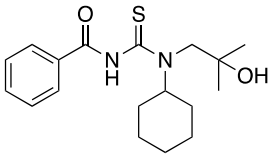

Yield: 95%; **^{1}H-NMR** ($CDCl_3$ 400 MHz): δ 1.21-1.27 (m, 2H); 1.32 (s, 6H); 1.40-1.46 (m, 2H); 1.72 (s, 3H); 1.80-1.84 (m, 2H); 1.91-1.94 (m, 2H); 3.37-3.39 (m, 2H); 7.45-7.50 (m, 2H); 7.54-7.58 (m, 1H); 7.82-7.86 (m, 2H).

***N*-(cyclopentyl(2-hydroxy-2-methylpropyl)carbamothioyl)benzamide 95g:**

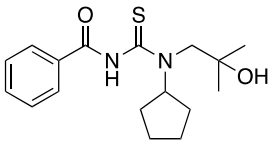

Yield: 93%; **^{1}H-NMR** ($CDCl_3$ 400 MHz): δ 1.29 (m, 2H); 1.53 (s; 6H); 1.72 (m, 5H); 1.99 (m, 2H); 3.32 (s, 2H); 4.61 (qt, 1H, J = 8 Hz); 7.44 (m, 2H); 7.85 (d; 1H; J = 8 Hz); 8.19 (d, 2H, J = 8 Hz).

***N*-(cycloheptyl(2-hydroxyethyl)carbamothioyl)benzamide 95h:**

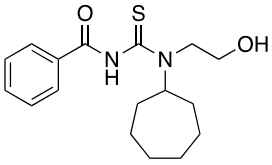

Yield: 95%; **^{1}H NMR** (DMSO-d_6, 400 MHz): δ 1.48 (m, 8H); 1.67 (m, 4H); 3.34 (m, 2H); 3.55 (q, 2H, J = 8 Hz); 7.50 (m, 3H); 7.87 (d, 2H, J = 4 Hz).

ethyl 4-(3-benzoyl-1-(2-hydroxyethyl)thioureido)cyclohexane-1-carboxylate 95m:

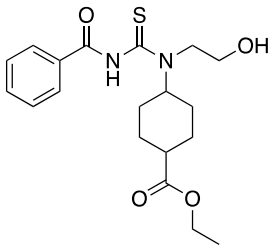

Yield: 46%; **^{1}H NMR** ($CDCl_3$, 400 MHz): δ 1.26-1.32 (t, 3H); 1.50-1.68 (m, 6H); 1.76-1.95 (m, 2H); 2.25-2.29 (t, 2H); 2.60-2.69 (m, 1H); 3.49-3.68 (m, 1H); 3.94-4.04 (t, 2H); 4.16-4.24 (q, 2H); 7.42-7.63 (m, 3H); 7.83-7.90 (m, 2H)

General Procedure for the Synthesis of compounds 96a-m:

Sodium (209 mg; 4.76 mmol) was added to dry MeOH (10.13 mL) under argon atmosphere and stirred until we obtained a solution, where NaOMe is formed. The proper intermediate (1.59 mmol) was added portion wise. The mixture was stirred under argon atmosphere at room temperature for 1 hour for **96a,c,d,e**, 2 hours for **96f-i**, and 3 hours for **96b,l,m** . The solvent was evaporated under vacuum. The crude was purified by flash chromatography using the proper eluent: **96a:** CH_2Cl_2/MeOH 95:5; **96b:** Hexane/EtOAc 8:2; **96c**: CH_2Cl_2/MeOH 93:7; **96d:** CH_2Cl_2/MeOH 96:4; **96e-i:** CH_2Cl_2/MeOH 98:2, **96l,m**: CH_2Cl_2/MeOH 93:7 plus 0.5% of formic acid

1-(2-hydroxy-2-methylpropyl)thiourea 96a:

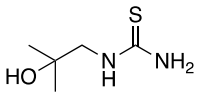

Yield: 90%; **MS** (ESI) $[M+H]^+$: 149,06 m/z; **^{1}H-NMR** (DMSO-d_6 300 MHz): δ 1.08 (s, 6H); 4.58 (m, 2H); 7.05 (s, 2H).

1-((1-hydroxycyclopentyl)methyl)thiourea 96b:

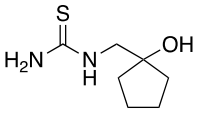

Yield: 35%; **^{1}H NMR** (DMSO-d_6, 300 MHz): δ 1.51 (m, 7H); 1.68 (m, 1H); 3.44 (m, 2H); 4.55 (bs, 1H); 7.04 (bs, 2H); 7.49 (bs, 1H).

1-(2,3-dihydroxypropyl)thiourea 96c:

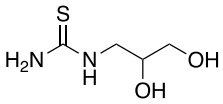

Yield: 80%; **^{1}H-NMR** (DMSO-d_6 300 MHz): δ 3.17 (s, 1H); 3.25-3.55 (m, 4H).

1,1-bis(2-hydroxyethyl)thiourea 96d:

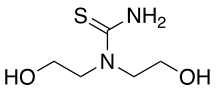

Yield: 30%; **MS** (ESI) $[M+H]^+$ = 165,13 m/z; **^{1}H-NMR** (DMSO-d_6 300 MHz): δ 3.58-3.69 (m, 8H); 4.87 (bs, 2H); 7.21 (s, 2H).

1-cyclohexyl-1-(2-hydroxy-2-methylpropyl)thiourea 96e:

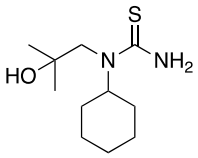

Yield: 33%; **MS** (ESI) $[M+H]^+$ = 231,19 m/z; **^{1}H-NMR** ($CDCl_3$ 400 MHz): 1.02-1.12 (m, 1H); 1.21-1.24 (m, 2H); 1.32 (s, 6H); 1.40-1.50 (m, 2H); 1.67-1.72 (m, 4H); 1.80-1.83 (m, 2H); 1.91-1.94 (m, 2H); 2.65 (bs, 1H).

1-cyclopentyl-1-(2-hydroxyethyl)thiourea 96f:

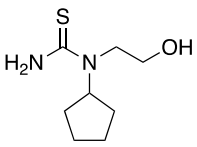

Yield: 50%; **^{1}H NMR** ($CDCl_3$, 400 MHz): δ 1.39 (m, 2H); 1.69 (m, 4H); 2.04 (m, 2H); 3.44 (m, 1H); 3.61 (m, 2H); 3.89 (m, 2H).

1-cyclopentyl-1-(2-hydroxy-2-methylpropyl)thiourea 96g:

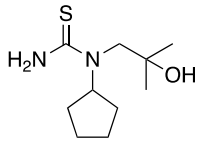

Yield: 30%; **^{1}H NMR** ($CDCl_3$, 400 MHz): δ 1.39 (s, 6H); 1.61-1.66 (m, 2H); 1.78-1.90 (m, 2H); 2.10-2.14 (m, 2H); 2.95 (s,1H); 3.47-3.50 (m, 1H); 6.03 (s, 2H).

1-cycloheptyl-1-(2-hydroxyethyl)thiourea 96h:

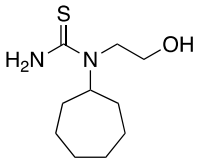

Yield: 37%; **^{1}H NMR** (DMSO-d_6, 400 MHz): δ 1.48 (m, 8H); 1.67 (m, 4H); 3.34 (m, 2H); 3.55 (q, 2H, J = 8 Hz); 5.23 (bs, 1H).

1-cycloheptyl-1-(2-hydroxy-2-methylpropyl)thiourea 96i:

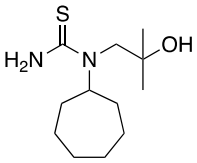

Yield: 50%; **^{1}H NMR** ($CDCl_3$, 400 MHz): δ 1.40 (s, 6H); 1.48 (m, 8 H); 1.67 (m, 3H); 3.34 (m, 2H); 3.55 (q, 2H, J = 8 Hz); 5.23 (bs, 1H).

3-(1-(2-hydroxyethyl)thioureido)cyclohexane-1-carboxylic acid 96l:

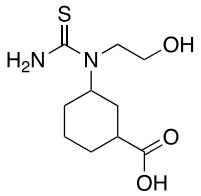

Yield: 24%; **^{1}H NMR** ($CDCl_3$, 400 MHz): δ 1.52 (m, 7H); 1.68 (m, 3H); 3.33 (m, 2H); 4.50 (m, 2H).

4-(1-(2-hydroxyethyl)thioureido)cyclohexane-1-carboxylic acid 96m:

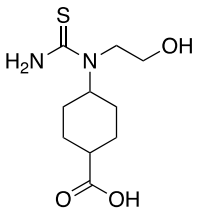

Yield: 35%; **^{1}H NMR** ($CDCl_3$, 400 MHz): δ 1.56 (m; 4H); 1.70 (m, 2H); 1.83 (m, 3H), 2.25 (m, 1H); 3.53 (m, 2H); 3.84 (m, 2H).

General Procedure for the Synthesis of compounds 96n-p:

TMSNCS (1 equivalent) and EtOH (2-5 mL) were added to a round-bottomed flask and the mixture was stirred for a couple of minutes. Triethylamine (1.5 equivalent) was added to the mixture and then

also the proper secondary amine **93h-l** (1 equivalent) was added. The mixture was heated at reflux for three hours. The progress of the reaction was monitored by TLC. Equal parts of a saturated aqueous NH_4Cl solution and ethyl acetate were added and the aqueous phase was extracted 5 times with ethyl acetate. The combined organic phases were dried over Na_2SO_4 and concentrated under vacuum.

1-cyclohexyl-1-((1-hydroxycyclopentyl)methyl)thiourea 96n:

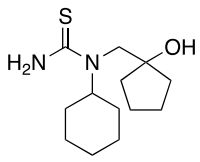

Yield: 81%; **^{1}H NMR** ($CDCl_3$, 400 MHz): δ 1.08-1.27 (m, 4H); 1.46-1.51 (m, 2H); 1.56-1.63 (m, 10H); 1.66-1.95 (m, 2H); 2.45-2.50 (m, 1H); 2.71 (s, 2H); 3.04 (s, 2H).

1-cyclopentyl-1-((1-hydroxycyclopentyl)methyl)thiourea 96o:

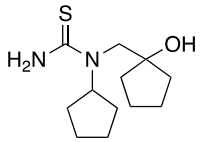

Yield: 50%; **^{1}H NMR** ($CDCl_3$, 400 MHz): δ 1.32-1.37 (m, 2H); 1.44-1.58 (m, 6H); 1.62-1.68 (m, 4H); 1.74-1.84 (m, 4H); 2.66 (s, 2H); 3.08-3.11 (m, 1H); 3.26 (s, 2H)

1-cycloheptyl-1-((1-hydroxycyclopentyl)methyl)thiourea 96p:

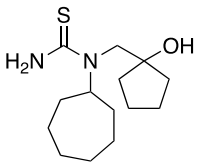

Yield: 50%; **^{1}H NMR** ($CDCl_3$, 400 MHz): δ 1.23-1.27 (m, 1H); 1.32-1.70 (m, 15H); 1.75-1.90 (m, 4H); 2.63 (s, 2H); 2.61-2.79 (m, 1H).

General procedure for the synthesis of compounds 103a-p:

A solution of N-(5-(2-bromoacetyl)-4-methylthiazol-2-yl)pivalamide **89** (86 mg; 0.27 mmol) and the proper thiourea **96a-p** (1 eq) in ethanol (2 mL) was stirred at reflux for 1 hour for compounds **103b**,**c**,**d**,**f**,**g**,**h**,**i**, 2 hours for compounds **103a** and **103e**, 3 hours for **103l,m** and overnight for **103n-p**. After evaporation of the solvent, saturated aqueous $NaHCO_3$ was added and the mixture was extracted three times with ethyl acetate. The combined organic phases were dried over $NaSO_4$ and concentrated under vacuum. The crude was purified by flash chromatography using the proper eluent: **103a,b,d,e,g,i**: CH_2Cl_2/MeOH 98:2; **103c,f,h:** CH_2Cl_2/MeOH 97:3; **103l,m**: CH_2Cl_2/MeOH 95:5 plus 0.5% of formic acid; **103n-p**: Hexane/EtOAc 7:2

N-(2'-((2-hydroxy-2-methylpropyl)amino)-4-methyl-[5,5'-bithiazol]-2-yl)pivalamide 103a:

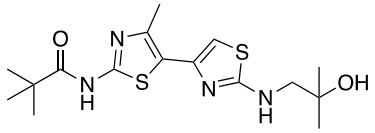

Yield: 96%; **MS** (ESI) $[M+H]^+$ = 369,20 m/z; **^{1}H-NMR** (DMSO-*d_6* 300 MHz): δ 1.14 (s, 6H); 1.23 (s, 9H); 2.44 (s, 3H); 3.23 (d, 2H, *J* = 4 Hz); 4.59 (s, 1H); 6.56 (s, 1H); 7.61 (t, 1H, *J* = 4 Hz); 11.64 (s, 1H). **^{13}C-NMR** (DMSO-*d_6*, 75 MHz): δ 17.35; 27.08; 27.88; 56.31; 70.06; 100.65; 121.23; 142.42; 142.92; 155.99; 169.06; 176.86.

***N*-(2-(((1-hydroxycyclopentyl)methyl)amino)-4'-methyl-[4,5'-bithiazol]-2'-yl)pivalamide 103b:**

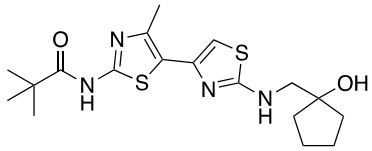

Yield: 77 %; **^{1}H NMR** ($CDCl_3$, 400 MHz): δ 1.34 (s, 9H); 1.74 (m, 4H); 1.87 (m, 4H); 2.52 (s, 3H); 3.49 (d, 2H, J = 8 Hz); 5.62 (t, 1H, J = 4 Hz); 6.41 (s, 1H); 8.92 (bs, 1H). **^{13}C-NMR** (DMSO-*d_6*, 75 MHz): δ 16.99; 24.03; 27.27; 38.26; 39.15; 54.86; 82.47; 101.37; 121.91; 142.65; 143.35; 155.57; 169.39; 175.90.

N-(2'-((2,3-dihydroxypropyl)amino)-4-methyl-[5,5'-bithiazol]-2-yl)pivalamide 103c:

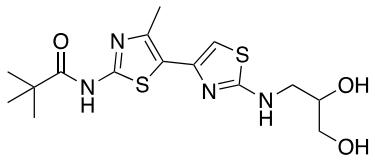

Yield: 67%; **MS** (ESI) $[M+H]^+$ = 371,05 m/z; **^{1}H-NMR** (DMSO-*d_6* 300 MHz): δ 1.23 (s, 9H); 2.51 (s, 3H); 3.37 (m, 1H); 3.68 (m, 1H); 4.63 (t, 1H, *J* = 8 Hz); 4.88 (d, 1H, *J* = 8 Hz); 6.59 (s, 1H); 7.68 (t, 1H, *J* = 4 Hz); 11.45 (s, 1H). **^{13}C-NMR** (DMSO-*d_6*, 75 MHz): δ 17.34; 27.08; 39.18; 48.35; 64.14; 70.67; 100.88; 121.09; 142.55, 143.03; 156.00; 168.81; 176.87.

N-(2'-(bis(2-hydroxyethyl)amino)-4-methyl-[5,5'-bithiazol]-2-yl)pivalamide 103d:

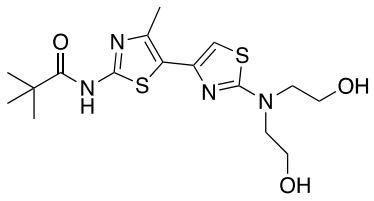

Yield: 62%; **MS** (ESI) $[M+H]^+$ = 385,33 m/z; **^{1}H-NMR** (DMSO-*d_6* 300 MHz): δ 1.23 (s, 9H); 2.45 (s, 3H); 3.54 (t, 4H, *J* = 4 Hz); 3.66 (q, 4H, *J* = 8 Hz); 4.89 (t, 2H, J = 8 Hz); 6.69 (s, 1H); 11.67 (s, 1H). **^{13}C-NMR** (DMSO-*d_6* 75 MHz): δ 17.29; 27.07; 39.17; 54.99; 58.58; 101.08; 121.05; 142.17; 143.87; 156.12; 169.17; 176.92.

N-(2'-(cyclohexyl(2-hydroxy-2-methylpropyl)amino)-4-methyl-[5,5'-bithiazol]-2-yl)pivalamide 103e:

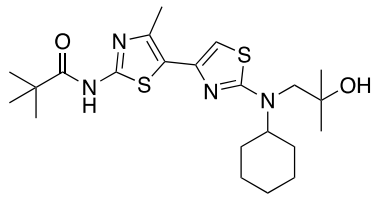

Yield: 20%; **MS** (ESI) $[M+H]^+$ = 451,31 m/z; **^{1}H-NMR** (MeOD 400 MHz): δ 1.24 (s, 6H); 1.31 (s, 9H); 1.41-1.45 (m, 3H); 1.67-1.70 (m, 3H); 1.88-1.91 (m, 4H); 2.47 (s, 3H); 3.33-3.41 (m, 1H); 3.49 (s, 2H); 6.65 (s, 1H). **^{13}C-NMR** (MeOD 100 MHz): δ 15.63; 25.03; 25.75; 25.89; 25.92; 26.85; 29.81; 38.74; 57.72; 64.30; 71.09; 74.52; 101.71; 120.74; 142.56; 142.88; 171.91.

***N*-(2-(cyclopentyl(2-hydroxyethyl)amino)-4'-methyl-[4,5'-bithiazol]-2'-yl)pivalamide 103f:**

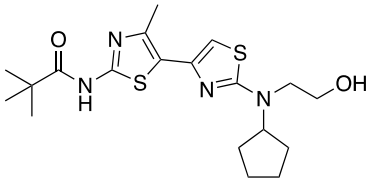

Yield: 78%; **^{1}H NMR:** ($CDCl_3$, 400 MHz) δ 1.33 (s, 9H); 1.63 (m, 4H); 1.77 (m, 2H); 2.07 (m, 2H); 2.51 (s, 3H); 3.64 (t, 2H, J = 4 Hz); 3.89 (t, 2H, J = 4 Hz); 3.94 (qt, 1H, J = 4 Hz); 4.53 (bs, 1H); 6.45 (s, 1H), 8.87 (bs, 1H). **^{13}C NMR** ($CDCl_3$, 100 MHz): δ 23.78; 27.27; 29.05; 39.1248.98; 63.63; 64.16; 101.29; 143.35; 171.64; 175.79.

***N*-(2-(cyclopentyl(2-hydroxy-2-methylpropyl)amino)-4'-methyl-[4,5'-bithiazol]-2'-yl)pivalamide 103g:**

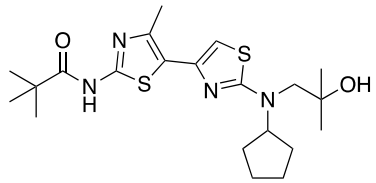

Yield: 60%; **^{1}H NMR:** ($CDCl_3$, 400 MHz) δ 1.27 (s, 9H); 1.39 (s, 6H); 1.61-1.68 (m, 2H); 1.77-1.90 (m, 4H); 2.08-2.15 (m, 2H); 2.65 (s, 3H); 2.95 (s, 2H); 3.47-3.52 (m, 1H); 6.45 (s, 1H); 8.82 (s, 1H). **^{13}C NMR** ($CDCl_3$, 100 MHz): δ 12.2; 24.1; 27.5; 28.0; 32.9; 39.3; 66.7; 70.8; 72.2; 104.8; 117.3; 142.5; 147.9; 155.8; 162.9; 176.7

***N*-(2-(cycloheptyl(2-hydroxyethyl)amino)-4'-methyl-[4,5'-bithiazol]-2'-yl)pivalamide 103h:**

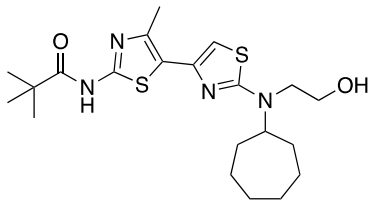

Yield: 64%; **MS** (ESI) $[M+H]^+$: 437.20 m/z; **^{1}H NMR** (DMSO-d_6, 400 MHz): δ 1.23 (s, 9H); 1.56 (m, 4H) 1.79 (m, 6H); 2.46 (s, 3H); 3.63 (t, 2H, J = 8 Hz); 3.73 (t, 2H, J = 8 Hz) 4.80 (m, 1H); 6.70 (s, 1H); 11.70 (s, 1H). **^{13}C NMR** ($CDCl_3$, 100 MHz): δ 16.23; 25.58; 28.45; 29.57; 30.70; 39.09; 59.19; 67.86; 101.90; 121.29; 142.04; 150.41; 155.80 171.91; 175.60.

_N_-(2-(cycloheptyl(2-hydroxy-2-methylpropyl)amino)-4'-methyl-[4,5'-bithiazol]-2'-yl)pivalamide 103i:

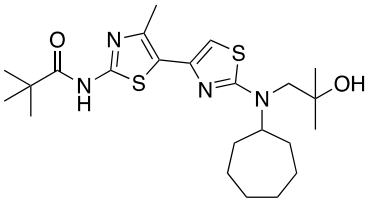

Yield: 98%; **^{1}H NMR** ($CDCl_3$, 400 MHz): δ 1.22 (s, 6H); 1.31 (s, 9H); 1.55 (m, 4H); 1.73 (m, 6H); 2.00 (m, 2H); 2.49 (s, 3H); 3.44 (s, 2H); 3.47 (qt, 1H, J = 8 Hz); 6.45 (s, 1H); 8.82 (bs, 1H). **^{13}C NMR** ($CDCl_3$, 100 MHz): δ 16.92; 25.47; 27.28; 28.45; 32.70; 39.09; 59.13; 59.16; 60.01; 68.86; 68.87; 101.95; 101.96; 121.29; 143.04; 155.41; 171.91; 175.60.

3-((2-hydroxyethyl)(4'-methyl-2'-pivalamido-[4,5'-bithiazol]-2-yl)amino)cyclohexane-1-carboxylic acid 103l:

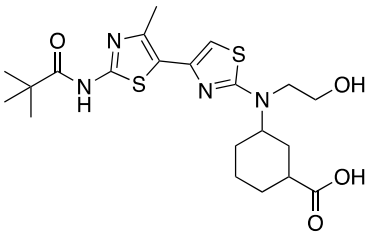

Yield: 89%; **MS** (ESI) $[M+H]^+$: 468.17 m/z; **^{1}H NMR** (DMSO-d_6, 400 MHz): δ 1.23 (s, 9H); 1.56 (m, 4H) 1.79 (m, 6H); 2.46 (s, 3H); 3.63 (t, 2H, J = 8 Hz); 3.73 (t, 2H, J = 8 Hz) 4.80 (m, 1H); 6.70 (s, 1H); 11.70 (s, 1H). **^{13}C NMR** ($CDCl_3$, 100 MHz): δ 15.73; 23.9; 26.98; 28.10; 34.72; 37.29; 39.41; 41.75; 61.37; 63.36; 69.72; 101.63; 120.79; 140.82; 143.00; 158.25; 170.97; 177.38; 180.31.

4-((2-hydroxyethyl)(4'-methyl-2'-pivalamido-[4,5'-bithiazol]-2-yl)amino)cyclohexane-1-carboxylic acid 103m:

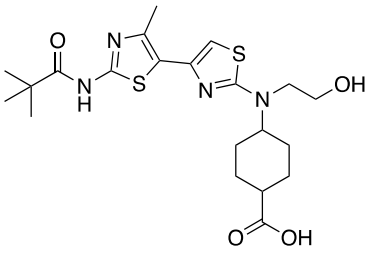

Yield: 33 %; **^{1}H NMR** ($CDCl_3$, 400 MHz): δ 1.34 (s, 9H); 1.59 (m, 2H); 1.84 (m, 4H); 2.05 (m, 1H); 2.38 (m, 2H); 2.49 (s, 3H); 3.44 (m, 1H); 3.63 (t, 2H, J = 8 Hz); 3.83 (q, 2H, J = 8 Hz); 6.44 (s, 1H). **^{13}C NMR** ($CDCl_3$, 100 MHz): δ 15.73; 23.9; 28.10; 28.51; 39.41; 41.75; 60.73; 66.59; 101.63; 120.79; 140.82; 143.00; 158.25; 170.97; 177.38; 180.31.

_N_-(2-(cyclohexyl((1-hydroxycyclopentyl)methyl)amino)-4'-methyl-[4,5'-bithiazol]-2'-yl)pivalamide 103n:

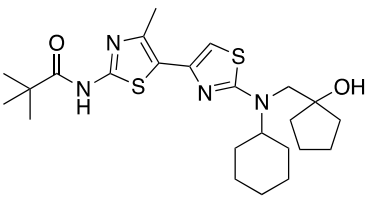

Yield: 15%; **^{1}H NMR** ($CDCl_3$, 400 MHz): δ 0.90 (s, 9H); 1.20-1.27 (m, 6H); 1.57-1.82 (m, 10H); 1.91-1.94 (m, 2H); 2.43-2.50 (m, 1H); 2.71 (s, 2H); 3.01 (s, 3H); 6.45 (s, 1H); 8.87 (bs, 1H). **^{13}C NMR** ($CDCl_3$, 100 MHz): δ 12.2; 23.9; 25.4, 25.7; 28.1; 39.4; 67.0; 67.1; 81.2; 104.8; 117.3; 142.5; 147.9; 155.8; 163.0; 176.9.

***N*-(2-(cyclopentyl((1-hydroxycyclopentyl)methyl)amino)-4'-methyl-[4,5'-bithiazol]-2'-yl)pivalamide 103o:**

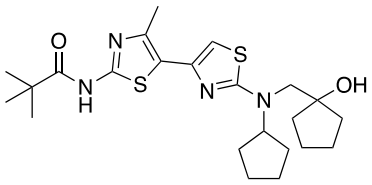

Yield: 21%; **^{1}H NMR:** ($CDCl_3$, 400 MHz): δ 1.33 (s, 9H); 1.59-1.67 (m, 10H); 1.76-1.78 (m, 4H); 2.03-2.12 (m, 2H); 2.51 (s, 3H); 2.71 (s, 2H); 3.94-4.02 (m, 1H); 4.53 (s, 1H); 6.45 (s, 1H); 8.87 (bs, 1H). **^{13}C NMR** ($CDCl_3$, 100 MHz): δ 12.2; 23.9; 24.1; 32.9; 39.7; 66.7; 67.0; 81.2; 104.8; 117.3; 142.5; 147.9; 155.8; 162.9; 176.7.

***N*-(2-(cycloheptyl((1-hydroxycyclopentyl)methyl)amino)-4'-methyl-[4,5'-bithiazol]-2'-yl)pivalamide 105p:**

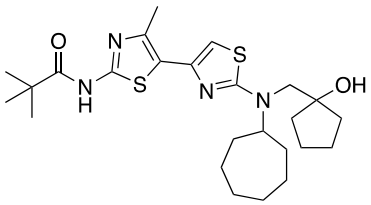

Yield: 13%; **^{1}H NMR:** ($CDCl_3$, 400 MHz): δ 1.22 (s, 9H); 1.56 (m, 14H); 1.66 (m, 4H); 1.90 (m, 7H); 2.11 (m, 2H); 2.75 (s, 3H); 3.01 (s, 2H); 3.13 (m, 1H); 3.85 (m, 1H); 6.97 (s, 1H); **^{13}C NMR** ($CDCl_3$, 100 MHz): δ 12.2; 23.9; 25.7; 28.0; 29.0; 29.7; 39.3; 39.7; 66.5; 67.3; 81.6; 103.8; 117.5; 142.6; 148.0; 156.5; 163.1; 176.9.

Conjugate

General Procedure for the Synthesis of Compound 2-(2-((2-phenoxyethyl)amino)-6-((3-(trifluoromethyl)phenyl)amino)-9*H*-purin-9-yl)ethyl 3-((4'-methyl-2'-pivalamido-[2,5'-bithiazol]-4-yl)amino)benzoate 105:

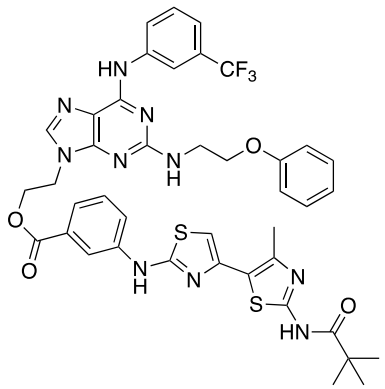

Compound **83,** synthesized according to the procedure reported in Rif. 226, was suspended in THF. $SOCl_2$ was added and the reaction mixture was stirred at r.t. for 30 min until the starting material was consumed. After this time, acyclic nucleoside **46d** was dissolved in THF, and Et_3N was added and afterward, the clear solution was added dropwise to the solution of acylic chloride. The reaction mixture was stirred at reflux for 9 h. The solvent was evaporated, EtOAc was added, and the reaction mixture was washed with NH_4Cl for three times. The organic layer was washed with brine, dried over Na_2SO_4 and dried under vacuum. The product was purified by silice gel chromatography with 98:2 CH_2Cl_2: MeOH and 0.5 % of formic acid as eluent. **Yield**: %; **MS** (ESI) $[M+H]^+$: 857.26 m/z; **^{1}H-NMR** (DMSO-*d*$_6$ 400 MHz): δ 1.24 (s, 9H); 2.52 (s, 3H); 3.70 (t, 2H, J = 8 Hz); 3.75 (t, 2H, J = 8 Hz); 4.12 (m, 4H); 6.95 (m, 5H); 7.27 (t, 3H, J = 8 Hz); 7.47 (m, 3H); 7.54 (dt, 1H, J = 1.4 Hz, J = 8 Hz); 7.88 (s, 1H); 7.99 (m, 1H); 8.24 (s, 1H); 10.51 (s, 1H); 11.76 (s, 1H); 12.91 (s, 1H); **^{13}C-NMR** (DMSO-*d*$_6$ 100 MHz): δ 26.36; 26.60; 28.98; 39.30; 45.38; 54.89; 59.16; 66.06; 103.05; 110.32; 113.74; 114.35; 114.87; 116.01; 117.57; 120.48; 120.72; 122.04; 123.35; 129.86; 129.84; 131.57; 139.32; 140.76; 141.18; 141.72; 142.96; 151.75; 154.19; 158.51; 162.19; 162.99; 164.28; 165.33; 167.22; 168.85; 170.58.

General Procedure for the Synthesis of Compound 1-(cyclohexyl(4'-methyl-2'-pivalamido-[4,5'-bithiazol]-2-yl)amino)-2-methylpropan-2-yl (2-(2-((2-phenoxyethyl)amino)-6-((3-(trifluoromethyl)phenyl)amino)-9*H*-purin-9-yl)ethyl) carbonate 107:

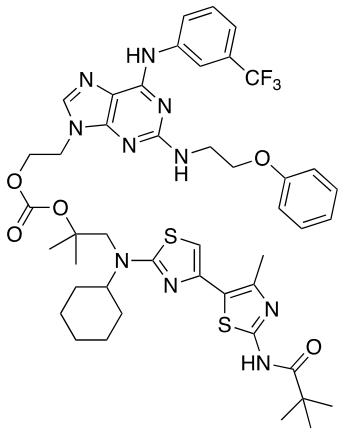

Dry THF was added to compound **46d**. 1,1'-carbonyldiimidazole and catalytic KOH were added, and the reaction mixture was heated at 45 °C with stirring for 4h until the starting material was consumed. Compound **103e** was dissolved in ACN. DBU was added and the reaction mixture was stirred for 1h. The obtained solution was added dropwise to the solution of intermediate imidazole carboxylic. The reaction mixture was stirred at 60 °C overnight. The reaction was cooled, concentrated in vacuo, and dissolved in CH_2Cl_2, and washed with water for three times. The solution was dried over Na_2SO_4 and concentrated under vacuum. The crude was purified by silica gel chromatography with 99:1 CH_2Cl_2:MeOH as eluent. **Yield**: %; **MS** (ESI) $[M+H]^+$: 935.36 m/z; **^{1}H-NMR** (DMSO-d_6 400 MHz): δ 1.16 (s, 6H); 1.24 (s, 9H); 1.82 (d, 5H; J = 8 Hz); 1.98 (q, 4H, J = 12 Hz); 2.46 (s, 3H); 2.57 (d, 2H, J = 8 Hz); 3.41 (s, 3H); 3.65 (s, 2H); 3.71 (m, 2H); 4.15 (m, 2H); 4.35 (t, 1H, J = 8 Hz); 4.42 (m, 1H); 4.48 (t, 2H; J = 8 Hz); 6.73 (s, 1H); 6.93 (m, 4H); 7.27 (m, 3H); 7.48 (m, 1H); 7.92 (s, 1H); 8.36 (bs, 1H); 8.52 (bs, 1H); 9.87 (s, 1H); 11.67 (s, 1H). **^{13}C-NMR** (DMSO-d_6 100 MHz): δ 14.42; 17.34; 25.60; 26.24; 26.86; 28.08; 27.86; 28.54; 29.47; 31.75; 42.17; 55.24; 63.93; 66.52; 71.05; 101.09; 105.60; 111.63; 114.83; 115.42; 115.68; 116.53; 120.92; 123.90; 128.75; 129.92; 139.27; 143.11; 152.24; 153.87; 156.13; 159.00; 159.30; 166.00; 170.47; 176.88.

4.2 Materials and methods of Mixtures analysis

HPLC/UV-MS Method. LC chromatographic analyses were performed by UV/LC-MS with an Agilent 1100 LC/MSD VL system (G1946C) (Agilent Technologies, Palo Alto, CA) equipped with a vacuum solvent degassing unit, a binary high-pressure gradient pump, an 1100 series UV detector, and a 1100 MSD model VL benchtop mass spectrometer. Chromatographic separations were obtained using an analytical Zorbax Eclipse XDB-C18 column (250 x 4.6 mm) (Agilent) with 5 µm particle size and gradient elution with a binary solution; (eluent A: H_2O acidified with formic acid (FA) 0.1% v/v, eluent B: ACN/MeOH 1:1 v/v) at room temperature (0.6 mL/min). The analysis started with 0% of B (from t = 0 to t = 2 min), then B was increased to 98% (from t = 2 to t = 16 min), then kept at 98% (from 16 to 20 min) and finally returned to 0% of eluent A in one minute, injection volume 5 µL. The MSD worked in dual mode and the UV detector operated at 254 nm. The ESI-MS parameters were: capillary voltage 1000 V, drying gas 5 L/min, drying gas temperature 300.0 °C, nebulizing gas 60.0 psi and vaporizing temperature 200°C. Nitrogen was used as nebulizer gas and drying gas.

Stability studies. Stability in DMSO and ACN was conducted for MR-379 at room temperature, protected from light, for more than 30 days analyzing the solutions (1 mg/mL) once a week in the above reported chromatographic condition. The comparison was made by comparing the relative chromatograms obtained at 254 nm.

Chromatographic separation. Fractionation of MR-379 was performed on a Varian ProStar apparatus equipped with two pumps and an UV detector using a semipreparative Zorbax Eclipse XDB-C18 column (250 x 9.4 mm) (Agilent). The mixture was dissolved in ACN/MeOH 1:1 v/v (5 mg/mL) and 200 µL injected each time. The separation was performed by using the same solvents as in the HPLC-UV-MS method at 2 mL/min and a modified gradient: 0% of B for 4 min then % of B was increased to 98% in 25 min, then kept at 98% for 10 min. Four fractions were collected from 0 to 14.8 min, 14.8 - 18.0 min, 18.0 – 21.5 min and 21.5-30.0 min. The collected fractions were dried under nitrogen flow, weighted, and submitted to biological evaluation after a chromatographic control.

Parallel Artificial Membrane Permeability Assay (PAMPA). In order to assess the apparent permeability of various components of the mixture, a stock solution in DMSO of MR-379 was prepared at the final concentration of 1 mM. By diluting the stocks 1:1 v/v with phosphate buffer (PBS 25 mM, pH 7.4), donor solutions were made.

To mimic the gastrointestinal (GI) phospholipidic bilayer, 10 µL of a 1% w/v dodecane solution of phosphatidylcholine (PC) was used to coat filters. The acceptor solution, made of 1:1 v/v

DMSO/PBS, was added to each well (300 µL), while the donor solution (150 µL) was added to each well of the filter plate. The sandwich plates were assembled and incubated for 5 h at room temperature. At the time point, the plates were separated, and the amount of compound passed through the phospholipid bilayer was measured by UV/LC-MS. Finally, apparent permeability (Papp) and membrane retention (MR%) were calculated for the main components.

4.3 ABTS radical assay

ABTS assay was performed according to the protocol reported on reference [240].
The stock solution was prepared by mixing ABTS (2, 2 azobis-(3-ethylbenzothiozoline-6-sulphonic acid), dissolved in water at 7 mm concentration, with 2.45 mM potassium persulphate, and leaving the mixture to stand in the dark at room temperature for 12-16 h before use. The latter solution, appropriately diluted in ethanol (1: 100, v/v), gave an absorbance of 0,70 (+/-0,02) at 734 nm and was used as a control solution. 3,0 ml of the latter control solution was added to 30 µl of the reference compound (ascorbic acid) or selected compounds dissolved in DMSO, at different concentrations (10 µM, 50 µM, 0.1 mM, 0.2 mM, 0.5 mM, 1 mM). The absorbance at 734 nm was read exactly after 10 minutes of incubation time. The scavenging activity has been estimated on the basis of the percentage of ABTS radicals scavenged by the following formula:

$\%scavenging = [(A_0 - A_s)/A_0] \times 100$

where A_0 is the absorption of the control solution (performed in each test), A_S is the absorption in the presence of the reference compound or tested compounds

4.4 Materials and methods of Electrochemistry-MS

Apparatus and analysis conditions. The electrochemical (EC) experiments were performed with the use of a ROXY™ system (Antec, Zoeterwoude, The Netherlands). This instrument consisted of a potentiostat, an electrochemical reaction cell and an infusion pump. The Dialog Elite software was used for control and data collection. The electrochemical cell consisted of a three-electrode arrangement including a working electrode (glassy carbon), counter electrode, and reference electrode (HyREF). The reaction cell of Roxy system had volume of 500 µl and was connected directly with a mass Bruker Esquire 6000 spectrometer(Bruker Daltonics, Billerica, MA).

Electrochemical and mass spectrometric conditions. For the simulation of phase I metabolism, the Roxy EC system was used connected to an ESI-MS instrument. Samples were dissolved in 5mM CH_3COONH_4 or CH_3COOH containing 50% acetonitrile and infused with a syringe pump at a flow

rate of 10 µl/min. The reaction chamber was kept at a constant temperature of 30 °C. The mass voltammograms were obtained by linear increasing of the working electrode potential from 0 to 2000 mV at the rate of 10 mV/s. It was observed that for each of the test compounds the maximum peak area was obtained for a working electrode potential of 1500 mV. Full-scan mass spectra were recorded within the mass range of *m*/*z* 100–1000. The following operation parameters of MS/MS were applied: gas flow rate 5.0 L min^{-1}; nebulizer gas pressure 10 psi. The capillary voltage of 4500 V and drying gas temperature 300 °C were applied

EC-ESI-MS data of the reference compound (adenosine) and tested samples were compared in order to determine the possible metabolites produced in electrochemical cell.

Sample preparation. The nucleoside solutions were prepared through dissolving stock solutions with the use of various solvents in order to optimize EC-ESI-MS conditions. Stock solutions were prepared for each compound: 1mg/1mL of 50% ACN or MeOH in H_2O. These were then diluted: 10 µL of stock solution + 495 µL of selected solvents (ACN or MeOH) + 495 µL of 5mM ammonium acetate (AA) or 5 mM acetic acid (CH_3COOH). Different conditions were used to investigate the behavior of selected compounds at different pH. The mixture was vortexed at 1200 rpm. Next the syringe pump was filled, and the sample was injected into EC–MS system.

5. ACKNOWLEDGEMENTS

I would like to thank the whole research group for the great time we spent together in the lab, for all the scientific and non-scientific talks and for having shared with me concerns, results and successes about our work.

For analytical analysis: Prof. Elena Dreassi and Dr. Enrico Rango from Dipartimento di Biotecnologie Mediche, Università degli Studi di Siena;

For antiviral assays: Prof. Maurizio Zazzi and Dr. Ilaria Vinceti from Dipartimento di Biotecnologie Mediche, Università degli Studi di Siena, and Prof. Lucia Nencioni from Department of Public Health and Infectious Diseases, Laboratory Affiliated to Istituto Pasteur Italia-Fondazione Cenci Bolognetti, Sapienza University of Rome, and Dr. Valeria Cagno from Laboratory of Antiviral Research Institut de Microbiologie, Lausanne, Switzerland;

For antibacterial assays: Prof. Jean-Denis Docquier from Dipartimento di Biotecnologie Mediche, Università degli Studi di Siena;

For enzymatic assays: Dr. Emmanuele Crespan and Dr. Giovanni Maga, from Istituto di Genetica Molecolare, IGM-CNR, Pavia, and Prof. Enzo Tramontano and Prof. Angela Corona from the University of Cagliari.

I am grateful to Prof. Jef Rozenski and Prof. Elisabetta Groaz for having given me the possibility to carry out a research period at the Rega Institute for Medical Research, Leuven, Belgium.

Finally, I would like to give my special thanks to my supervisor Prof. Marco Radi for his guidance during my PhD project.

6. REFERENCES

[1] Abebe G.M.,Emerging and Re-Emerging Viral Diseases: The Case of Coronavirus Disease-19 (COVID-19). *Int J Virol AIDS* ***2020****, 7, 067.*

[2] Meganck R. M. & Baric R. S., Developing therapeutic approaches for twenty-first-century emerging infectious viral diseases, *Nature Medicine* ***2021****, 27, 401–410.*

[3] Pierson T.C. & Diamond M.S., The continued threat of emerging flaviviruses, *Nature Microbiology* ***2020*** *5, 796–812.*

[4] Debing Y., Neyts J., Delang L., The future of antivirals: broad-spectrum inhibitors, *Current Opinion in Infection Diseases* ***2015****, 28 (6), 596-602.*

[5] Vigant F., Santos N.C., Lee B., Broad-spectrum antivirals against viral fusion, *Nat. Rev Microbiol.* ***2015****, 13(7), 426–37.*

[6] Modjarrad, K.; Vermund, S. H., Effect of Treating Co-Infections on HIV-1 Viral Load: A Systematic Review. *Lancet Infect. Dis.* **2010**, *10 (7), 455–463.*

[7] Sidwell, R. W.; Huffman, J. H.; Khare, G. P.; Allen, L. B.; Witkowski, J. T. Robins, R. K., Broad-Spectrum Antiviral Activity of Virazole: 1-β-D-Ribofuranosyl-1,2,4-triazole-3-carboxamide, *Science* ***1972****, 177 (4050), 705-706.*

[8] Graci, J. D.; Cameron, C. E., Mechanisms of Action of Ribavirin against Distinct Viruses. Rev, *Med. Virol.* ***2006****, 16 (1), 37–48.*

[9] Parker W. B., Metabolism and Antiviral Activity of Ribavirin, *Virus Res.* ***2005****, 107 (2), 165–171.*

[10] Andersen P.I., Ianevski A., Lysvand H., Vitkauskiene A., Oksenych V., Bjørås M., Telling K., Lutsar I., Dumpis U., Irie Y., Tenson T., Kantele A., Kainov D.E., Discovery and development of safe-in-man broad-spectrum antiviral agents, *Int. J. Infect. Dis.* **2020**, 9, 268–276.

[11] Rosenke K., Feldmann H., Westover J.B, Hanley P. W., Martellaro C., Feldmann F., Saturday G., Lovaglio J., Scott D. P., Furuta Y., Komeno T., Gowen B.B. and Safronetz D., Use of Favipiravir to Treat Lassa Virus Infection in Macaques, *Emerging Infectious Diseases* ***2018****, 24(9), 1696-1699.*

[12] Raabe V.N., Kann G., Ribner B.S., Morales A., Varkey J.B., Mehta A.K., Lyon G.M., Vanairsdale S., Faber K., Becker S., Eickmann M., Strecker T., Brown S., Patel K., De Leuw P., Schuettfort G., Stephan C., Rabenau H., Klena J.D., Rollin P.E., McElroy A., Ströher U., Nichol S., Kraft C.S., Wolf T., Favipiravir and Ribavirin Treatment of Epidemiologically Linked Cases of Lassa Fever. *Clin Infect Dis.* ***2017****, 65(5), 855-859.*

[13] Safrin S., Cherrington J., Jaffe H.F., *Rev Med Virol.* ***1997****, 7, 145–156.*

[14]Dunning J., Kennedy S.B., Antierens A., Whitehead J., Ciglenecki I., Carson G., Kanapathipillai R., Castle L., Howell-Jones R., Pardinaz-Solis R., Grove J., Scott J., Lang T., Olliaro P., Horby P.W., Experimental Treatment of Ebola Virus Disease with Brincidofovir., *PLoS One.* ***2016****, 11(9):e0162199.*

[15] Toth K., Ying B., Tollefson A. E., Spencer J. F., Balakrishnan L., Sagartz J. E., Wold, W. S., Valganciclovir inhibits human adenovirus replication and pathology in permissive immunosuppressed female and male Syrian hamsters, *Viruses* ***2015****, 7(3), 1409-1428.*

[16] Agostini M.L., Andres E.L., Sims A.C., Graham R.L., Sheahan T.P., Lu X., Smith E.C., Case J.B., Feng J.Y., Jordan R., Ray A.S., Cihlar T., Siegel D., Mackman R.L., Clarke M.O., Baric R.S., Denison M.R., Coronavirus Susceptibility to the Antiviral Remdesivir (GS-5734) Is Mediated by the Viral Polymerase and the Proofreading Exoribonuclease, *mBio.* ***2018****, 9(2):e00221-18.*

[17] De Clercq E., Clinical potential of the acyclic nucleoside phosphonates cidofovir, adefovir, and tenofovir in treatment of DNA virus and retrovirus infections, *Clinical microbiology reviews* ***2003****, 16(4), 569-596.*

[18] Chu C.M., Cheng V.C., Hung I.F., Wong M.M., Chan K.H., Chan K.S., Kao R.Y., Poon L.L., Wong C.L., Guan Y., Peiris J.S., Yuen K.Y., Role of lopinavir/ritonavir in the treatment of SARS: initial virological and clinical findings. *Thorax.* ***2004****, 59(3), 252-256.*

[19] Rossignol J.F., Nitazoxanide: a first-in-class broad-spectrum antiviral agent, *Antiviral Res.* ***2014****, 110, 94-103.*

[20] Zheng W., Thorne N., McKew J.C., Phenotypic screens as a renewed approach for drug discovery. *Drug Discov Today* ***2013****, 18(21-22), 1067-1073.*

[21] Swinney D.C. & Anthony J., How were new medicines discovered?, *Nat. Rev. Drug Discov.* ***2011****, 10, 507–519*

[22] Sams-Dodd F., Is poor research the cause of the declining productivity of the pharmaceutical industry? An industry in need of a paradigm shift, *Drug Discov Today* ***2013****, 18(5-6), 211-217.*

[23] Sams-Dodd F., Target-based drug discovery: is something wrong?, *Drug Discov Today* ***2005****, 10(2), 139-147.*

[24] Hopkins A.L., Network pharmacology: the next paradigm in drug discovery, *Nat Chem Biol.* ***2008****, 4(11), 682-690.*

[25] Butcher E.C., Can cell systems biology rescue drug discovery? *Nat Rev Drug Discov.* ***2005****, 4(6), 461-467.*

[26] Swinney D.C., Phenotypic vs. target-based drug discovery for first-in-class medicines, Clin Pharmacol Ther. **2013**, 93(4), 299-301.

[27] Lee J.A., Uhlik M.T., Moxham C.M., Tomandl D., Sall D.J., Modern phenotypic drug discovery is a viable, neoclassic pharma strategy, *J Med Chem.* ***2012****, 55(10), 4527-4538.*

[28] Koonin E.V., Dolja V.V., Krupovic M. Origins and evolution of viruses of eukaryotes: The ultimate modularity. *Virology* ***2015****, 479-480, 2-25.*

[29] *Kitadai N. Shigenori M.,* Origins of building blocks of life: A review, *Geoscience Frontiers* ***2018****, 9, 1117.*

[30] Chaudhuri S., Symons J.A., Deval J., Innovation and trends in the development and approval of antiviral medicines: 1987-2017 and beyond, *Antiviral Res* ***2018****, 155, 76–88.*

[31] Chitalia V.C., Munawar A.H., A painful lesson from the COVID-19 pandemic: the need for broad-spectrum, host-directed antivirals. *J Transl Med* ***2020****, 18(1), 1–6.*

[32] Locarnini S., Bowden S., Drug resistance in antiviral therapy, *Clin Liver Dis* ***2010****, 14, 439–459.*

[33] Kumar N., Sharma S., Kumar R., Tripathi B.N., Barua S., Ly H., Rouse B.T., Host-Directed Antiviral Therapy, *Clin Microbiol Rev.* ***2020***, 33(3):e00168-19.

[34] Field H.J., Herpes simplex virus antiviral drug resistance--current trends and future prospects. *J Clin Virol.* ***2001****, 21(3), 261-269.*

[35] Pillay D., Zambon M., Antiviral drug resistance. *BMJ.* ***1998****, 317(7159), 660-662.*

[36] Bartholomeusz A., Locarnini S.A., Antiviral drug resistance: clinical consequences and molecular aspects. *Semin Liver Dis.* ***2006****, 26(2), 162-170.*

[37] Witkowski J.T., Robins R.K., Sidwell R.W., Simon L.N., Design, synthesis, and broad spectrum antiviral activity of 1--D-ribofuranosyl-1,2,4-triazole-3-carboxamide and related nucleosides, *J Med Chem.* ***1972****, 15(11), 1150-1154.*

[38] Gebre M., Nomburg J.L., Gewurz B.E., CRISPR-Cas9 genetic analysis of virus-host interactions, *Viruses* ***2018****, 10, 55.*

[39] Puschnik A.S., Majzoub K., Ooi Y.S., Carette J.E., A CRISPR toolbox to study virus-host interactions, *Nat Rev Microbiol* ***2017****, 15, 351–364.*

[40] Lazcano A. & Forterre P. The molecular search for the last common ancestor, *J. Mol. Evol.* ***1999****, 49, 411–412.*

[41] Koonin E.V., Comparative genomics, minimal gene-sets and the last universal common ancestor. *Nat Rev Microbiol.* ***2003****, 1(2), 127-36.*

[42] Fournier G.P., Andam C.P., Gogarten J.P., Ancient horizontal gene transfer and the last common ancestors, *BMC Evol Biol.* ***2015****, 15, 70.*

[43]Ouzounis C.A., Kunin V., Darzentas N., Goldovsky L., A minimal estimate for the gene content of the last universal common ancestor-exobiology from a terrestrial perspective, *Res Microbiol.* ***2006****, 157(1), 57-68.*

[44] Martina M.G., Giannessi L., Radi M., Multicomponent Synthesis of Purines and Pyrimidines: From the Origin of Life to New Sustainable Approaches for Drug-Discovery Applications, *Eur. J. Org. Chem.* ***2023****, 26, e202201288.*

[45] Kendall E. C. and B. F. McKenzie, dl-ALANINE, *Org. Synth.* ***1929****, 9, 4.*

[46] Clarke H. T. and Bean H. J., α-AMINOISOBUTYRIC ACID, *Org, Synth.* ***1931****, 11, 4.*

[47] C. N. Mattews, *Cellular Origin and Life in Extreme Habitats and Astrobiology*, **2004**, 121–135.

[48] Pino, S.; Sponer, J.E.; Costanzo, G.; Saladino, R.; Mauro, E.D. From Formamide to RNA, the Path Is Tenuous but Continuous. Life **2015**, 5, 372-384.

[49] Saladino R., Crestini C., Ciciriello F., Costanzo G., Di Mauro E., Formamide chemistry and the origin of informational polymers. *Chem Biodivers.* ***2007****, 4(4), 694-720.*

[50] Saladino R., Botta G., Pino S., Costanzo G., Di Mauro E., Genetics first or metabolism first? The formamide clue, *Chem Soc Rev.* ***2012****, 41(16), 5526-5565.*

[51] Saladino R., Botta G., Pino S., Costanzo G. & Di Mauro E., From the one-carbon amide formamide to RNA all the steps are prebiotically possible, Biochimie **2012,** 94,1451–1456.

[52] Saladino R., Barontini M., Cossetti C., Di Mauro E. & Crestini C. The effects of borate minerals on the synthesis of nucleic acid bases, amino acids and biogenic carboxylic acids from formamide, *Orig. Life Evol. Biosph.* **2011**, 41, 317-330.

[53] Cossetti C., Crestini C., Saladino R. & di Mauro E., Borate minerals and RNA stability, Polymers (Basel) **2010**, 2, 211–228.

[54] Deamer, D. W. The molecular origins of life (ed. A. Brack), **1998**, pp. 189–205. Cambridge, UK: Cambridge University Press.

[55] Fiore M., Strazewski P., Prebiotic Lipidic Amphiphiles and Condensing Agents on the Early Earth. *Life*. **2016**, 6(2), 17.

[56] Deamer D. W., Role of amphiphilic compounds in the evolution of membrane structure on the early Earth. Origins of Life and Evolution of the Biosphere **1986**, 17(1), 3-25.

[57] Georgiou D.C., Deamer D.W. Lipids as universal biomarkers of extraterrestrial Life. *Astrobiology* **2014**, *14*, 541–549.

[58] Segré D., Ben-Eli D.; Deamer D.W.; Lancet, D. The lipid world. *Orig. Life Evol. Biosph.* **2001**, *31*, 119–145.

[59] Lombard J., López García P.; Moreira D. The early evolution of lipid membranes and the three domains of Life, *Nat. Rev. Microbiol.* **2012**, *10*, 507–515.

[60] Oró, J., Chemical synthesis of lipids and the origin of life. *J. Biol. Phys.* **1994**, *20*, 135–147.

[61] Deamer D.W., Role of amphiphilic compounds in the evolution of membrane structure on early Earth. *Orig. Life* ***1986****, 17, 3–25.*

[62] Ruiz-Mirazo K., Briones C., de la Escosura A., Prebiotic systems chemistry: new perspectives for the origins of life. *Chem Rev.* ***2014****, 114(1), 285-366.*

[63]Cui S., The possible roles of water in the prebiotic chemical evolution of DNA, *Phys Chem Chem Phys* ***2010****, 12(35), 10147-10153.*

[64] Saa J.M., Frontera A., On the Role of Water as a Catalyst in Prebiotic Chemistry, *Chemphyschem.* ***2020****, 21(4), 313-320.*

[65] Vincetti P., Costantino G., Martina M.G., and Radi M., Probing the Reactivity of 2,4-Dichlorofuro[3,4-d]pyrimidin-7-one: A Versatile and Underexploited Scaffold to Generate Substituted or Fused Pyrimidine Derivatives, *Synlett* **2019**, 30, 2010- 2014.

[66] Russo R., Corasaniti M.T., Bagetta G., Morrone L.A., Exploitation of Cytotoxicity of Some Essential Oils for Translation in Cancer Therapy, *Evidence-Based Complementary and Alternative Medicine,* ***2015****, 2015, 1-9.*

[67] Governa P., Manetti F., Miraldi E., & Biagi M. Effects of in vitro simulated digestion on the antioxidant activity of different Camellia sinensis (L.) Kuntze leaves extracts. *European Food Research and Technology,* ***2022****, 248(1), 119-128.*

[68] Thursky K.A., Worth L.J. Can mortality of cancer patients with fever and neutropenia be improved?, *Curr Opin Infect Dis.* ***2015****, 28(6), 505-513.*

[69] RSC Drug Discovery Series, RSC Publ, Cambridge 2012.

[70] Bizzarri M., Giuliani A., Monti N.,Verna R., Pensotti A., & Cucina A., Rediscovery of natural compounds acting via multitarget recognition and noncanonical pharmacodynamical actions. *Drug Discovery Today,* ***2020*** *25(5), 920-927.*

[71] Bbosa N., Kaleebu P., Ssemwanga D. HIV subtype diversity worldwide., *Curr Opin HIV AIDS* ***2019****, 14(3), 153-160.*

[72] Vincetti P., Caporuscio F., Kaptein S., Gioiello A., Mancino V., Suzuki Y., Yamamoto N., Crespan E., Lossani A, Maga G., Rastelli G., Castagnolo D., Neyts J., Leyssen P., Costantino G., Radi M. Discovery of Multitarget Antivirals Acting on Both the Dengue Virus NS5-NS3 Interaction and the Host Src/Fyn Kinases. *J Med Chem.* ***2015****, 58(12), 4964-4975.*

[73] Kaptein S.J.F., Vincetti P., Crespan E., Rivera J.I.A., Costantino G., Maga G., Neyts J., Radi M, Identification of Broad-Spectrum Dengue/Zika Virus Replication Inhibitors by Functionalization of Quinoline and 2,6-Diaminopurine Scaffolds, *ChemMedChem.* ***2018****, 13(14), 1371-1376.*

[74] Park J., Avila-Perez G., Nogales A., Blanco-Lobo P., de la Torre J., Martínez-Sobrido L., Identification and characterization of novel compounds with broad spectrum antiviral activity against influenza A and B viruses, *J. Virol.* ***2020****, 94, e02149-19.*

[75] Wang M., Cao R., Zhang L., Yang X., Liu J., Xu M., Shi Z., Hu Z., Zhong W., Xiao G., Remdesivir and chloroquine effectively inhibit the recently emerged novel coronavirus (2019-NCoV) in vitro, *Cell Res.* ***2020****, 30, 269-271.*

[76] Duarte L.F.B., Oliveira R.L., Rodrigues K.C., Voss G.T., Godoi B., Schumacher R.F., Perin G., Wilhelm E.A., Luchese C., Alves D., Organoselenium compounds from purines: synthesis of 6-arylselanylpurines with antioxidant and anticholinesterase activities and memory improvement effect, *Bioorg. Med. Chem.* ***2017****, 25, 6718-6723.*

[77] Brathe A., Andresen G., Gundersen L.-L., Malterud K.E., Rise F., Antioxidant activity of synthetic cytokinin analogues: 6-alkynyl- and 6-alkenylpurines as novel 15-lipoxygenase inhibitors, *Bioorg. Med. Chem.* ***2002****, 10, 1581-1586.*

[78] Djuidje E.N., Dissette V., Bino B., Benetti S., Balzarini J., Liekens S., Manfredini S., Vertuani S., Baldisserotto A., A multitarget approach toward the development of 8- substituted purines for photoprotection and prevention of UV-related damage, *ChemMedChem* ***2017****, 12, 760-769.*

[79] Vicenti I., Dragoni F., Giannini A., Giammarino F., Spinicci M., Saladini F., Boccuto A., Zazzi M., Development of a cell-based immunodetection assay for simultaneous screening of antiviral compounds inhibiting Zika and dengue virus replication, *SLAS Discov.*, ***2020****, 25, 506-514.*

[80] Puertas M.C., Buzon M.J., Ballestero M., Van Den Eede P., Clotet B., Prado J.G., Martinez-Picado J., Novel two-round phenotypic assay for protease inhibitor susceptibility testing of recombinant and primary HIV-1 isolates, *J. Clin. Microbiol.* ***2012****, 50, 3909-3916.*

[81] F. Saladini, A. Giannini, A. Boccuto, I. Vicenti, M. Zazzi, Agreement between an in-house replication competent and a reference replication defective recombinant virus assay for measuring phenotypic resistance to HIV-1 protease, reverse Transcriptase, and integrase inhibitors, *J. Clin. Lab. Anal.* **2017**, 32, e22206.

[82] Park J., Ávila-Pérez G., Nogales A., Blanco-Lobo P., de la Torre J., Martínez-Sobrido L., Identification and Characterization Of Novel Compounds With Broad-Spectrum Antiviral Activity Against Influenza A and B Viruses, *J. Virol.* ***2020****, 94, e02149-19.*

[83] Park J. G., Ávila-Pérez G., Nogales A., Blanco-Lobo P., de la Torre J. C., & Martínez-Sobrido L. Identification and characterization of novel compounds with broad-spectrum antiviral activity against influenza A and B viruses. *Journal of Virology* ***2020****, 94(7), e02149-19.*

[84] Wang M., Cao R., Zhang L., Yang X., Liu J., Xu M., Shi Z., Hu Z., Zhong W., Xiao G., Remdesivir and Chloroquine Effectively Inhibit the Recently Emerged Novel Coronavirus (2019-NCoV) in Vitro. *Cell Res.* **2020**, *30*, 269–271.

[85] Pruijssers A., George A., Schafer A., Leist S., Gralinksi L., Dinnon K., Yount B., Agostini M., Stevens L., Chappell J., Lu X., Hughes T., Gully K., Martinez D., Brown A., Graham R., Perry J., Du Pont V., Pitts J., Ma B., Babusis D., Murakami E., Feng J., Bilello J., Porter D., Cihlar T., Baric R., Denison M., Sheahan T., Remdesivir inhibits SARS-CoV-2 in human lung cells and chimeric SARS-CoV expressing the SARS-CoV-2 RNA polymerase in mice, *Cell Rep*. ***2020****, 32, 107940.*

[86] De Meyer S., Bojkova D., Cinatl J., Van Damme E., Buyck C., Van Loock M., Woodfall B., Ciesek S., Lack of antiviral activity of darunavir against SARS-CoV-2, *Int. J. Infect. Dis.* ***2020****, 97, 7-10*.

[87] Choy K., Wong A., Kaewpreedee P., Sia S., Chen D., Hui K., Chu D., Chan M., Cheung P., Huang X., Peiris M., Yen H., Remdesivir, lopinavir, emetine, and homoharringtonine inhibit SARS-CoV-2 replication in vitro, *Antivir. Res. 2020, 178, 104786.*

[88] Dubankova A., Boura, E., Structure of the Yellow Fever NS5 Protein Reveals Conserved Drug Targets Shared among Flaviviruses. *Antiviral Res.* **2019**, *169*, 104536.

[89] Wu J., Liu W., Gong P., A Structural Overview of RNA-Dependent RNA Polymerases from the Flaviviridae Family. *Int. J. Mol. Sci.* **2015**, *16*, 12943–12957.

[90] Zou G., Chen Y.-L., Dong H., Lim C. C., Yap L. J., Yau Y. H., Shochat S. G., Lescar J., Shi P.-Y., Functional Analysis of Two Cavities in Flavivirus NS5 Polymerase. *J. Biol. Chem.* **2011**, *286*, 14362-14372.

[91] Tay M. Y. F., Vasudevan S. G., The Transactions of NS3 and NS5 in Flaviviral RNA Replication. *Adv. Exp. Med. Biol.* **2018**, *1062*, 147–163.

[92] Wu J., Liu W., Gong P., A structural overview of RNA-dependent RNA polymerases from the flaviviridae family, *Int. J. Mol. Sci.* ***2015****, 16, 12943-12957.*

[93] Sarto C., Kaufman S. B., Estrin D. A., Arrar M., Nucleotide-Dependent Dynamics of the Dengue NS3 Helicase. *Biochim. Biophys. Acta Proteins Proteom.* **2020**, *1868*, 140441.

[94] Wu J., Bera A. K., Kuhn R. J., Smith J. L., Structure of the Flavivirus Helicase: Implications for Catalytic Activity, Protein Interactions, and Proteolytic Processing. *J. Virol.* **2005**, *79*, 10268–10277.

[95] Saw W. G., Pan A., Subramanian Manimekalai M. S., Grüber A., Grüber G., Structure and Flexibility of Non-Structural Proteins 3 and -5 of Dengue- and Zika Viruses in Solution. *Progress Biophys. Mol. Bio.* **2019**, *143*, 67–77.

[96] Tay M. Y. F., Saw W. G., Zhao Y., Chan K. W. K., Singh D., Chong Y., Forwood J. K., Ooi E. E., Grüber G., Lescar J., Luo D., Vasudevan S. G., The C-Terminal 50 Amino Acid Residues of Dengue NS3 Protein Are Important for NS3-NS5 Interaction and Viral Replication. *J. Biol. Chem.* **2015**, *290*, 2379–2394.

[97] Selisko B., Peyrane F. F., Canard B., Alvarez K., Decroly E., Biochemical Characterization of the (Nucleoside-2'O)-Methyltransferase Activity of Dengue Virus Protein NS5 Using Purified Capped RNA Oligonucleotides 7MeGpppACn and GpppACn. *J. Gen. Virol.* ***2010****, 91 (1), 112–121.*

[98] Coutard B., Barral K., Lichière J., Selisko B., Martin B., Aouadi W., Lombardia M. O., Debart F., Vasseur J.-J., Guillemot J. C., Canard B., Decroly E., Zika Virus Methyltransferase: Structure and Functions for Drug Design Perspectives. *J. Virol*. **2017**, *91* (5), e02202-16, e02202-16.

[99] Meineke R., Rimmelzwaan G., Elbahesh H., Influenza Virus Infections and Cellular Kinases. *Viruses* **2019**, *11* (2), *171.*

[100] Weisberg E., Parent A., Yang P. L., Sattler M., Liu Q., Liu Q., Wang J., Meng C., Buhrlage S. J., Gray N., Griffin J. D., Repurposing of Kinase Inhibitors for Treatment of COVID-19. *Pharm. Res.* **2020**, *37* (9), 167.

[101] Huang H., Ma J., Shi J., Meng L., Jiang H., Ding J., Liu H., Discovery of novel purine derivatives with potent and selective inhibitory activity against c-src tyrosine kinase. *Bioorg. Med. Chem.* **2010**, *18, 4615−4624.*

[102] Jordheim L.P., Durantel D., Zoulim F., Dumontet C. Advances in the development of nucleoside and nucleotide analogues for cancer and viral diseases. *Nat Rev Drug Discov.* ***2013****, 12(6), 447-464.*

[103] Benhamou Y., Tubiana R., & Thibault V., Tenofovir disoproxil fumarate in patients with HIV and lamivudine-resistant hepatitis B virus. *New England Journal of Medicine* ***2003****, 348(2), 177-178.*

[104] Ray A. S., Fordyce M. W., & Hitchcock M. J., Tenofovir alafenamide: a novel prodrug of tenofovir for the treatment of human immunodeficiency virus. *Antiviral research* ***2016****, 125, 63-70.*

[105] Yu-Shan H., Sui-Yuan C., Wang-Huei S., Hsin-Yun S., Kuan-Yeh L., Yu-Chung C., Yi-Ching S., Wen-Chun L., Chien-Ching H, Shan-Chwen C., Virological Response to Tenofovir Disoproxil Fumarate in HIV-Positive Patients with Lamivudine-Resistant Hepatitis B Virus Coinfection in an Area Hyperendemic for Hepatitis B Virus Infection, PlosOne **2016**, 11(12): e0169228.

[106]Lam Y.F., Seto W.K., Wong D., Cheung K.S., Fung J., Mak L.Y., Yuen J., Chong C.K., Lai C.L., Yuen M.F., Seven-Year Treatment Outcome of Entecavir in a Real-World Cohort: Effects on Clinical Parameters, HBsAg and HBcrAg Levels. *Clin Transl Gastroenterol.* ***2017****, 8(10), e125.*

[107]Stedman, C., Sofosbuvir, a NS5B polymerase inhibitor in the treatment of hepatitis C: a review of its clinical potential. *Therapeutic advances in gastroenterology* ***2014****, 3, 131-140.*

[108]Clercq E.D., & Holý,A., Acyclic nucleoside phosphonates: a key class of antiviral drugs. Nature Reviews Drug Discovery **2005**, 4(11), 928-940.

[109]Cano-Soldado P., & Pastor-Anglada M., Transporters that translocate nucleosides and structural similar drugs: structural requirements for substrate recognition. *Medicinal research reviews* ***2012****, 32(2), 428-457.*

[110] Milisavljevic N., Konkolová E., Kozák J., Hodek J., Veselovská L., Sýkorová V., Čížek K., Pohl R., Eyer L., Svoboda P., Růžek D., Weber J., Nencka R., Bouřa E., and Hocek M., Antiviral Activity of 7-Substituted 7-Deazapurine Ribonucleosides, Monophosphate Prodrugs, and Triphoshates against Emerging RNA Viruses *ACS Infect. Dis.* ***2021****, 7, 471−478.*

[111] Najjar A., Karaman R., Successes, failures, and future prospects of prodrugs and their clinical impact. Expert Opin Drug Discov. **2019**, 14(3), 199-220.

[112] Mehellou Y., & De Clercq E., Twenty-six years of anti-HIV drug discovery: where do we stand and where do we go?, *Journal of medicinal chemistry* ***2010****, 53(2), 521-538.*

[113] De Clercq E., Strategies in the design of antiviral drugs. Nature Reviews drug discovery **2002,** 1(1), 13-25.

[114]De Clercq E., A 40-year journey in search of selective antiviral chemotherapy. *Annual review of pharmacology and toxicology **2011**, 51(1), 1-24.*

[115]Murphy E. L., Collier A. C., Kalish L. A., Assmann S. F., Para M. F., Flanigan T. P., Kumar P. N., Mintz L., Wallach F. R., Nemo G. J., Highly active antiretroviral therapy decreases mortality and morbidity in patients with advanced HIV disease. *Annals of internal medicine **2001**, 135(1), 17-26.*

[116] De Clercq E., & Li G. Approved antiviral drugs over the past 50 years. *Clinical microbiology reviews **2016**, 29(3), 695-747.*

[117] Margolis D. M., Mukherjee A. L., Fletcher C. V., Hogg E., Ogata-Arakaki D., Petersen T., Rusin D., Martinez A., W. Mellors J., AIDS **2007**, 21, 2025–2032.

[118] Gripshover B. M., Ribaudo H., Santana J., Gerber J. G., Campbell T. B., Hoggs E., Jarocki B., Hammer S. M., Kuritzkes D. R., *Antiviral Ther. **2006**, 11, 619–623.*

[119] Homsi J., Garrett C. R., Hepatic arterial infusion of chemotherapy for hepatic metastases from colorectal cancer, *Cancer Control **2006**, 13, 42-47.*

[120] Carroll S. S., Ludmerer S., Handt L., Koeplinger K., Zhang N. Y. R., Graham D., Davies M. E., MacCoss M., Hazuda D., Olsen D. B., *Antimicrob. Agents Chemother. **2009**, 53, 926–934.*

[121] Watanabe K. A., Su T. L., Klein R. S., Chu C. K., Matsuda A., Chun M. W., Lopez C., Fox J. J., J. *Med. Chem. **1983**, 26, 152–156.*

[122] Bzowska A., Kulikowska E., & Shugar D., Purine nucleoside phosphorylases: properties, functions, and clinical aspects, *Pharmacology & therapeutics **2000**, 88(3), 349-425.*

[123] Kifli N., De Clercq E., Balzarini J., & Simons C. Novel imidazo [1, 2-c] pyrimidine base-modified nucleosides: synthesis and antiviral evaluation. *Bioorganic & medicinal chemistry **2004**, 12(15), 4245-4252.*

[124] Herdewijn, P., Modified nucleosides: in biochemistry, biotechnology and medicine. *John Wiley & Sons, (Ed.) (**2008**).*

[125] Amblard F., Fromentin E., Detorio M., Obikhod A., Rapp K. L., McBrayer T. R., Whitaker T., Coats S.J., Schinazi R.F. Synthesis, antiviral activity, and stability of nucleoside analogs containing tricyclic bases. *European journal of medicinal chemistry **2009**, 44(10), 3845-3851.*

[126] Xia Y., Qu F., Peng L., Triazole nucleoside derivatives bearing aryl functionalities on the nucleobases show antiviral and anticancer activity. *Mini Rev Med Chem. **2010**, 10(9), 806-821*.

[127] Meneghesso S., Vanderlinden E., Stevaert A., McGuigan C., Balzarini J., Naesens L., Synthesis and biological evaluation of pyrimidine nucleoside monophosphate prodrugs targeted against influenza virus. *Antiviral Res. **2012,** 94(1), 35-43.*

[128]Seneviratne U., Wickramaratne S., Kotandeniya D., Groehler A. S., Geraghty R. J., Dreis, C., Pujari S.S., Tretyakova, N. Y., Synthesis and biological evaluation of pyrrolidine-functionalized nucleoside analogs. Medicinal Chemistry Research **2021**, 30(2), 483-499.

[129] Focher F., Spadari S., & Maga G., Antivirals at the mirror: the lack of stereospecificity of some viral and human enzymes offers novel opportunities in antiviral drug development. *Current Drug Targets-Infectious Disorders **2003**, 3(1), 41-53.*

[130] Mathé C.,Gosselin G., L-nucleoside enantiomers as antivirals drugs: a mini-review. *Chemother. Antiviral Chem. **2000,** 11, 165-190.*

[131] Collect. Czech. Chem. Commun., 29(**1964**), pp. 2809-2813.

[132] Int. Antiviral News, 3 (**1995**), pp. 74-77.

[133] Nair V., Jahnke T. S. Antiviral activities of isometric dideoxynucleosides of D-and L-related stereochemistry. *Antimicrobial agents and chemotherapy **1995**, 39(5), 1017-1029.*

[134] Gumina G., Chong Y., Choo H., Song G. Y., & Chu, C. K., L-Nucleosides: antiviral activity and molecular mechanism. *Current topics in medicinal chemistry **2002**, 2(10), 1065-1086.*

[135] Wang P., Hong J. H., Cooperwood J. S., & Chu C. K., Recent advances in L-nucleosides: chemistry and biology. *Antiviral research **1998**, 40(1-2), 19-44.*

[136] Gumina G., Song G. Y., & Chu C. K. L-Nucleosides as chemotherapeutic agents. *FEMS microbiology letters **2001**, 202(1), 9-15.*

[137] Moore M. D., & Jaykus L. A., Virus–bacteria interactions: implications and potential for the applied and agricultural sciences. *Viruses **2018**, 10(2), 61.*

[138]Azevedo M., Mullis L., & Agnihothram S., Viral and bacterial co-infection and its implications. *SciFed virology research journal **2017**, 1(1).*

[139]Contou D., Claudinon A., Pajot O., Micaëlo M., Flandre P. L., Dubert M, Cally R., Logre E., Fraissé M., Mentec H., Plantefève G., Bacterial and viral co-infections in patients with severe SARS-CoV-2 pneumonia admitted to a French ICU. *Ann. Intensive Care **2020**, 10, 119.*

[140]Thomson J. M., Lamont I. L., Nucleoside analogues as antibacterial agents. *Frontiers in microbiology, **2019**, 10, 952.*

[141] Serpi M., Ferrari V., Pertusati F., Nucleoside Derived Antibiotics to Fight Microbial Drug Resistance: New Utilities for an Established Class of Drugs? *J Med Chem. **2016**, 59(23), 10343-10382.*

[142] Bugg T.D.H., Kerr R.V., Mechanism of action of nucleoside antibacterial natural product antibiotics. *The Journal of Antibiotics. **2019**, 72(12), 865-876.*

[143] Zenchenko A.A., Drenichev M.S., Il'icheva I.A., Mikhailov S.N. Antiviral and Antimicrobial Nucleoside Derivatives: Structural Features and Mechanisms of Action. *Mol Biol. **2021**, 55(6), 786-812.*

[144] Rice, L. B., The clinical consequences of antimicrobial resistance. *Current opinion in microbiology, **2009**, 12(5), 476-481.*

[145] Winn M., Goss R.J., Kimura K., Bugg T.D., Antimicrobial nucleoside antibiotics targeting cell wall assembly: recent advances in structure-function studies and nucleoside biosynthesis. *Natural Product Reports **2010**, 27(2), 279-304.*

[146] Stoeckler J.D., Poirot A.F., Smith R.M., Parks R.E., Ealick S.E., Takabayashi K., Erion M.D. Purine nucleoside phosphorylase. 3. Reversal of purine base specificity by site-directed mutagenesis. *Biochemistry **1997**, 36(39), 11749-11756.*

[147] John A. Montgomery, Shri Niwas, Jerry D. Rose, John A. Secrist III, Y. Sudhakar Babu, Charles E. Bugg, Mark D. Erion, Wayne C. Guida, and Steven E. Ealick Structure-based design of inhibitors of purine nucleoside phosphorylase. 1. 9-(Arylmethyl) derivatives of 9-deazaguanine, *J. Med. Chem. **1993**, 36, 1, 55–69.*

[148] Bzowska A., Kulikowska E., Shugar D., Purine nucleoside phosphorylases: properties, functions, and clinical aspects. *Pharmacol Ther. **2000**, 88(3), 349-425.*

[149] Canduri F., Fadel V., Basso L. A., Palma M.S., Santo D. S., de Azevedo Jr W. F., New catalytic mechanism for human purine nucleoside phosphorylase, *Biochemical and Biophysical Research Communications **2005**, 327(3), 646-649.*

[150] Garner P., Yoo J. U., & Sarabu R. Synthesis of 2-aminopurine nucleosides via regiocontrolled glycosylation. *Tetrahedron **1992**, 48(21), 4259-4270.*

[151] Garner P., & Ramakanth S. A regiocontrolled synthesis of N7-and N9-guanine nucleosides. *The Journal of Organic Chemistry **1988**, 53(6), 1294-1298.*

[152] Cahard D., McGuigan C., Balzarini J., Aryloxy Phosphoramidate Triesters as Pro-Tides, *Mini-Reviews in Medicinal Chemistry **2004**, 4 (4), 371-381.*

[153] McGuigan C., Knaggs S., Daluge S. M., Gudmundsson K. S., McLean E. W., Burnette T. C., Marr H., Hazen R., Condreay L. D., Johnson L., De Clercq E., Balzarini J., Application of phosphoramidate pronucleotide technology to abacavir leads to a significant enhancement of antiviral potency, *Journal of Medicinal Chemistry **2005**, 48 (10), 3504-3515.*

[154] Mehellou Y., Balzarini J., McGuigan C., Aryloxy Phosphoramidate Triesters: a Technology for Delivering Monophosphorylated Nucleosides and Sugars into Cells **2009**, 4(11), 1779-1791.

[155] Mehellou Y., Rattan H.S., Balzarini J., The ProTide Prodrug Technology: From the Concept to the Clinic. *J Med Chem. **2018**, 61(6),2211-2226.*

[156] Bobkov G. V., Brilliantov K. V., Mikhailov S. N., Rozenski J., Aerschot A. V., Herdewijn P., *Collect. Czech. Chem. Commun. **2006**, 71, 804.*

[157] Zhong M., Nowak I., Cannon J. F., Robins M. J., Structure and Synthesis of 6-(Substituted-imidazol-1-yl)purines: Versatile Substrates for Regiospecific Alkylation and Glycosylation at N9, *J. Org. Chem. **2006**, 71, 11, 4216–4221.*

[158] Johansson T., Weidolf L., Jurva U., Mimicry of phase I drug metabolism--novel methods for metabolite characterization and synthesis. *Rapid Commun Mass Spectrom. **2007**, 21(14), 2323-2331.*

[159] Studzińska S., Siecińska L., Buszewski B., On-line electrochemistry/electrospray ionization mass spectrometry (EC-ESI-MS) system for the study of nucleosides and nucleotides oxidation products, *Journal of Pharmaceutical and Biomedical Analysis **2018**, 158, 416-424.*

[160] I. Vicenti, M.G. Martina, A. Boccuto, M. De Angelis, G. Giavarini, F. Dragoni, S. Marchi, C.M. Trombetta, E. Crespan, G. Maga, C. Eydoux, E. Decroly, E. Montomoli, L. Nencioni, M. Zazzi, M. Radi, System-oriented optimization of multi-target 2,6-diaminopurine derivatives: Easily accessible broad-spectrum antivirals active against flaviviruses, influenza virus and SARS-CoV-2, *European Journal of Medicinal Chemistry*, ***2021***, *224, 113683.*

[161] A. Brai, V. Riva, F. Saladini, C. Zamperini, C.I. Trivisani, A. Garbelli, C. Pennisi, A. Giannini, A. Boccuto, F. Bugli, M. Martini, M. Sanguinetti, M. Zazzi, E. Dreassi, M. Botta, G. Maga, DDX3X inhibitors, an effective way to overcome HIV-1 resistance targeting host proteins, *European Journal of Medicinal Chemistry*, ***2020***, *200, 112319.*

[162] Clinical Laboratory Standard Institute, Methods for dilution antimicrobial susceptibility tests for bacteria that grow aerobically, Document M07-A10, 2015, Twelfth Edition, Wayne, PA, USA.

[163] Liang C., Tian L., Liu Y., Hui N., Qiao G., Li H., Shi Z., Tang Y., Zhang D., Xie X., Zhao X., A promising antiviral candidate drug for the COVID-19 pandemic: A mini-review of remdesivir, *European Journal of Medicinal Chemistry* ***2020***, *201, 112527.*

[164] Eastman R.T., Roth J.S., Brimacombe K.R., Simeonov A., Shen M., Patnaik S., Hall M.D., Remdesivir: A Review of Its Discovery and Development Leading to Emergency Use Authorization for Treatment of COVID-19. *ACS Cent Sci.* ***2020***,*6(5),672-683.*

[165] Sofia M. J., Bao D., Chang W., Du J., Nagarathnam D., Rachakonda S., Reddy P. G., Ross B.s., Wang P., Zhang H-R., Bansal S., Espiritu C., Keilman M., Lam A. M., Steuer H. M. M., Niu C., Otto M. J., Furman P. A., Discovery of a β-d-2′-Deoxy-2′-α-fluoro-2′-β-C-methyluridine Nucleotide Prodrug (PSI-7977) for the Treatment of Hepatitis C Virus, *Journal of Medicinal Chemistry* ***2010***, *53, 19, 7202-7218.*

[166] Siegel D., Hui H.C., Doerffler E., Clarke M.O., Chun K., Zhang L., Neville S., Carra E., Lew W., Ross B., Wang Q., Wolfe L., Jordan R., Soloveva V., Knox J., Perry J., Perron M., Stray K.M., Barauskas O., Feng J.Y., Xu Y., Lee G., Rheingold A.L., Ray A.S., Bannister R., Strickley R., Swaminathan S., Lee W.A., Bavari S., Cihlar T., Lo M.K., Warren T.K., Mackman R.L.. Discovery and Synthesis of a Phosphoramidate Prodrug of a Pyrrolo[2,1-f][triazin-4-amino] Adenine C-Nucleoside (GS-5734) for the Treatment of Ebola and Emerging Viruses. *J Med Chem.* ***2017***, *60(5), 1648-1661*.

[167] Thornton P.J., Kadri H., Miccoli A., Mehellou Y., Nucleoside Phosphate and Phosphonate Prodrug Clinical Candidates. *J Med Chem.* ***2016***, *59(23),10400-10410.*

[168] Warren T., Jordan R., Lo M. et al, Therapeutic efficacy of the small molecule GS-5734 against Ebola virus in rhesus monkeys. *Nature* ***2016***, *531, 381–385.*

[169] Alanazi A. S., James E., and Mehellou Y., The ProTide Prodrug Technology: Where Next? *ACS Med. Chem. Lett.* ***2019***, *10, 1, 2–5.*

[170] Lohman T.M., Tomko E.J., Wu C.G., Non-hexameric DNA helicases and translocases: mechanisms and regulation. *Nat Rev Mol Cell Biol.* ***2008***, *9(5), 391-401.*

[171] Gorbalenya A. E., Koonin E. V., Helicases: amino acid sequence comparisons and structure-function relationships, *Current Opinion in Structural Biology* ***1993***, *3 (3), 419-429.*

[172] Lehmann K. C., Snijder E. J., Posthuma C. C., Gorbalenya A. E., What we know but do not understand about nidovirus helicases, *Virus Research* ***2015***, *202, 12-32.*

[173] Ivanov K.A., Thiel V., Dobbe J.C., van der Meer Y., Snijder E.J., Ziebuhr J., Multiple enzymatic activities associated with severe acute respiratory syndrome coronavirus helicase. *J Virol.* ***2004***, *78(11), 5619-5632.*

[174] Fairman-Williams M.E., Guenther U.P., Jankowsky E., SF1 and SF2 helicases: family matters. *Curr Opin Struct Biol.* ***2010***,*20(3), 313-324.*

[175] Tanner J.A., Watt R.M., Chai Y.B., Lu L.Y., Lin M.C., Peiris J.S., et al. The severe acute respiratory syndrome (SARS) coronavirus NTPase/helicase belongs to a distinct class of 5' to 3' viral helicases. *J Biol Chem.* ***2003,*** *278(41), 39578-39582.*

[176] Seybert A., Hegyi A., Siddell S.G., Ziebuhr J., Thehuman coronavirus 229E superfamily 1 helicase has RNA and DNA duplex-unwinding activities with 5'-to-3' polarity. *RNA* ***2000***, *6(7), 1056-1068.*

[177] Lehmann K. C., Snijder E. J., Posthuma C. C., Gorbalenya A. E.,What We Know but Do Not Understand about Nidovirus Helicases.*Virus Res.* ***2015***, *202, 12−32.*

[178] Adedeji A. O., Marchand B., Te Velthuis A. J. W., Snijder E. J., Weiss, S., Eoff R. L., Singh K., Sarafianos S. G., Mechanism of NucleicAcid Unwinding by SARS-CoV Helicase. *PLoS One* ***2012***, *7(5), e36521.*

[179] Van Hemert M.J., van den Worm S.H.E., Knoops K., Mommaas A.M., Gorbalenya A.E., Snijder E.J. SARS coronavirus replication/transcription complexes are membrane-protected and need a host factor for activity in vitro. *PLoS Pathog.* ***2008****, 4(5):e1000054.*

[180] Frick D.N., Lam A.M. Understanding helicases as a means of virus control. *Curr Pharm Des.* ***2006****, 12(11), 1315-1338.*

[181] Chen J., Malone B., Llewellyn E., Grasso M., Shelton P.M.M., Olinares P.D.B., et al. Structural Basis for Helicase-Polymerase Coupling in the SARS-CoV-2 Replication-Transcription Complex. *Cell.* ***2020****, 182(6), 1560-1573.*

[182] Fang S., Chen B., Tay F.P., Ng B.S., Liu D.X., An arginine-to-proline mutation in a domain with undefined functions within the helicase protein (Nsp13) is lethal to the coronavirus infectious bronchitis virus in cultured cells. *Virology* ***2007****, 358(1), 136-147.*

[183] Wu A., Peng Y., Huang B., Ding X., Wang X., Niu P., et al. Genome Composition and Divergence of the Novel Coronavirus (2019-nCoV) Originating in China. *Cell Host Microbe* ***2020****, 27(3), 325-328.*

[184] Shum K.T., Tanner J.A., Differential inhibitory activities and stabilisation of DNA aptamers against the SARS coronavirus helicase. *Chembiochem.* ***2008****, 9(18), 3037-3045.*

[185] Adedeji A.O., Singh K., Kassim A., Coleman C.M., Elliott R., Weiss S.R., Frieman M.B., Sarafianos S.G., Evaluation of SSYA10-001 as a replication inhibitor of severe acute respiratory syndrome, mouse hepatitis, and Middle East respiratory syndrome coronaviruses. *Antimicrob Agents Chemother.* ***2014****, 58(8), 4894-4898.*

[186] V'kovski P., Kratzel A., Steiner S., Stalder H., Thiel V., Coronavirus Biology and Replication: Implications for SARS-CoV-2. *Nat. Rev. Microbiol.* ***2021****,19, 155.*

[187] Saikrishnan K., Powell B., Cook N. J., Webb M. R., Wigley D.B., Mechanistic Basis of 5′-3′Translocation in SF1B Helicases. *Cell* ***2009****, 137(5), 849−859.*

[188] Hao W., Wojdyla J. A., Zhao R., Han R., Das R., Zlatev I., Manoharan M., Wang M., Cui S., Crystal Structure of Middle EastRespiratory Syndrome Coronavirus Helicase. *PLoS Pathog.* ***2017****,13(6), e1006474.*

[189] White M. A., Lin W., and Cheng X., Discovery of COVID-19 Inhibitors Targeting the SARS-CoV-2 Nsp13 Helicase, *J.Phys.Chem.Lett.* ***2020****, 11, 9144−9151*

[190] Yazdi A. K., Pakarian P., Perveen S., Hajian T., Santhakumar V., Bolotokova A., Li F., and Vedadi M., Kinetic Characterization of SARS-CoV-2 nsp13 ATPase Activity and Discovery of Small-Molecule Inhibitors. *ACSInfect.Dis.* ***2022****,8,1533−1542.*

[191] Corona A., Wycisk K., Talarico C., Manelfi C., Milia J., Cannalire R., Esposito F., Gribbon P., Zaliani A., Iaconis D., Beccari A. R., Summa V., Nowotny M., and Tramontano E., Natural Compounds Inhibit SARS-CoV-2 nsp13 Unwinding and ATPase Enzyme Activities. *ACS Pharmacol. Transl. Sci.* ***2022****, 5, 226−239.*

[192] Yu M. S., Lee J., Lee J. M., Kim, Y., Chin Y. W., Jee J. G., Keum Y. S., Jeong Y. J., Identification of Myricetin and Scutellarein asNovel Chemical Inhibitors of the SARS Coronavirus Helicase, NsP13.Bioorg. *Med. Chem. Lett.* ***2012****,22(12), 4049−4054.*

[193]Keum Y. S., Lee J. M., Yu M. S., Chin Y. W., Jeong Y. J., Inhibition of SARS Coronavirus Helicase by Baicalein. *Bull. Korean Chem. Soc.* ***2013****, 34 (11), 3187–3188.*

[194] van Hemert M.J., van den Worm S.H., Knoops K., Mommaas A.M., Gorbalenya A.E., Snijder E.J., SARS-coronavirus replication/transcription complexes are membrane-protected and need a host factor for activity in vitro. *PLoS Pathog.* ***2008****, 4(5):e1000054*..

[195] Sharma A., Boris-Lawrie K., Determination of Host Rna Helicases Activity in Viral Replication. *Method Enzymol* **2012**, *511*, 405-435.

[196] Ranji A., Boris-Lawrie K., RNA helicases: emerging roles in viral replication and the host innate response. *RNA Biol* **2010**, *7*, 775-787.

[197] Lai M. C., Sun H. S., Wang S. W., Tarn W. Y., DDX 3 functions in antiviral innate immunity through translational control of PACT. *The FEBS journal* ***2016****, 283(1), 88-101.*

[198] Lin S., Chang P., He J., Coyaud E., Pierce B. E., and Zhang Y.J., RNA helicase DDX3 interacts with the capsid protein of hepatitis E virus and plays an indispensable role in the viral replication, Preprints.org; **2020**. DOI: 10.20944/preprints202012.0557.v1

[199] Maga G., Falchi F., Radi M., Botta L., Casaluce G., Bernardini M., Irannejad H., Manetti F., Garbelli A., Samuele A., Zanoli S., Esté J.A., Gonzalez E., Zucca E., Paolucci S., Baldanti F., De Rijck J., Debyser Z., Botta M. Toward the discovery of novel anti-HIV drugs. Second-generation inhibitors of the cellular ATPase DDX3 with improved anti-

HIV activity: synthesis, structure-activity relationship analysis, cytotoxicity studies, and target validation. *ChemMedChem* ***2011*** *6(8), 1371-1389.*

[200] Radi M., Falchi F., Garbelli A., Samuele A., Bernardo V., Paolucci S., Baldanti F., Schenone S., Manetti F., Maga G., Botta M., Discovery of the first small molecule inhibitor of human DDX3 specifically designed to target the RNA binding site: towards the next generation HIV-1 inhibitors. *Bioorg Med Chem Lett.* ***2012****, 22(5):2094-2098.*

[201] Flynn R.A., Belk J.A., Qi Y., Yasumoto Y., Wei J., Alfajaro M.M., Shi Qzi C.R., Wilen C.B., Satpathy A.T., Discovery and functional interrogation of SARS-CoV-2 RNA-host protein interactions. *Cell.* ***2021****, 184(9), 2394-2411.e16.*

[202] Squeglia F., Romano M., Ruggiero A., Maga G. and Berisio R., Host DDX Helicases as Possible SARS-CoV-2 Proviral Factors: A Structural Overview of Their Hijacking Through Multiple Viral Proteins. *Front. Chem. Sec. Chemical Biology* ***2020****, 8, 1-17.*

[203] Service R. S., Newly discovered 'magic methyl' reaction could turbocharge the potency of some drugs. *Science* ***2020****, doi: 10.1126/science.abb7567.*

[204] Zhao J., Zhang D., Zhang W., Stashko M. A., DeRyckere D., Vasileiadi E., Parker R. E., Hunter D., Liu Q., Zhang Y., Norris-Drouin J., Li B., Drewry D. H., Kireev D., Graham D. K:, Earp H. S., Frye S. V., and Wang X. Highly selective MERTK inhibitors achieved by a single methyl group. *Journal of Medicinal Chemistry,* ***2018****, 61(22), 10242-10254.*

[205]Khan K.M., Shah Z., Ahmad V.U., Khan M., Taha M., Rahim F., Ali S., Ambreen N., Perveen S., Choudhary M.I., Voelter W. 2,4,6-Trichlorophenylhydrazine Schiff bases as DPPH radical and super oxide anion scavengers. *Med Chem.* ***2012****, 8(3), 452-461.*

[206]Demurtas M., Baldisserotto A., Lampronti I., Moi D., Balboni G., Pacifico S., Vertuani S., Manfredini S., Onnis V. Indole derivatives as multifunctional drugs: Synthesis and evaluation of antioxidant, photoprotective and antiproliferative activity of indole hydrazones. *Bioorg Chem.* ***2019****, 85, 568-576.*

[207] But T.Y., Toy P.H. Organocatalytic Mitsunobu reactions. *J Am Chem Soc.* ***2006****, 128(30), 9636-9637.*

[208] Bino A., Baldisserotto A., Scalambra E., Dissette V., Vedaldi D. E., Salvador A., Durini E., Manfredini S., Vertuani S. Design, synthesis and biological evaluation of novel hydroxy-phenyl-1H-benzimidazoles as radical scavengers and UV-protective agents. *Journal of Enzyme Inhibition and Medicinal Chemistry* ***2017****, 32(1), 527-537.*

[209] Adedeji A. O., Singh K., Calcaterra N. E., DeDiego M. L., Enjuanes L., Weiss S., Sarafianos S. G., Severe Acute Respiratory Syndrome Coronavirus Replication Inhibitor That Interferes with the Nucleic Acid Unwinding of the Viral Helicase. *Antimicrob. AgentsChemother.* ***2012****, 56(9), 4718−4728.*

[210] Provencher V. M. I.; Coccaro E., Lacasse J. J.; Schang L. M., Antiviral Drugs that Target Cellular Proteins May Play Major Roles in Combating HIV Resistance, *Current Pharmaceutical Design* ***2004*** *10(32), 4081-4101.*

[211]Schang L. M. Effects of pharmacological cyclin-dependent kinase inhibitors on viral transcription and replication. *Biochimica et Biophysica Acta (BBA)-Proteins and Proteomics* ***2004****, 1697(1-2), 197-209.*

[212] Scutigliani E.M., and Kikkert M., Interaction of the innate immune system with positive-strand RNA virus replication organelles. *Cytokine Growth Factor Rev.* ***2017****, 37, 17–27*

[213] Wolff G., Melia C. E., Snijder E. J., Bárcena M., *Trends Microbiol.* ***2020****, 28 (12), 1022–1033.*

[214] Paul D., Bartenschlager R., Architecture and biogenesis of plus-strand RNA virus replication factories. *World J. Virol.* **2013**, *2* (2), 32-48.

[215] van der Schaar H. M., Dorobantu C. M., Albulescu L., Strating J. R. P. M., van Kuppeveld F. J. M., Fat(al) attraction: Picornaviruses Usurp Lipid Transfer at Membrane Contact Sites to Create Replication Organelles. *Trends Microbiol.* **2016**, *24* (7), 535–546.

[216] Beziau A., Brand D., Piver E. The role of phosphatidylinositol phosphate kinases during viral infection. *Viruses* ***2020****, 12(10), 1–16.*

[217] Altan-Bonnet N., Balla T., Phosphatidylinositol 4-kinases: Hostages harnessed to build panviral replication platforms. *Trends Biochem Sci* **2012**, 37(7), 293–302.

[218] Yang N., Ping M., Lang J., Zhang Y., Deng J., Ju X., Zhang G., Jiang C., Phosphatidylinositol 4-kinase IIIβ is required for severe acute respiratory syndrome coronavirus spike-mediated cell entry. *J Biol Chem* ***2012****, 287(11), 8457–8467.*

[219] Doerflinger S.Y., Cortese M., Romero-Brey I., Menne Z., Tubiana T., Schenk C., White P.A., Bartenschlager R., Bressanelli S., Hansman G.S., Lohmann V., Membrane alterations induced by nonstructural proteins of human norovirus. PLoS Pathog. **2017**, 13(10):e1006705.

[220] Melia C.E., van der Schaar H.M., de Jong A.W.M., Lyoo H.R., Snijder E.J., Koster A.J., van Kuppeveld F.J.M., Bárcena M. The Origin, Dynamic Morphology, and PI4P-Independent Formation of Encephalomyocarditis Virus Replication Organelles. *mBio.* ***2018****, 9(2):e00420-18.*

[221] Romero-Brey I., Merz A., Chiramel A., Lee J.Y., Chlanda P., Haselman U., Santarella-Mellwig R., Habermann A., Hoppe S., Kallis S., Walther P., Antony C., Krijnse-Locker J., Bartenschlager R., Three-dimensional architecture and biogenesis of membrane structures associated with hepatitis C virus replication. *PLoS Pathog.* ***2012****, 8(12):e1003056.*

[222] Knoops K., Kikkert M., Worm S.H., Zevenhoven-Dobbe J.C., van der Meer Y., Koster A.J., Mommaas A.M., Snijder E.J., SARS-coronavirus replication is supported by a reticulovesicular network of modified endoplasmic reticulum. *PLoS Biol.* ***2008****, 6(9):e226.*

[223] de Wilde A.H., Raj V.S., Oudshoorn D., Bestebroer T.M., van Nieuwkoop S., Limpens R.W.A.L., Posthuma C.C., van der Meer Y., Bárcena M., Haagmans B.L., Snijder E.J., van den Hoogen B.G., MERS-coronavirus replication induces severe in vitro cytopathology and is strongly inhibited by cyclosporin A or interferon-α treatment. *J Gen Virol.* ***2013,*** *94(Pt 8):1749-1760.*

[224] Snijder E.J., Limpens R.W.A.L., de Wilde A.H., de Jong A.W.M., Zevenhoven-Dobbe J.C., Maier H.J., Faas F.F.G.A., Koster A.J., Bárcena M., A unifying structural and functional model of the coronavirus replication organelle: Tracking down RNA synthesis. *PLoS Biol.* ***2020****, 18(6):e3000715.*

[225] Delang L., Paeshuyse J., Neyts J., The role of phosphatidylinositol 4-kinases and phosphatidylinositol 4-phosphate during viral replication. *Biochem Pharmacol* ***2012****, 84(11), 1400–1408.*

[226] Strating J.R., van Kuppeveld F.J., Viral rewiring of cellular lipid metabolism to create membranous replication compartments. *Curr Opin Cell Biol.* ***2017****, 47, 24-33.*

[227] Ci Y., Yang Y., Xu C., Qin C.-F., Shi L., Electrostatic Interaction Between NS1 and Negatively Charged Lipids Contributes to Flavivirus Replication Organelles Formation. *Front. Microbiol.* **2021**, *12*, 641059.

[228] H. Yang, X. Zhao, M. Xun, L. Xu, B. Liu, H. Wang, Cytoplasmic domain and enzymatic activity of ACE2 is not required for PI4KB dependent endocytosis entry of SARS-CoV-2 into host cells, *bioRxiv* **2021**. 03.01.433503.

[229] Tassini S., Sun L., Lanko K., Crespan E., Langron E., Falchi F., Kissova M., Armijos-Rivera J. I., Delang L., Mirabelli C., Neyts J., Pieroni M., Cavalli A., Costantino G., Maga G., Vergani P., Leyssen P., Radi M., Discovery of Multitarget Agents Active as Broad-Spectrum Antivirals and Correctors of Cystic Fibrosis Transmembrane Conductance Regulator for Associated Pulmonary Diseases. *J. Med. Chem.* ***2017****, 60, 1400−1416.*

[230] S. Tassini, E. Langron, L. Delang, C. Mirabelli, K. Lanko, E. Crespan, M. Kissova, G. Tagliavini, G. Fontò, S. Bertoni, S. Palese, C. Giorgio, F. Ravanetti, L. Ragionieri, C. Zamperini, A. Mancini, E. Dreassi, G. Maga, P. Vergani, J. Neyts, M. Radi, Multitarget CFTR Modulators Endowed with Multiple Beneficial Side Effects for Cystic Fibrosis Patients: Toward a Simplified Therapeutic Approach. *J. Med. Chem.* **2019**, *62*, *10833-10847*.

[231] Golubev V., Zubkov F., Krasavin M. A simple, three-component synthesis of 2-aminothiazoles using trimethylsilyl isothiocyanate. *Tetrahedron Lett.* ***2013****, 54(36), 4844–4847.*

[232] Martina M. G., Vicenti I., Bauer L., Crespan E:, Rango E., Boccuto A., Olivieri N., Incerti M., Zwaagstra M., Allodi M., Bertoni S., Dreassi E., Zazzi M., van Kuppeveld F. J. M., Maga G., and Radi M., Bithiazole Inhibitors of Phosphatidylinositol 4-Kinase (PI4KIIIβ) as Broad-Spectrum Antivirals Blocking the Replication of SARS-CoV-2, Zika Virus, and Human Rhinoviruses, *ChemMedChem* ***2021****, 16, 1–6*

[233] Bauer L., Manganaro R., Zonsics B., Hurdiss D. L., Zwaagstra M., Donselaar T., Welter N. G. E., van Kleef R. G. D. M., Lopez M. L., Bevilacqua F., Raman T., Ferla S., Bassetto M., Neyts J., Strating J. R. P. M., Westerink R. H. S., Brancale A., van Kuppeveld F. J. M., *PLoS Biol.* ***2020****, 18 (11), e3000904.*

[234] MacLeod A. M., Mitchell D. R., Palmer N. J., Van de Poël H., Conrath K., Andrews M., Leyssen P., Neyts J., Identification of a Series of Compounds with Potent Antiviral Activity for the Treatment of Enterovirus Infections. *ACS Med. Chem. Lett.* ***2013****, 4 (7), 585–589.*

[235] Strating J. R., van Kuppeveld F. J., Viral rewiring of cellular lipid metabolism to create membranous replication compartments. *Curr. Opin. Cell Biol.* ***2017****, 47, 24–33.*

[236] Vicenti I., Boccuto A., Giannini A., Dragoni F., Saladini F., Zazzi M., Comparative analysis of different cell systems for Zika virus (ZIKV) propagation and evaluation of anti-ZIKV compounds in vitro. *Virus Res.* **2018**, *244*, 64–70.

[237] Vicenti I., Dragoni F., Giannini A., Giammarino F., Spinicci M., Saladini F., Boccuto A., Zazzi M., Development of a Cell-Based Immunodetection Assay for Simultaneous Screening of Antiviral Compounds Inhibiting Zika and Dengue Virus Replication, *SLAS Discov,* ***2020****, 25(5), 506-514.*

[238] Rango E., D'Antona L., Iovenitti G., Brai A., Mancini A., Zamperini C., Trivisani C. I., Marianelli S., Fallacara A. L., Molinari A., Cianciusi A., Schenone S., Perrotti N., Dreassi E., Botta M., Si113-prodrugs selectively activated by plasmin against hepatocellular and ovarian carcinoma, *European Journal of Medicinal Chemistry, **2021**, 223, 113653*

[239] Barthel B. L., Rudnicki D. L., Kirby T. P., Colvin S. M., Burkhart D. J., Koch T. H., *J. Med. Chem. **2012**, 55, 6595–6607.*

[240] Re R., Pellegrini N., Proteggente A., Pannala A., Yang M., Rice-Evans C., Antioxidant activity applying an improved ABTS radical cation decolorization assay. *Free Radic Biol Med. 1999, 26(9-10), 1231-1237.*